CARBON NANOFILLER MODIFIED CARBON FIBER EPOXY COMPOSITE FOR STRUCTURAL APPLICATION

Ph.D. THESIS

by

ANKITA BISHT

DEPARTMENT OF METALLURGICAL AND MATERIALS ENGINEERING
INDIAN INSTITUTE OF TECHNOLOGY ROORKEE
ROORKEE – 247667, INDIA
JULY, 2019

CARBON NANOFILLER MODIFIED CARBON FIBER EPOXY COMPOSITE FOR STRUCTURAL APPLICATION

A THESIS

Submitted in partial fulfilment of the requirements for the award of the degree

of

DOCTOR OF PHILOSOPHY

in

METALLURGICAL AND MATERIALS ENGINEERING

by

ANKITA BISHT

DEPARTMENT OF METALLURGICAL AND MATERIALSENGINEERING
INDIAN INSTITUTE OF TECHNOLOGY ROORKEE
ROORKEE – 247667, INDIA
JULY, 2019

INDIAN INSTITUTE OF TECHNOLOGY ROORKEE
ROORKEE

CANDIDATE'S DECLARATION

I hereby certify that the work which is being presented in the thesis entitled **"CARBON NANOFILLER MODIFIED CARBON FIBER EPOXY COMPOSITE FOR STRUCTURAL APPLICATION"** in partial fulfilment of the requirements for the award of the Degree of Doctor of Philosophy and submitted in the Department of Metallurgical and Materials Engineering of the Indian Institute of Technology Roorkee, Roorkee is an authentic record of my own work carried out during a period from July, 2014 to July, 2019 under the supervision of Dr. Debrupa Lahiri, Associate Professor, Department of Metallurgical and Materials Engineering, Indian Institute of Technology Roorkee, Roorkee.

The matter presented in this thesis has not been submitted by me for the award of any other degree of this or any other Institution.

(ANKITA BISHT)

This is to certify that the above statement made by the candidate is correct to the best of my knowledge

Date:

(Debrupa Lahiri)
Supervisor

ABSTRACT

Carbon fiber (CF) reinforced epoxy composites are the most widely used fiber reinforced polymer composites (FRPs) in aerospace, automobiles, lightweight structures and many other industries. Properties, like, high strength and stiffness, coupled with low density, corrosion and fatigue resistance, make it better as compared to the conventional metallic counterparts. Despite these advantages, the anisotropic properties of FRPs and the brittle nature of the matrix often results in delamination and premature failure of structures. Hence, there is a need to improve the transverse and out of plane properties, without sacrificing the axial properties and maintaining low weight. The interfacial interaction between CF and epoxy has to be strong to achieve this. A number of techniques have been adopted to strengthen the interface, most of which involve modifying CF surface. Studies on modifying the matrix using nanofillers is quite limited, due to the difficulty in dispersion. Hence, this study aims at modifying the epoxy matrix using carbon nanofillers, as they have similar surface chemistry and properties as CF. It also focuses on improving the dispersion of carbon nanofillers inside epoxy matrix, by taking advantage of the synergy that exist among nanofillers having different morphologies.

Thus, the overall aim of the current research is to explore the potential of synergistic effect of carbon nanofillers, with different morphologies, on CF epoxy composite for structural application. The carbon nanofillers of interest here are carbon nanotubes (CNT) with 1D structure, graphene (Gr) with 2D shape and nanodiamond (ND) with 3D morphology. The potential of ND, as a reinforcement to epoxy matrix, is investigated and compared with CNT and Gr, in terms of mechanical and thermal properties for a range of content 0.1-1 wt%. ND improves tensile strength (56%), elastic modulus (94%), hardness (470%) and % strain (66%) of epoxy, simultaneously,

which is very remarkable as compared to Gr or CNT. Investigation on fractured surface of CNT-epoxy and Gr-epoxy composite revealed agglomeration as the prime reason behind the restricted efficiency of the reinforcement phases. Nanodiamonds showed great reinforcement efficiency to epoxy matrix. NanoDMA was performed on ND-epoxy composite to assess and understand the micron level phase distribution of ND in epoxy matrix and its effect on mechanical properties. The spherical morphology of ND has less tendency to agglomerate. So, its positive contribution towards dispersion, in binary combinations with CNT and Gr in epoxy composite, is investigated. Both mechanical and thermal properties are improved for CNT- epoxy and Gr-epoxy composite with the addition of ND, due to the improved exfoliation. No agglomerations were seen even at much higher reinforcement content. The improved exfoliation of Gr, with addition of ND, is quantified through scanning probe microscopy (SPM). Its effect on toughening behaviour of epoxy was predicted through numerical analysis, which were in good agreement with experimental results.

After verifying the potential of ND, as an individual reinforcement and in binary combination, its role in boosting the synergy between Gr-CNT hybrid is investigated. Addition of ND to Gr-CNT hybrid helped in achieving a well exfoliated close knitted 3D network of reinforcement, which improved both tensile strength and fracture toughness quite significantly. This well exfoliated close knitted 3D network of nanofiller is then added to epoxy matrix. The CF laminated composite, fabricated through vacuum assisted resin transfer technique, using 3D network of nanofiller modified epoxy matrix. It is then evaluated for mechanical, thermal and interfacial properties. Improvement in interlaminar fracture toughness by ~260% and interfacial shear strength by ~16% with the addition of 3D network of nanofiller establishes the potential of the approach/route followed.

ACKNOWLEDGEMENT

There are so many people who helped me during this work, which I owe my profound gratitude to:

First, I would like to express my heartfelt gratitude and sincere thanks to my supervisor Dr. Debrupa Lahiri, Associate Professor, Department of Metallurgical and Materials Engineering, Indian Institute of Technology, Roorkee. Her valuable guidance, constant encouragement, untiring help, and supporting attitude has been a great source of motivation at every stage of research and preparation of thesis. She provided great research facilities and maintained a great working environment in the research group. She devoted hours discussing research works and gave valuable suggestions which helped improve the quality of my research. Her constant motivation and encouragement helped me in achieving my research goals, despite of several failures. Not only has she helped me with her research outlook, clarity and knowledge. Her abilities to multitask, dedication towards every task, enthusiasm towards new findings and learning new things, work ethics and principles which are non-negotiable, self-belief/confidence and most importantly being brave and standing for yourself has helped and taught me a lot. To her, I shall remain, professionally and personally indebted for life.

I express my sincere thanks to Dr. Indranil Lahiri, Associate Professor Department of Metallurgical and Materials Engineering, Indian Institute of Technology, Roorkee who gave access to his research lab and facilities for carrying out my research work.

I greatly acknowledge the contributions of my research committee members Dr. Anjan Sil Professor, Department of Metallurgical and Materials Engineering, IIT Roorkee, Dr. Bhanu Mishra, Professor, Department of Mechanical and Industrial Engineering, IIT Roorkee, Dr. Ujjwal Prakash, Professor, Department of Metallurgical and Materials Engineering, IIT Roorkee, who spared their valuable time for critical assessment of my work.

I would like to thank Dr. Kinshuk Dasgupta, Scientist, Bhabha Atomic Research Centre, Mumbai, for sparing his valuable time for critical assessment of my research work. Incorporation of his constructive suggestions has greatly enhanced the quality of my research work.

I am thankful to Head of the Department Dr. G. P. Chaudhari, Professor, Metallurgical and Materials Engineering Department, for his help and providing the facilities in the department for my research work. I would also like to show my appreciation to all our departmental faculties and our technical staff who have helped me through the experimental work, especially, Mr. R. K. Sharma for supporting me in the usage of departmental facilities.

I am grateful to my seniors, colleagues and juniors Dr. Swati Haldar, Dr. Manoj Kumar R., Dr. Vijayesh Kumar, Dr. Raj Kumar, Dr. Sandan Kumar Sharma, Pramod Kumar, Satish Jaiswal, Anshu Dubey, Vaibhav Jain, Kanike Rajesh, Siddharth Sharma, Pradeep Thakur, Nitam Tayade, Mukul Srivastava, Bhagyadhar Das, Ketan Khamgaonkar, Rakesh, Gurjinder Kaur, Narashima Vinod, Atif Suhail, Akanksha Urade, Palash Maity, Rita Joshi and other BMML & NAL lab members who have supported and helped me by providing such a good working atmosphere, making my journey a memorable one.

I wish to acknowledge and thank my dear friends Soumyaranjan Nayak, Souvik Ghosh, Vishal Panwar, Janki Supyal, Sakshi Chauhan, Seema Negi, Sonika Chauhan, Laxmi Adhikari, Konika Bhateja, Pratibha Negi, Vineeta Kanwal, Ruchi, Khyati Tamta and Nisha Tamta who have mentally and emotionally supported me throughout this journey.

My family deserves special attention for their unconditional love and support throughout my life and during my research work. This thesis would not have been possible without their support, advice, time, never-ending patience, constant encouragement and faith in me. Words fail to express the sacrifices my parents Mr. Prakash Chandra Bisht and Mrs. Vimla Bisht, have made to bring me to this position. Specially my mother, who sacrificed her professional career, so that she could be there

for me and my sisters. I express my profound regards to my grandparents Mr. Heera Ballabh Pangaria and Chandra Pangaria for their blessings, unconditional love, care and being the source of inspiration. I would specially like to thank my sisters Ms. Monika Bisht and Ms. Niharika Bisht and my niece Khanak for pouring in the positive energy and enthusiasm in me, whenever I felt discouraged or demotivated. They have taught me to have a positive outlook towards every situation.

Special thanks to my dear friend Mr. Sanjay Singh Samant, Assistant Professor, Department of Mechanical Engineering, GBPIET, Pauri, for helping me with the numerical analysis studies presented in my thesis and all the technical discussions, which has helped a lot in verifying and supporting my experimental findings. More importantly for his moral support and encouragement which helped me to culminate this work into a success.

I am also thankful to the Ministry of Human Resources and Development, Government of India for providing the financial assistantship during the tenure of my research work. Board of Research in Nuclear Sciences (BRNS), India (36(2)/14/17/2016-BRNS) and the faculty initiation grant (FIG-100613) by IIT Roorkee, for the financial support for carrying out this research. The non-teaching and administrative staff who has rendered their help in all possible ways during my Ph.D. work.

Further, I thank with an apology to all those people whose contributions to this work have escaped my attention and, thus, have gone unnoticed.

ANKITA BISHT

TABLE OF CONTENTS

ABSTRACT i

ACKNOWLEDGEMENT iii

TABLE OF CONTENTS vi

LIST OF FIGURES xii

LIST OF TABLES xviii

1 INTRODUCTION 1

2 LITERATURE REVIEW 10

2.1 Introduction to Fiber Reinforced Polymer Composites 10

2.2 Commonly used Carbon Nanofillers as a Reinforcement to Polymer Matrix 12

2.3 Different Approaches to Integrate Carbon Nanofillers in a Multiscale Composite 16

2.3.1 Nano-engineering the Carbon Fiber Surface 16

2.3.1.1 Electrophoretic Deposition 16

2.3.1.2 Carbon Vapour Deposition (CVD) 20

2.3.1.3 Interleaving 22

2.3.1.4 Chemical Grafting 23

2.3.1.5 Dip Coating 24

2.3.2 Nanofiller Modified Polymer Matrix 25

2.3.3 Nanofiller Modified Sizing 26

2.4 Techniques for Fabricating Fiber Reinforced Polymer Composites 26

2.4.1 Vacuum Assisted-Resin Transfer Moulding (VARTM/RTM) 26

2.4.2 Autoclave 27

2.4.3 Hand lay up 27

2.4.4 Other Techniques 28
2.5 Carbon Nanoparticle-Carbon Fiber Epoxy System 28
2.5.1 CNT-CF Epoxy Composites 28
2.5.2 Gr and its derivatives -CF Epoxy Composites 29
2.6 Assessing the Role of Interfacial Bonding in CF-Epoxy Composite 32
2.7 Effect of Nanofiller Addition on Mechanical Properties CF-Epoxy Composite 38
2.7.1 Tensile Strength 38
2.7.2 Interlaminar Shear Strength and Interlaminar Fracture Toughness 41
2.7.3 Flexural strength 44
2.7.4 Other Properties 46
2.8 Numerical Simulation to Predict the Effect of Nanofiller Modification on CF Epoxy Composite 48
2.9 Summary of the Literature Reviewed 51
3 EXPERIMENTAL TECHNIQUES 53
3.1 Materials 53
3.2 Processing 54
3.2.1 Dispersion of Nanofillers in Epoxy Matrix 54
3.2.2 Fabrication of Different Composite Systems 55
3.2.2.1 Nanofiller Epoxy Composite 55
3.2.2.2 Multiscale Carbon Fiber Epoxy Composite 56
3.3 Characterizations 57
3.3.1 Microstructural and Structural Characterization of Nanofillers and Composite 57
3.3.1.1 Scanning Electron Microscopy 57
3.3.1.2 Transmission Electron Microscopy 57

3.3.1.3 Scanning Probe Microscopy 58
3.3.1.4 Modulus Mapping 58
3.3.2 Mechanical Characterization of Composite 58
3.3.2.1 Tensile Test 59
3.3.2.2 Fracture Toughness 59
3.3.2.3 Nanoindentation Elastic modulus and Hardness 59
3.3.3 Interlaminar Properties of Laminated Fiber Composite 60
3.3.3.1 Interlaminar fracture Toughness 60
3.3.3.2 Interlaminar Shear Strength 61
3.3.4 Thermal Degradation Analysis of Composites 61
3.3.5 Thermo-Mechanical Characterization of Composites 61
3.3.6 Contact Angle Measurement 62
3.3.7 Numerical Analysis 62
4 RESULTS AND DISCUSSION 64
4.1 Investigating and Comparing the Potential of Nanodiamonds with Carbon Nanotubes and Graphene as a Reinforcement to Epoxy Matrix 64
4.1.1 Microstructural Characterization of Nanofillers to Confirm Morphology and Dispersion 65
4.1.2 Fracture Surface Analysis of Epoxy and Nanofiller Reinforced Epoxy Matrix 67
4.1.3 Mechanical Behavior of Epoxy and Nanofiller Reinforced Epoxy Composite 69
4.1.3.1 Hardness and Elastic Modulus of Nanofiller Reinforced Composite 69
4.1.3.2 Tensile Properties to Assess the Strengthening Imparted by Nanofillers to Epoxy Matrix 72
4.1.3.3 Fracture toughness to Assess the Toughening Imparted by Nanofillers to Epoxy Matrix 76

4.1.4 Thermal Analysis of Epoxy and Nanofiller Reinforced Epoxy Composites 80
4.1.4.1 Effect of Nanofiller Addition on Thermal Degradation of Epoxy matrix 80
4.1.4.2 Thermo-Mechanical Analysis of Epoxy and Nanofiller Reinforced Epoxy Composite 83
4.1.5 Summary 86
4.2 Evaluating the Micron Level Phase Distribution of Nanodiamond in Epoxy Matrix and its Effect on Mechanical Behaviour 88
4.2.1 TEM Analysis to Confirm Uniform Distribution and Strong Integration of Nanodiamond in Epoxy Matrix 89
4.2.2 Analyzing Functional Distribution of ND in Epoxy Matrix through Nano-Scale Modulus Mapping 91
4.2.3 Evaluation of Elastic Property using Numerical Analysis 99
4.2.4 Summary 105
4.3 Synergistic Effect of Nanodiamond in Binary Combinations with Carbon Nanotube and Graphene in Epoxy Composite 106
4.3.1 Microstructural Characterization to Confirm Morphology of Binary Combinations of Nanofillers 107
4.3.2 Fracture Surface Analysis to Confirm Dispersion, Proper Integration and Strengthening Imparted by Binary Combinations of Nanofillers to Epoxy Matrix 109
4.3.3 Mechanical Behaviour of Epoxy Matrix Reinforced with Binary Combinations of Nanofillers 112
4.3.3.1 Tensile test to Assess the Strengthening Imparted by Binary Combinations of Nanofillers to Epoxy Matrix 112
4.3.3.2 Fracture toughness to Assess the Toughening Imparted by Binary Combinations of Nanofillers to Epoxy Matrix 116
4.3.4 Thermal Analysis of Epoxy Reinforced with Binary Combinations of Nanofillers 118

4.3.4.1 Effect of Addition of Binary Combinations of Nanofillers on Thermal Degradation of Epoxy Matrix 118
4.3.4.2 Thermo-Mechanical Analysis for Different Combinations of Binary Nanofiller Reinforced Epoxy Composite 121
4.3.5 Summary 125
4.4 Nanodiamonds Assisted Exfoliation of Graphene and its Effect on Toughening Behaviour of Epoxy 126
4.4.1 TEM Analysis to confirm the Nanodiamonds Assisted Exfoliation of Graphene 126
4.4.2 Assessing Exfoliation of Graphene with Addition of Nanodiamond by Surface Topography Imaging 129
4.4.3 Numerical Analysis to Predict the Effect of Exfoliation on Toughening Behaviour of Epoxy 133
4.4.4 Summary 141
4.5 Investigating the Potential of Nanodiamonds in Boosting the Synergistic Effect of Gr-CNT Hybrid Filler in Epoxy 143
4.5.1 Microstructural Characterization to Verify the Synergistic Effect of Nanodiamond Addition on Graphene-Carbon Nanotube Hybrid filler 143
4.5.2 Fracture Surface Analysis of Epoxy Reinforced with Gr-CNT, and Gr-CNT-ND hybrid 148
4.5.3 Mechanical Behaviour of Gr-CNT and Gr-CNT-ND Reinforced Epoxy Composites 151
4.5.3.1 Tensile Studies to Assess the Strengthening Imparted to Epoxy by Gr-CNT and Gr-CNT-ND fillers 151
4.5.3.2 Fracture Toughness to Assess the Toughening Imparted to Epoxy by Gr-CNT and Gr-CNT-ND fillers 155
4.5.4 Thermal Analysis of Gr-CNT Epoxy and Gr-CNT-ND Epoxy Composites 157
4.5.4.1 Effect of Addition of Gr-CNT and Gr-CNT-ND fillers on the Thermal Stability of Epoxy 157

4.5.4.2 Thermomechanical Analysis of Gr-CNT and Gr-CNT-ND Epoxy Composites 160
4.5.5 Summary 163
4.6 Role of 3D Network of Carbon Nanofillers in Improving the Properties of Carbon Fiber Epoxy Laminated Composite 165
4.6.1 Investigating the Wettability and Infiltration of Carbon Fiber by Epoxy and Nanofiller Modified Epoxy 166
4.6.2 Fracture Surface Analysis to Confirm Role Played by 3D Network of Nanofiller in Strengthening and Improving the Interfacial Bonding between CF and Epoxy matrix 167
4.6.3 Investigating Mechanical Properties of Multiscale Composites 172
4.6.3.1 Tensile Test for CF Epoxy and Nanofiller Reinforced Carbon Fiber Epoxy Composite 172
4.6.3.2 Intralaminar Fracture Toughness for CF Epoxy and Nanofiller Reinforced Carbon Fiber Epoxy Composite 175
4.6.4 Assessing the Role of 3D Network of Carbon Nanofillers in Modifying the Interfacial Properties of Multiscale Composite 176
4.6.4.1 Mode - I Interlaminar Fracture Toughness 176
4.6.4.2 Interlaminar Shear Strength 178
4.6.5 Thermal Analysis of Carbon Fiber and Nanofiller Reinforced Carbon Fiber Epoxy Composite 181
4.6.5.1 Effect of Addition of Nanofillers on Thermal Stability of CF Epoxy Composite 181
4.6.5.2 Thermomechanical Analysis of CF Epoxy Composite with and without Nanofillers 183
4.6.6 Summary 185
5 CONCLUSIONS 186
6 RECCOMENDATION FOR FUTURE WORK 188
LIST OF PUBLICATIONS 189
REFERENCES 192

LIST OF FIGURES

Figure 1 Flow chart of the research plan 9

Figure 2.1 (a) Schematic of electrophoretic deposition of CNTs on CF surface, FE-SEM images of **(b)** SWNTs, **(c)** MWNTs on annealed in vacuum and nitric acid treated CF and **(d)** MWNTs on as received CF surface 18

Figure 2.2 Schematic of setup for electrophoretic deposition of GO on CF surface (right), FE-SEM images of **(a)** as-received CF, **(b)** (2 V, 0.02 A) GO-CF, **(c)** (10 V, 0.11 A) GO-CF, **(d)** (30 V, 0.27 A) GO-CF epoxy composite 18

Figure 2.3 Optical images of CF sheets **(a, b)** as-received, after electrophoretic deposition of **(c, d)** oxidized carbon nanofibers (CNF) and **(e, f)** with sizing amidized CNFs 19

Figure 2.4 Schematic showing CNT grafting on CF surface by CVD 21

Figure 2.5 Interleaving vertically aligned CNT forest through transfer-printing process on a pre-preg **(a)** Illustration and **(b)** fully transplanted to the surface of CF epoxy pre-preg sheet; **(c, d)** FE-SEM images at different magnifications showing two sheets aligned CNT interlayer hybrid composite 22

Figure 2.6 Schematic of vacuum assisted resin transfer moulding 27

Figure 2.7 Scanning electron microscopy (FE-SEM) images of the **(i) (a)** CF without sizing **(b)** CF with commercial sizing, **(c)** CF-1 wt% GO sizing, **(d)** CF-5 wt% GO sizing, **(e)** CF-10 wt% GO sizing, **(f)** magnified image of **(e)**; **(ii)** fractured surface of ILSS **(a, a′)** CF with commercial sizing-epoxy **(b, b′)** CF-1 wt% GO sizing-epoxy, **(c, c′)** CF-5 wt% sizing-epoxy; **(d, d′)** CF-10 wt% GO-epoxy composite 30

Figure 2.8 FTIR spectra of GO and functionalised GOs 32

Figure 2.9 FE-SEM images for fracture surface of **(a, b)** CF-epoxy and **(c, d)** CNT-CF epoxy composite 37

Figure 2.10 Schematic illustrating different fiber pull out failure modes for CNT/CF epoxy 37

Figure 2.11 FE-SEM images of **(a)** CF epoxy, **(b)** 0.3 wt% GO-CF epoxy, **(c)** 0.5 wt% DDS-FGO CF epoxy, **(d)** 0.3 wt% EDA-FGO, **(e)** 0.3 wt% PPD-FGO CF epoxy composite in axial direction **(f)** 0.5 wt% GO CF epoxy, **(g)** with 0.5 wt% EDA- 40

FGO CF epoxy, and **(h)** agglomeration of 0.5 wt% DDS-FGO CF epoxy composite in transverse direction to tensile load

Figure 2.12 Schematic of the **(a)** vertically aligned CNTs placed in between two sheets of a laminated composite, **(b)** schematic and **(c)** FE-SEM image showing vertically aligned CNTs bridging the crack between the two sheets 42

Figure 2.13 Mode-I fracture surface for **(a)** CF epoxy, **(b)** GO1-CF epoxy, **(c)** GO2-CF epoxy and **(d)** GO3-CF epoxy composite 44

Figure 2.14 FE-SEM images for fractured surface **(a)** non-coated CFs, **(b)** epoxy coated CFs, and **(c)** Gr coated CFs after **(i)** flexural 90° and **(ii)** flexural 0° 46

Figure 2.15 Images along with corresponding schematic of water droplets lying on **(a)** hydrophilic CF surface and **(b)** hydrophobic CNT-CF surface 47

Figure 2.16 (a) Shows FEA models of DCB specimen, load vs COD plots for numerical and experimental analysis of **(b)** plain CF epoxy sample and **(c)** GO-CF epoxy sample 48

Figure 3 FE-SEM images of as received **(a)** CNT, **(b)** Gr and **(c)** ND 54

Figure 4.1 FE-SEM and TEM images of **(a, d)** CNTs, **(b, e)** Gr and **(c, f)** NDs 66

Figure 4.2 FE-SEM images for fractured surface of **(a-c)** epoxy, **(d-f)** CNT-epoxy composite, **(g-i)** Gr-epoxy composite and **(j-l)** ND-epoxy composite 68

Figure 4.3 Representative load vs. displacement and elastic modulus-hardness plots for different composition of **(a, b)** CNT-epoxy, **(c, d)** Gr-epoxy and **(e, f)** ND-epoxy composites 71

Figure 4.4 Stress-Strain curve for various composition of **(a)** CNT-epoxy, **(b)** Gr-epoxy and **(c)** ND-epoxy composite 73

Figure 4.5 Fracture toughness variation as a function of reinforcement content 77

Figure 4.6 (i) Schematic representation and **(ii)** FE-SEM images showing dominant fracture mechanism in **(a)** epoxy, **(b)** Gr-epoxy, **(c)** CNT-Epoxy and **(d)** ND-Epoxy composite 78

Figure 4.7 TGA thermogram for epoxy and various compositions of **(a)** CNT- epoxy, **(b)** Gr-epoxy and **(c)** ND-epoxy composite 82

Figure 4.8 Typical storage modulus and plots tanδ for various composition of **(a, b)** CNT-epoxy, **(c, d)** Gr-epoxy and **(e, f)** ND-epoxy composite as a function of temperature 85

Figure 4.9 (i) TEM image of the uniformly dispersed NDs embedded in the epoxy matrix and **(ii)(a)** HRTEM image of the ND-epoxy composite, **(b)** IFFT simulated image for the selected section and **(c)** Profile of IFFT simulated image. 90

Figure. 4.10 Schematic of tensile sample used for modulus mapping 92

Figure 4.11 Storage modulus maps for epoxy and ND-epoxy before tensile stress is applied 92

Figure 4.12 Storage modulus maps for **(a)** epoxy before tensile and the ND-epoxy composite **(b)** before tensile and **(c)** after tensile test 95

Figure 4.13 Storage modulus maps arranged in 3D for **(a)** epoxy before tensile and for the ND-epoxy composite **(b)** before tensile and **(c)** after tensile 96

Figure 4.14 Storage modulus map for ND-epoxy composite having severe agglomeration 97

Figure 4.15 Storage modulus maps for **(a)** epoxy and **(b)** ND-epoxy composite at ~1-2 mm away from the fractured surface tip 97

Figure 4.16 (a) Schematic representation of the homogenization approach for the periodic microstructure, **(b)** meshed RVE containing randomly distributed circular particles in the continuous matrix, **(c)** RVE subjected to the uniaxial tensile strain, **(d & e)** reaction force and strain energy curve obtained under the specific loading and boundary conditions, **(f)** convergence study for modulus evaluation against number of elements, **(g)** comparative variation of the effective elastic modulus with weight fraction of the ND obtained from the numerical and experimental analysis and **(g)** the von Mises stress distribution for the RVE. 101

Figure 4.17 von Mises stress distribution for **(a)** 0.1 wt% ND-epoxy, **(b)** 0.2 wt% ND-epoxy, **(c)** 0.3 wt% ND-epoxy and **(d)** 0.5 wt% ND-epoxy composites 104

Figure 4.18 TEM and FE-SEM images for **(i) (a, b)** CNT, **(i) (c, d)** CNT-ND, **(ii) (a, b)** Gr and **(ii) (c, d)** Gr-ND 108

Figure 4.19 FE-SEM images for fractured surface of **(a)** 0.5 wt% CNT, **(b)** 0.5 wt% Gr, (c) 0.5 wt% ND, **(d)** 0.5 wt % (75Gr:25ND), **(f)** 0.5 wt% (50Gr:50ND), **(g)** 0.5 wt 111

% (25Gr:75ND), **(h)** 0.6 wt% (75 CNT:25ND), **(i)** 0.6 wt% (50CNT:50ND) and **(j)** 0.6 wt% (25CNT:75ND) epoxy composite

Figure 4.20 Representative stress-strain plots for various combinations of Gr-ND epoxy with **(a)** 0.3 wt% & **(b)** 0.5 wt% reinforcement 113

Figure 4.21 Fracture toughness plot for various combinations of **(a)** CNT-ND epoxy composite and **(b)** Gr- ND epoxy composite 117

Figure 4.22 TGA thermogram for various combinations of **(a, b)** CNT-ND epoxy composite and **(c, d)** Gr- ND epoxy composite 119

Figure 4.23 Storage modulus for various combinations of **(a)** 0.3 wt% CNT-ND epoxy, **(b)** 0.6 wt% CNT-ND epoxy, (c) 0.3 wt% Gr-ND epoxy and **(d)** 0.5wt% Gr-ND epoxy composite as function of temperature 122

Figure 4.24 tanδ for various combinations of **(a)** 0.3 wt% CNT-ND epoxy, **(b)** 0.6 wt% CNT-ND epoxy, (c) 0.3 wt% Gr-ND epoxy and **(d)** 0.5 wt% Gr-ND epoxy composite as function of temperature 123

Figure 4.25 TEM images at different magnifications for **(a, f)** 0.5 wt% (100Gr:0ND), **(b, g)** 0.5 wt% (75Gr:25ND) unsonicated, **(c, h)** 0.5 wt% (75Gr:25ND) sonicated **(d, i)** 0.5 wt% (50Gr:50ND) and **(e, j)** 0.5 wt% (25Gr:75ND) 127

Figure 4.26 Surface morphology, 3D profiling and line scan with showing variation of thickness for **(a)** NDs, **(b)** Gr, **(c)** 75Gr:25ND unsonicated, **(d)** 75Gr:25ND sonicated, **(e)** 50Gr:50ND unsonicated and **(f)** 25Gr:75ND sonicated, processed through SPIP^{TM} software 131

Figure 4.27 Surface morphology and line scan with surface thickness at three different locations **(a)** NDs, **(b)** Gr, **(c)** 75Gr:25ND unsonicated, **(d)** 75Gr:25ND sonicated, **(e)** 50Gr:50ND unsonicated and **(f)** 25Gr:75ND sonicated, processed through SPIP^{TM} software 132

Figure 4.28 (a) Schematic representation of the SENB specimen, **(b)** meshed SENB specimen and **(c)** RVE subjected to the uniaxial tensile strain 136

Figure 4.29 Comparison of load vs displacement plot obtained from numerical analysis of SENB analysis through Hashin-Shtrikman bounds and experimentally for **(a)** epoxy, **(b)** 0.5 wt% (100Gr:0ND) epoxy, **(c)** 0.5 wt% (75Gr:25ND) epoxy, **(d)** 0.5 wt% (50Gr:50ND) epoxy and **(e)** 0.5 wt% (25Gr:75ND) epoxy composite 137

Figure 4.30 SENB specimen containing different volume fraction of Gr, distributed in the continuous epoxy matrix for **(a)** Gr and **(b)** 75Gr:25ND 139

Figure 4.31 von-Mises stress distribution for **(a)** epoxy, **(b)** 0.5 wt% (100Gr:0ND) epoxy, **(c)** 0.5 wt% (75Gr:25ND) epoxy, **(d)** 0.5 wt% (50Gr:50ND) epoxy and **(e)** 0.5 wt% (25Gr:75ND) epoxy composite 140

Figure 4.32 TEM images of **(a)** Gr, **(b)** Gr-CNT, **(c)** Gr-ND, **(d)** CNT-ND, **(e)** Gr-CNT-ND (exfoliated) and **(f)** Gr-CNT-ND agglomerated 145

Figure 4.33 FE-SEM images of **(a)** Gr, **(b)** Gr-CNT, **(c)** Gr-ND, **(d)** CNT-ND, **(e)** Gr-CNT-ND (exfoliated) and **(f)** Gr-CNT-ND agglomerated 147

Figure 4.34 FE-SEM images for fractured surface of **(a)** 0.3 wt% Gr, **(b)** 0.3 wt% CNT, **(c)** 0.3 wt% ND, **(d)** 0.5 wt% Gr, **(e)** 0.5 wt% CNT, **(f)** 0.5 wt% ND, **(g)** 0.5 wt % (75Gr:25CNT), **(h)** 0.5 wt% (50Gr:50CNT), **(i)** 0.5 wt % (25Gr:75CNT), **(j)** 0.8 wt% (50Gr:25CNT:25ND), **(k)** 0.8 wt% (25Gr:50CNT:25ND), **(l)** 0.8 wt% (25Gr:25CNT:50ND) and **(m)** 0.8 wt% (33Gr:33CNT:33ND) epoxy composite 149

Figure 4.35 Representative stress-strain plots for various combinations of **(a)** 0.3 wt% Gr-CNT, **(b)** 0.5 wt% Gr-CNT, **(c)** 0.5 wt% Gr-CNT-ND and **(d)** 0.8 wt% Gr-CNT-ND epoxy composite 152

Figure 4.36 Fracture toughness plots for various compositions and combinations of **(a)** Gr-CNT and **(b)** Gr-CNT-ND epoxy composite 156

Figure 4.37 TGA thermogram for various combinations of **(a, b)** Gr-CNT epoxy composite and **(c, d)** Gr- CNT-ND epoxy composite 159

Figure 4.38 Storage modulus for various combinations of **(a)** 0.3 wt% Gr-CNT epoxy, **(b)** 0.5 wt% Gr-CNT epoxy, **(c)** 0.5 wt% Gr-CNT-ND epoxy and **(d)** 0.8 wt% Gr-CNT-ND epoxy composite as function of temperature 161

Figure 4.39 tanδ for various combinations of **(a)** 0.3 wt% Gr-CNT epoxy, **(b)** 0.5 wt% Gr-CNT epoxy, **(c)** 0.5 wt% Gr-CNT-ND epoxy and **(d)** 0.8 wt% Gr-CNT-ND epoxy composite as function of temperature 162

Figure 4.40 Images showing wetability and infiltration of epoxy on CF without and with addition of nanofillers as a function of time 166

Figure 4.41 FE-SEM images of the fractured surface cross-sections both along and transverse to the direction of applied load for **(a(1-5))** CF-Epoxy, **(b(1-5))** 225 GCN 169

CF-Epoxy, **(c(1-5))** 252 GCN CF-Epoxy and **(d(1-5))** 333 GCN CF-Epoxy composites at different magnifications

Figure 4.42 FE-SEM images at different magnifications for delaminated **(a-c)** CF-epoxy, **(d-f)** 25Gr:25CNT:75ND CF-epoxy, **(g-i)** 25Gr:50CNT:25ND CF-epoxy and **(j-l)** 33Gr:33CNT:33ND CF-epoxy composites 171

Figure 4.43 Stress-Strain plots for various combination of Gr:CNT:ND CF-epoxy composite 172

Figure 4.44 Fracture toughness plots for various combination of Gr:CNT:ND CF-epoxy composite 175

Figure 4.45 (a) Representative load vs displacement curves obtained from modified beam theory (MBT) method **(b)** variation of ILFT as a function of crack length for different combination of Gr:CNT:ND CF-epoxy composite 177

Figure 4.46 (a) Representative load vs displacement curves obtained from short beam shear test **(b)** ILSS plots for CF-epoxy and various combination of Gr:CNT:ND CF-epoxy composite and **(c)** digital images of failed samples 179

Figure 4.47 TGA thermogram for epoxy, CF epoxy composite and CF nanofiller modified epoxy composite 182

Figure 4.48 Typical DMA results (a) Storage modulus and (b) tanδ curve for various composition of Gr:CNT:ND CF epoxy composite as a function of temperature 184

LIST OF TABLES

Table 1. Presents the various routes adapted for nanofiller modification and fabrication of CF epoxy composite and their effect on different properties 49

Table 2. % improvement in properties of epoxy with CNT, Gr and ND reinforcement 87

Table 3. Load, strain energy and elastic modulus of the ND-Epoxy composites obtained from numerical analysis 103

`**Table 4.** Ultimate tensile strength, % strain, % improvement in fracture toughness for epoxy and various composition and combination of Gr-ND epoxy composite 114

Table 5. Shows the value for thickness and change in thicknee for different combinations of Gr:ND 131

Table 6. Ultimate tensile strength, % strain, % improvement in fracture toughness for various composition and combination of Gr-CNT and Gr-CNT-ND epoxy composites 153

Table 7. Elastic modulus, ultimate tensile strength and % strain, for various composition and combination of Gr:CNT:ND CF-epoxy composites 174

CHAPTER 1

INTRODUCTION

Fiber reinforced polymer composites (FRPs) are widely used polymer matrix composites (PMCs) in applications, such as, aerospace, automobiles, lightweight structures and many more. The major advantage of using FRPs is their high strength to weight ratio, corrosion and fatigue resistance, which is much better as compared to the conventional metallic counterparts. Carbon fibers (CFs) are the most widely used class of fibers for structural application, due to their high specific strength, stiffness, high fatigue resistance, low coefficient of thermal expansion etc. However, the macro-sized fibers, with their specific orientation, often result into anisotropic properties in the composites structures. The fiber orientation in structural composite structures is usually in x- direction and y-direction, leading to fiber dominated material properties in these directions, whereas the z-direction remains matrix dominated. The conditions that leads to delamination can vary from out-of-plane tensile loads to in-plane compressive loads, with crack initiating at structural discontinuities such as edges, notches, voids or impurities/foreign particles [1].

Thermoset resins are the most widely used class of polymers for fabricating fiber-reinforced structures for structural applications. They are generally stiffer, stronger and cost-effective as compared to their thermoplastic counterparts [1]. Epoxies are one of the most preferred thermoset resin for matrix material of PMCs for structural application. Low density, higher stiffness, good adhesion to most reinforcements, high thermal stability, low shrinkage, low moisture absorption and ease of processing makes them the most suitable choice. However, the biggest drawback is their brittle nature.

Carbon fiber epoxy composites have a wide variety of structural applications [2-4]. The properties essential for such applications include high strength, toughness, shear strength both along axial and transverse direction of fibers. There are different factors that decide the performance of composites, which include the mechanical properties of the matrix, individual CFs, as well as, sheets, fiber-matrix interface, and processing conditions [5]. Since the load in the composites is transferred from the matrix to the fiber through the shear stress, the control of the fiber-matrix interface is crucial in ensuring good interfacial shear strength (IFSS), interlaminar shear strength (ILSS) and interlaminar fracture toughness (ILFT). For a composite to perform well, the interfacial bonding between the CF and polymer should be higher than the cohesive bonding of the matrix [6, 7]. Interface is the one that controls the improvement in properties of the composite structure. Thus, properties are often inferior due to the inherently poor interfacial bonding between CF and epoxy. This is a major drawback of CF epoxy composite that has been there for years.

Over the years, a lot of research has been done to overcome this drawback. The conventional methods to improve interfacial bonding of CF and epoxy include modifying or treating CF surface. Sizing (application of polymer to CF surface), acid modification, electrochemical modifications, plasma surface, high energy irradiation, thermal modification, ozone treatments, etc. [8-10] are the most commonly used techniques for fiber surface treatment. However, the discovery of nanofillers has attracted the interest of researchers in the field to use submicron to nanometer level reinforcement phases. The advantage of nano-scaled filler, over micro-scaled fillers, is their very high surface area, which can act as an interface for stress-transfer. Widespread availability and excellent properties make carbon nanofillers the most preferred choice for this purpose [11-13]. The addition of carbon nanofillers into CF- epoxy composite have been reported to offer promising results in improving the properties, like interlaminar fracture toughness (ILFT) [14, 15], interlaminar

shear strength (ILSS) [8, 14-19], tensile strength [20, 21], fatigue life [22] etc. [8, 9, 15, 18-21, 23, 24].

There are two different approach for incorporating nanofillers in the CF-epoxy system, namely, growing/grafting/depositing/coating or nano-engineering CF surface and then using it as a reinforcement to the composite system. Nano-engineering the surface of the CF reinforcement is one of the most common approach. There are different techniques used to achieve nano-engineered CF surface, e.g., carbon vapour deposition (CVD) [25], electrophoretic deposition [19, 26, 27], chemical grafting [28-32], dip coating [18], graphitic structure by design (GSD) [22, 33] etc. However, biggest limitation of these approaches that involve modifying fiber surface is degradation in fiber properties due to fiber damage. Apart from that, difficulty in scaling up the process and too many parameters to control, limits the practical application of these techniques for structural application.

The other approach, is to add or disperse the carbon nanofillers throughout the matrix of bulk composite. However, the mechanical behaviour of such nano-phase reinforced composites greatly depend on the quality of distribution. As, it dictates the interaction of reinforcement phase with matrix and the homogeneity of the cumulative response towards mechanical loading. The high tendency of agglomeration, in nano-size entities, make the task of dispersion even more challenging and limits their efficiency as a reinforcement. Different techniques and dispersing mediums have been adopted to improve dispersion, namely, functionalization of nanofillers, use of gamma radiations to activate nanofillers, etc. Damage to nanofillers shape and size, residue chemicals restricted the efficiency of the above mentioned techniques. However, a new approach that utilizes the synergistic effect of addition of Gr and CNT together on dispersion [34-38]. This approach is quite simple and clean. However, there are only few studies reported so far and these are also very

limited in approach, especially with binary combinations i.e. carbon nanotube (CNT) and graphene (Gr) or its derivatives. None of the studies are done systematically, by first optimizing the nanofillers content with single filler, followed by studying binary filler for different ratios. Further, the entanglement of CNTs, due to fiber like morphology, is seen to limit its contribution in dispersing Gr. Addition of another nanoparticle that can improve the synergy between Gr and CNT can overcome this limitation.

Nanodiamond (ND) is the most suitable candidate to improve the synergy between Gr-CNT hybrids. Small size, similar surface chemistry and mechanical properties as Gr/CNT and the particle like morphology that has a less tendency to show severe agglomeration. The spherical shape is less favourable for a reinforcement phase especially for the applications that require high tensile strength and fracture toughness. So, before investigating its potential in improving the synergy of Gr-CNT its efficiency as a reinforcement to epoxy needs to be investigated. Also, the synergy of ND with CNT and Gr in binary combinations needs to be assessed.

Therefore, the aim of the research, carried out and reported in this thesis, is to investigate and reveal the potential of synergistic effect of carbon nanofillers with different morphology, namely, CNT (1D), Gr (2D) and ND (3D) on CF epoxy composite for structural application, in terms of mechanical, interfacial and thermal properties. This overall objective can be achieved through following specific objective:

- *Modifying epoxy matrix and evaluating its mechanical and thermal properties as a function of*
  - *Different morphologies of nanofillers*
  - *Different combinations of nanofillers i.e. binary and ternary combinations*
- *Evaluating the distribution of nanophase reinforcement in polymer matrix through FE-SEM, TEM and their behaviour during loading through nanoDMA and numerical analysis*

- *Revealing the synergy between different nanofillers for various combinations through high resolution electron microscopy and SPM*
- *Establishing a suitable fabrication route for hybrid multiscale carbon fiber reinforced composite with modified nanofiller reinforced epoxy matrix*
- *Comparative evaluation of multiscale carbon fiber reinforced composite with modified nanofiller reinforced epoxy matrix with that of only carbon reinforced composite in terms of mechanical and thermal properties*

The plan of research work is illustrated in the flow chart shown in figure 1. The dissertation has been arranged in different chapters, sections and subsections to present a clear picture about the background and the state of the art; the methods adopted in this study; the analysis of the outcomes with scientific interpretation and the future scope of research and improvement.

Chapter 1 contains a brief introduction on FRPs, carbon nanofillers, CF and epoxy. It also includes current research and developments on carbon fiber reinforced epoxy composites and objectives of the present study.

Chapter 2 provides a comprehensive literature review on this topic. It also highlights the research areas that have not been paid much attention yet and the scope of present work based on literature.

Chapter 3 presents the detailed account of the methodology adopted in this research.

Chapter 4 provides explanation of results and scientific analysis of outcomes in context with objectives of this research.

Chapter 4.1 investigates and compares the potential of ND as reinforcement to epoxy matrix with CNT and Gr for a range of nanofiller content (0.1 - 1wt. %). Composites, containing different amount of nanofillers, are synthesized using ultrasonic cavitation (probe sonicator), a strong tool for effective dispersion of nanofillers in matrix. Mechanical (tensile and fracture) properties are studied

thoroughly. The mechanical properties are analysed in terms of Young's modulus, ultimate tensile strength, % strain (at break), and fracture toughness. Thorough microstructural studies are performed to evaluate dispersion, strengthening, and toughening mechanisms operating. Dynamic mechanical analysis (DMA) is used to study the effect of temperature on mechanical properties, like, storage modulus, glass transition temperature and damping capacity of the composites as a function of different reinforcement types and content. Thermogravimetric analysis (TGA) was done to study the thermal stability of epoxy with different reinforcement type and content. The results obtained from all the tests are thoroughly analysed to comprehend the individual effect of each of these nanofillers, on the performance of the composites during service in structural applications.

Chapter 4.2 has taken an initiative to understand the distribution of nanophase reinforcement in polymer matrix and their behaviour during loading, using 2D modulus mapping. The composite system, being studied here, is a nanodiamond reinforced epoxy matrix. Modulus mapping gives an idea of distribution of nanodiamond in matrix, in terms of spatial distribution of micron level higher modulus regions in the composite structure. The modulus mapping studies have been carried out on composites with and without application of uniaxial tensile stresses. The analysis of the maps has been carried out to reveal the role of nanodiamond on the mechanical behaviour of the epoxy matrix and the evolution of distribution of the former with application of stress. The stiffening effect of nanodiamond dispersed in epoxy matrix was evaluated through FEM of representative volume element (RVE). The predicted results were then compared with the experimental results obtained from the nanoindentation.

Chapter 4.3 reveals the synergistic effect of addition of ND on CNT and Gr in binary combinations of nanofillers, using very simple, easily adoptable and scalable technique, i.e. ultrasonication. The extent of exfoliation, with binary combinations of fillers, as compared to unary fillers, was verified

through FE-SEM and TEM. The capacity of synergistically exfoliated binary fillers, as a potential reinforcement to epoxy matrix, is then explored in terms of mechanical properties. Tensile test and fracture toughness test were performed for composites to evaluate their mechanical performance. The fractured surfaces of the tensile samples were investigated through FE-SEM to give insight of dispersion, interfacial interaction of fillers with matrix and active strengthening mechanism.

Chapter 4.4 explores nanodiamonds assisted exfoliation of graphene and its effect on toughening behaviour of epoxy. High quality exfoliated Gr sheets, decorated with ND particles is obtained, which is confirmed through FE-SEM, TEM and SPM. High resolution electron microscopy gave a qualitative confirmation of the role played by the ND in hindering restacking of graphene by restricting the π–π stabilization. While SPM, quantitatively confirmed the same by giving thickness distribution both before and after exfoliation in the presence of ND. The toughening effect of ND assisted exfoliated Gr dispersed in epoxy matrix, evaluated through experiment is also in concurrence with results predicted using finite element method (FEM).

Chapter 4.5 investigates potential of ND in improving synergistic effect of Gr-CNT hybrid and there after its potential as a reinforcement to epoxy matrix is explored. In depth TEM and FE-SEM analysis of fillers at different stages of exfoliation, with different combinations of nanofillers are investigated. Once the desired exfoliation was achieved, the composite was fabricated and tested for mechanical properties. The fractured surfaces of the tensile samples were then assessed through FE-SEM to get insight of dispersion, interfacial interaction of fillers with matrix and thus validating the differential mechanical properties across compositions.

Chapter 4.6 aims to investigate the effect of addition of this well exfoliated close knitted 3D network of Gr-CNT-ND into the epoxy matrix of a conventional carbon fiber-reinforced composites. Thorough evaluation of mechanical properties, which include tensile test, interlaminar shear

strength, interlaminar and intralaminar mode I fracture toughness, were conducted to investigate the effect of addition of 3D network of Gr-CNT-ND on interfacial properties of CF-epoxy composite. In depth fracture surface analysis, through FE-SEM, was carried out to get an insight into the active strengthening and toughening mechanism in the interface as well as matrix regions of the laminated composites structure.

Chapter 5 presents overview of the main outcomes with the key points of the research

Chapter 6 presents future scope of research

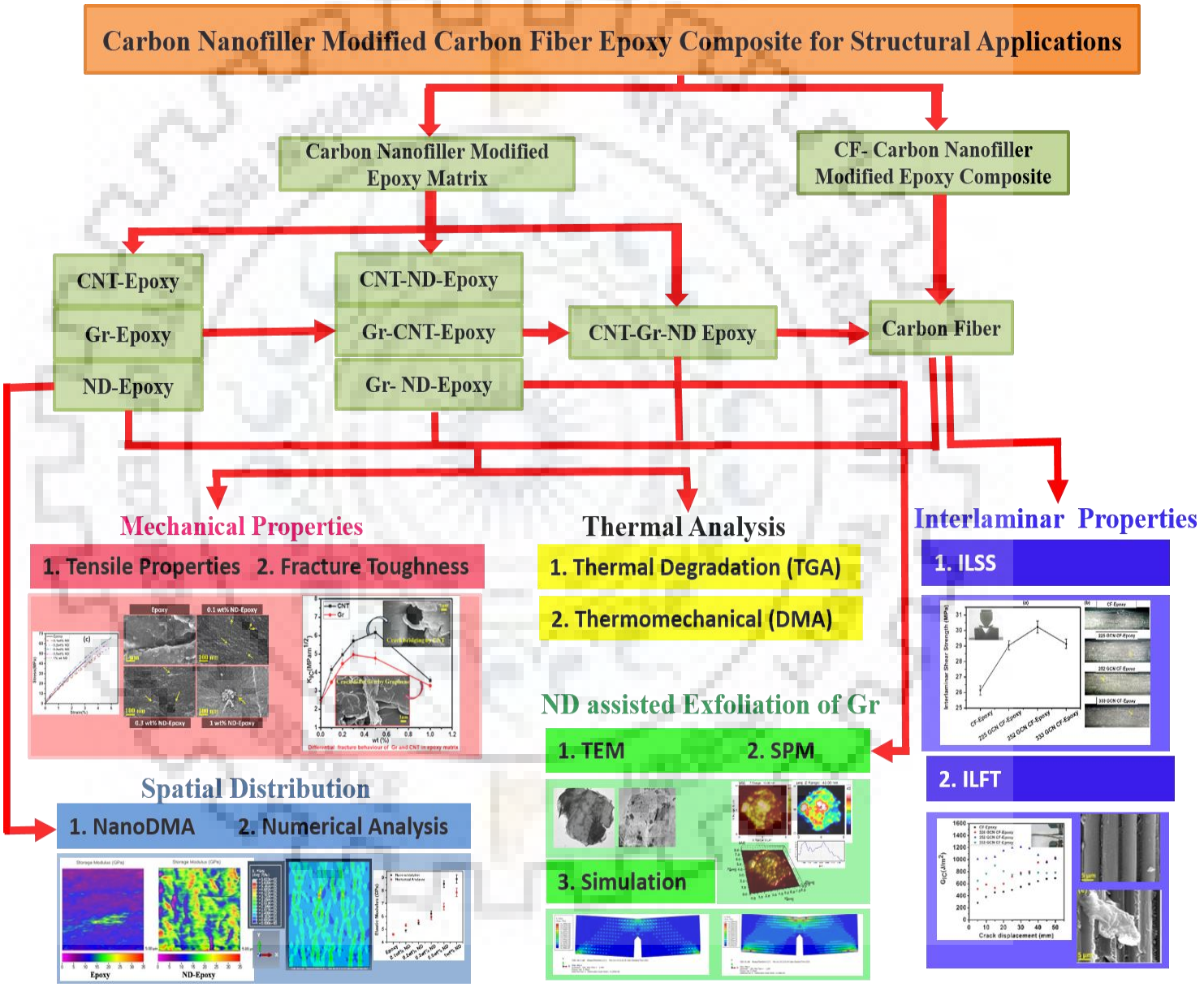

Figure 1 Flow chart of the research plan

CHAPTER 2

LITERATURE REVIEW

This chapter gives a comprehensive summary of the available literature on carbon nanofiller modified carbon fiber epoxy composites, for structural applications. It starts with a brief introduction to the most commonly used carbon nanoparticles as a filler to polymer matrix, followed by the techniques used for successfully integrating carbon nanofillers to the CF epoxy composite. A detailed description of the effects of the carbon nanoparticles on interfacial bonding and mechanical response of different carbon nanofiller CF-epoxy system is also covered. In-depth review and analysis of the past and on-going research in the field helped in finding the areas that need attention and led to the planning of this study.

2.1 Introduction to Fiber Reinforced Polymer Composites

Composites are being used as an increasingly attractive alternative to the conventional counterparts [39]. The requirement of light weight in structural applications have created the demand of polymer matrix composites (PMCs). Outstanding mechanical properties, corrosion resistance, improved fatigue life along with light weight are some of the properties, which have increased the use of fiber reinforced polymer composites (FRPs), over their conventional counterparts, in automobile, marine, aeronautical, defense, sports and construction industries. Carbon fiber is one of the strongest and extensively used fiber available for reinforcing polymer matrix for structural applications. High strength and stiffness, coupled with low density, high chemical resistance, low coefficient of thermal expansion, better fire resistance etc. makes it superior to other commercially available options [35]. However, the major limitation of CF is its non-polar surface, chemical

inertness, surface lipophobicity, smoothness and less adsorption, which lead to weaker bond with the matrix material [6, 41, 42].

Thermoset resins are the most widely used class of polymers for fabricating FRPs especially for structural applications, as they are stiffer, stronger and cost effective than most thermoplastics. Epoxy is one of the most preferred thermoset resins, used in matrix material of polymer matrix composites (PMCs) for structural application. Low density, higher stiffness, good adhesion to most reinforcements, high thermal stability, low shrinkage, low moisture absorption and ease of processing makes them the major choice. However, the biggest drawback is their brittle nature, which makes FRPs more prone to interfacial or interlaminar failure.

Over the past few decades, with the improvement in technology, the design limit of optimizing composites with conventional micrometer scale fiber reinforcement and resin matrix is realized. The limitations, encountered, are macroscopic defects appearing because of the uneven dispersion of fibers in the matrix, presence of matrix-rich regions formed in the gaps between the fiber in a woven fabric and specific orientation of fibers, which often result into anisotropic properties in the composites structure. These defects often are the major causes of material failure. Crack originates at reinforcement-matrix interface, and at structural discontinuities such as edges, notches, voids or impurities/foreign particles, reinforcement free regions and gradually moves forward. Such regions are difficult to reinforce with microscale reinforcement. Therefore, it is very difficult to develop composites, consisting of conventional fiber and resin system, to serve to a wide variety of applications.

Addition of nanofillers to the matrix can improve the interfacial properties of CF-epoxy composites, due to their high surface area, which can act as interface for stress-transfer, as well as, improve the toughness of the polymer matrix. Due to the higher mechanical properties, offered by

materials in their nanoscale forms as compared to their macroscale forms, various nanoscale materials have been explored for selective reinforcement of matrix-rich regions [43-47]. However, with the discovery of carbon based nanofillers in the recent past, a new approach for fabrication of conventional FRP composites is in use, which involves incorporation of carbon nanoparticles. Based on their shapes, the most commonly used carbon nanofillers are categorized in three different groups, namely, one-dimensional or cylindrical fillers, two-dimensional or sheet particles and three dimensional or spherical fillers. The examples for each of these three categories are carbon nanotubes (CNTs), graphene (Gr) and nanodiamonds (NDs), respectively.

2.2 Commonly used Carbon Nanofillers as a Reinforcement to Polymer Matrix

For last two decades, the potential of CNTs as nanofillers has been examined for wide variety of matrices and for various applications [48-59]. High aspect ratios and exceptional physical properties of carbon nanotubes (CNTs) make them a potential candidate for improving the properties of polymer composites [11, 12, 49]. The introduction of CNTs in the matrix of continuous macro-fiber reinforced composites gives a chance for combining merits of nanoscale reinforcement with that of fiber reinforced composites, in the hybrid multiscale composites structure [60, 61]. Increased production and economic feasibility of CNTs [62] with time has increased the probability of developing a new generation material having optimum mechanical, thermal as well as electrical properties, which represent a good agreement between performance and cost for most applications.

CNTs, because of their high aspect ratio, great flexibility, outstanding strength and elasticity, show a remarkable improvement in mechanical and physical properties of FRPs, while maintaining low density and ease of fabrication [63]. But the extent, to which the properties could be improved by the use of CNTs, has been restricted due to non-uniform distribution of CNTs in the composite.

The reinforcement efficiency depends upon the alignment, content, aspect ratio, extent of dispersion, morphology and waviness of CNTs. Therefore, the efficient transfer of excellent properties of CNTs into the final hybrid multiscale composites is still a challenging task. Few research groups have evaluated the potential of the composite by hybridization of the reinforcement. The mechanical properties, like, shear strength, fracture toughness, elastic properties and other important properties of the final multiscale composites showed a remarkable improvement [29,30, 64-67]. Thus, they have high scope of applications in further reduction of mass and enhancement of electrical and thermal conductivity [64].

Graphene is an atomically thick, two-dimensional (2D) sheet composed of sp^2 carbon atoms, which are arranged in a honeycomb structure. The first reported method for production of graphene nanosheets can be recorded back to 1970s [68]. But, the successful segregation of free single layer graphene was reported in 2004, using micromechanical cleavage [69]. With ultimate strength of 130 GPa and elastic modulus of 1 TPa, single-layer graphene is the strongest material ever measured [70]. It registered a thermal conductivity of 5000 W/(m^3K), which is so far the highest values reported for SWCNT [71]. High electrical conductivity, up to 6000 S/cm [72] and very high surface area signifies graphene's great ability to improve mechanical, electrical, thermal properties of polymer. Such excellent properties and the low cost of graphene, as compared all other carbon based nanomaterials, have made it a great choice for researchers in various applications [73-76]. A simple search with graphene polymer composite as a keyword, using only one common database from 'scopus' since 2005, produced a list of ~12989 publications, out of which ~8407 are from material science background. If we further refine our search by using the keyword graphene/epoxy composites, ~1795 papers are listed down.

The above data gives a clear picture that graphene has been a great area of interest for researchers from all backgrounds over the past few decades. Its use for composites due to extremely good properties has attracted interest for using it as one of the reinforcement in polymer based composite [77, 78]. Graphene has very high surface area, which makes it a perfect option for being used as filler in conventional fiber reinforced polymer composite [79]. But, the major problem that arises during the fabrication is the improper dispersion of graphene, which adversely affects the interfacial interactions between polymer-graphene and the final properties of the composite structure.

Among all carbonaceous nanomaterials, graphene and carbon nanotubes are most widely reinforced to epoxy matrix [80-102].

Nanodiamond (ND) is a spherical shape carbon-based nanoparticle, having sp^3 hybridization, with an average diameter of 4−6 nm, very large specific surface area of ~250-450 m^2/g, high strength, stiffness and light weight [103-106]. The spherical shape of NDs (a geometrical feature offering an entanglement-free nanoparticle) practically offers maximum interfacial area, as compared to platelets and rod like nanoparticle, owing to the agglomerating tendency of these two latter ones. Rich surface chemistry, along with high mechanical properties and thermal conductivity, makes ND a desirable candidate in numerous applications, such as, composite [107-111], biomedical [112-115], electrochemical [116] etc. [117].

As far as structural applications are concerned, in recent past, there has been a significant number of studies focused on incorporation of ND into thermoplastic and thermoset polymers [109]. The studies, specific to epoxy matrix [105, 106, 118-130], have used ND as reinforcement, both at filler content as low as 0.05 wt% [123] and as high as 47 wt% [119], with and without functionalization [105, 118-126, 129, 130]. The composites have been evaluated for mechanical

[118, 119, 121-124, 126, 127, 130], tribological [105, 106, 126] and thermomechanical [125, 129] behaviour.

While few of the above mentioned studies claimed agglomeration above 0.1 wt% ND loading, some reports claimed up to 30 wt% ND addition, using functionalisation. Uniformly distributed ND, having strong interfacial interaction with epoxy, leads to better load sharing and provides high resistance to the matrix against deformation. Thus, as seen from the literature, as far as tensile and fracture behaviour are concerned, not more than 1 wt% ND loading is found suitable, even after functionalization. However, as compared to CNTs or any other carbon based nanomaterial, there is limited research conducted on polymeric composite materials containing nanodiamonds.

Carbon based nanofillers can be a solution for imparting isotropic properties in polymer based composites. But, the extent to which the properties could be improved by the use of carbon based nanofillers, has been restricted due to difficulty in dispersion of these entities in the matrix [6-8]. Therefore, the efficient transfer of excellent properties of carbon nanofillers into composites is still a challenging task. Various dispersion methods, agents, as well as, surface functionalization techniques have been used to overcome these issues. However, only partial success has been received so far.

Recently, few studies have come up with a new approach to combine 2D Gr sheets with 1D CNTs [34-38]. CNTs are suitable for this purpose due to their long fibrous structure and high flexibity, which help in bridging the adjacent Gr [11, 48, 131-133]. The CNTs along with Gr form 3D structure, which inhibits face to face stacking of Gr, thus increasing the surface area between reinforcement and matrix. Various techniques, ranging from sonication [34], three roll mill [35], mechanical stirring [38] to growing CNTs on Gr surface through CVD [37], were applied for

achieving highly exfoliated entanglement free 3D structure. However, the high aspect ratio, torturous tube like morphology and the strong van der Waals forces between CNTs tend to entangle them, which restricts their effect in exfoliating Gr and as a reinforcement. On the other hand, once the CNTs are grown on Gr surface by CVD, Gr cannot be exfoliated further. As a result, none of the above mentioned methods could provide a significant improvement in properties.

2.3 Different Approaches to Integrate Carbon Nanofillers in a Multiscale Composite

There are two different approach for incorporating nanofillers in the CF-polymer (epoxy) system i.e. growing/grafting/depositing/coating or nano-engineering CF surface and then using it as a reinforcement to a polymer matrix. While, the other is to add or disperse them in the polymer which is used either as a matrix of bulk composite or the sizing material.

2.3.1 Nano-engineering the Carbon Fiber Surface

Nano-engineering the surface of the CF reinforcement is one of the most common approach. Interlaminar and interfacial strength is possibly the weakest link for FRPs, with nanofillers oriented perpendicular to the interface significant improvement may be sought. There are different techniques used to achieve nano-engineered CF surface, however the efficiency of each technique is governed by various parameters which is discussed in detail in the sections below.

2.3.1.1 Electrophoretic Deposition

Electrophoresis is an efficient technique for the deposition of CNTs, Gr and its derivatives i.e. graphene oxide (GO) or reduced graphene oxide (RGO) on CFs surface [19, 26, 27, 134-137]. It is quite simple and versatile technique that can be easily up-scaled, automated and used for industrial applications. This technique utilizes the ability of carbon nanofillers to respond to an electric field

to deposit them on the surface of carbon fibers. As seen from figure 2.1, on applying a dc potential between the CF and the counter electrodes, CNTs are uniformly deposited on the surface of CF from aqueous CNT dispersions. The negative charge, present on carbon nanotubes surface, is attributed to the functional groups, like, carboxylic acid [26], introduced on the CNT surface as a result of pre-treatment and/or adsorption from the dispersing medium [26]. The negative charge helps CNTs in migrating towards the positive carbon fiber electrode and get deposited on the fiber surface (figure 2.1). This behaviour of CNTs has been widely used for other purposes, like, separating conducting and FE-SEM conducting CNTs [134], purification [135] etc. [136]. Giving ultrasonic assistance to electrolyte, through bath sonicator, during electrophoretic deposition is seen to improve the amount and uniformity of nanofiller deposition on CF surface, as it prevents the trapped gas pockets from impeding the deposition [27, 137]. Using this process, the deposition can be achieved both with and without the removal of fiber sizing. Electrophoretic deposition process permits deposition of uniform films of CNTs on fiber panels, having complex shapes and rough surfaces. Some studies have even suggested the electrophoretic deposition of nanofiller on the fiber surface in-situ, to make them more efficient [138], as shown in figure 2.2. Post fiber processing electrophoretic deposition leads to uneven deposition of the nanofillers, especially when it is a woven fabric [139], as fibers tend to overlap each other [26], as shown in figure 2.3. The uneven distribution of CNTs on CF surface suggests insignificant improvement in properties. Electrophoretic deposition of graphene oxide (GO) on CF surface, even acts as a sizing, as seen from figure 2.2 [27]. Post deposition, the CF were annealed and GO reduced to RGO [27]. GO was covalently attached to CF surface through various functional groups, which appeared post annealing as confirmed through X-ray photoelectron spectroscopy (XPS) [27]. This results in increased surface roughness and covalent bonding between CF and RGO, improving the interfacial properties of the RGO-CF epoxy composite.

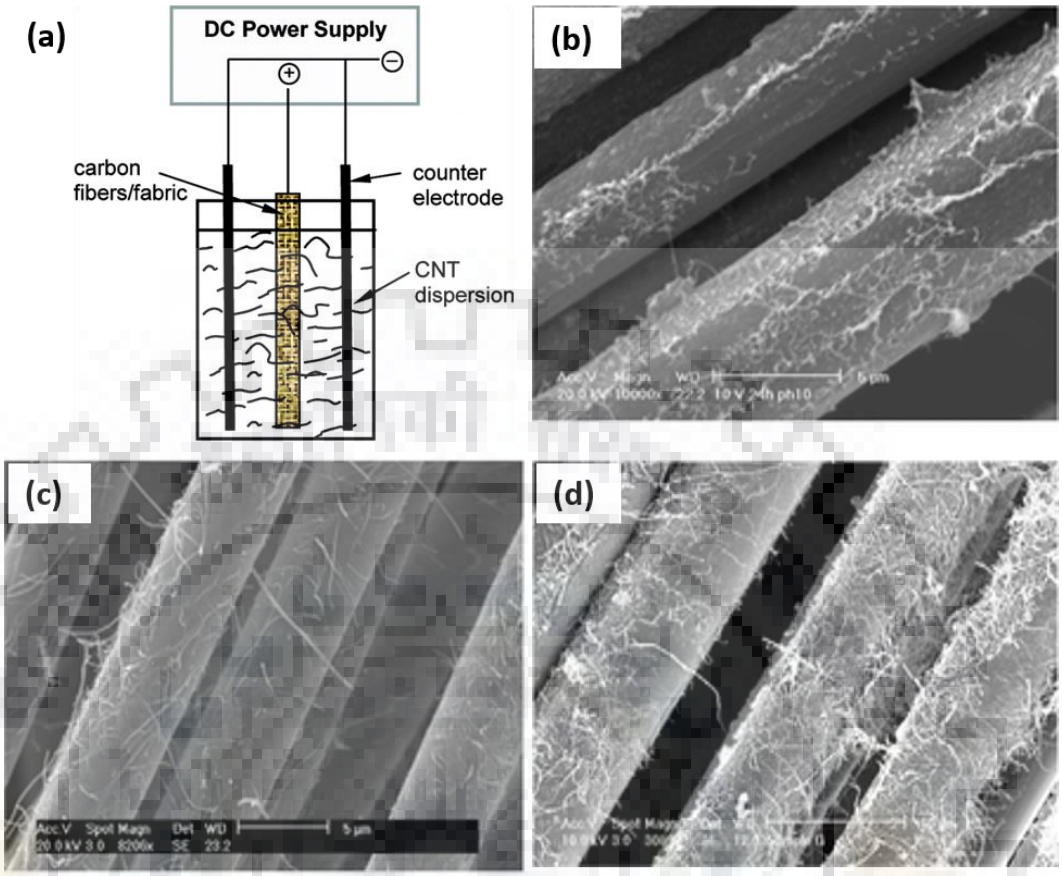

Figure 2.1 (a) Schematic of electrophoretic deposition of CNTs on CF surface, FE-SEM images of **(b)** SWNTs, **(c)** MWNTs on annealed in vacuum and nitric acid treated CF and **(d)** MWNTs on as received CF surface [26].

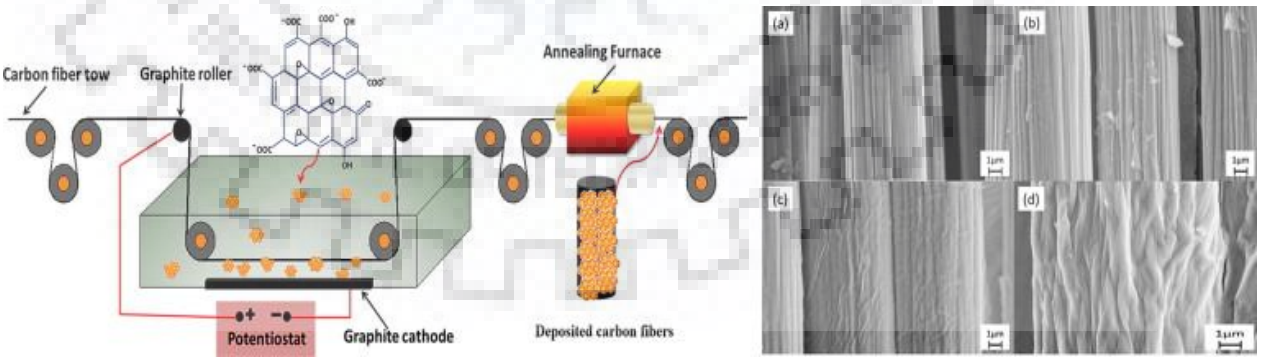

Figure 2.2 Schematic of setup for electrophoretic deposition of GO on CF surface (right), FE-SEM images of **(a)** as-received CF, **(b)** (2 V, 0.02 A) GO-CF, **(c)** (10 V, 0.11 A) GO-CF, **(d)** (30 V, 0.27 A) GO-CF epoxy composite [27].

Factors like, applied DC voltage, nanofiller concentration, deposition time, type of pre-treatment on CF surface, as well as, the morphology of nanofiller, are seen to govern the deposition rate on CF surface [26, 27]. The nano-engineered CF structures can then be utilized as a reinforcement for structural composites

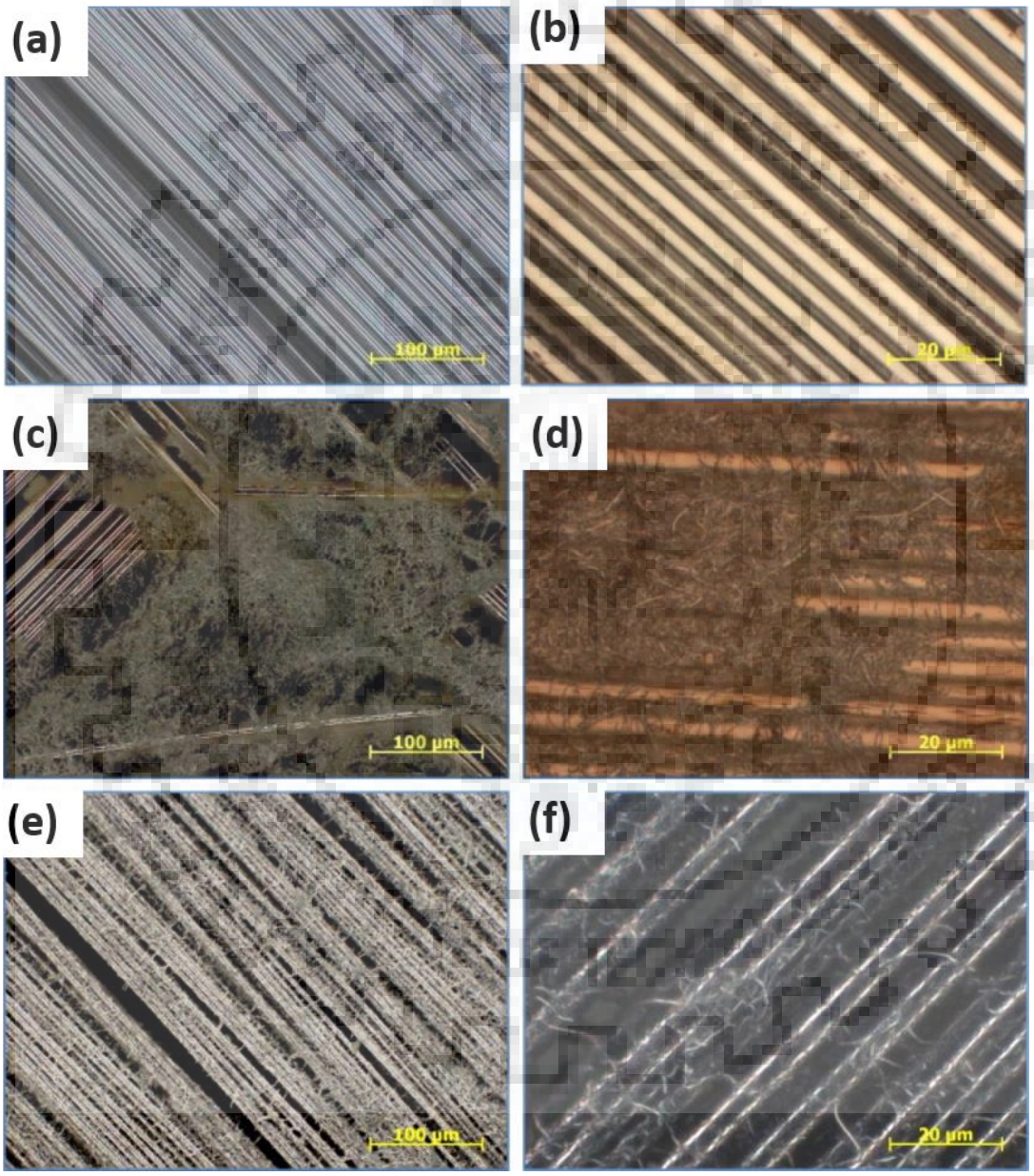

Figure 2.3 Optical images of CF sheets **(a, b)** as-received, after electrophoretic deposition of **(c, d)** oxidized carbon nanofibers (CNF) and **(e, f)** with sizing amidized CNFs [139]

2.3.1.2 Carbon Vapour Deposition (CVD)

CVD is a method, which involves the decomposition of hydrocarbon gases, at relatively high temperatures, over catalytically active metallic centres on the substrate surface (figure 2.4). The CVD system provides a method for CNTs/Gr growth in different environments, variety of temperatures mostly between 650 ºC to 1000 ºC, pressures which is usually lower than atmospheric pressure, variety of catalysts (Fe, Co, Ni, or other transitional metal nanoparticles and alloys), a number of hydrocarbon gases, like, methane, ethane etc. as a carbon precursor and different substrates (alumina, clays, silicon, graphite etc.) [140, 141]. It is the most widely used technique for growing CNTs/Gr on a variety of fiber surfaces. Growing CNTs/Gr by CVD is therefore not a simple technique, as there are number of parameters and conditions, like, temperature [140, 142], time [140], atmosphere [140], different carbon sources and their flow rates [140, 143-145], type and concentration of the catalyst [140, 146] and others [140], which need to be controlled precisely.

Use of high temperature in CVD might improve the CNT/Gr growth, but it removes any sizing, which may have been applied to the fiber surface during its manufacturing, making it vulnerable to degradation by CVD reaction. Another drawback of using CVD method is CF surface degradation due to catalyst adhesion [140, 147]. The concentration of catalyst is increased to achieve higher density of CNTs on CF surface. This, results in few catalyst particles migrating into the CF filaments. At high temperatures (>700 ºC), the common metal catalyst typically starts to dissolve/melt, which degrades CF surface and deteriorate its properties [140, 146, 147]. If not controlled properly, all the above mentioned parameters will affect the CNT growth and damage CF surface, which eventually result in declined mechanical properties of CFs [27, 29, 147-152]. Thus, the performance of CF-reinforced composites is significantly degraded as the mechanical properties

of the macroscale reinforcement are deteriorated. The reduced tensile strength of hierarchical CFs is not feasible for use in advanced composites.

Quite a few studies have been carried out to inhibit the degradation of CFs during the CNT growth process by using unsized CF [153], lowering the CNT growth temperature below the eutectic temperature [154], decreasing the CNT density [155], use of barrier coatings to shield CF surface from catalyst [156, 157], utilizing the aerosol-assisted chemical vapor deposition (CVD) [152, 158], oxidative dehydrogenation reaction between C_2H_2 and CO_2, that allowed growing CNTs on CF at 500 °C [159]. Even though, all these studies reported reduction in degradation of the CF strength under the controlled condition, but it could not be eliminated [152]. The use of high temperature, catalysts and difficulties in scaling up the process for large fiber panels limits the practical application of this technique for the fabrication of CNT CF-epoxy composite for structural applications.

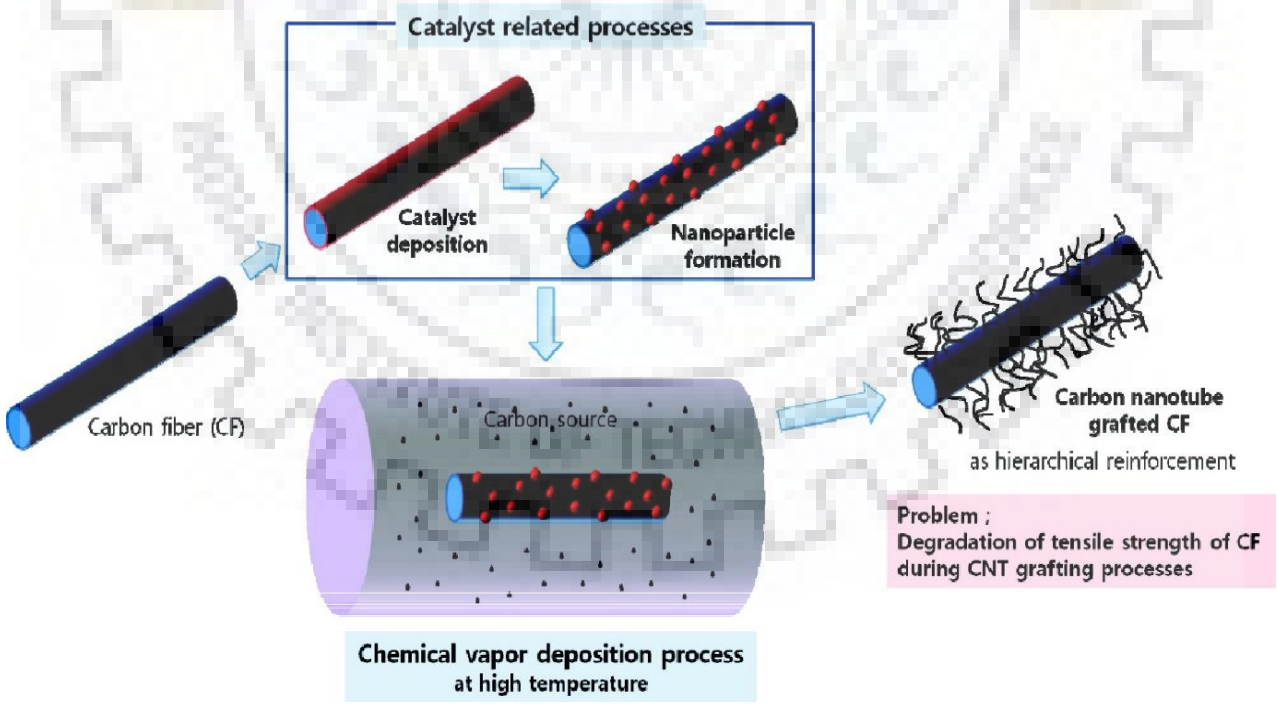

Figure 2.4 Schematic showing CNT grafting on CF surface by CVD [146]

2.3.1.3 Interleaving

Interleaving is a method of inserting a layer of nanoscale reinforcement in between/at the interface of two CF sheets [59, 160-163]. There are different approaches available in literature to interleave nanofillers in CF epoxy composite. One of which include inserting CNT in the form of bucky paper (BP) as interleave/interply between CF sheets [64]. The composite was fabricated by autoclave processing. The resin flow first occurred through thickness from CF pre-preg to dry BP. Once the BP were completely filled with resin, it began to bleed along the in-plane direction of the laminates. However, high resin absorbance and low permeability of dry BP caused voids and defects in BP-CF hybrid composites.

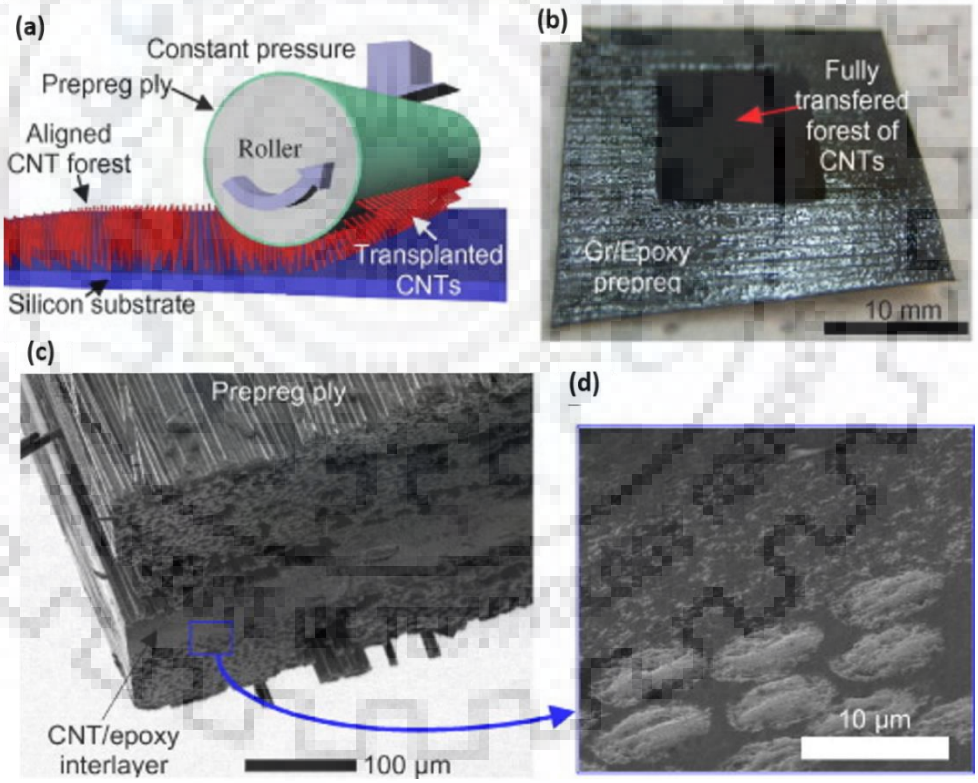

Figure 2.5 Interleaving vertically aligned CNT forest through transfer-printing process on a pre-preg **(a)** Illustration and **(b)** fully transplanted to the surface of CF epoxy pre-preg sheet; **(c, d)** FE-SEM images at different magnifications showing two sheets aligned CNT interlayer hybrid composite [162].

In another effort, the researchers transplanted the CNTs, grown on silicon substrate using CVD, to a CF epoxy pre-preg sheet using a roller as shown in figure 2.5 [162]. FE-SEM images in figure 2.5(c & d) clearly confirms effective impregnation of polymer in the CNT forest (interlayer). The polymer was drawn by the CNT forest from both the sides from the pre-preg sheets to form an aligned CNT interlayer. The thickness of interlayer is similar to the height of the vertically aligned CNT, before curing.

Another way to use nanofiller interleave is to add nanofiller to epoxy paste and use that paste as interleave. GO-epoxy paste interleave is prepared by dispersing GO in DMF through ultrasonication, followed by mixing epoxy through planetary centrifugal mixer. The mixture was then ultrasonicated and kept in vacuum oven to remove DMF. The dry paste was then spread on CF surface using metallic roller, which served as an interleaf to CF epoxy laminates [163]. Apart from the above mentioned approaches, use of CNTs, grown on short CF as interleave, for CF epoxy laminated composite is also reported [161]. The biggest challenge encountered in case of interleaving is the voids and defects arising due to resin deficit. As, interleaves are quite dense structures, they have less permeability. Therefore, good supply of resin is required to properly impregnate them, which is often not available as the main source of polymer are the adjacent pre-preg layers. This leads to the polymer deficit regions both in CF pre-preg sheet, as well as, in interleave.

2.3.1.4 Chemical Grafting

The nanofillers are also grafted onto the CF surface through chemical functionalization of nanofillers and grafting surface. In case of CNTs, the end caps are functionalized with amine group and the CF surface with carboxyl and hydroxyl group [28-32]. The interfacial shear strength (IFSS) showed significant improvement due to improved load sharing ability with the formation of

crosslinks between CNT and the epoxy matrix. Similarly, use of polyhedral oligomeric silsesquioxane (POSS) [30] improve the interfacial adhesion of the resulting composites. The numerous epoxy groups of POSS increase surface wettability of fiber with the epoxy resin, which react with the hardener to enhance chemical bonding. On the other hand, the CNTs, grafted on the fiber surface, act as extra branches or arms that dig into the matrix. This increases the overall surface area, enhances mechanical interlocking, strengthen and stiffen the interface, which results in improved interfacial strength [30].

2.3.1.5 Dip Coating

Dip coating is one of the simplest techniques, which involves dispersing the carbon nanofiller in a solvent bath using ultrasonication. Once the carbon nanofiller is properly dispersed, the CF is then immersed in that solution. The mixture is sonicated in the presence of CF to promote adsorption of carbon nanofiller on CF surface. The CF might be removed from the solution once coated and oven dried or left in the solution, which is heated till all the solution is evaporated. The later one is given the name liquid phase deposition strategy [164]. Both of these approaches are suitable for short fibers or sheets. Continuous solution coating process is employed for long fibers [8].

It is very important to verify the carbon nanofillers formation, morphology and adhesion to CF substrate for all the techniques that involve nano-engineering of CF surface. Scanning electron micrography is the most commonly used technique to confirm the growth, shape, size and density of nanofillers [165]. Raman Spectroscopy is also employed to confirm the graphitic structure, while DTA/TGA are carried out to confirm the purity of nanofillers grown/grafted/deposited/coated [165] on fiber surface. Single fiber fragmentation test and single fiber pull out tests, equipped with a

camera, are the most common tests to examine the strength and modulus of nano-engineered CF [157, 165].

2.3.2 Nanofiller Modified Polymer Matrix

Apart from the factors leading to non-uniform and weak interfacial bonding, localization of plastic strain in the polymer matrix restrained by surrounding fibers and triaxial stress state in the polymer are majorly responsible for the premature failure of laminates, in directions other than fiber alignment [65, 166]. Addition of nanofillers to the matrix can improve the interfacial properties of CF-epoxy composites, due to the high surface area, which can act as interface for stress-transfer. It even leads to the extension of localized plastic strain from polymer matrix regions near the interface to the entire matrix, uniformly. Homogeneous dispersion of reinforcement phase, along with strong interfacial interaction with the matrix, are the keys to strong composite structures. However, poor dispersion of nanofillers, due to the higher surface energy, restricts their potential as reinforcement. Therefore, it is important to exfoliate nanofillers and uniformly disperse them in polymer matrix, without forming agglomerates, in order to take advantage of its high surface area. Various techniques are in use to disperse nanofillers, which include ultrasonication [65, 167], magnetic stirring, mechanical mixing, shear mixing and three roll milling [24]. All of these techniques either directly disperse nanofillers into the polymer or use solvents, like, methanol, acetone, ethanol etc. to disperse nanofillers first, followed by mixing this dispersion into the polymer. To take full advantage of the potential of nanofillers added to the CFRP composite, they can even be aligned transverse to the fiber alignment direction by means of an electric or magnetic field [65].

2.3.3 Nanofiller Modified Sizing

Another route that has the potential to improve the interface between CF and polymer matrix is the use of nanofillers in the fiber sizing (polymer coating applied to fiber surface to prevent damage). This route has received very limited attention till date [168, 169]. It takes advantage of the developed techniques for the dispersion of nanofillers in polymer and then grafting that nanofiller sizing to CF. Thus, it is possible to even scale up the process for industrial applications. In order to eliminate the potential effects of commercial sizing, the fiber needs to be desized first, which can be done by using methods like refluxing in acetone for hours [168] or thermal degradation of sizing. De-sizing needs to be controlled in order to prevent any damage to the fiber. The desized or raw CFs are pulled through the nanofiller modified sizing with subsequent drying. The speed at which the CF is extracted should be maintained slow enough to achieve good and uniform wetting of the CF, while the excess resin is allowed to be drained.

2.4 Techniques for Fabricating Fiber Reinforced Polymer Composites

2.4.1 Vacuum Assisted-Resin Transfer Moulding

This is the most efficient and most commonly used technique for fabricating multiscale FRPs [26, 157, 161, 164, 168]. Both vacuum assisted-resin transfer moulding (VARTM) and resin transfer moulding (RTM) are closed mould processes, where pressure is used to inject resin into the mould. In case of VARTM, the vacuum pressure is used for resin inflow. It uses only bottom half of the mould, while a flexible outer bag creates the other half. Specifically, there is a huge increase in the surface area of reinforcement for carbon nanofillers deposited/grown/grafted/coated CF panels reinforced composite structures, which obstruct the infiltration of epoxy into the fiber bundles. VARTM is a much efficient technique and helps in infiltration of epoxy into the fibers, uniformly

[26, 157, 161, 168]. High-permeability distribution media/resin flow channels are incorporated in the layup pile to improve the resin flow. A schematic for the process is reproduced in figure 2.6. Post resin infusion, the composite may be cured at room temperature or even at high temperature in oven [164].

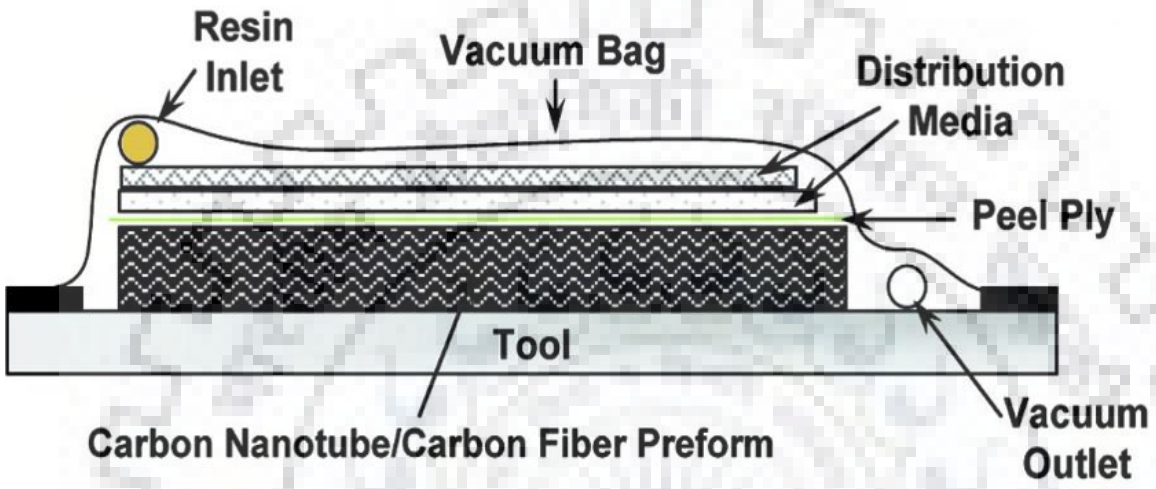

Figure 2.6 Schematic of vacuum assisted resin transfer moulding [26]

2.4.2 Autoclave

This technique is used to process the composites that require elevated temperature and pressure for curing and fabrication. This technique is frequently used for fabricating pre-preg based composite [24, 162, 170] or for the composite that require post curing at high temperature and vacuum, after being fabricated through VARTM [63, 168].

2.4.3 Hand lay up

It is a very simple technique that uses brush and rollers to apply polymer to CF surface. Once the pre-pregs are made, they are stacked together and compressed using either compression moulding, hot press [161, 163], VARTM [167] or even autoclave [8, 167].

2.4.4 Other Techniques

Compression moulding, hot press [161, 163], filament winding [24], drum winding [8] are the other techniques used for fabricating CF epoxy composites. Compression moulding and hot press [161, 163] techniques are used post epoxy impregnation. These techniques can be used itself or in combination with the other.

2.5 Carbon Nanoparticle-Carbon Fiber Epoxy System

2.5.1 CNT-CF Epoxy Composite

CNTs are the most widely studied carbon nanofiller as reinforcement to the conventional FRPs, due to their fiber like morphology (can be aligned along z direction), high flexibility, nanoscale diameter, high aspect ratio, exceptional mechanical, electrical and thermal properties. Hence, incorporation of CNTs to FRP can help to improve the interfacial and interlaminar properties along with electrical, thermal and other mechanical properties that lead to significant improvement in their performance [1, 9, 10]. This approach helps in exploring benefits of microscale traditional fibers along with the additional reinforcement offered by nanoscale carbon nanotubes. The addition of CNT not only strengthens the polymer matrix, but also the interface, which lead to improved fiber-polymer interfacial load transfer. CNTs can be integrated to a conventional CFRPs either in bulk or deposited/grown/grafted/coated on CF surface.

CNT-CF epoxy composites, are generally fabricated using CF with CNTs deposited/grown/grafted/coated in it, through electrophoretic deposition [26], CVD [165], graphitic structure by design (GSD) [30], laser ablation, dip coating and chemical grafting [9, 10]. Successful deposition of CNT on CF surface, using electrophoretic deposition, is shown in figure 2.1. For the electrophoretic deposition of carbon nanotubes, the carbon fabric was annealed at 700 °C in vacuum

to remove the polymer sizing applied to the fabric, followed by oxidative treatment that consists of refluxing in nitric acid. The oxidative treatment aims at introducing functional groups, removing the weak outer layers of the fiber, and texturing the fiber surface. However, if not controlled properly, the strong oxidative conditions can result in non-uniform etching of the carbon fiber and loss of fiber tensile strength [26].

The infiltration of epoxy into CNTs, deposited/grown/grafted/coated CF panels, is quite a challenging task. There is a huge increase in the surface area of reinforcement with the attachment of CNT on the CF surface, which obstruct the infiltration of epoxy into the fiber bundles [26]. The CF epoxy composites, with nano-engineered CF surface, has shown significant improvement in out of plane properties. However, the in plane properties does not show any significant change, as the in-plane properties of FRPs are fiber dominated. Modifying epoxy matrix by addition of CNTs to epoxy matrix is seen to improve flexural modulus of the CF epoxy composite [65]. Attaching magnetite particle to CNT surface by adsorption help in achieving preferred orientation [65] and improve the properties further. The effect of different techniques, used for modifying CF epoxy interface, on different properties is presented in table 1.

2.5.2 Gr and its derivatives-CF Epoxy Composite

The high aspect ratio and two-dimensional sheet like morphology of Gr and its derivatives make it highly effective in improving the interface between the micro fiber and matrix interface of composites. Along with the improvement in interlaminar fracture toughness (ILFT) and interlaminar shear strength (ILSS), properties, like, flexural strength, electrical conductivity and other also are seen to improve, as shown in table 1. The different methods, used for the incorporating Gr in a multiscale CF epoxy composites, include electrophoretic deposition pre or post CF processing [19, 27], which may or may not be followed by thermal annealing, in epoxy sizing [168], interleaving

[163], liquid phase deposition (extended dip coating), three roll mill and filament winding [24], continuous coating (dip coating for long fibers) [8].

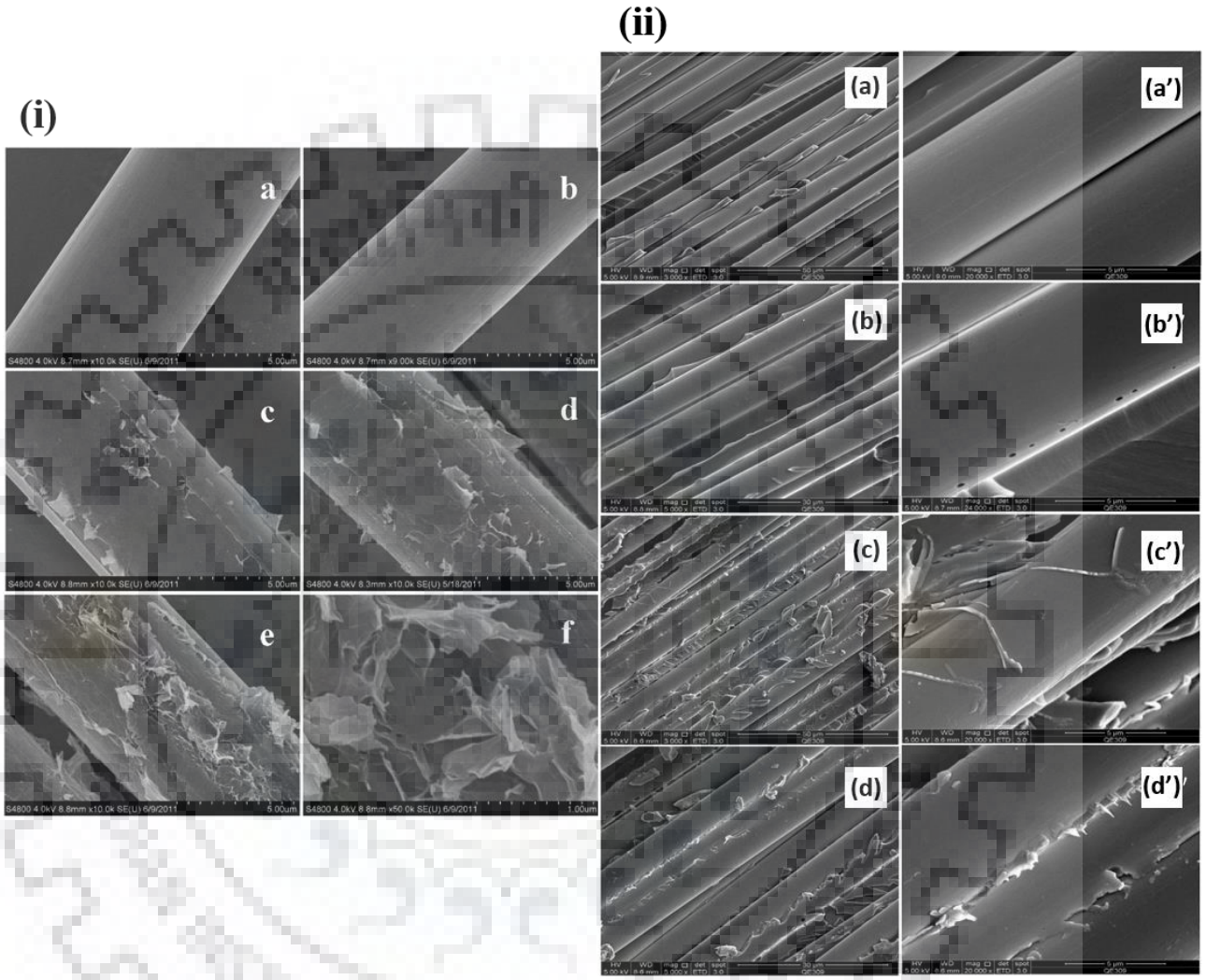

Figure 2.7 Scanning electron microscopy (FE-SEM) images of the **(i) (a)** CF without sizing **(b)** CF with commercial sizing, **(c)** CF-1 wt% GO sizing, **(d)** CF-5 wt% GO sizing, **(e)** CF-10 wt% GO sizing, **(f)** magnified image of **(e)**; **(ii)** fractured surface of ILSS **(a, a′)** CF with commercial sizing-epoxy **(b, b′)** CF-1 wt% GO sizing-epoxy, **(c, c′)** CF-5 wt% sizing-epoxy; **(d, d′)** CF-10 wt% GO-epoxy composite [168]

Dispersing Gr in sizing and then coating the surface of CF with modified sizing is one of the least explored approach available in literature, not only for Gr or its derivatives, but for overall, carbon nanofiller CF epoxy composite. Addition of graphene oxide (GO) in epoxy sizing improved the interfacial performance for single CF epoxy matrix, as well as, interlaminar performance for unidirectional CFs on epoxy matrix [168]. FE-SEM images in figure 2.7 for the fractured surface even corroborates the same. The IFSS for CFs epoxy matrix is improved by ~73 % due covalent bonding and improved mechanical interlocking, with the addition of GO [27]. The exfoliated Gr-CF epoxy composite, prepared by liquid phase deposition strategy (extended dip coating), showed improvement in both ILSS and flexural strength of the composites [164]. Improved interfacial bonding between CF and epoxy with the addition of Gr lead to better load sharing between CF and epoxy.

Above mentioned studies clearly reveal the role played by Gr and its derivates, as well as, by different techniques used to incorporate them in CF epoxy interface. Further, the effect of functionalization was studied by Ashrori et. al. GO was functionalized using three different diamines, namely 4,40 - diaminodiphenyl sulfone (DDS), ethylenediamine (EDA), and p-phenylenediamine (PPD), used as reinforcement to epoxy matrix, with the objective to improve interfacial bonding strength of CF-epoxy composite [167]. Fourier transform infrared spectroscopy (FTIR) spectra, as shown in figure 2.8, confirmed the conversion of oxygenated functional groups of GO to different functional groups, post reactions with the above-mentioned diamines.

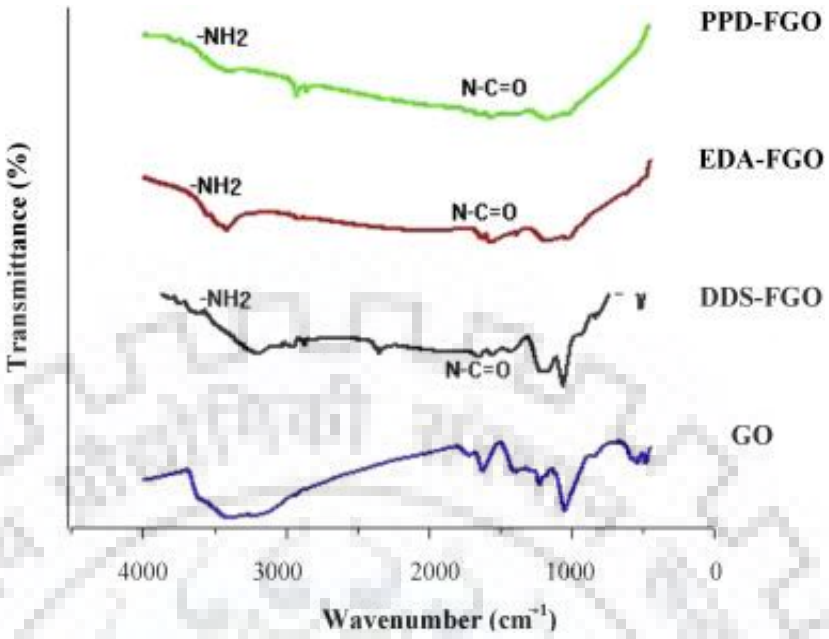

Figure 2.8 FTIR spectra of GO and functionalised GOs [167]

The spectra for the functionalised GOs (FGO) have several new peaks w.r.t GO spectrum. The peaks appearing at 3500-3700 cm^{-1} and 1600-1700 cm^{-1} correspond to amide N-H stretch and amide CO stretch, respectively. While, the disappearance of the peaks located at 1720, 1396, and 1264 cm^{-1} in the GO spectrum suggests that the carboxyl and epoxide groups of the GO have reacted with the NH_2 groups of the diamines. Tensile and flexural properties showed improvement both with GO and FGO, which is due to the improved interface adhesion [167].

2.6 Assessing the Role of Interfacial Bonding in CF-Epoxy Composite

CF epoxy composites have a wide variety of applications [2-4]. The properties, essential for such applications, include high strength, toughness and shear strength both along longitudinal, as well as, transverse direction. Different factors decide the performance of composites, which include the mechanical properties of the matrix and individual CFs, fiber-matrix interface and processing conditions [5]. The load transfer in case of composites is from the matrix to fiber through the shear

stress. Effective control of the fiber matrix interface is important to ensure good interfacial shear strength (IFSS), as the performance is restricted due to the inherently poor interfacial bonding between CF and polymer matrix. This has been a major drawback of CF polymer composite. Over the years, a lot of research has been done to overcome this drawback. Strong van der Waal's forces and hydrogen bonding are preferred to exist between CF and epoxy [6, 7]. The interface is generally assessed by the interfacial shear strength (IFSS) and interlaminar shear strength (ILSS).

As mentioned earlier, the biggest limitation of CF is its non-polar surface, chemical inertness, surface lipophobicity, smoothness and less adsorption, which lead to weaker bond with the matrix material [3-5]. Different treatments are done to modify fiber surface to combat the inertness of CF. Sizing (application of polymer to CF surface) [171, 172], acid modification [173, 174], electrochemical modifications [175, 176], electro-polymer [177-178], plasma surface [175, 179], high energy irradiation [180, 181], Ni surface [182], thermal modification [183], ozone treatments [184], nanofiller addition [8] are the different techniques used to treat CF surface inertness [9, 10].

Sizing is a method, which protects filaments of fiber from getting damaged as well as, provides structural integrity during manufacturing and usage, by applying a coat of polymers, like, polyimide [185], polyurethane [185], epoxy [186, 187] etc. to CF surface [171, 172, 188]. It even facilitates fiber-matrix adhesion and composite processability. The addition of coupling agent to sizing material is further responsible for improving the chemical interaction of CF with the matrix, through oxy-carbonated functional group [189]. The strength of this interaction depends upon the fiber sizing compatibility. The molecular weight of sizing also influences interfacial properties. Low molecular weight sizing leads to soft and more compatible interface region [190]. However, there is a segregation of high concentration of polymer chains at the interface, which reduces mechanical properties [191, 192]. On the contrary, higher molecular weight sizing leads to brittle and less

compatible interface [190, 193]. The diffusion of fiber sizing into polymer matrix leads to formation of interface that protect fiber and hinder crack propagation. Most of the commercially available sizing for CF are compatible to epoxy than any other polymers [172, 185, 194-196]. The sizing alone, as well as, along with coupling agent is seen to affect tensile, flexural, compressive, fatigue, fracture toughness, interfacial, interlaminar etc. properties of the composite [187, 195].

Acid treatment is another commonly used technique for modifying CF surface. The acid corrodes the fiber surface and introduces flaws and pits, which improves fiber-polymer mechanical interlocking, but at the expense of single fiber strength [173, 197-200]. Nitric acid, maleic anhydride, etc. are the commonly used acids for surface treatments [173, 174]. The effect of acid modification on fiber surface is generally characterized using techniques such as FTIR [173], FTIR-attenuated total reflection (ATR) [200], Raman spectroscopy [174] and XPS [201]. The acid treated CF, when reinforced in polymer, is seen to significantly improve the properties like ILSS [197, 202], flexural strength [202], impact strength, tribological behaviour, electrical conductivity etc. Electrochemical treatment on the other hand, uses electrolyte to introduce specific functional groups on CF surface which improves interfacial properties [175, 176]. However, if parameters, like, treatment time, electrolyte concentration and type are not chosen properly, it may lead to reduced single fiber strength.

As compared to other techniques, plasma treatment causes the least damage to the CF [169, 203-205]. It, leads to inclusion of reactive functional groups, like, hydroxyl, ether, carbonyl etc., on CF surface, improving its surface reactivity and adhesion to polymer matrix. Another efficient and environment friendly technique for fiber surface modification, without significant fiber damage, is high energy irradiation grafting [180, 181, 206 and 207]. This method changes the fiber surface roughness by displacement of atoms, which create site for bonding the functional group of matrix.

Generally, the interfacial bonding is a chemical bonding, due to the presence of functional groups at the fiber surface. However, due to the higher temperatures involved in surface modification techniques, most of the functionality disappear, which in some cases, can rise again during composite processing [208, 209]. Therefore, it is always difficult to define whether the interfacial bonding is mechanical interlocking or chemical bonding.

An alternate to all the above mentioned techniques is utilization of nanoparticles for modifying the CF surface, which has recently gained a lot of attention. Carbon based nanoparticles are the most promising candidate as reinforcement to CF polymer, due to their nanoscale dimension, high aspect ratio, exceptional properties, the attributes required for modification of interfacial properties. The incorporation of carbon nanofillers in matrix, as well as, on the CF surface of a multiscale composite, has been extensively studied by researchers. The grafting, depositing, growing or coating of carbon based nanofillers, specially CNTs, Gr and its derivate, increases the surface area and promotes mechanical interlocking. The improved interfacial interaction enhances the overall strength and stiffness, owing to the improved stress transfer from the matrix to the fibers. The most popular micromechanical technique to study interface of single fiber in a matrix are pull-out test, micro-droplet test or fragmentation test [29, 148, 152, 165, 168, 210].

As seen from the literature, CVD has been quite an efficient technique to grow CNTs on CF surface with different yield, shape, size etc. Interfacial shear strength, as high as ~94 %, was achieved with aerosol assisted CVD CNT-CF epoxy composite [152]. The presence of CNTs changes the interface behaviour. CNTs, grown on carbon fiber surface, increased the specific surface area and mechanical interlocking between the fibers and the epoxy. The difference in the fracture morphology of the pulled out fiber and the hole left behind confirms the same as seen in figure 2.9. There are three possible modes in which the nano-engineered CF polymer composite can fracture. All three

modes are schematically shown in figure 2.10. The CF is pulled out in type 1 failure mode, while the CNTs remain embedded inside the matrix owing to a weak bonding force between the CF and CNT. In type 2 failure, CNTs along with CF is debonded from the matrix, as a result of strong adhesion between the CNTs and CF. However, in case of type 3 failure, the fibers are fragmented, with a part of CNT still connected to the pulled out fiber, while the rest is buried within the matrix. Correlating fractured surface images in figure 2.9 with different failure modes suggested in figure 2.10 verifies type 2, as the dominant failure mode in this study [152]. The orientation and length of CNTs grown on CF surface also controls the interfacial properties of the composite. CNTs with high aspect ratio, aligned perpendicular to CF displayed higher IFSS in epoxy composites. Improvement of up to 115% with CNTs having length 47.2 μm and aligned perpendicular to CF was reported as compared to that of randomly oriented entangled CNTs. Improved wettability and increased interface between the CNT-CF and epoxy were the reason behind the improved IFSS [148]. Higher growth time lead to longer CNTs. However, the symmetric structure of CNTs were seen to be disrupted for growth time longer than 60 min, which reduces IFSS [148]. This is attributed to the circumferential tension exceeding the inherent lateral strength of the grown MWCNT [211]. High temperature, non-uniform distribution, pre-deposited catalyst, along with difficulties in scaling up the process are the factors, which limit the practical application of this technique [26].

Chemically grafting CNTs on CF surface are seen to improve the IFSS by over 150% with less than 1 wt% content [29]. The improvement in ILSS is a cumulative output of improved crosslinking between CNT and the matrix, increased surface area of CF with CNT grafting, mechanical interlocking induced due to fiber surface roughness and improved surface wettability due to active chemical groups [29].

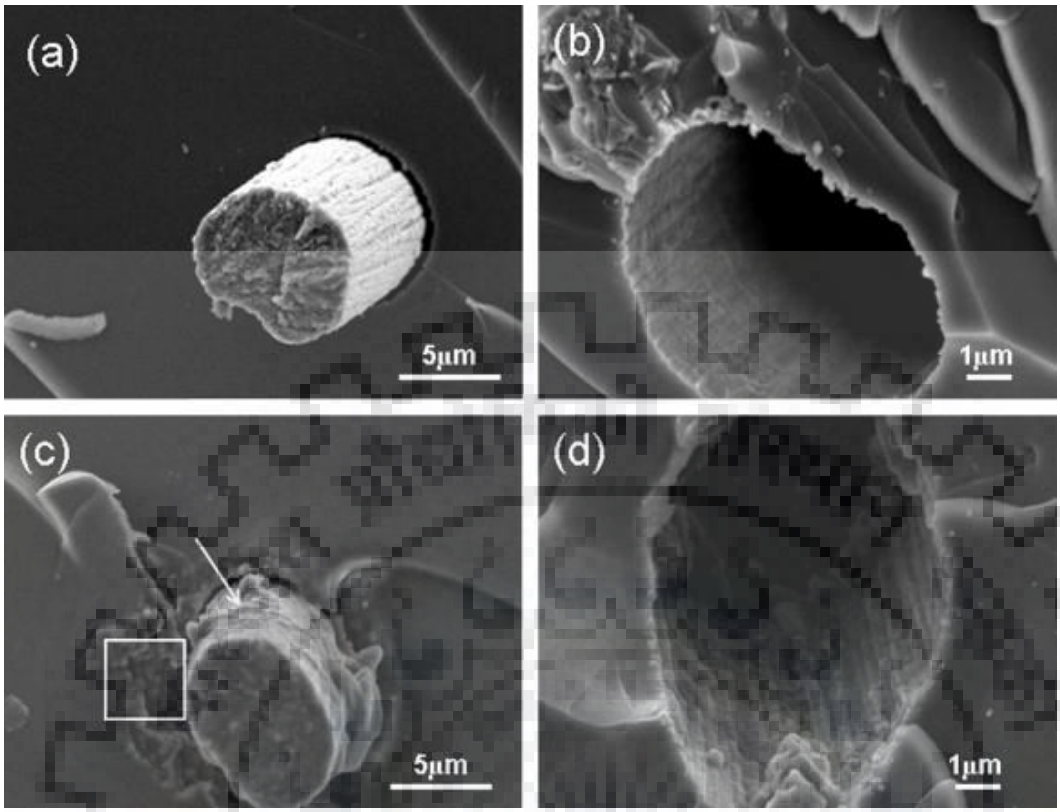

Figure 2.9 FE-SEM images for fracture surface of **(a, b)** CF-epoxy and **(c, d)** CNT-CF epoxy composite [152]

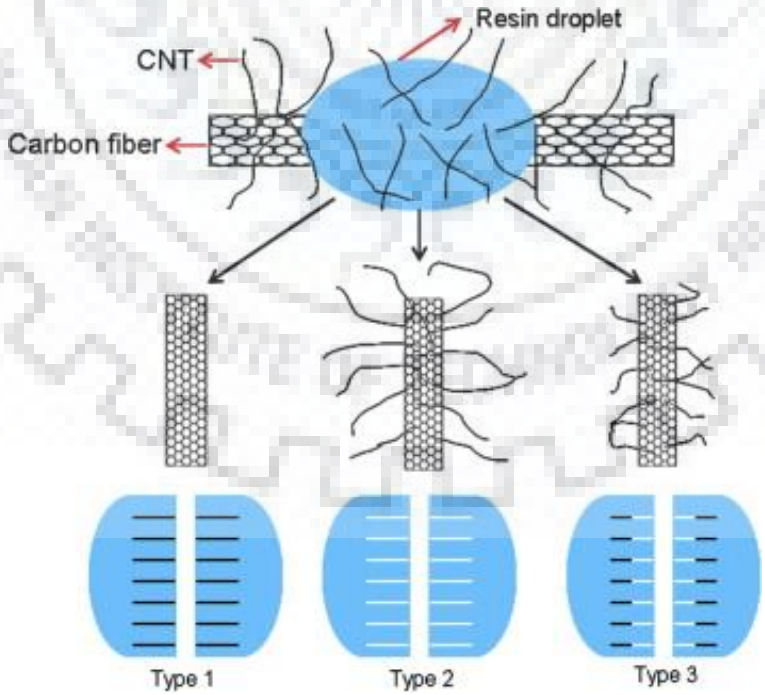

Figure 2.10 Schematic illustrating different fiber pull out failure modes for CNT/CF epoxy [152]

Incorporating graphene oxide to epoxy sizing improves IFSS of CF epoxy composite by ~71% and ~36% as compared to unsized and commercially sized CF, respectively with 7.5 wt% GO [168]. Even though the technique is clean and scalable, the improvement achieved in interfacial properties is not quite significant, considering the high reinforcement content.

2.7 Effect of Nanofiller Addition on Mechanical Properties CF-Epoxy Composite

The aim behind addition of nanofillers to CF epoxy composite is to improve out of plane or transverse mechanical properties which include flexural strength, interlaminar fracture toughness, interlaminar shear strength. At the same time, maintaining the in plane properties like axial/longitudinal tensile strength and Young's modulus. The improvement in the properties depends on various factors, which include fabrication technique, nanofiller content, dispersion and particle geometry. Apart from controlling the degree of consolidation, fabrication techniques also affect the dispersion of the reinforcement phase. For all the nanofiller CF-epoxy multiscale composites studies reported so far, the primary mechanical properties studies include tensile properties, interlaminar shear strength, interlaminar fracture toughness and flexural strength [1, 9, 10].

Reinforcing the epoxy matrix with nano-engineered CF surface is seen to significantly improve mechanical properties of CFRP as the properties in this direction are matrix dominated. The in-plane mechanical properties, on the other hand, does not show substantial difference as they are typically dominated by fiber reinforcement [26].

2.7.1 Tensile Strength

The effect of addition of different nanofillers, e.g., graphite, GO, RGO, Gr, CNT and carbon black, on UTS, E and failure strain of CF-epoxy composite is studied extensively. Fiber being the major reinforcement in nanofillers reinforced FRPs, the tensile properties are governed by the

properties of microscale fibers. For nano-engineered CF epoxy composite, it is very important to study the tensile property of fiber both before and after the nanofillers are grown, grafted, deposited or coated. This is critical, as the techniques used for modifying the CF surface have adverse effect on fibers. Reinforcing such fibers to epoxy matrix do not give desirable improvement in properties for structural application. Therefore, for proper evaluation of nanofillers modified CF epoxy composite, both fiber strength and composite strength needs to be studied. Single fiber tensile test is the most common test to verify the strength of a fiber before reinforcing it into a composite [148, 210]. The strength of the CFs is seen to drop after the growth of CNTs on CF surface through CVD [148, 210]. The degradation of strength is attributed to the surface damage of the CFs by the thermal degradation and catalyst. The CF strength reduced by ~39% post CNT growth by injection CVD [148].

Electrophoretic deposition technique is also seen to degrade the fiber properties. The tensile strength reduced even though the out of plane properties like ILSS showed improvement [26]. Interleaving CNTs in the form of bucky paper in CF epoxy composite reduced its tensile strength and modulus both with 4.95 wt% and 7.99 wt% CNTs. This is due to the voids and defects created as a result of high resin absorbance and less permeability of BP [64]. Thus, nanofillers reinforced CF-epoxy composite, fabricated by dispersing nanofillers in epoxy composite, needs to be investigated as another option. Adding GO to the sizing is seen to improve tensile properties of carbon fiber composites. Both tensile strength and tensile modulus are higher than that of the normal composites [168]. To, further improve the interaction GO can be functionalized. Functionalization of GO, using three different diamines 4,4′-diaminodiphenyl sulfone (DDS), ethylenediamine (EDA), and p-phenylenediamine (PPD) was done, which was then dispersed in epoxy matrix for 0.1, 0.3 and 0.5 wt%. The CF epoxy composite, fabricated with this modified epoxy, is seen to improve tensile

strength by ~23% with 0.3 wt% PPD-CNT CF epoxy composite. Tensile modulus of CF epoxy also improved with the addition of both functionalized and non-functionalized GO [167]. Functional groups played a significant role in increasing the interaction energy between the CF and epoxy matrix, which can be evidenced from FE-SEM images for the fractured tensile samples in figure 2.11. However, properties decreased due to agglomeration above 0.3 wt% GO, even with functionalization.

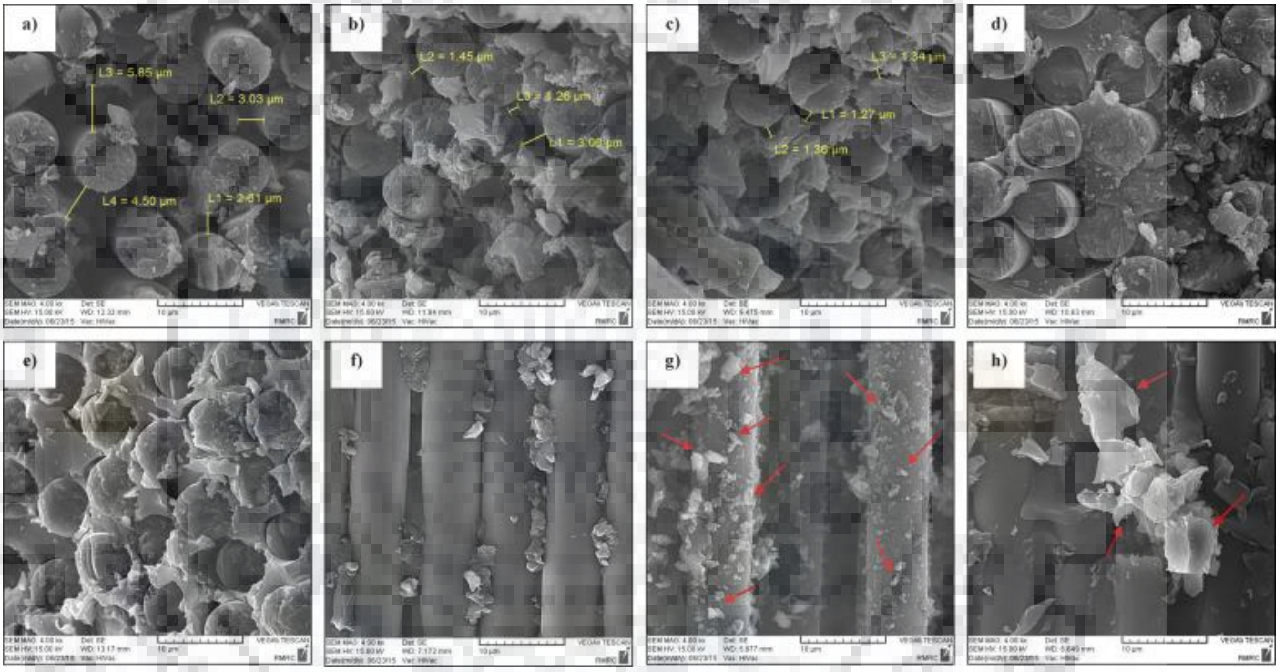

Figure 2.11 FE-SEM images of **(a)** CF epoxy, **(b)** 0.3 wt% GO-CF epoxy, **(c)** 0.3 wt% DDS-FGO CF epoxy, **(d)** 0.3 wt% EDA-FGO, **(e)** 0.3 wt% PPD-FGO CF epoxy composite in axial direction **(f)** 0.5 wt% GO CF epoxy, **(g)** with 0.5 wt% EDA-FGO CF epoxy, and **(h)** agglomeration of 0.5 wt% DDS-FGO CF epoxy composite in transverse direction to tensile load [167]

For GO-CF epoxy and functionalized GO (FGO)-CF epoxy composite, the voids between the pulled-out CFs and the epoxy matrix are small as compared to only CF epoxy composite. Further, matrix is seen attached to the pulled-out CF surfaces for functionalized specimens, as compared with the control specimen. This indicates interfacial adhesion to be relatively strong for GO-CF composite

and much stronger for functionalized GO-CF epoxy composite, as compared to CF epoxy composite. For the composites with EDA- and PPD-FGO (figure 2.11(d & e)), the amount of epoxy matrix attached on the pulled-out CFs surfaces is more and the gaps between the CFs and the matrix are smaller. With increase in the GO and FGO contents to 0.5 wt%, the interfacial adhesion reduced, due to agglomeration as evidenced in figure 2.11(h) [167].

4.2.7.2 Interlaminar Shear Strength and Interlaminar Fracture Toughness

Failure to delamination is another major drawback of laminated composite structures. The fiber orientation in structural composite is usually planar, in x- and y-direction, leading to fiber dominated material properties in these directions, whereas the z-direction remains matrix dominated. The conditions that leads to delamination can vary from out-of-plane tensile loads to in-plane compressive loads, with crack initiating at structural discontinuities such as edges, notches, voids or impurities/foreign particles. The poor interfacial bonding between fiber and epoxy matrix, along with the low strength and brittle nature of epoxy, make the FRPs more prone to the interlaminar failure. Therefore, improving properties, like, interlaminar shear strength (ILSS), interlaminar fracture toughness (ILFT) and interlaminar fracture strength (ILFS) would help in restricting the generation and propagation of delamination. Processing techniques, like, stitching, braiding, 3D weaving and embroidery, have been used extensively in past to improve the interlaminar properties [1, 212-215]. However, the misalignment during stitching, as well as, the resin pockets in the stitching zones are considered as causes for the degradation, as, it is more prone to generation of microcracks [1].

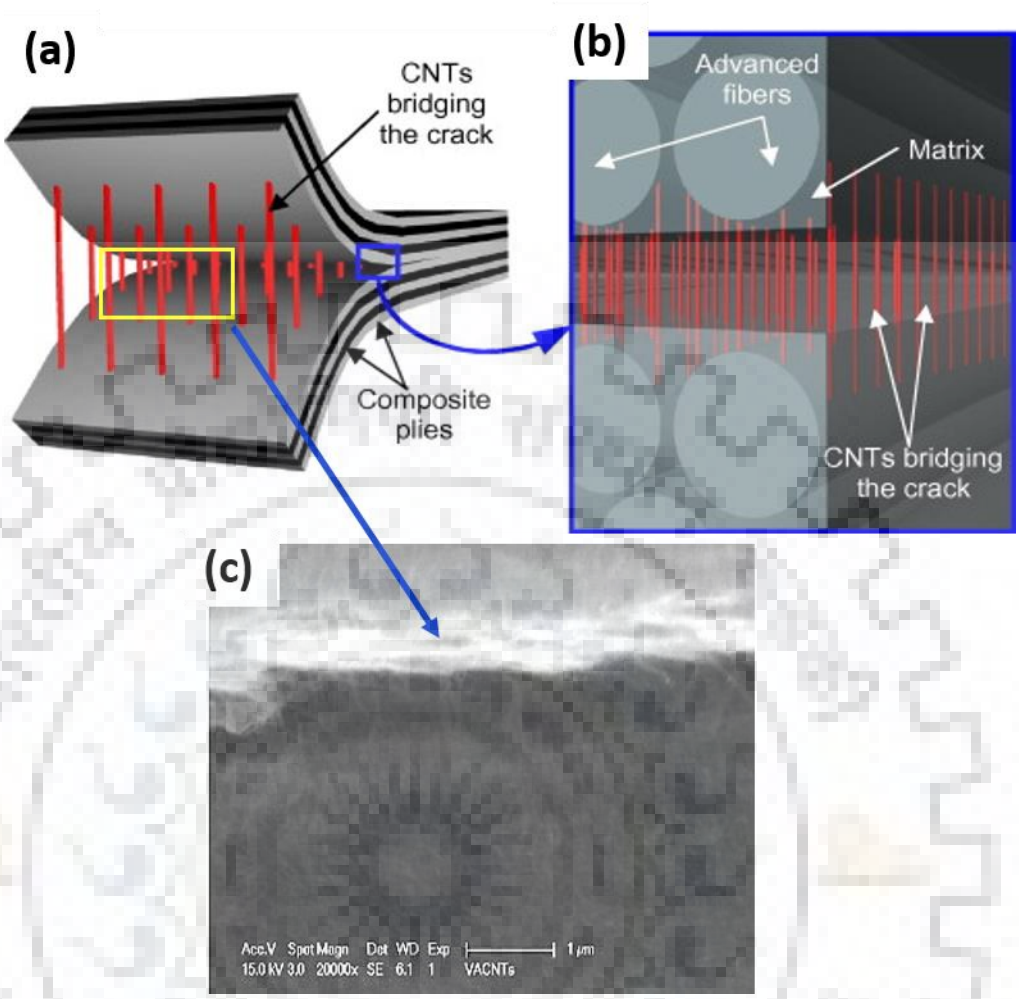

Figure 2.12 Schematic of the **(a)** vertically aligned CNTs placed in between two sheets of a laminated composite, **(b)** schematic and **(c)** FE-SEM image showing vertically aligned CNTs bridging the crack between the two sheets [162].

Use of carbon based nanoparticles for improving the interlaminar properties of FRPs, using techniques, like, interleaving [162], nano-engineered CF surface by growing/grafting/depositing/ coating and modifying the epoxy resin to promote better fiber-matrix interaction, have been the most promising ones. The exfoliated Gr-CF epoxy composite, prepared by liquid phase deposition strategy (extended dip coating), showed an improvement in ILSS by 28% with 1 wt% Gr [164]. The improvement is attributed to the increase of the interface layer modulus with the deposition of Gr. CVD grown vertically aligned CNT forest, transfer printed to the pre-preg was used by another group

as interleave between CF pre-preg sheets to improve the interlaminar properties [162]. The pre-preg was attached to a cylinder that was rolled over CNT forest, at room temperature. The CNTs were transferred from the growth substrate to pre-preg taking advantage of tack of the pre-preg. Mode I and II test on a DCB sample showed an improvement in interlaminar fracture toughness, of ~150% and ~62% respectively, over CF epoxy composite. Crack bridging by vertically aligned CNT, forest as seen from figure 2.12, is claimed to be the main toughening mechanism.

The fracture toughness of CFRPs is a function of toughness of matrix and the interfacial bonding between carbon fiber and matrix. Thus, improvement in ILFT is due to typical energy dissipation mechanisms, such as, matrix deformation, crack deflection and arrest, fiber debonding and pull-out. Strong interfacial bonding between CF and epoxy was witnessed after introducing the GO sheets to the interfacial regions of carbon fibers and epoxy, when added to epoxy sizing, enhancing ILSS by ~12.7% compared with commercially sized CF composites [168]. Applying a thick paste of GO-epoxy as an interleaf, is seen to improve the ILFT and fracture resistance [163]. GO with three different area density 1 g/m^2 (GO1), 2 g/m^2 (GO2) and 3 g/m^2 (GO3) were used in this study. GO2-CF epoxy composite, gives a remarkable improvement of 171% and 108%, in Mode-I fracture toughness and resistance, respectively over CF epoxy composite. Strong interfacial adhesion is the reason for improved property. It can be clearly corroborated to more irregular/rough fracture surface as well as the epoxy matrix adhering to CF surface specimen toughened by GO-epoxy interleaf (figure 2.13).

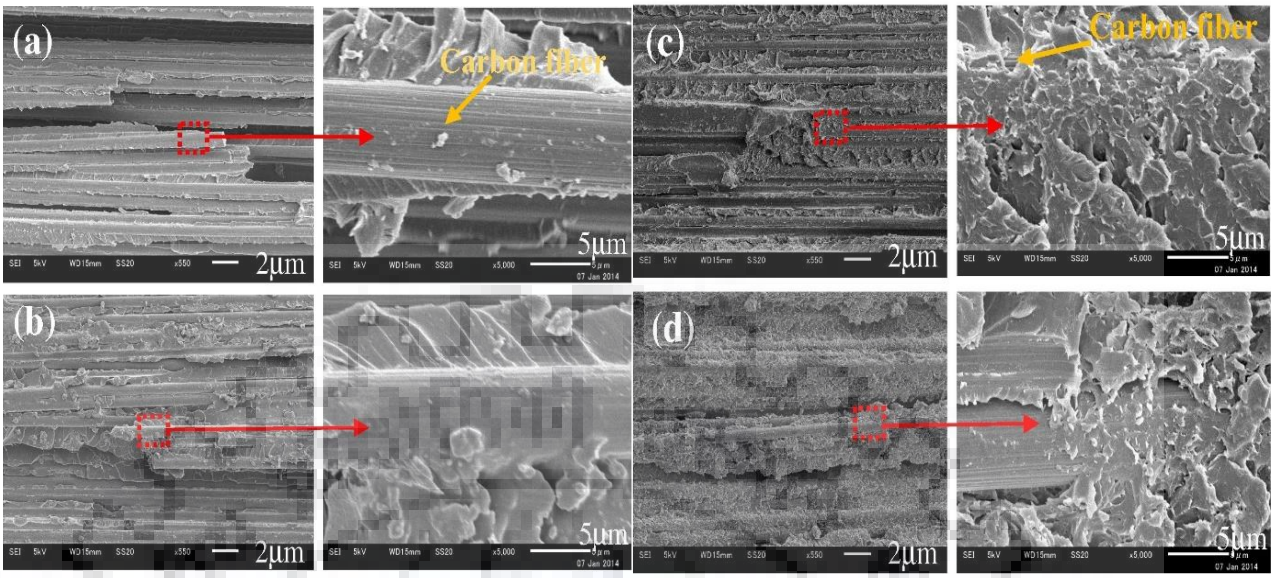

Figure 2.13 Mode-I fracture surface for **(a)** CF epoxy, **(b)** GO1-CF epoxy, **(c)** GO2-CF epoxy and **(d)** GO3-CF epoxy composite [163]

2.7.3 Flexural strength

Another out of plane property of FRPs that needs to be investigated is flexural strength, which is measured using three-point bending tests [65]. It was seen that addition of CNTs to the CF epoxy laminated composite resulted in significant improvement in the load carrying capacity and the flexural modulus of the composite. Further aligning the CNTs in magnetic field, by adsorbing magnetite particle on CF surface in the transverse direction to CF, increased the flexural modulus by ~46%. While, for the randomly oriented CNTs, the flexural modulus increased by ~21%. Besides, the CNTs increased the load carrying capacity of CF epoxy composite. The maximum load carried under three-point bend test is increased by 33% and 15%, with aligned and random CNTs CF epoxy composite compared to CF epoxy composite [65]. Both the flexural strength and modulus is seen to improve for CF epoxy composite after depositing Gr through electrophoretic deposition [19]. Increase in the interfacial surface area of the CF with deposition of Gr improves the load carrying capacity of CF epoxy composite in transverse direction [19]. Similarly, exfoliated Gr-CF epoxy

composite, prepared by liquid phase deposition strategy (extended dip coating), and showed improvement in ILSS by ~ 28% with 1 wt% Gr-CF epoxy over CF epoxy composite [164]. To further confirm the interfacial strengthening flexural strength and modulus were investigated [164], which showed improvement with addition of exfoliated Gr.

The effect of functionalization of GO on flexural strength and modulus of CF epoxy composite was also verified [167]. GO was functionalized with three different diamines i.e. EDA, DDS and PPD, which incorporated amide group on GO surface, which was confirmed through FTIR in figure 2.8. The flexural strength of CF epoxy increases with increase in the GO content from 0.1 wt% to 0.3 wt% both with GO and FGO. The improvement was not very significant. The highest improvement was ~12% improvement with DDS functionalized 0.3 wt% FGO-CF epoxy composite. With further increase in GO content to 0.5 wt%, the flexural strength decreased for EDA and DDS functionalised GO due to agglomeration. While, the non-functionalized GO and PPA functionalized GO showed an improvement of ~50 % and ~73% respectively, over CF epoxy composite [168]. The improvement in flexural strength with 0.5 wt% with non-functionalized GO over EDA and DDS functionalized GO is surprising, as functionalization reduces agglomeration. Functionalization, if not controlled properly, can induce lot of surface defects. Therefore, Raman spectroscopy and single fiber test should have been done to confirm any functionalization related defects before fabricating composite.

The 90° (transverse) flexural strength is the most sensitive interfacial property of a unidirectional fiber composite. So, in order to investigate the reinforcing effect of ozone treated and dip coated unidirectional Gr-CF in epoxy matrix flexural strength was measured both along and transverse to the fiber alignment direction [8]. The epoxy coated fibers showed 82% and 51% increase in 90° flexural strengths for Gr coated fibers, as compared to uncoated and epoxy coated

fibers. On contrary, the improvement in 0° flexural strengths was only 7% [8]. Improved interfacial strength between CF and epoxy matrix with Gr addition, as seen from figure 2.14, is the reason behind improved flexural strength.

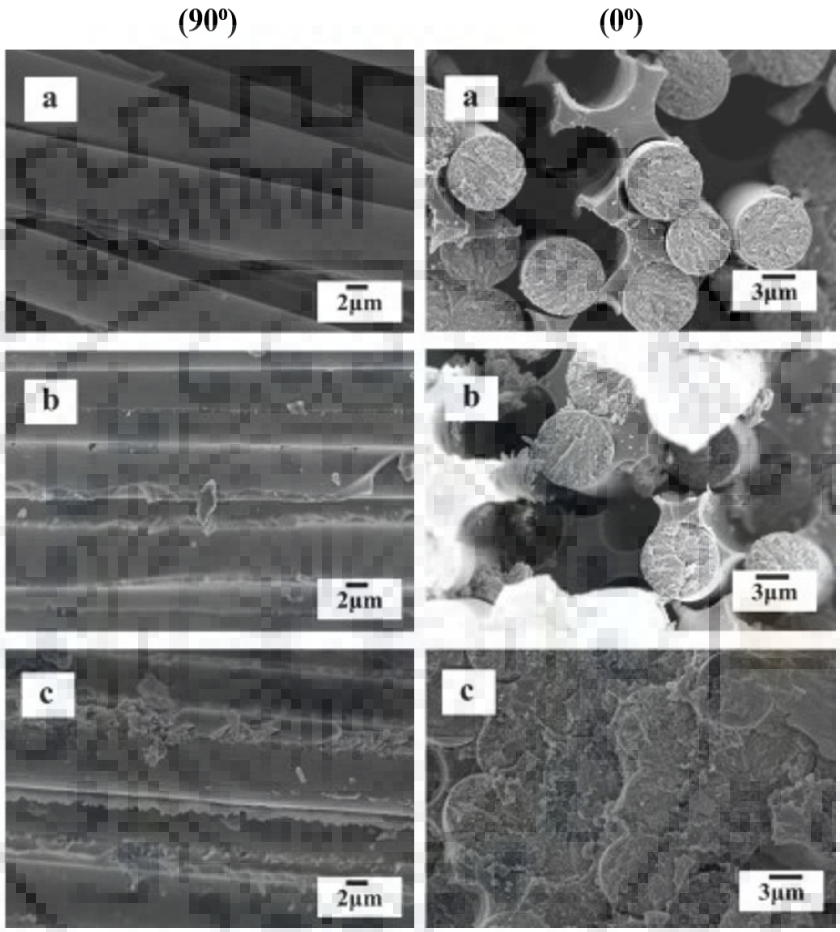

Figure 2.14 FE-SEM images for fractured surface **(a)** non-coated CFs, **(b)** epoxy coated CFs, and **(c)** Gr coated CFs after **(i)** flexural 90° and **(ii)** flexural 0° [8]

2.7.4 Other Properties

Wettability and surface area measurement are two very important properties as these two properties majorly governs the improvement in mechanical properties. Brunauer–Emmett–Teller (BET) method for specific surface area [148, 210] and contact angle measurement using drop on fiber technique for wettability [148, 210] are the most commonly used techniques.

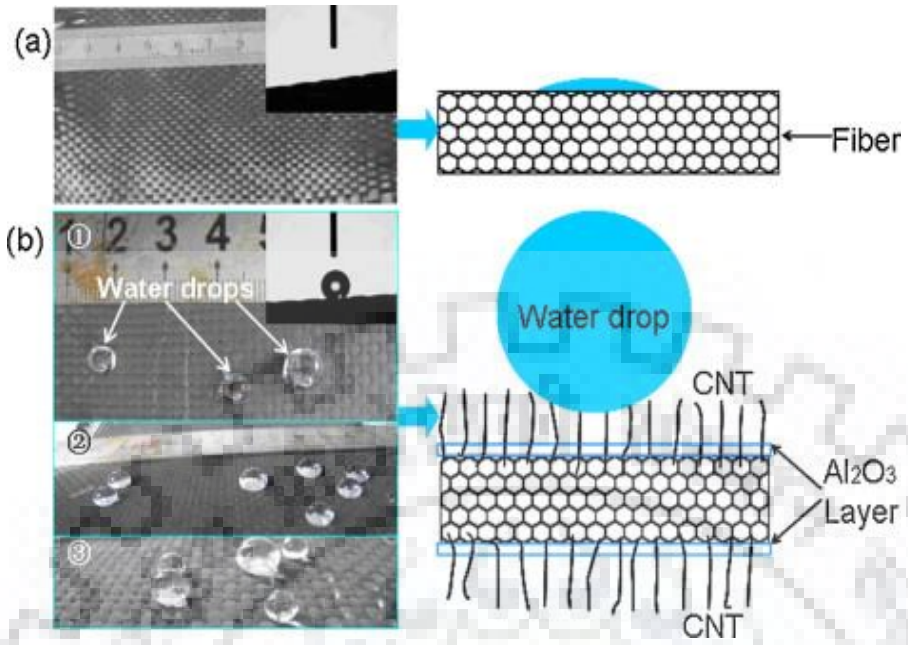

Figure 2.15 Images along with corresponding schematic of water droplets lying on **(a)** hydrophilic CF surface and **(b)** hydrophobic CNT-CF surface [210]

The as received CF and CNT grown CF were cut into short segments, which were then exposed to nitrogen at -196ºC. The nitrogen adsorption by each surface was than measured using adsorption apparatus, which was used to calculate the specific surface area through BET method. Increase in surface area by a ~200% was obtained with CNT grafting [210]. The specific surface area is influenced by orientation and length of CNTs [210]. Grafting CNT showed a remarkable increase in surface area, however the wettability reduced. Grafting CNT on CF surface showed an increase in contact angle, as confirmed from digital images and schematic explaining this increase (figure 2.15). The contact angles were measured with water, diiodomethane and epoxy. There was increase in contact angle with CNT grafting in all three cases, which indicate poor wettability. This increase is attributed to increase in surface roughness with CNT grafting. Hence, proper wettability and infiltration of epoxy resin into densely grown/grafted/deposited/coated nanofillers on CF surface can be difficult to achieve.

2.8 Numerical Simulation to Predict the Effect of Nanofiller Modification on CF Epoxy Composite

Finite element analysis (FEA) is a very important tool to predict the behaviour of nanofiller reinforced CF epoxy composite. The predicted behaviour can then be compared to the experimental results, in order to evaluate the reinforcement efficiency achieved using a particular technique. 2D Finite Element Analysis model was made using ABAQUS to simulate crack initiation and successive propagation in double cantilever beam (DCB) specimens as shown in figure 2.16. It was used to investigate the interlaminar properties of CF epoxy composite reinforced by GO-epoxy interleaf [163]. The laminate was modelled by plane strain element CPE4I with incompatible modes. The interface between two lamellas was modelled by zero thickness cohesive elements (COH_2D_4). The total number of elements in the models was 2100 for DCB specimen. The load vs crack opening displacement (COD) plots obtained from experimental and simulation were a very close match (figure 2.16) [163].

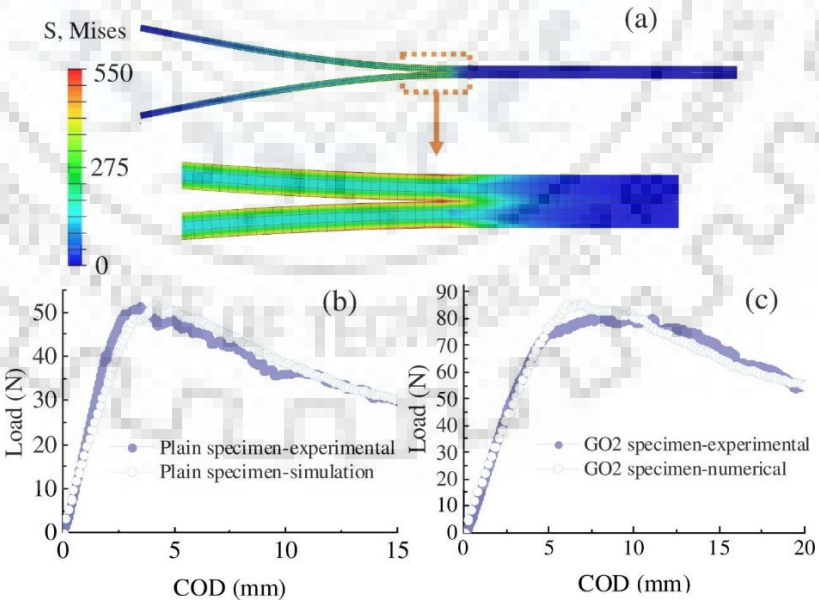

Figure 2.16 (a) Shows FEA models of DCB specimen, load vs COD plots for numerical and experimental analysis of **(b)** plain CF epoxy sample and **(c)** GO-CF epoxy sample [163]

Table 1. Presents the various routes adapted for nanofiller modification and fabrication of CF epoxy composite and their effect on different properties

Composition	Nanofiller Modification and Fabrication Routes	Properties	References
3 wt% Gr/CNT/CB-CF Epoxy	Nanofiller modification - epoxy matrix through mechanical mixing Fabrication- Vacuum assisted resin transfer moulding.	Mode I ILFT- improved by ~60% (Gr) and ~44% (CNT)\ reduced by ~42% (CB) Mode II ILFT- improved by ~53% (Gr) and ~29% (CNT) reduced by ~43% (CB)	[216]
0.25 wt% CNT- CF Epoxy	Nanofiller modification - CF surface through electrophoretic deposition Fabrication- Vacuum assisted resin transfer moulding	ILSS – improved by 27% Out of plane electrical conductivity – improved by 30%	[26]
CNT- CF Epoxy	Nanofiller modification- CF surface through CVD Fabrication- Casted in silicon rubber mould and cured in vacuum oven	ILSS- improved by 14%	[165]
CNT- CF Epoxy	Nanofiller modification- CF surface through CVD Fabrication-Autoclave	ILSS-improved by 4% Tensile Strength- reduced by 10%	[152]
CNT- CF Epoxy	Nanofiller modification- CF surface through chemical grafting Fabrication- dry oven	IFSS-improved by 150%	[29]
CNT- CF Epoxy	Nanofiller modification- CF surface through ICVD Fabrication- dry oven	IFSS-improved by 175%	[148]
CNT- CF Epoxy	Nanofiller modification- CF surface through CCVD Fabrication- dry oven	Tensile Strength-reduced by 10% ILSS-increased by 110%	[210]
CNT- CF Epoxy	Nanofiller modification- CF surface through chemical grafting Fabrication- dry oven	ILSS-improved by 37%	[30]
CNT- CF Epoxy	Nanofiller modification - CF surface through electrophoretic deposition Fabrication- Vacuum assisted resin transfer moulding	IFSS-improved by ~69% Tensile Strength by ~16% Weibull Modulus by ~41%	[137]
(4.99 wt% and 7.99 wt%) CNT-CF Epoxy	Nanofiller modification- CNT buckypaper sheet as interleave between CF and epoxy matrix Fabrication- Autoclave	Tensile strength reduced ~4.1% (4.95 wt.%) and 25% (7.99 wt.%) Tensile modulus reduced ~6.3% (4.95 wt.%) and 31.4% (7.99 wt.%) In plane electrical conductivity transverse direction increased by 350 times (4.95 wt%) and 419 times (7.99 wt%) In plane electrical conductivity axial directions 228% (4.95 wt%) and 176% (7.99 wt%) Out of plane electrical conductivity increased by 350% (4.95 wt%) and 425% (7.99 wt%)	[64]
1.5 wt%CNT-CF Epoxy	Nanofiller modification - to epoxy matrix through ultrasonication	Flexural modulus increased by ~46% with aligned CNTs	[65]

	Fabrication- Vacuum assisted resin transfer moulding CNTs surface modification - magnetite particles were used to impose preferred orientation on carbon nanotube in a composite matrix	Flexural modulus increased by ~21% with random CNTs Flexural strength increased by ~33% with aligned CNTs Flexural strength increased by ~15% with random CNTs	
CNT-CF Epoxy	Nanofiller modification- CNT grafted onto short CF reinforced epoxy interleave at the interface of CF epoxy laminate Fabrication- hand layup, vacuum bag and hot press	Interleaved composite G_{IC} improved by ~125% with 1mg/cm^2 Bulk composite G_{IC} improved by ~367% & K_{IC} by ~142% with 2.5 wt% SCF CF epoxy composite	[161]
CNT-CF Epoxy	Nanofiller modification- CNT grafted onto CF pre-preg surface through transfer printing which act as an interleave Fabrication-autoclave	Mode I interlaminar fracture toughness increased by ~150% Mode II interlaminar fracture toughness improved by ~62%	[162]
5 wt% GO- CF Epoxy	Nanofiller modification- GO added to sizing using normal mixing Fabrication- dry oven, resin infusion and autoclave	ILSS- improved ~12.7% IFSS-improved by ~70% Tensile Strength by ~13.7% Weibull Modulus by ~45.8%	[168]
GO-CF Epoxy	Nanofiller modification- CF surface through electrophoretic deposition	IFSS improved by ~ 73%	[27]
GO-CF Epoxy	Nanofiller modification- GO grafted short CF reinforced epoxy interleaf at the interface of CF epoxy laminate Fabrication- hand layup, vacuum bag and hot press	ILFT improved ~171% with 2 g/m^2 GO Fracture resistance improved ~108% with 2 g/m^2 GO	[163]
Gr/Cu-CF Epoxy	Nanofiller modification- CF surface through electrophoretic deposition	Flexural Strength improved by ~76% with 40V applied voltage Flexural Modulus improved by ~37% with 50V applied voltage	[19]
Exfoliated Gr-CF Epoxy	Nanofiller modification- exfoliated Gr on CF surface liquid phase deposition strategy (extended dip coating) Fabrication- Resin transfer moulding	ILSS improved ~28.3% with 1 wt% Gr	[164]
Diamine GO-CF Epoxy	Nanofiller modification- to epoxy matrix with and without functionalized GO Fabrication- hand layup, VARTM, autoclave	Tensile strength improved ~23% Flexural strength and modulus showed insignificant improvement	[167]
3 wt% Gr-CF Epoxy	Nanofiller modification-dip coating of CF Fabrication- drum winding, hand layup, autoclave	Flexural strength (90^o) improved by ~52% Flexural strength (0^o) improved by ~7% ILSS improved by 19% Electrical conductivity through thickness direction by 165%	[8]

2.9 Summary of the Literature Reviewed

Interface is the one that controls the improvement in properties of FRPs. The inert nature of CF limits its potential as a reinforcement to the epoxy matrix, due to the inherently poor interfacial bonding between them. This is a major drawback of CF epoxy composite and a lot of research has been done to overcome this drawback over the past few years. Modifying or treating the CF surface, to induce roughness (mechanical interlocking) or functional group (chemical bonding), is the most conventional approach to improve its interfacial properties. The most common techniques based on conventional approach for fiber treatment include sizing, acid modification, electrochemical modifications, plasma surface, high energy irradiation, thermal modification and ozone treatments. Wide spread availability, excellent properties, high surface area have made carbon nanofillers the most preferred choice for this purpose. Techniques, like, CVD, electrophoretic deposition, chemical grafting, dip coating etc., are being used to modify CF surface by grafting/depositing/growing/ coating nanofiller, to improve its interfacial bonding with epoxy matrix. However, the limitations associated with this approach or the techniques are fiber damage, controlling multiple parameters simultaneously, harsh conditions along with the difficulty in scaling up these process. Carbon based nano-fillers have shown a lot of promise in improving the mechanical properties, like, tensile, fracture, flexural strength etc. of epoxy matrix both in bulk as well as multiscale composite. Moreover, the morphology of the carbon nanofillers also have differential effect on the final properties of the structure. Thus, it is evident that an optimum combination of 1D, 2D and 3D carbon based nanofillers can accumulate all the structure specific attributes to the CF epoxy composite. Also, the synergistic effect of carbon nanofillers is hardly studied in polymer based composites, except for few studies on Gr-CNT epoxy composite. The improvement achieved in mechanical, thermal, electrical and other properties is limited as both Gr and CNT tend to agglomerate. The

morphology, as well as, the high surface area of nanofillers tend to reduce their reinforcement efficiency. No study is reported in literature, till date, on use of hybrid combination of carbon nanofillers, with a combination of three different morphologies. Thus, this study would explore the potential of a morphologically hybrid carbon nanofiller reinforcement in epoxy matrix, which has every possibility to produce a multiscale composite with improved mechanical properties than existing ones.

Further, advancements in macro carbon fiber based polymer composites is also facing the problem with directionally anisotropic mechanical properties and premature fracture from voids and stress concentration regions present in matrix. This study would look into developing a suitable carbon nanofiller reinforced matrix for the CFRP structures, to introduce improved interfacial adhesion and isotropic behaviour in terms of toughness and strength. This multiscale hybrid nanostructure is a novel one that can take care of existing problems with commercially used CFRPs.

CHAPTER 3

EXPERIMENTAL TECHNIQUES

This chapter describes the experimental techniques that are used to develop the carbon nanofiller modified carbon fiber epoxy composite for structural application. The details of materials composition and processing route, followed to successfully modify the matrix, are explained. Method used for fabricating multiscale composite using modified matrix is also given. This is followed by details of techniques used for characterizing the microstructural, mechanical, thermal and interfacial behaviour of the fabricated multiscale composite.

3.1 Materials

Epoxy monomer Epofine LY5052 (1, 4-butanediol diglycidyl ether) and hardener HY5052 (cycloaliphatic amine) were procured from Fine Finish Organics Pvt. Ltd., Mumbai, India. Multiwalled Carbon Nanotube (CNT), having more than 95% purity, outer diameter of 40-70 nm, length of 1-3 μm and density of 2.1 gm/cm^3, was procured from Inframat Corporation (Willington, CT) (figure 3 (a)). Graphene nanoplatelets (Gr), having purity more than 95%, surface area of 120-150 m^2/g and average lateral size of 15 μm, were procured from XG Sciences, USA as shown in figure 3(b). Nanodiamonds (NDs), having purity more than 97% and average size of < 10 nm, were procured from Sigma Aldrich, India (figure 3(c)). Bidirectional carbon fabric (HinFab™ HCP 301) was supplied by Hindoostan Composites Solutions, India, with filament diameter 7 μm and density 1.8 gm/cm^3.

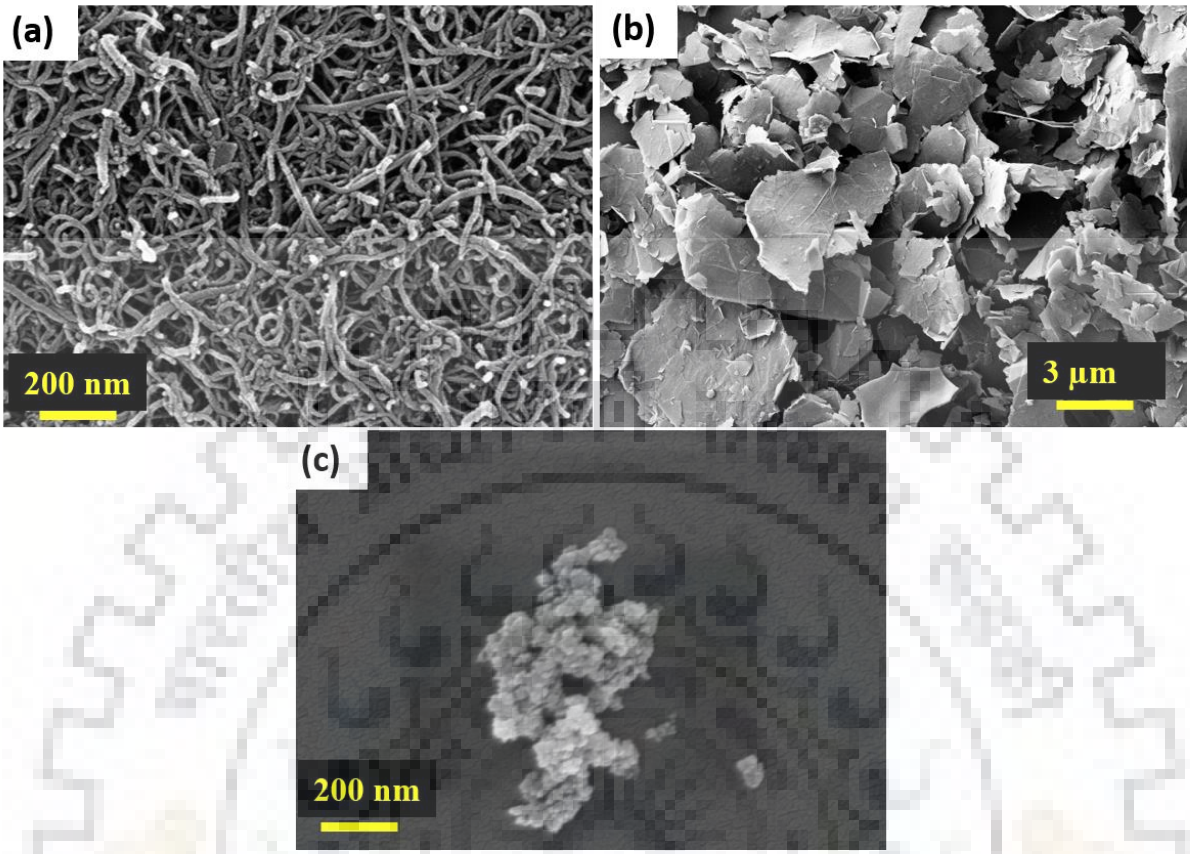

Figure 3. FE-SEM images of as received **(a)** CNT, **(b)** Gr and **(c)** ND

3.2 Processing

3.2.1 Dispersion of Nanofillers in Epoxy Matrix

Gr, CNT and ND were individually dispersed in acetone using probe sonicator (PKS-750F, PCI Analytics, Mumbai, India), at an amplitude of 70% for 60 min, with 5 seconds ON and 3 seconds OFF cycle and temperature ≤ 10ºC (maintained in ice bath). To achieve uniform dispersion, 0.01gm of filler/20 ml of acetone was taken for sonication.

For Gr-ND, Gr-CNT, and CNT-ND hybrid, one half of the homogeneously sonicated ND, CNT and ND solution was added to the homogeneously sonicated Gr, G and CNT solution, respectively, followed with sonication for 10 min after the other half of the solution is poured.

While, for Gr-CNT-ND hybrid, the homogeneously sonicated ND solution was equally divided into two halves. The one half of the ND solution was mixed into Gr solution in parts, while the other half was mixed into CNT solution in parts, followed with sonication for 10 min after each time the solution is poured. Finally, both the binary solutions were then mixed together and sonicated for another 20 min till the homogeneous solution is prepared.

After the fillers were homogeneously dispersed in each case, epoxy was poured into the solution in three equal parts with intermittent mixing. Care was taken to confirm proper dispersion of viscous epoxy solution by sonicating the solution for 10 min in between each part of epoxy is added. Sonication was continued for around 20 min after all the epoxy is poured. The solution was then kept over hot plate magnetic stirrer at 70ºC, for 6-7 hours, rotating at 400 rpm, to remove all the acetone completely.

3.2.2 Fabrication of Different Composite Systems

3.2.2.1 Nanofiller Epoxy Composite

Once the acetone is removed completely, the hardener is added to epoxy in the ratio of epoxy: hardener as 100:38 parts by weight. The mixture (resin) is then subjected to vacuum to remove the trapped air and reduce porosity. It is finally poured into silicon rubber moulds and left for room temperature curing. The unary composites were fabricated for 0, 0.1, 0.2, 0.3, 0.5 & 1 wt% reinforcement content. For binary composite, two compositions were selected, i.e. the highest value out of the individual best (optimized unary composition) and the sum of individual best of Gr/CNT/ND epoxy composite. Both compositions were tested for 5 different ratios i.e. 100:0, 75:25, 50:50, 25:75, 0:100.

Similarly, for ternary combination two compositions were selected i.e. the sum of individual best (optimized composition) of Gr/CNT/ND epoxy composite and the other composition is the one

which gave best combination of properties for binary composite. Both the composition were tested for 4 different ratio of Gr:CNT:ND i.e. 25:25:50, 25:50:25, 50:25:25 and 33:33:33.

3.2.2.2 Multiscale Carbon Fiber Epoxy Composite

Once the acetone is removed completely, the hardener is added to epoxy in the ratio of epoxy: hardener as 100:38 parts by weight. The mixture (resin) is then subjected to vacuum to remove the trapped air and reduce porosity. The composite laminate was than fabricated from eight layers of bidirectional carbon fabric using the nanofiller modified epoxy, as well as, neat epoxy. The laminated composite was fabricated using vacuum resin transfer moulding process, where a steel plate was kept underneath. A teflon film was inserted at one edge in the mid plane to provide a starter pre-crack notch for interlaminar fracture toughness samples, before sealing the sample inside the vacuum bag. After resin infusion, the bag was then left for 24 h at room temperature for curing.

The compositions selected here are optimized from the systematic studies conducted in for each nanofillers at different compositions and combinations. The composite laminate was fabricated for pure epoxy, 0.8 wt% (25Gr:25CNT:50ND), 0.8 wt% (25Gr:50CNT:25ND) and 0.8 wt% (33Gr:33CNT:33ND) and will be referred hereafter as, CF-epoxy, 225 GCN CF-epoxy, 252 GCN CF-epoxy and 333 GCN CF-epoxy composite. The samples were then cut from the laminates for uniaxial tensile test, interlaminar as well as intralaminar fracture toughness and interlaminar shear strength.

3.3 Characterizations

3.3.1 Microstructural and Structural Characterization of Nanofillers and Composite

3.3.1.1 Scanning Electron Microscopy

Once the nanofillers are homogeneously dispersed and exfoliated in acetone, prior to epoxy addition, a drop of the solution is suspended on carbon tape and left to air dry. The carbon tapes were then exposed to Field Emission Scanning Microscope (FE-SEM, Carl-Zeiss Ultra Plus) operated at 20 kV operating voltage to confirm the morphology, dispersability and arrangement of nanofillers in unary, binary and ternary combinations. The fractured surfaces of composites were investigated for defects (porosity, cracks etc.), interfacial interaction, active strengthening and toughening mechanism in composites. All samples were sputter coated with gold before observing in FE-SEM.

3.3.1.2 Transmission Electron Microscopy

After the nanofillers are homogeneously dispersed and exfoliated in acetone, prior to epoxy addition, a drop of the solution is suspended on Cu coated Transmission Electron Microscopy (TEM) grid placed on Teflon sheet and left to dry. The TEM grid is then exposed to Transmission Electron Microscope (TEM, Jeol, JEM 3200FS, USA) operating at 300 kV to verify morphology, dispersability and arrangement nanofillers in unary, binary and ternary combinations and interfacial interaction (between matrix and fillers). For verifying, the interaction between ND and epoxy matrix, sections having thickness ~70 nm were cut from the composites, through ultramicrotome (leica, EM UC6/UC7, Germany) equipped with diamond knife.

3.3.1.3 Scanning Probe Microscopy

The size distribution of ND, Gr and ND decorated Gr were analyzed through Scanning Probe Microscopy (SPM) module of Hysitron TI950 triboindenter equipped with three sided berkovich indenter with tip radius of 100 nm. The samples were prepared by suspending a drop of Gr, ND and ND decorated Gr, produced by wet-mechanical exfoliation (sonication) on silicon wafer. The thickness of ND, Gr and Gr-ND were evaluated by processing SPM images through SPIP^{TM} software (Image Metrology A/S, Horsholm, Denmark).

3.3.1.4 Modulus Mapping

Storage modulus maps of polished surface were obtained in nanoDMA mode using Hysitron TI-950 Triboindenter (Hysitron Inc, USA), equipped with three sided berkovich indenter with tip radius of 100 nm. The scanning of the surfaces during mapping employs the scanning probe module integrated to the nanoindenter. Modulus mapping was done at static load of 2 µN, dynamic load of 0.3 µN and frequency of 200 Hz. The 2D maps, used to assess the dispersion as well as estimate the size, morphology and density of ND rich regions inside epoxy at higher magnification, covers an area of 5 µm x 5 µm and 2 µm x 2 µm, respectively. While all other 2D maps used in this study cover an area of 10 µm x10 µm on the sample surface. Each map includes a matrix of equally spaced 256 x 256 points, resulting in 65,536 measurements in each scanning.

3.3.2 Mechanical Characterization of Composite

Mechanical properties were analyzed through tensile test, three-point bend test and nanoindentation. The tensile test and three-point bend test was done using H25K-S UTM from Tinius Olsen Testing Machine Company, USA.

3.3.2.1 Tensile Test

Dog bone samples were made for tensile test according to ASTM D638 (V) standard for nanofiller reinforced epoxy composite. The samples were tested at a strain rate of 1 mm/min. While for multiscale composite tensile test samples were made according to ASTM D3039. The samples were tested at a strain rate of 1 mm/min. The stress-strain curves of the tensile test specimens were used for determination of Young's modulus (E), tensile strength and % strain (at break).

3.3.2.2 Fracture Toughness

Single etched notched beam (SENB) samples were tested using 3-point bend test set-up at a strain rate of 1 mm/min. Force-displacement curve was used to determine fracture toughness of pure epoxy and composites. ASTM D5045-99 was used for calculating fracture toughness.

Five samples for each composition were tested for the repeatability of the results and the average of these quantities, with standard deviation, were reported. Failed samples from tensile and fracture toughness tests were characterized using FE-SEM to understand the failure mechanism.

3.3.2.3 Nanoindentation Elastic modulus and Hardness

Nanoindentation test was performed using Hysitron TI-950 Triboindenter (Hysitron Inc, USA), equipped with three sided berkovich indenter with tip radius of 100 nm, to determine the modulus (E) and hardness (H) of the composite. It was operated at a loading rate of 100 μN/s, up to maximum load of 1000 μN for CNT/Gr epoxy composite and 500 μN for ND epoxy composite with 2 s holding at peak load. To prevent any damage to the tip due to the high hardness of ND in comparison to Gr and CNT, the peak load was chosen less. Fifteen indents were taken on each

sample to evaluate the average hardness of the composite. Young's Modulus was determined from the unloading part of the load vs depth plot of the indents following the Oliver–Pharr method.

3.3.3 Interlaminar Properties of Laminated Fiber Composite

Interlaminar properties were analyzed through tensile test, short beam shear test, three-point bend test and double cantilever beam test using H25K-S UTM from Tinius Olsen Testing Machine Company, USA.

3.3.3.1 Interlaminar fracture Toughness

Interlaminar fracture toughness test was done using H25K-S UTM from Tinius Olsen Testing Machine Company, USA. ASTM D5528, modified beam theory (MBT) method was used for calculating interlaminar fracture toughness. Double cantilever beam (DCB) samples that were 165 mm in length, 20 mm in width and initial crack length 50 mm were tested at a strain rate of 1 mm/min. The samples were cut from a 180 mm × 160 mm composite plate, fabricated by stacking 8 layers of carbon sheets. A non-adhesive vacuum bagging plastic film of length 63 mm, sprayed with mould release agent, was inserted at the mid plane to form an initiation site for delamination. Load vs displacement plot was recorded to measure the interlaminar fracture toughness using the equation given below.

$$G_1 = \frac{3P\delta}{2b(a+|\Delta|)} \quad (1)$$

Where, P is the load, δ is the load point displacement, b is the specimen width and a is the delamination length, |Δ| may be determined experimentally by generating least square plot of cube

root of compliance $\sqrt[3]{C}$ as function of delamination length. Compliance *C* is the ratio of load point displacement to the applied load.

3.3.3.2 Interlaminar Shear Strength

Short beam shear test was used to measure the interlaminar shear strength (ILSS) of composites according to ASTM D2344. The sample was loaded under 3 point bending with strain rate of 2 mm/min. Load vs displacement plot was recorded for each sample. The length to thickness and span to thickness ratio were kept constant at 7 and 2. The interlaminar shear strength is calculated using equation 2.

$$ILSS = \frac{3P}{4bt} \quad (2)$$

Where P is the load, b is the specimen width and t is the specimen thickness.

Five samples for each composition were tested for the repeatability of the results and the average of these quantities, with standard deviation, were reported. Failed samples from interlaminar fracture toughness tests were characterized using FE-SEM to understand the failure mechanism.

3.3.4 Thermal Degradation Analysis

Thermogravimetric analysis (TGA) was performed using SII 6300 EXSTAR TG/DSC instrument to study the change in thermal stability of pure epoxy with addition of nanofillers and carbon fiber reinforcement. For TGA, 10 mg of sample in powder form was heated from 25ºC to 600ºC for nanofiller reinforced epoxy and 25ºC to 1000 ºC for multiscale composite, in alumina pan at a rate of 10ºC/min, under nitrogen purging at a flow rate of 200 ml/min. The thermal degradation is studied in terms of percentage weight retention of composite powder with increase in temperature.

3.3.5 Thermo-Mechanical Characterization of Composites

Dynamic mechanical analysis (DMA) (Model 8000, Perkin-Elmer) was used to determine the thermomechanical properties of epoxy and composites. Rectangular specimens of dimensions 30 x 10 x 2 mm were tested in a single cantilever mode. All the tests were performed for the temperature range of 25ºC to 250ºC at the heating rate 2 ºC/min for a constant frequency of 1 Hz. and dynamic loading range of 0 to 10 N. DMA is used here to study the effect of addition of fillers on the mobility of surrounding polymer through properties storage modulus, damping capacity, etc. as a function of temperature as well as glass transition temperature of composite system.

3.3.6 Contact Angle Measurement

After the nanofillers were properly exfoliated and integrated into 3D network, epoxy was poured into the solution in parts with intermittent mixing. Care was taken to confirm proper dispersion of viscous epoxy solution by sonicating the solution for 10 min in between each part of epoxy is added. After the epoxy is poured and mixed properly the solution was then kept over hot plate magnetic stirrer at 70ºC, for 6-7 hours, rotating at 400 rpm, to remove all the acetone completely. The uncured epoxy containing well connected 3D network of ternary nanofiller was dropped on the carbon fiber surface to study the wettability and infiltration 62ehavior between the two, i.e. with and without nanofillers, using sessile drop method (DSA25, KRÜSS GmbH, Germany). The contact angle was measured using ImageJ software at different time intervals.

3.3.7 Numerical Analysis

Numerical analysis of RVE was carried out in finite element software ABAQUS using python script to evaluate the elastic modulus of randomly dispersed circular shaped particles of ND

in epoxy matrix. Uniform displacement boundary condition overestimates the effective properties, while uniform traction boundary condition underestimates them. Therefore, periodic boundary conditions have been used to evaluate elastic properties in this study.

To predict the effect of improved exfoliation of Gr with the addition of ND on toughening behaviour of epoxy numerical analysis was done. 2D analysis of SENB specimen was performed under plane stress condition using finite element code in ABAQUS software. Elastic properties obtained using Hashin-Shtrikman approach were used in the FE analysis. As a response, force and displacement were obtained under specific loading and boundary conditions.

CHAPTER 4

RESULTS AND DISCUSSION

4.1 Comparing the Potential of Nanodiamonds, Carbon Nanotubes and Graphene as Reinforcement to Epoxy Matrix

The present study investigates the effect of CNT, Gr and ND as individual reinforcements in epoxy matrix, for a range of nanofiller content (0.1 – 1 wt%). A number of articles are available in open literature regarding the mechanical, thermal, electrical and thermomechanical properties of CNTs, Gr and ND in polymers, used individually as reinforcement, especially in epoxy resins. However, it is difficult to get a comparative view on the effect of these reinforcements on epoxy, just from articles studies made individually, as the compositions, fabrication techniques and processing conditions vary widely from case to case. These are important factors, having significant effect on the final property of the composite. The behaviour of these nanofillers and their interaction with epoxy matrix can be quite different, considering their vastly different morphologies. At the nano-scale length, morphologies become very significant in defining the behaviour of any material, as compared to their bulk counterparts. Thus, it is highly possible that CNTs, Gr and NDs might show their best effect/outcome as reinforcement at different contents. This requires comparative analysis of the effect of reinforcement for a range of content.

Thus, composites, containing different amount of nanofillers, are fabricated using ultrasonic cavitation (probe sonicator), a strong tool for effective dispersion of nanofillers in matrix. Mechanical (tensile and fracture) properties are studied thoroughly. The mechanical properties are analysed in terms of Young's modulus, ultimate tensile strength, % strain (at break) and fracture toughness. Thorough microstructural studies are performed to evaluate dispersion, strengthening and toughening mechanisms operating. DMA is used to study the effect of temperature on

mechanical properties, like, storage modulus and glass transition temperature, crosslinking density and damping capacity of the composites, as a function of different reinforcement types and content. The results, obtained from all the tests, are thoroughly analysed to comprehend the individual effect of each of these nanofillers, i.e., CNT, GNP and ND, on the performance of the composites, during service condition in structural applications.

4.1.1 Microstructural Characterization of Nanofillers to Confirm Morphology and Dispersion

FE-SEM and TEM micrographs, revealing the morphology of CNT, Gr and ND, are as shown in figure 4.1. The micrographs in figure 4.1(a, d) reveals the tube like morphology of CNT with outer diameter of ~40 nm. CNTs are found entangled together due to their high aspect ratio. The morphology of Gr is in the form of stacked wrinkled nanoplatelets, as revealed in figure 4.1(b). The opaque dark black color in TEM image in figure 4.1(e) confirm the stacking of Gr. The nanosheet has dimensions of ~15 µm along the length and ~10 µm along the width (figure 4.1b). Due to the smaller size and high surface energy, the NDs can be seen forming small clusters (figure 4.1(c & f)). However, the agglomeration in case of ND is not that severe. This is due to the spherical morphology of ND, which has a less tendency to agglomerate as compared to the sheet or tube like morphology. The average size of NDs is ~10 nm. Comparatively analysis of figure 4.1 with figure 2 clearly shows the extent of dispersion achieved, post sonication.

Stacking of Gr nanosheets, entanglement of CNTs and clustering of NDs reduce the overall exposed surface area. Thus, the total interface area with the polymer matrix is reduced in the composite structure. Due to high surface energies, nanofillers have the tendency to agglomerate. Thus, their effective dispersion is always a challenge.

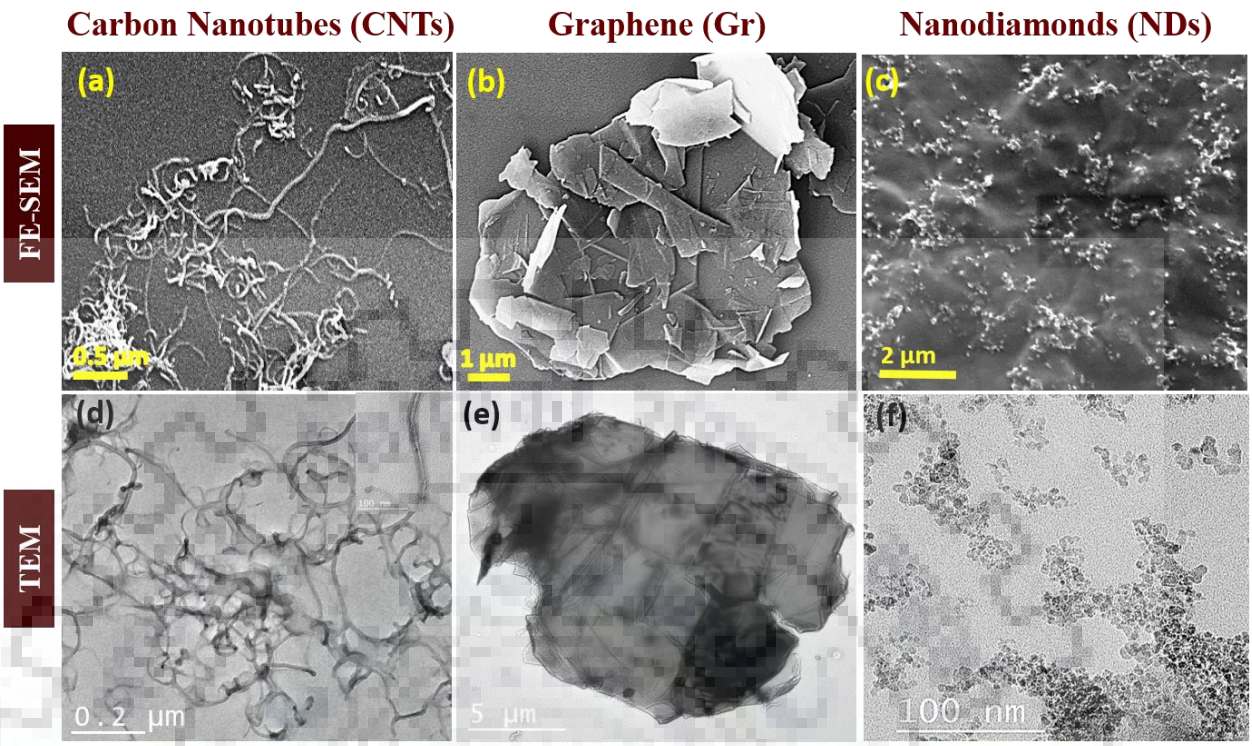

Figure 4.1 FE-SEM and TEM images of **(a, d)** CNTs, **(b, e)** Gr and **(c, f)** NDs

In order to achieve maximum improvement in properties, ultrasonic cavitation (probe sonicator), a strong tool for effective dispersion, was used. The parameters used for sonication play a major role. Too low of either amplitude or timing may lead to improper dispersion, whereas too high of amplitude or timing may severely damage the surface and reduce the size of CNT/ Gr due to breakage [217, 218]. Even the sonication temperature has a detrimental effect on their exfoliation [219]. Thus, the parameters of sonication have been optimized in this study to have the optimized dispersion without damaging.

The sonication parameters were optimized and some important modifications were incorporated in the fabrication technique as well. The fabrication technique, used in the present study, is simple, but at the same time, widely suitable and preferred for bulk production. So, to make it more efficient, nanofillers were first thoroughly exfoliated in the solvent and then epoxy was added

to it in batches (and not in one go), with significant interval of time in-between. This modification in technique has led to better dispersion of fillers and strong interaction with epoxy, leading to significant improvement in mechanical behaviour of the composite structure.

4.1.2 Fracture Surface Analysis of Epoxy and Nanofiller Reinforced Epoxy Matrix

Fractured surfaces of epoxy and CNT/Gr/ND epoxy composites are shown in figure 4.2. CNTs, Gr and NDs are found uniformly dispersed and properly embedded in epoxy matrix, revealing strong interfacial interaction and effective load transfer (figure 4.2(d, g & j)). The dispersion is highly affected by sonication time and amplitude. Higher amplitude and longer sonication times often lead to nanofiller damages, like, crumbling and crimpling, leading to deteriorated mechanical properties. However, none of these is observed in the present study (figure 4.2). The presence of effectively embedded Gr on fracture surface is indicated by the sharp edges of the 2D sheets (figure 4.2(g)). In addition, the wrinkled morphology on the fractured surface denotes a strong interaction between epoxy and Gr. This strong interfacial interaction causes epoxy to reflect the wrinkles present on the Gr surface, as marked by arrows in figure 4.2(g). The graphene sheets are seen completely wrapped within the epoxy matrix with no traces of partially pulled out Gr (figure 4.2(g)). Unlike Gr, uniformly distributed and effectively nested CNT can be seen protruding out of the fractured surface (figure 4.2(d & e)).

Good dispersion and strong interfacial interaction between ND and epoxy can be clearly evidenced from figure 4.2(j & k). No free lying ND or any traces of porosity/hole, due to debonding, can be seen on the fractured surface, even at very high magnification. In fact, fracture surface gives an impression of being coated with polymer layer, indicating effective load transfer.

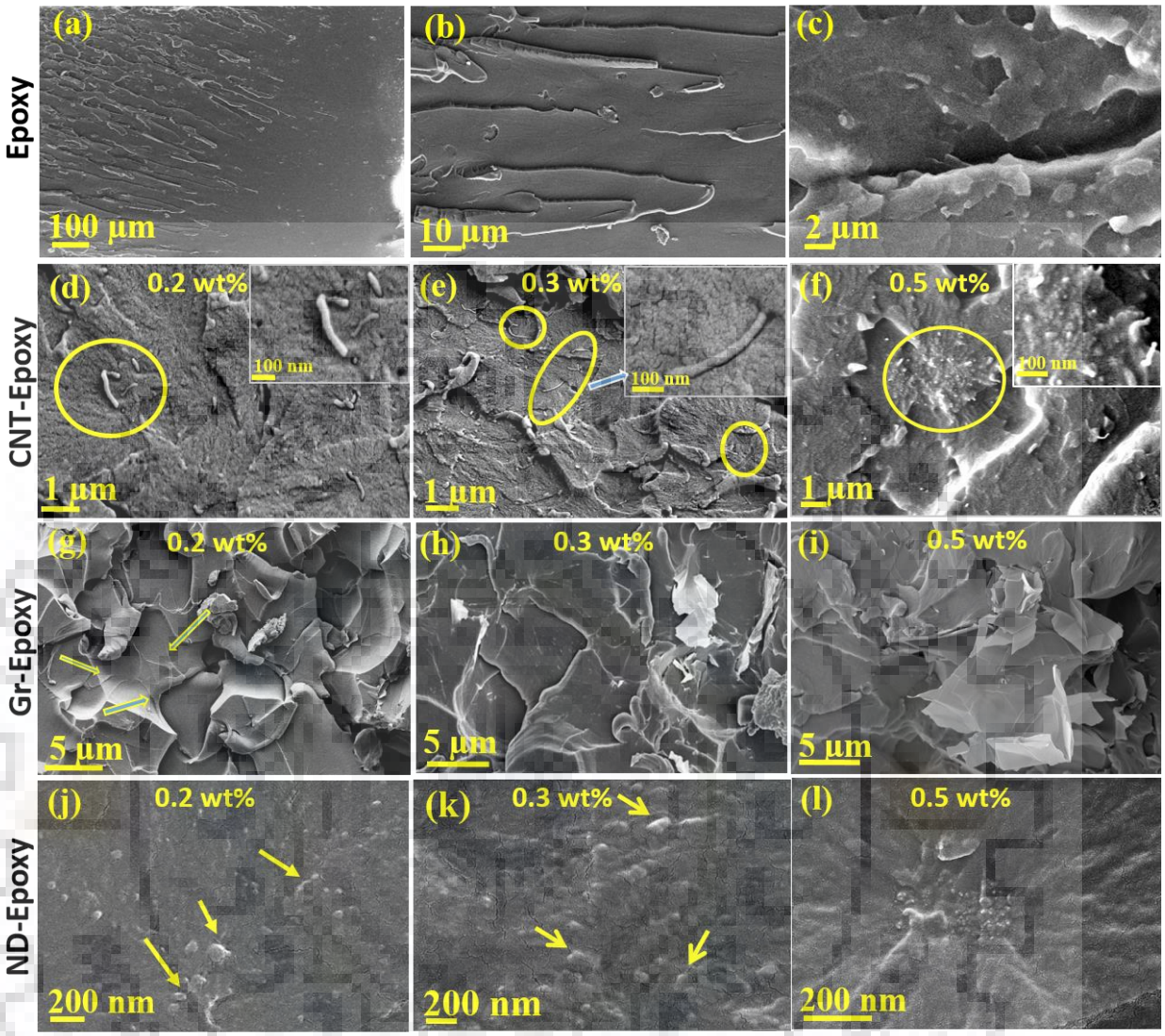

Figure 4.2 FE-SEM images for fractured surface of **(a- c)** epoxy, **(d- f)** CNT-epoxy composite, **(g-i)** Gr-epoxy composite and **(j-l)** ND-epoxy composite

The strengthening effect of CNT/Gr/ND on epoxy can be clearly seen from difference in the morphology of fractured surface of pure epoxy and epoxy-CNT/Gr/ND composites. Figure 4.2(a) shows the fractured surface of epoxy. The crack, once generated in this surface, propagates through until fracture, creating larger single crevices (figure 4.2(b)). However, in case of nanofiller reinforced epoxy (figure 4.2(e, h & k)), the fractured surface contains many smaller crevices. These are created as a result of resistance to crack propagation, offered by nanofillers.

Dispersion of nanofillers is very challenging and with increasing filler content it becomes even more severe. As seen from figure 4.2(f, i & l), increase in the Gr and CNT content leads to agglomeration. However, none of the fractured surfaces in present study showed traces of porosity or holes. These features indicate low adhesion or poor compatibility of nanofiller with epoxy. At higher concentrations, the Gr sheets appear to be on the surface with only one end embedded in the matrix, while the rest of it is dangling out with no epoxy traces on the surface. On the contrary, even at higher concentrations of CNTs, the agglomerate size is smaller and less severe than Gr. Thus, CNTs can retain good adhesion with the matrix. While in case of ND, the agglomerate size is quite small and completely coated with epoxy, making it less likely to undergo catastrophic failure. The present study also corroborates this differential behaviour of CNT, Gr and ND in epoxy matrix. The micrographs clearly show that instead of acting as an anchor to crack propagation, the agglomerated reinforcement phases act as sites for stress concentration and crack generation. Thus, apart from nanofiller content, its dispersion and interaction with the matrix is influenced by its shape, which in turn governs the mechanical properties.

As seen from these micrographs, due to the small size and spherical shape of NDs, it becomes really difficult to even trace them at low content. Therefore, though claimed by many reports [123, 127, 220, 221], only FE-SEM analysis is neither enough nor satisfactory to prove proper dispersion of nanofillers and strengthening effect offered by them.

4.1.3 Mechanical Behaviour of Epoxy and Nanofiller Reinforced Epoxy Composite

4.1.3.1 Hardness and Elastic Modulus of Nanofiller Reinforced Composite

Instrumented indentation technique was used to measure the hardness and elastic modulus of the epoxy and its composites. Figure 4.3(a, c & e) shows the representative load vs displacement

plots obtained from nanoindentation test for CNT-epoxy, Gr-epoxy and ND-epoxy, in load control mode. ND-epoxy composites have shown less indentation depth as compared to pure epoxy, for all compositions, which indicates higher hardness of the composite. The maximum improvement in hardness was 79%, 69% and 470%, for 0.3 wt% CNT, 0.2 wt% Gr and 1 wt% ND, respectively. Beyond these contents, the indentation depth increases marginally with increase in CNT/Gr concentration, which is due to the porosity and irregularities generated by agglomeration of nano-fillers. Figure. 4(b, d & f) shows the average hardness and their standard deviation for all compositions. Reinforcing epoxy with nanofillers increases hardness. This improvement is due to the presence of uniformly distributed stronger reinforcement, which shares the load transferred to the matrix and provides high resistance to the matrix against deformation. The improvement in hardness, is much higher with ND, than CNT or Gr. This is due to the higher hardness of the former, which offers more resistance to deformation. Also, less agglomeration and uniformly distribution throughout the matrix at higher concentration results into more number of hard particles resisting deformation. Hence, the cumulative resistance to deformation is much higher.

Similar trend was observed with elastic modulus, as seen from figure. 4.3 (b, d & f). The modulus of epoxy increased with increase in nanofiller content. The highest improvement was 31%, 23% and 94%, with 0.2 wt% Gr, 0.3 wt% CNT and 1 wt% ND, respectively. The strong interfacial interaction between the uniformly distributed stiff reinforcement phase and the epoxy matrix resists the deformation and help in effective load sharing. The properties deteriorate at further higher contents of CNT and Gr, due to the agglomeration, which leads to less population of individual stiff reinforcement phase available to resist the deformation of matrix.

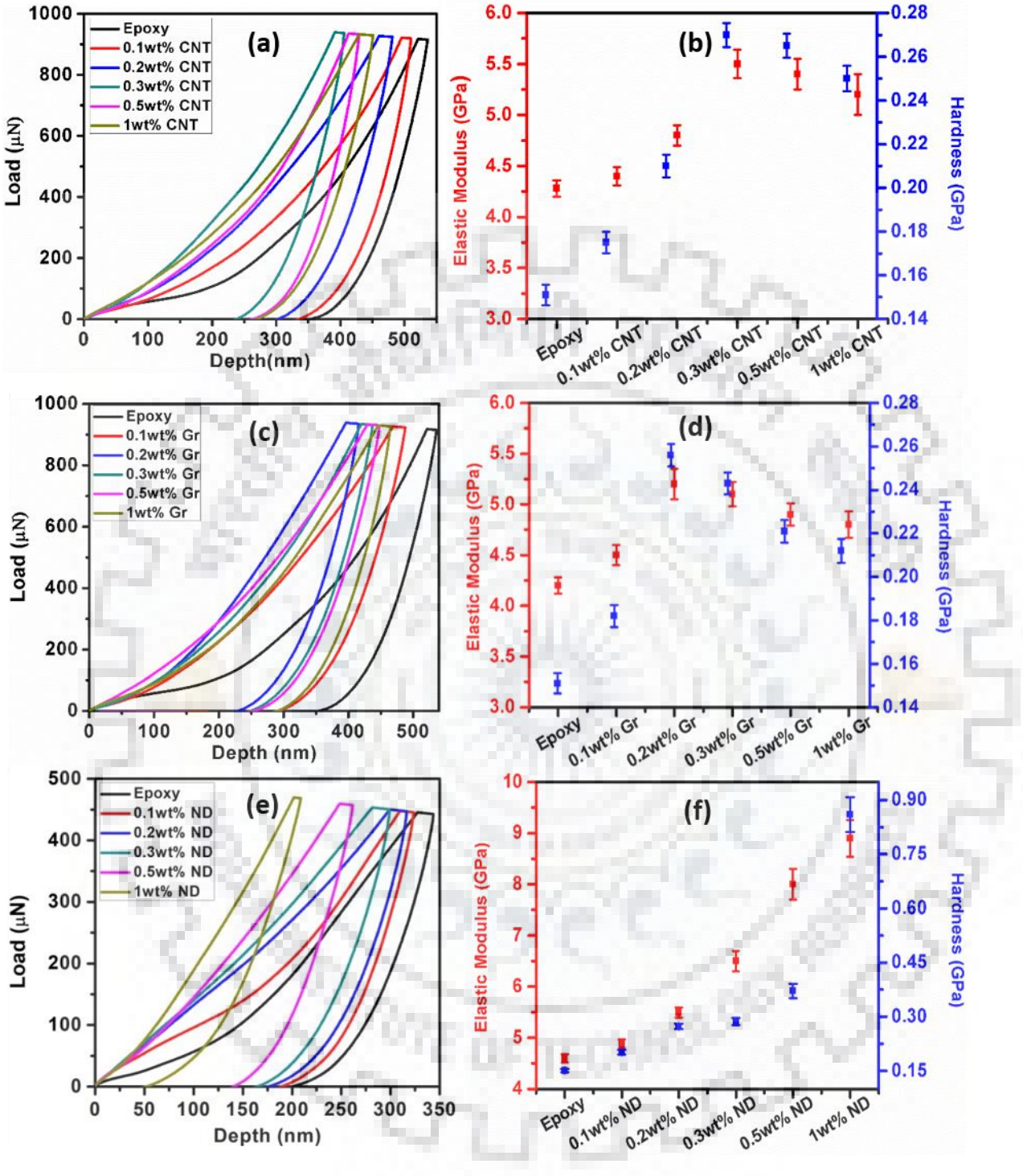

Figure 4.3 Representative load vs. displacement and elastic modulus-hardness plots for different composition of **(a, b)** CNT-epoxy, **(c, d)** Gr-epoxy and **(e, f)** ND-epoxy composites

In case of ND, the improvement in modulus of epoxy increased up to 1 wt% ND. However, the improvement was not as significant as with 0.5 wt% ND, even though the reinforcement content was doubled. This is due to the agglomeration and irregularities that start to appear with increase in ND content, leading to poor interfacial interaction. The improvement in hardness is quite significant, as compared to elastic modulus, which clearly shows that hardness is less sensitive to agglomeration. This is because hardness is improved by inhibiting deformation of matrix, which might be achieved by agglomerated NDs also. On the other hand, strong bonding between matrix and reinforcement or a good interface is the key reason behind the improvement of elastic modulus. Hence, even a small irregularity/non uniformity in structure or discontinuity in interface, due to agglomeration, is quite detrimental to modulus of the composite. Thus, the severity of agglomeration affects both hardness and elastic modulus, but to different extent.

4.1.3.2 Tensile Properties to Assess the Strengthening Imparted by Nanofillers to Epoxy Matrix

The typical stress strain response for uniaxial tensile tests of pure epoxy and composites are shown in figure 4.4(a, b & c). The properties determined from stress strain curve include ultimate tensile strength (UTS) and % strain (at break). A minimum of five samples per composition were tested for the repeatability of the results and average of these are reported with the standard deviation presented as error bars. As seen from figures 4.4, the addition of nanofillers increases strength and elastic modulus of epoxy matrix. The UTS of epoxy increased by ~18 %, ~24% and 56% with 0.3 wt% CNT, 0.2 wt% Gr and 0.3 wt% ND, respectively. The effective load transfer is the main strengthening mechanism in case of composites. The key ingredient to this is good dispersion of reinforcement in matrix and the strong interfacial interaction between the two.

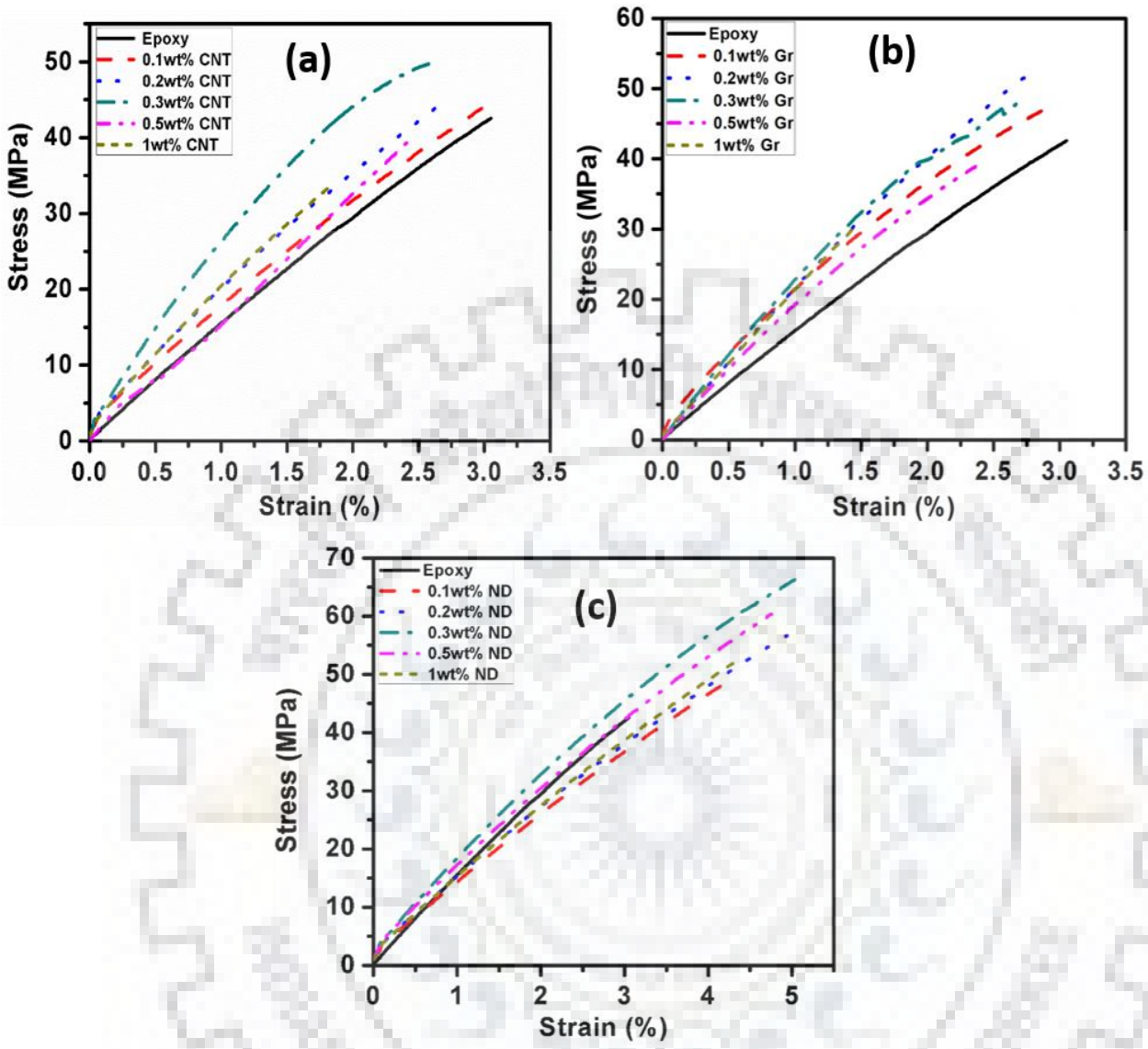

Figure 4.4 Stress-Strain curve for various composition of **(a)** CNT-epoxy, **(b)** Gr-epoxy and **(c)** ND-epoxy composite

However, a decrease in tensile strength was seen with the increase in CNT content above 0.3 wt%, Gr above 0.2 wt% and ND above 0.3 wt%. In fact, for Gr/CNT epoxy composite, above 0.5 wt%, the UTS became less than that of pure epoxy. The decrease in tensile strength at high nanofiller content is due to the high surface energy of nanofiller, which results in aggregation. As shown in figure. 4.2(g), the graphene sheets are completely wrapped within the epoxy matrix. No traces of partially pulled out Gr from the matrix could be seen on the fractured surface for 0.2 wt% Gr

composite. While, at higher concentrations, the sheets appear to be on the surface with only one end embedded in the matrix and the rest of it is dangling out with no epoxy traces on the surface (figure 4.2(i)). This suggests a weak interface between the nanofiller and the epoxy matrix.

For CNT-epoxy composite structures, the CNTs, which are aligned along the direction of applied load, could be seen protruding out of the fractured surface due to debonding with the matrix. This signifies fiber pull out due to weak adhesion (figure 4.2(d)). CNTs, aligned in other direction, could be seen with their surface exposed (inset figure 4.2(e)). The encircled region in figure 4.2(f) clearly shows the agglomerates of CNTs at some places, which acted as sites for stress concentration and crack generation. The improved modulus of composite, even after agglomeration, can be correlated to the very high modulus of nanofillers (~1 TPa).

High nanofiller content for ND-epoxy composite leads to decrease in the tensile strength, due to agglomeration. However, in all cases, the UTS was better than that for pure epoxy. This is because the agglomeration is not that severe even at the highest ND content (1 wt%), as seen in figure 4.2(l). The aggregated NDs are seen to be completely impregnated with epoxy, with no free lying ND on the surface. Any discontinuity in the network will act as a weakest link for load transfer and matrix will fail, when subjected to external loading. However, the severity of agglomeration dictates how much prone to fracture the composite is and at what load the composite would fail.

Gr-epoxy composite performs better than CNT-epoxy composite at low filler content (≤ 0.2 wt%). Uniformly dispersed sheet of Gr and relatively good sheet/matrix interaction effectively improve load transfer efficiency with the matrix and increase the tensile strength. Wrinkled surface morphology of graphene sheets is an added advantage as it promotes mechanical interlocking with the matrix [78][221]. Further, the rectangular (2-D) shape of graphene increases the packing density, thus reducing voids or defects. The poor reinforcement effect of graphene at higher concentration is

possibly due to the agglomeration of sheets, leading to weak interfacial interaction. Dispersability becomes difficult at higher concentration, due to high specific surface area. However, it is encouraging to find out that significant improvement in mechanical behaviour of Gr-epoxy is achieved at a very low weight fraction of reinforcement.

However, for > 0.2 wt% filler content, CNT-epoxy performed better than Gr-epoxy. As already discussed, the main strengthening mechanism is effective load transfer and the key ingredient to that is good dispersion and strong interfacial interaction. Intercalated 2D planar structure, high surface area and the extra π-π bond make dispersion of Gr difficult. On the other hand, CNTs are comparatively easy to disperse until they have very high aspect ratio [223]. If we compare the loading (0.5 wt%) at which both composites show agglomeration, it can be clearly seen that the severe agglomeration with no trace of even a thin interfacial layer of epoxy is imaged in the pulled out agglomerated Gr (figure 4.2(i)). While, in case of CNTs, the agglomeration was not that intense. In fact, the CNTs present in the agglomerate showed decent interaction with the epoxy (inset figure 4.2(f)). Therefore, the main reason for failure seems to be stress concentration, rather than weak interfacial interaction. Thus, CNT is a more effective reinforcement at high filler concentration, due to relatively better dispersion, strong interaction and efficient load transfer. Another added advantage is the high aspect ratio or tubular structure of CNT, which increases the efficiency of load transfer for the CNTs, aligned along the applied load direction. The probability of such occurrence increases with increase in CNT content.

If we compare ND-epoxy composite with CNT-epoxy and Gr-epoxy composite, the improvement in UTS in case of ND epoxy composite is better at every composition. This is quite unusual for a spherical morphology, as for effective load sharing the aspect ratio should be high. The tensile strength reduced after 0.3 wt% reinforcement content, which is due to clustering of NDs.

Though, it was better than epoxy for all cases. Interestingly, with the improvement in strength, simultaneous improvement in % strain of epoxy matrix is recorded with ND, with the highest improvement of 66% at 0.3 wt%. This improvement in strain with strength is quite unusual, considering the brittle nature of matrix. Addition of a hard and stiff reinforcement, is expected to make it more brittle. This finding demands further analysis of the mechanism dominating the mechanical behaviour of this composite. The spherical morphology of NDs is also believed to play the key role. Once a tensile stress is applied to a ND epoxy polymer composite, sliding of the polymer chains starts. The motion/rotation of NDs further facilitates this process, thus increasing failure strain or ductility [223]. However, this mechanism alone can't bring such huge improvement. Hence, this behaviour of ND in epoxy needs to be further investigated.

4.1.3.3 Fracture toughness to assess the Toughening Imparted by Nanofillers to Epoxy Matrix

Figure 4.5 presents fracture toughness as a function of CNT, Gr and ND content. Fracture toughness of all the nanofiller reinforced epoxy is higher than that of epoxy. The highest improvement in Gr-epoxy composite was 102%, obtained with 0.3 wt% reinforcement content. The same for CNT-epoxy and ND-epoxy composite was 152% with 0.5 wt% CNT and 85% with 0.3 wt% ND.

At least five samples, per composition, were tested for the repeatability of the results. Fracture toughness, reported here, is the average values from five tests, with the standard deviations presented as error bars. Figure 4.6(i) is the pictorial representation, depicting the fracture toughening mechanism active in epoxy, Gr-epoxy, CNT-epoxy and ND-epoxy composite. Figure 4.6(ii) shows the FE-SEM micrographs for fracture surfaces of epoxy and its composites. The crack initiated at the notched edge under tension for all specimen. As shown in figure 4.6(ii)(a), epoxy resin displays

a relatively smooth fracture surface indicating brittle behaviour, which is responsible for the low fracture toughness of epoxy. A crack, once initiated, propagates without any obstruction (i.e. bridging, deflection or pinning) up till fracture. In case of epoxy, the distance between the two cleavages is comparatively wide and smooth. However, with the introduction of reinforcement, fracture mode changes, as reinforcement obstruct the path of crack. As shown in figure 4.6(ii)(b & c), the rippled or stepped fracture surface of composite suggests toughening by reinforcement.

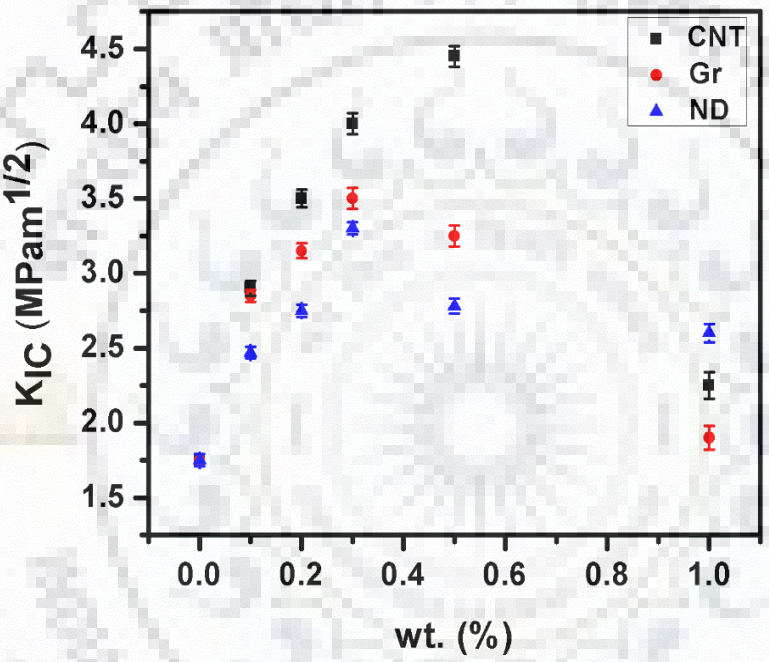

Figure 4.5 Fracture toughness variation as a function of reinforcement content

In case of Gr reinforced composite, the crack front encounters impenetrable obstacle in the form of Gr sheets during propagation. As a result, the crack is deflected, which increases the requirement of energy for progression of fracture [225]. A crack encounters multiple such obstacles before fracture, increasing the total amount energy absorbed before fracture. A series of obstacles on the way causes the crack to bow out between particles, known as crack pinning. It can be clearly seen on the fractured surfaces as arched or bow-shaped lines (figure 4.6(ii)(b)). In another instance, the crack may find a path of least resistance after repetitive deflection and finally propagates causing

failure. In either case, the fractured specimen does not show straight line brittle fracture, or any specific crack orientation. Fracture surface for Gr-epoxy, evidenced here, is a rough surface with randomly oriented cracks. The wrinkled surface morphology of graphene sheets improves the interfacial adhesion by mechanical interlocking with the epoxy matrix, which further resisted crack growth.

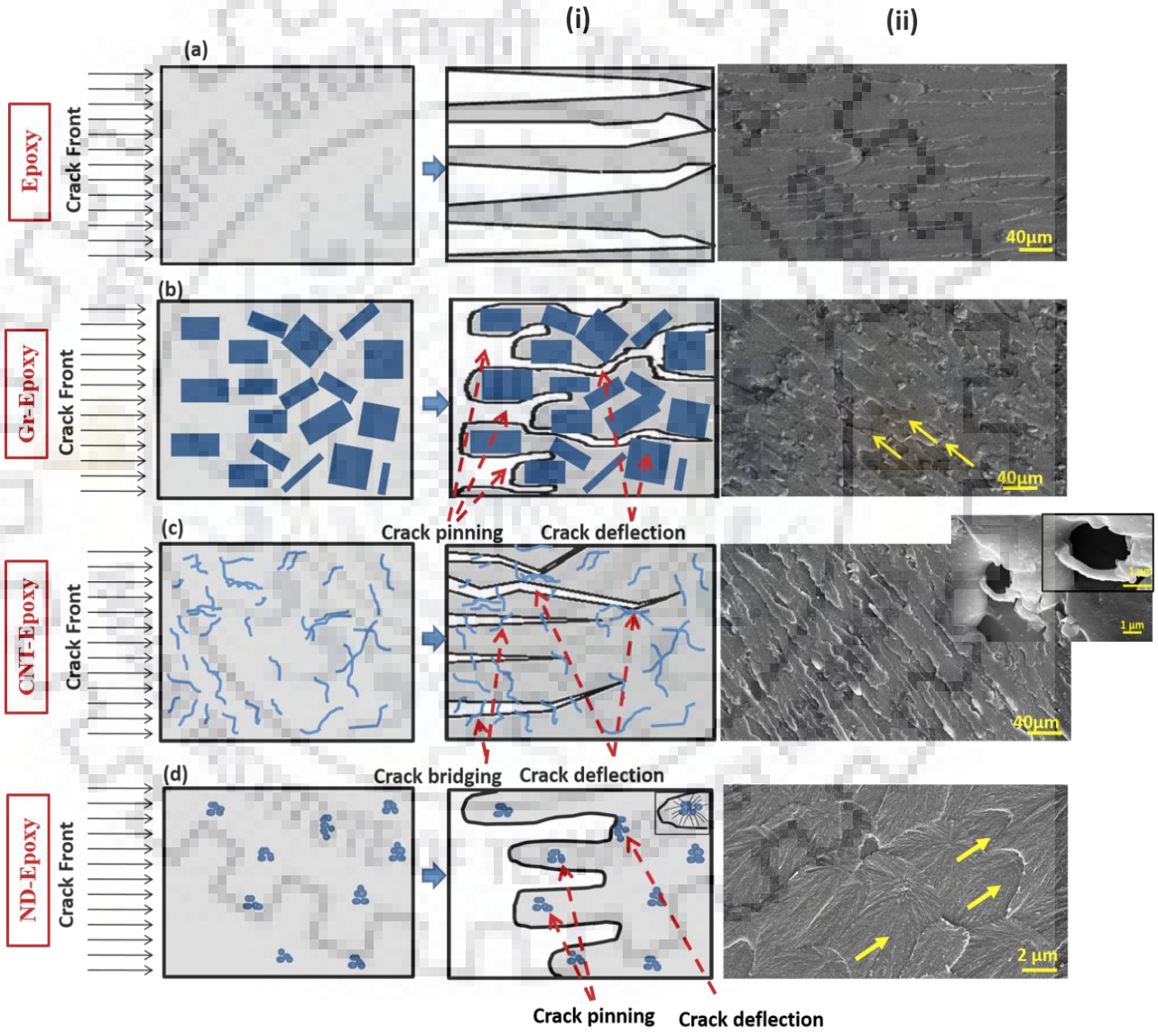

Figure 4.6 (i) Schematic representation and **(ii)** FE-SEM images showing dominant fracture mechanism in **(a)** epoxy, **(b)** Gr-epoxy, **(c)** CNT-Epoxy and **(d)** ND-Epoxy composite

Fracture toughness results suggest CNT introduced better toughening to epoxy matrix than Gr. Figure 4.6(ii)(c) shows the fractured surface for 0.5 wt % CNT, revealing reduction in cleavage plane and increment in surface roughness. These features are the result of the distorted path followed by crack tip at the wake of CNTs. The toughening in CNT-epoxy composite is caused by matrix deformation (elastic deformation or rupture), CNT rupture, interfacial debonding, crack deflection, CNT pullout and crack bridging [101]. The most dominant mechanism, out of them, is the crack bridging mechanism. CNTs are found acting as bridge in preventing the propagation of crack tip, as shown by a blow-out image in figure 4.6(ii)(c). With increase in CNT loading, the aggregates of CNTs can be seen (figure 4.2(f)). When subjected to low stress, the agglomerated particle increased the stiffness of the material. But, as the stress level is increased, these agglomerated particles act as a site for stress concentration or crack generation, finally leading to failure due to crack propagation.

In case of ND-epoxy composite, the crack propagation from the pre-notched line was either deflected in different angles or crack bows between particles (crack pinning), giving a hemispherical morphology (figure 4.6(ii)(d)) on the fractured surface. This is due to the presence of uniformly distributed nanodiamonds, which pin the cracks. Due to the presence of uniformly distributed nanodiamond, the development of cracks was effectively disturbed. Although the number of the cracks increased with increase in ND content, the average size of the cracks reduced as the nanodiamond content is increased. Meanwhile, many sub-cracks were induced in the fracture surface of the composites. The breakdown of propagating cracks, due to the presence of ND, certainly reduced local applied stress and thus contributed to the resistance of fracture. This is one of the main reasons for the improvement of the fracture toughness.

The highest fracture toughness, achieved for both Gr and CNT epoxy composite, is at a higher reinforcement content, than the one shown for maximum UTS and E. Higher amount of filler

leads to higher active sites for polymer to interact with reinforcement. In strengthening, load transfer efficiency is the main mechanism, which requires strong interfacial interaction. But, for toughening, the main strengthening mechanism is crack pinning, crack deflection or crack bridging. This requires more number of reinforcement interaction points in the path of a propagating crack, to deflect and bridge the same. At higher filler content, the crack front encounters more number of impenetrable obstacles. As a result, it either gets deflected or pinned down, losing all its energy. However, at very high filler content, nanofillers start agglomerating in larger masses and total number of obstacles on the path of the crack decreases.

The toughness, imparted by ND to epoxy matrix, was significant, but less than that by Gr and CNT, at same reinforcement content. This is because crack bridging is the most dominant toughening mechanism, especially for brittle material. In case of CNT-epoxy, it is the most active toughening mechanism, due to the fiber like morphology of CNT. It is also seen active in Gr-epoxy system due to the high aspect ratio of Gr. However, in case of ND-epoxy composites, crack pinning is the active toughening mechanism, while crack deflection is also seen at ND rich region or cluster, but no bridging occurs.

4.1.4 Thermal Analysis of Epoxy and Nanofiller Reinforced Epoxy Composites

4.1.4.1 Effect of Nanofiller Addition on Thermal Degradation of Epoxy matrix

Thermal stability of epoxy and nanofiller composites were investigated by thermogravimetric analysis (TGA) in nitrogen atmosphere. Degradation in mass as a function of temperature is presented in figure 4.7(a-c). Mechanical and/or thermal properties of CNT/Gr/ND-epoxy composites depend on the extent of dispersion and interfacial interaction between the nanofiller and epoxy matrix. Only 5% mass loss occurs up to 300°C for nanofiller reinforced

composites, which is due to the evaporation of moisture or volatile impurities. The degradation temperature was found to be ~340°C in each case, which is defined as the point of inflection on the TGA curve. The major mass loss of about 50% occurs between 350°C to 450°C. The incorporation of nanofillers did not have any significant effect on the thermal stability of epoxy. A careful observation at the initial degradation temperature between 300 °C and 400 °C (inset in the figure 4.7(b)) showed that the thermal stability of composite with 0.1 wt% Gr is slightly increased by ~5°C. Thermal stability is reduced at ≥ 0.3 wt% Gr content and the graph shifted towards low temperature in comparison with the epoxy. The improvement in thermal stability of the Gr composite is postulated due to a sheet barrier effect or torturous path effect, which prevents the entry of oxygen and exit of volatile products evolved at high temperature or during thermal degradation [80, 82, 222].

As already discussed in previous section, Gr starts to agglomerate at ≥ 0.3 wt%. As a result, the uncured epoxy, with reduced cross link density and the oxygen, trapped inside the pores of agglomerates, reduces the thermal stability. In addition, the surfaces of the Gr, present in the agglomerates, are not completely wrapped with epoxy or are exposed freely. This leads to easy oxidation of amorphous carbon present in Gr at high temperature and reduces the stability. However, the reduction in thermal stability is not quite significant (~5°C).

On the other hand, CNT reinforced epoxy composite showed lower thermal stability as compared to epoxy for all compositions (Figure 4.7(a)). The reason for reduction in thermal stability of CNT composites is the formation of conductive network by CNTs. Agglomeration and oxidation of amorphous carbon present on the exposed surface of uncoated CNT, similar to graphene, is an added reason for degradation at higher loading. However, the decrease in degradation is also non-significant in case of CNT by ~5°C only. As the higher nanofiller content reduced the thermal stability, the TGA analysis for 1 wt% Gr and CNT composites was not conducted.

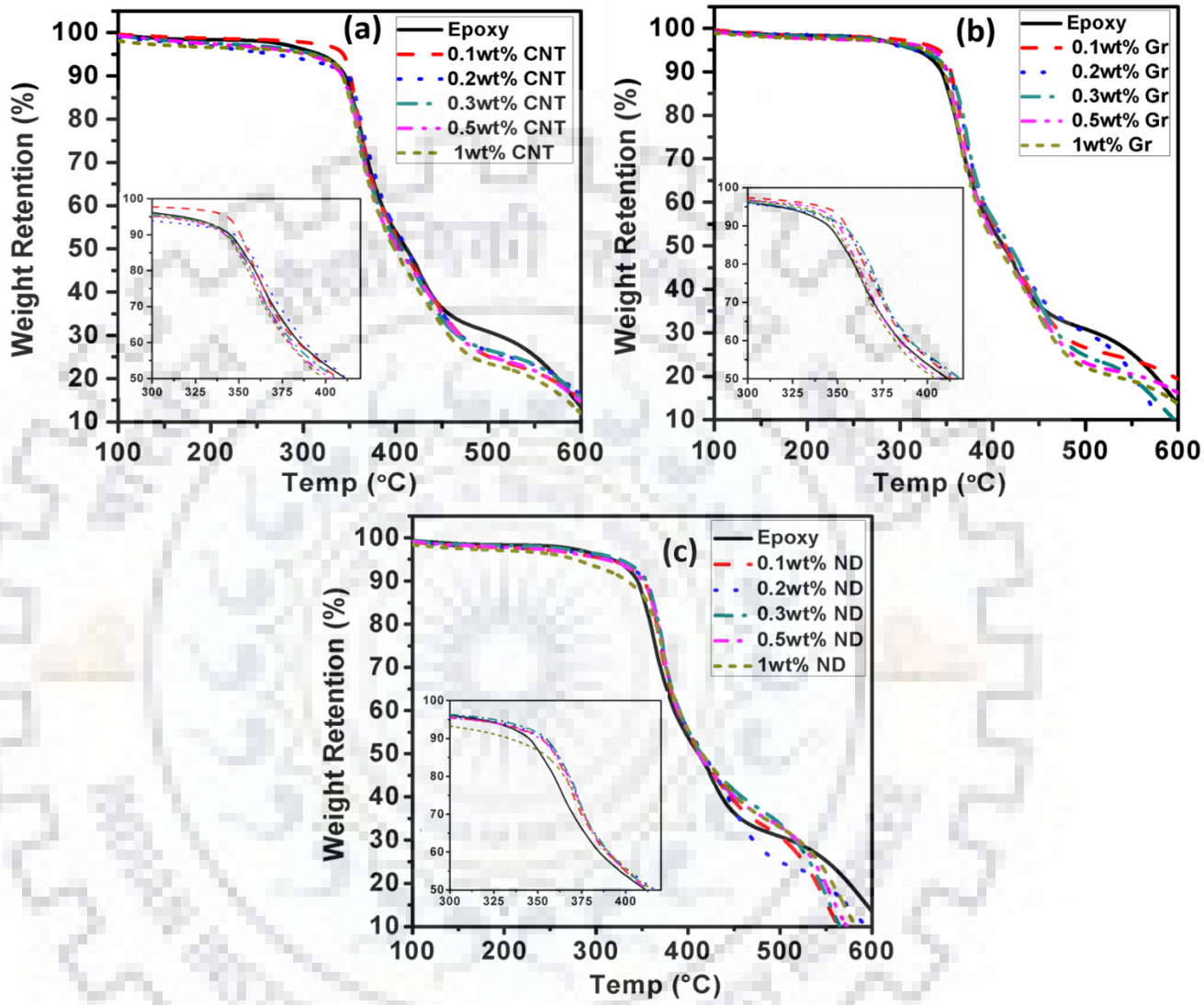

Figure 4.7 TGA thermogram for epoxy and various compositions of **(a)** CNT- epoxy, **(b)** Gr-epoxy and **(c)** ND-epoxy composite

Similarly, ND reinforced epoxy composite showed better thermal stability as compared to epoxy for all composition (figure 4.7(c)). As, ND has particle like morphology hence they cannot form long conducting networks. Also, ND has high thermal stability, so adding it to epoxy improves

its thermal stability by ~5°C only. The improvement is not quite significant as the concentration of ND is also very low.

In short, the addition of nanofillers did not show very significant effect on the thermal stability. Thus, the nanofiller addition did not have any negative effect on the thermal stability of epoxy, while offering impressive improvement in mechanical behaviour.

4.1.4.2 Thermo-Mechanical Analysis of Epoxy and Nanofiller Reinforced Epoxy Composite

Temperature-dependent mechanical properties of a material system, like, storage modulus, is evaluated by subjecting the structures to dynamic loading. Dynamic mechanical analysis was performed using single cantilever mode at a ramp rate of 2^0C/min, constant frequency of 1 Hz and dynamic loading range of 0 to 10 N. DMA is used here to study the effect of addition of fillers on the mobility of surrounding polymer. The typical DMA plots of storage modulus, as a function of temperature, for CNT-epoxy, Gr-epoxy and ND-epoxy composites are shown in figure 4.8(a, c & e). The value of storage modulus signifies stiffness of material, which tends to increase with the addition of CNT, Gr and ND. When added in small amount ≤ 0.1 wt%, the nanofillers did not offer remarkable effect on the storage modulus of epoxy. This is apparently due to the low amount of filler available to interact with the matrix. Increasing the content of CNT, Gr and ND resulted in a significant increase of modulus. The maximum improvement of ~29 %, ~26 % and 68% was obtained in storage modulus with 0.3 wt% CNT, 0.2 wt% Gr and 0.3 wt% ND, respectively. With filler content ≤ 0.2 wt%, Gr showed better reinforcing effect than CNT and ND, which is due to the intercalated structure and higher surface area of Gr leading to better load sharing ability. However, at 0.3 wt% filler content, CNT proved to be better reinforcement than Gr and ND. Gr tends to

aggregate, thus reducing filler matrix interaction. While, ND did not provide much reinforcing effect due to its spherical morphology.

With further increase in filler content to > 0.3 wt%, the modulus starts to increase for ND and reaches highest at 1 wt%. On the contrary, it starts to reduce for Gr and CNT, due to severe agglomeration. The retention of higher modulus by composites above room temperature, as compared to neat epoxy, is due to the restricted segmental mobility of polymer structure [82]. Storage modulus and elastic modulus are different properties. Thus, the values obtained for them are quite different. But the trend followed by them is same.

Figure. 4.8 (b, d & e) are representative tan δ (loss factor) vs. temperature plots, the peak value of which suggest the glass transition temperatures (T_g) [84, 86, 100, 226]. The increase or decrease in T_g and tan δ peak is thoroughly influenced by the interaction between the CNT/Gr/ND and epoxy, as it dictates the segmental mobility of polymer chain. This behaviour can be explained by dual monolayer theory which proposes the formation of 2 layers around the nanofillers inside the polymer matrix [227]. The first layer, formed close to the filler surface, is tightly clinched to the stiff filler hindering the motion of polymer chain. The second layer is formed little away from particle surface and is loosely bound. As the filler content increases, inter-particle distance reduces. The volume of immobile region also increases as more first layers are formed with higher filler content. These happenings lead to higher T_g and lower tan δ. The glass transition temperature is ~75^{0}C for pure epoxy, ~100^{0}C for 0.3 wt% CNT, ~104.8^{0}C for 0.2 wt% Gr and ~85.3^{0}C for 0.3wt% ND, which are the maximum T_g obtained for each type of composite. On addition of filler ≥ 0.5 wt%, the T_g dropped and became less than pure epoxy for Gr-epoxy. It can be attributed to higher mobility of uncured epoxy chains caged inside the filler aggregates at high content. The value of loss factor (tan δ) signifies damping behaviour, which is a measure of dissipation of energy under cyclic load.

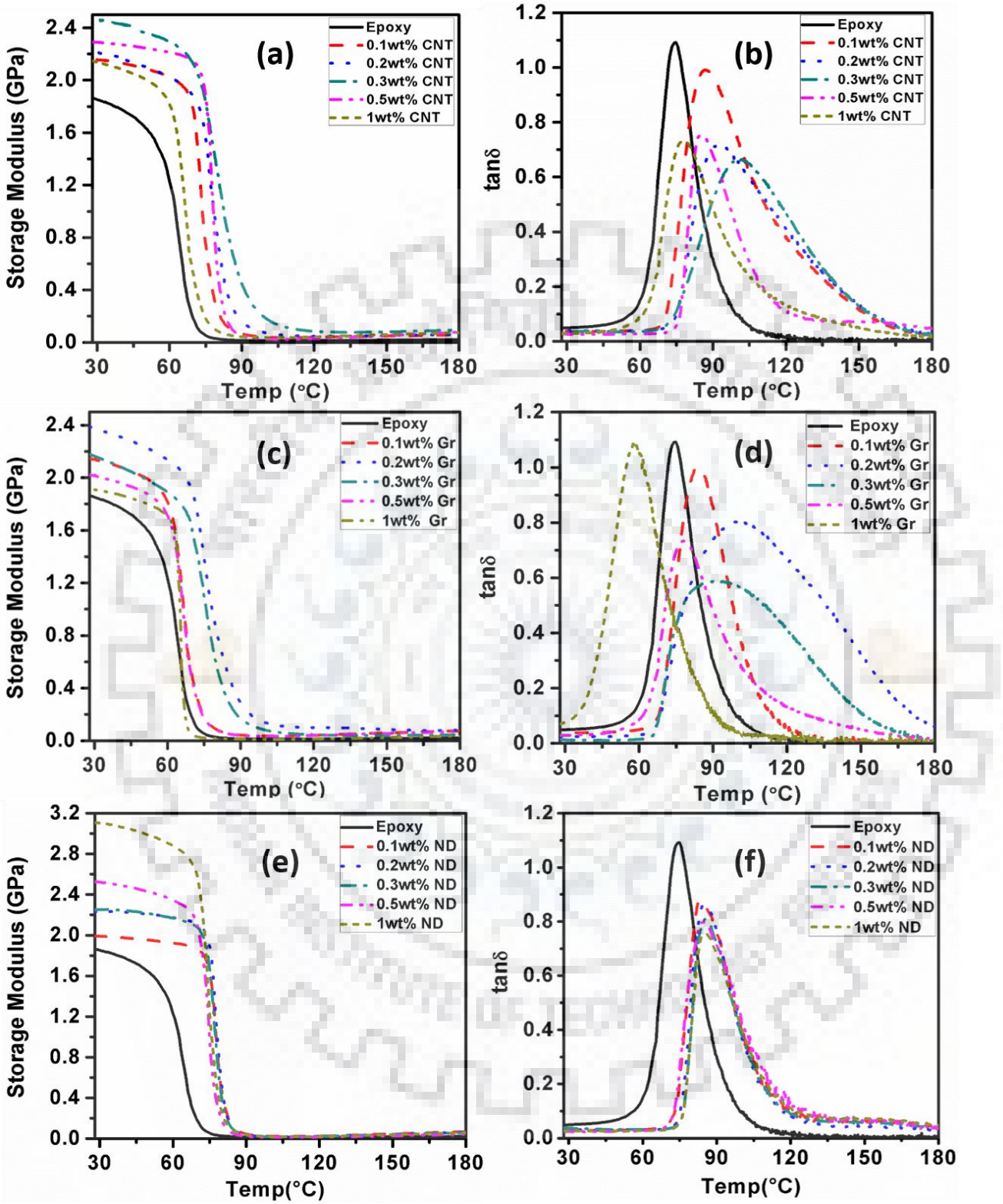

Figure 4.8 Typical storage modulus and plots tanδ for various composition of **(a, b)** CNT-epoxy, **(c, d)** Gr-epoxy and **(e, f)** ND-epoxy composite as a function of temperature

The capacity of composite to absorb the energy by polymer chain sliding is reduced with the addition of nanofillers. This is due to the formation of higher volume of immobile region, which ultimately leads to reduced tan δ. A low tanδ value is indicative of a material that has a high elastic component, while a high value indicates one that is more inelastic. For pure epoxy, the value of tanδ was 1.1, whereas with the addition of CNT/Gr/ND it decreased as low as 0.63, 0.58 and 0.75, with 0.3 wt% CNT, 0.2 wt% Gr and 1 wt% ND.

The increase in T_g, for ND-epoxy composites, was almost similar for all compositions. Further, the highest improvement in T_g with ND was less, as compared to the other two fillers. This is due to the spherical morphology of ND, which tends to rotate, when loaded, thereby increasing the segmental mobility of polymer chain.

The properties, calculated from DMA, are the functions of (a) free volume, (b) cross linking density and (c) interfacial interaction between filler and matrix, which controls the segmental mobility of chain. The results clearly showed that the addition of Gr and CNT resulted in a remarkable increase in the thermo-mechanical stability of the material at higher temperature.

4.1.5 Summary

Addition of carbon based nanofillers (CNT, Gr and ND) are found to improve the mechanical and thermal properties of the epoxy matrix. Where CNT showed highest improvement in fracture toughness ~152% by crack bridging, ND showed highest improvement in UTS of 56%, despite its spherical morphology (less preferable than the other two). Crack pinning, crack deflection and crack bridging being the active toughening mechanism. Sudden decrement in properties were observed for all three morphologies with ≥ 0.3 wt% content, due to agglomeration. DMA results indicate the improvement in glass transition temperature and storage modulus over pure epoxy. Which is

attributed to good dispersion of filler, increase in cross linking density, reduced free volume and restricted segmental mobility with improved interfacial interaction. Incorporation of nanofillers did not have any significant effect on the thermal stability of epoxy. The highest improvement with each filler for all properties is presented in table 2.

Table 2. % improvement in properties of epoxy with CNT, Gr and ND reinforcement

Nanofiller	Improvement (filler content wt%)					
	UTS	E	H	K_{IC}	T_g	E_b
CNT	18% (0.3)	31% (0.3)	79% (0.3)	**154% (0.5)**	25 (0.3)	29% (0.3)
Gr	24% (0.2)	23% (0.2)	69% (0.2)	102% (0.3)	**29.8 (0.2)**	26% (0.2)
ND	**56% (0.3)**	**94% (1)**	**470% (1)**	85% (0.3)	10.3 (0.3)	**68% (1)**

As seen from table 2, the improvement in majority of properties for CNT is at 0.3 wt%, Gr at 0.2 wt% and ND at 0.3 wt%. Therefore, these reinforcement content are the optimized content for each filler for unary reinforcement.

In addition, ND has shown great reinforcement efficiency with highest improvement in modulus, hardness, storage modulus and strength along with strain. This behaviour of ND necessitates an in-depth investigation.

4.2 Evaluating the Micron Level Phase Distribution of Nanodiamond in Epoxy Matrix and its Effect on Mechanical Behaviour

The present study has taken an initiative to understand the distribution of nanophase reinforcement in polymer matrix and their behaviour during loading, using 2D modulus mapping. High resolution electron microscopy is commonly used for evaluating the quality of dispersion of the reinforcement phase in polymer matrix. However, this is not a very suitable technique, considering the small sample size used for these microscopy techniques. Further, it is not possible to clearly distinguish the nano-sized reinforcement phases in polymer matrix, in some cases. As a result, the microscopic images might not be the most effective ones to understand the matrix-reinforcement interaction and their behavior during load sharing. The composite system, being studied here, is a nanodiamond reinforced epoxy resin matrix. Modulus Mapping gives an idea of distribution of nanodiamond in matrix, in terms of spatial distribution of micron level higher modulus regions in epoxy matrix. The modulus mapping studies, carried out on composites with and without application of uniaxial tensile stresses, reveals the active role being played by nanodiamond in modulating the mechanical behaviour of the epoxy matrix and the evolution of distribution of the former with application of stress. The stiffening effect of nanodiamond dispersed in epoxy matrix was evaluated through FEM of representative volume element (RVE). The predicted results were then compared with the experimental results obtained from the nanoindentation. ND dispersion and interaction with epoxy matrix was even analyzed through TEM.

4.2.1 TEM Analysis to Confirm Uniform Distribution and Strong Integration of Nanodiamond in Epoxy Matrix

TEM analysis was done to study the dispersion, interaction and incorporation of ND in epoxy. Due to the smaller size and high surface energy, the NDs tend to agglomerate, making its dispersion and incorporation in the polymer matrix a challenging task. However, ultrasonication technique, as well as, the fabrication method proved to be quite promising in successful dispersion and incorporation of ND in epoxy. Figure. 4.9(i) shows region in the matrix of ND-epoxy composite, where many round shaped ND particles with varied sizes are randomly dispersed within matrix. It can be clearly seen that the NDs are uniformly dispersed and apparently show good interaction with the matrix.

To further confirm the interfacial interaction HRTEM analysis was done. No discontinuity can be seen at ND epoxy interface, even at higher resolution, high enough to reveal the fringes of ND (figure 4.9(ii)(a)). HRTEM image analysis (figure. 4.9(ii)) also proves that the structures of the particles were obvious, with the {111} planes of diamond with interplanar spacing of 0.21 nm. Although the area scanned in TEM is quite small to claim uniform dispersion, but the presence of the individual ND, having good interface with the epoxy, reveals proper incorporation of ND in epoxy matrix. Good dispersion of fillers and strong interface with matrix lead to strengthening of structure.

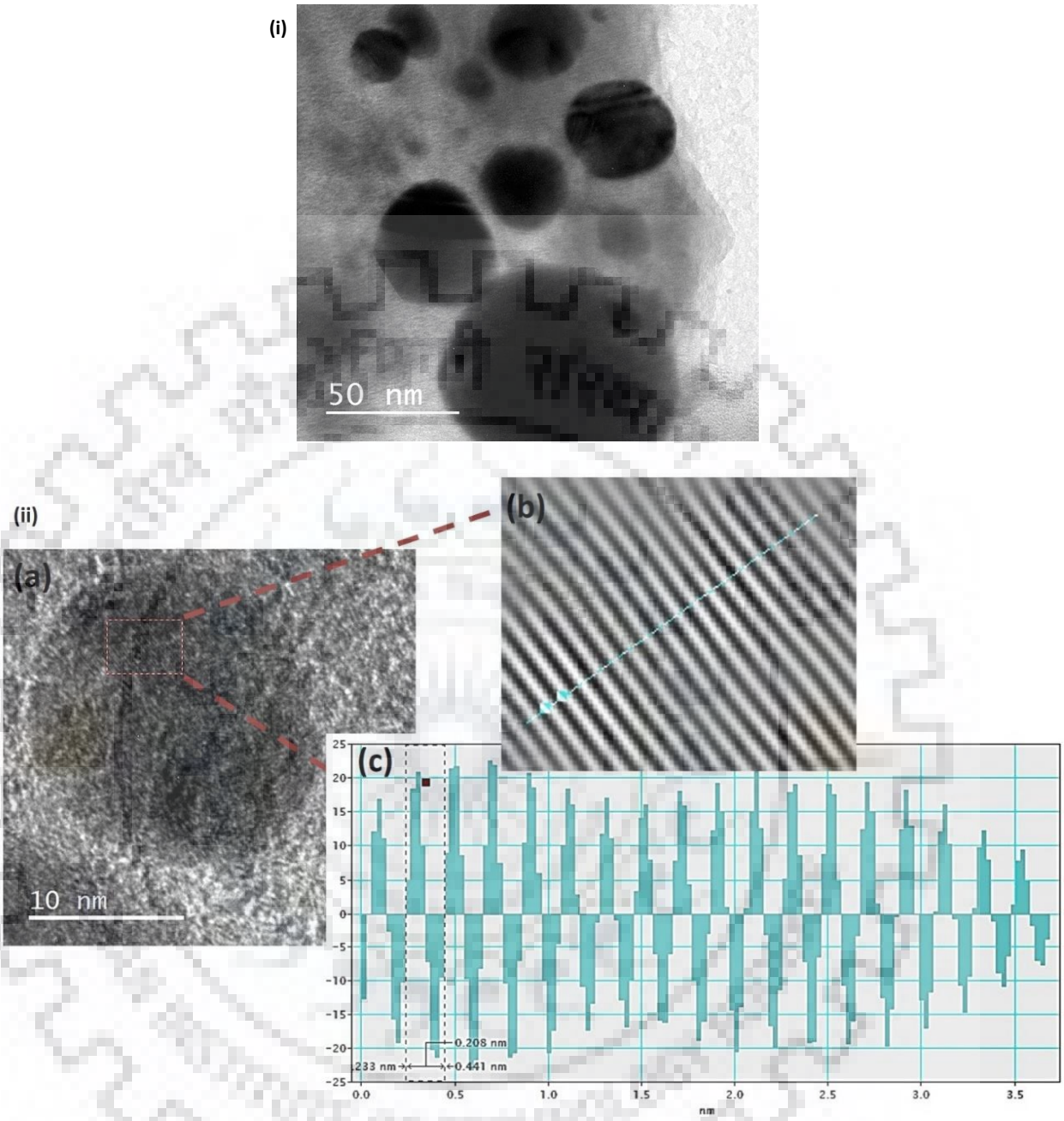

Figure 4.9 (i) TEM image of the uniformly dispersed NDs embedded in the epoxy matrix and **(ii)(a)** HRTEM image of the ND-epoxy composite, **(b)** IFFT simulated image for the selected section and **(c)** Profile of IFFT simulated image.

4.2.2 Analyzing Functional Distribution of ND in Epoxy Matrix through Nano-Scale Modulus Mapping

Microstructural analysis gave a picture about the dispersion of ND as well as its successful incorporation within epoxy matrix. However, distribution of elastic modulus at nanoscale is studied to understand, how good is the interfacial interaction between the epoxy and ND and how does the composite behave when external load is applied with different filler content.

Microstructural features and mechanical behaviour of structure needs to be assessed in order to comprehend the effect of addition of ND on the performance of the composites during service in structural applications. However, neither of the study is sufficient and capable enough to understand the actual quality of reinforcement dispersion, matrix-reinforcement interaction and their behaviour during load sharing. An area map of the cross section of composite, showing the distribution of modulus, at different conditions, can be helpful in this regard. 2D modulus mapping using Hysitron triboindenter, was performed on all the three planes (X, Y and Z) of the epoxy and ND-epoxy composites, both before and after being subjected to uniaxial tensile stress.

The samples for modulus Mapping were collected from the failed tensile specimen. The one half of the dog bone sample, which failed under tensile loading was used for modulus mapping. While, exact same sample was prepared by cutting the dog bone sample into two halves using hack saw for before loading condition. Both the samples i.e. before and after being subjected to tensile loading, were cloth polished to mirror finish. Schematic in figure 4.10 shows the sample sections on which modulus mapping was done. The modulus mapping was done near to the fractured surface on the gauge length.

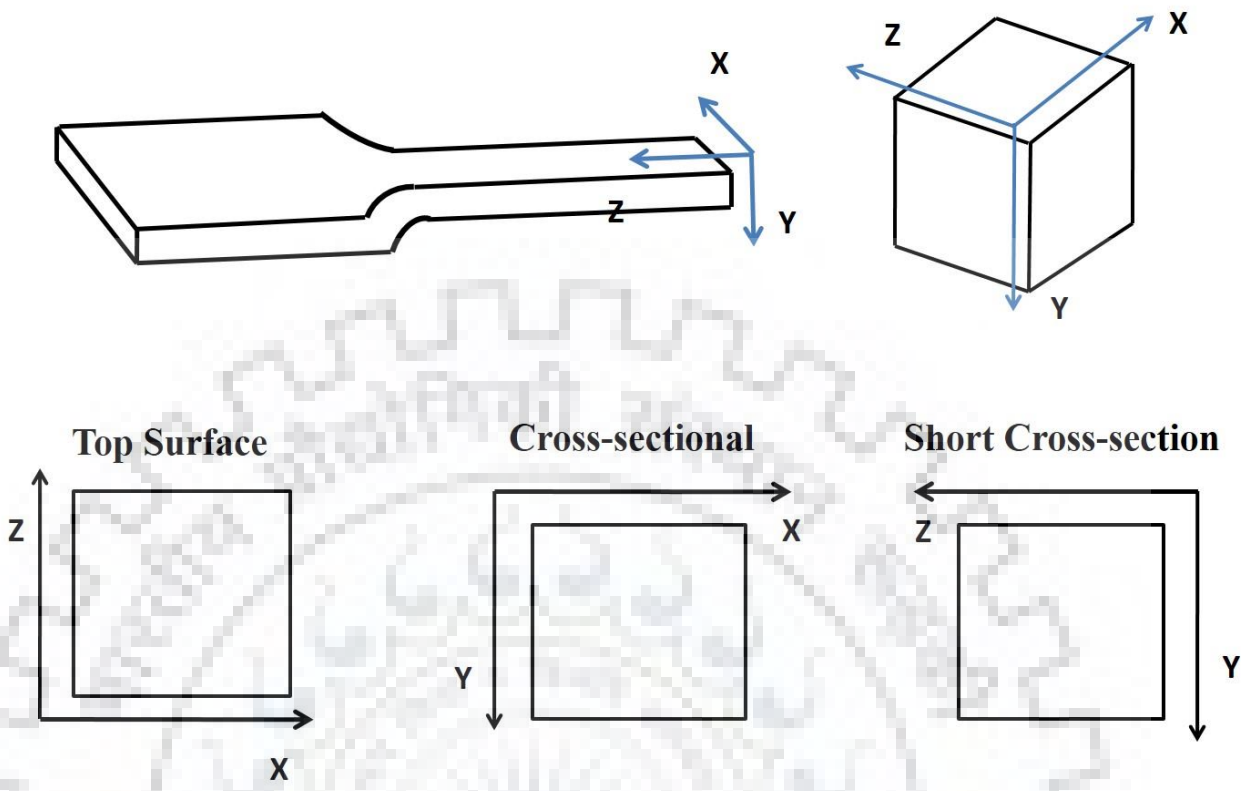

Figure. 4.10 Schematic of tensile sample used for modulus mapping

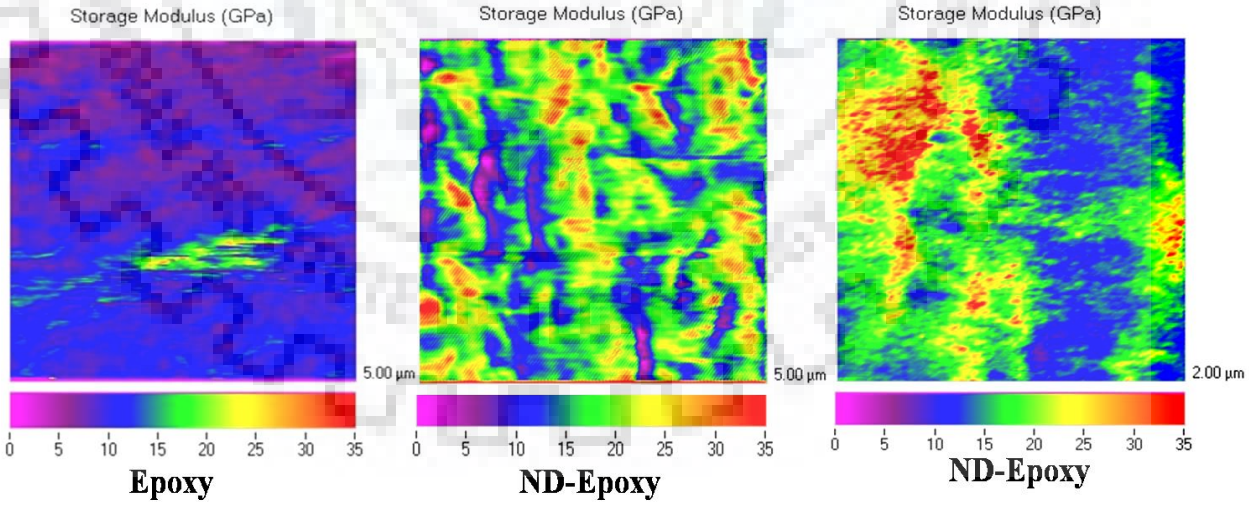

Figure 4.11 Storage modulus maps for epoxy and ND-epoxy before tensile stress is applied

Figure 4.11 shows the storage modulus maps obtained for epoxy and ND-epoxy composite before the uniaxial tensile stress was applied. Storage modulus represents the stiffness of a viscoelastic material and is proportional to the energy stored during a loading cycle. In this process, the probe is sinusoidally oscillated over the polished surface with a given frequency and load. The value of storage modulus signifies stiffness of material, which tends to increase with the addition of ND. The first map in figure 4.11 show the modulus of epoxy, while the other two show the modulus of ND epoxy composite at different magnifications. Since, it is a very high resolution 2D mapping, it can distinguish spatial position of matrix and reinforcement in composite structure.

The regions of high modulus denote the area having higher concentration of ND, which is shown in red color. The continuous gradient of modulus (yellow and green) around this high moduli region (red) indicates better load sharing by ND. The presence of these regions suggests better interface and good load sharing ability between the ND and epoxy. The color scale for all the modulus maps are kept same for the sake of comparison. It can be clearly seen from the maps that the average storage modulus obtained for the same area of 5 μm x 5 μm has increased from ~6 GPa to around ~15 GPa with the addition of 1 wt% ND. The NDs were uniformly distributed throughout the matrix, with domain size of ~500 nm - 600 nm, which are slightly more ND rich than rest of the matrix. These domains are uniformly distributed in random directions throughout the matrix. Further magnified view in 2 μm x 2 μm map (figure 4.11) clearly reveals that these domains are not the agglomerations, as they show smooth transition of modulus towards epoxy matrix.

Representative property map for the storage modulus of epoxy and ND-epoxy composite in all the three planes (X, Y and Z), both before and after applying the tensile stress, are shown in figure 4.12. 2D modulus maps, as shown in figure 4.11 and 4.12, are taken from the area, which is about 6-8 mm away from the tip of fractured surface. In order to get a larger picture and develop a better

understanding, 10 μm x 10 μm area was scanned in all the three planes. Modulus maps, thus obtained, were arranged in 3D to get a volumetric view of the structure, as presented in figure 4.13. It can be clearly seen from figure. 4.12(b) that nanodiamonds are uniformly distributed throughout the matrix, offering very strong interaction with the epoxy matrix. This feature leads to proper load sharing, thereby increasing the average modulus of the epoxy matrix. The red color regions, having high ND concentration, as seen for ND epoxy composite in figure 4.11, are not seen in figure 4.12(b). This is just because the range of colour scale has been changed from 0-35 GPa to 0-65 GPa, for the sake of comparison with samples after tensile loading. After the epoxy and its composite were subjected to uniaxial tensile loading, the modulus mapping was performed again to understand if the applied stress has brought about any significant change in the internal structure of the composite and their active strengthening mechanism.

Comparison of Figures 4.12(b) and 4.12(c) clearly shows that with application of uniaxial tensile stress there is a change in the internal structure of the composite. Upon application of stress, the polymer chains and ND tend to redistribute and align themselves in the stress direction, thus reducing the domain size. The internal structure of ND epoxy composite looks like a well aligned connected network of fibers. These uniformly distributed and aligned NDs, having very strong interface with epoxy matrix, lead to improved modulus and strength, due to better load sharing as evidenced by the rise of high modulus red color regions.

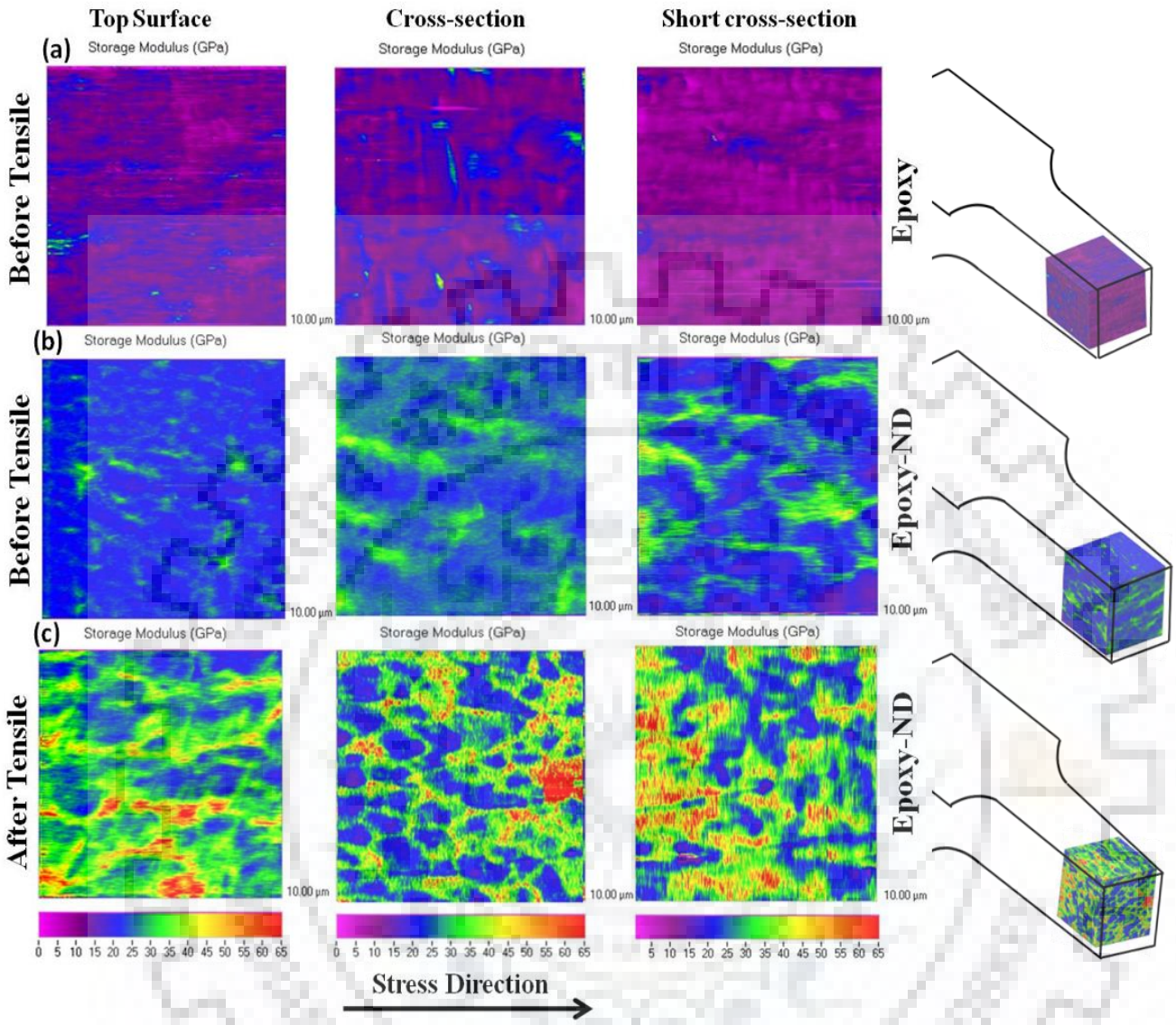

Figure 4.12 Storage modulus maps for **(a)** epoxy before tensile and the ND-epoxy composite **(b)** before tensile and **(c)** after tensile test

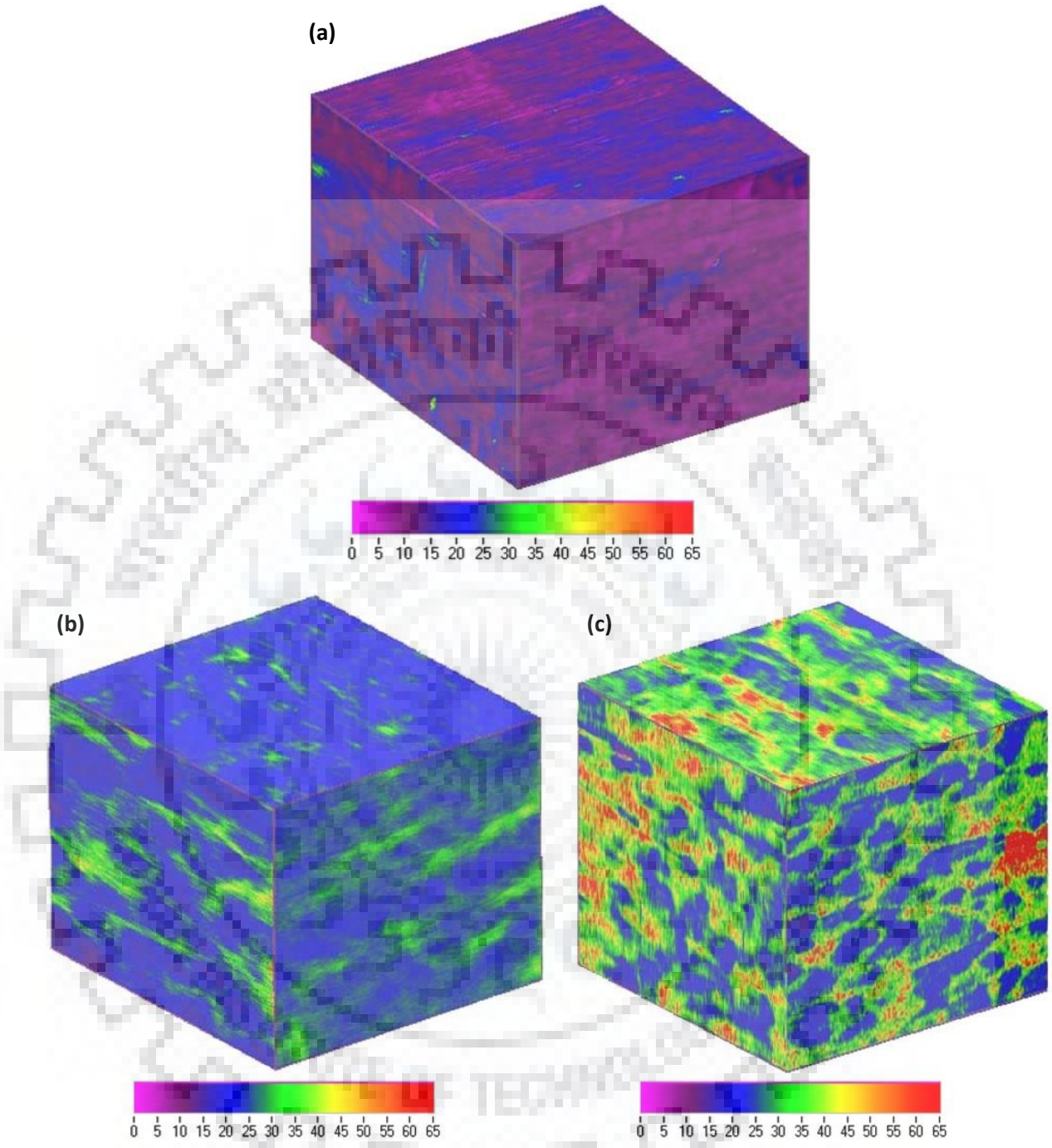

Figure 4.13 Storage modulus maps arranged in 3D for **(a)** epoxy before tensile and for the ND-epoxy composite **(b)** before tensile and **(c)** after tensile

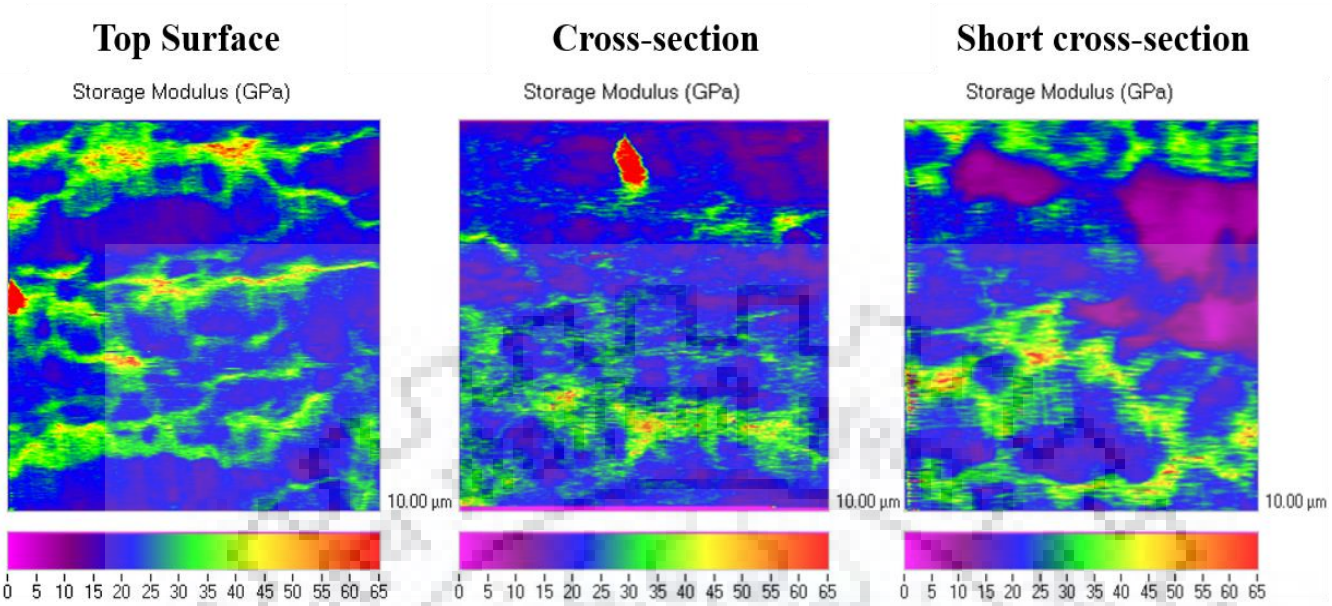

Figure 4.14 Storage modulus map for ND-epoxy composite having severe agglomeration

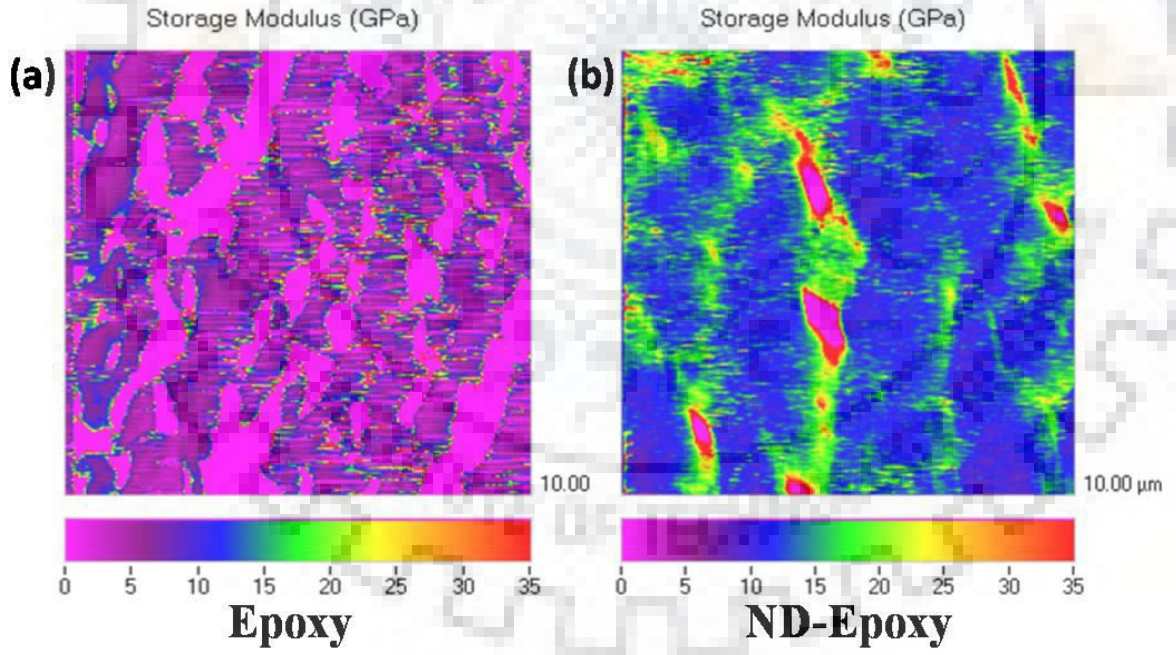

Figure 4.15 Storage modulus maps for **(a)** epoxy and **(b)** ND-epoxy composite at ~1-2 mm away from the fractured surface tip.

Storage modulus map with severe ND agglomeration is shown in figure 4.14. It can be clearly observed from comparing the storage modulus maps for cross section in figure 4.14 to figure (4.12 & 4.11). The red region, in figure 4.14 shows a sudden decline in the modulus from 65 GPa (red region) to somewhere around 10-15 GPa (surrounding area). While, in figure (4.12 & 4.11) the decrease in the modulus is gradual as we move away from red region. This sudden change in modulus leads to very high stress concentration, thereby leading to premature failure at very low load

Modulus maps shown in figure 4.15 are taken from the distance ~1-2 mm away from the fracture surface tip. Comparison of maps in figure 4.15 clearly shows that the population and extent of cracks, denoted by the light pink region having almost zero modulus, are much less in case of ND-epoxy as compared to epoxy. It can be clearly evidenced from the maps that in case of epoxy the cracks, once generated on the surface, propagates through till failure. However, the segregation of ND, as seen in figure 4.15(b) as red regions, along the boundary of cracks tend to anchor the cracks and prevent them from growing. Further, the agglomeration of ND on the crack tips (red regions) and in between the cracks (green regions) prevent them from merging. This restricts the through and through failure, thus increasing the % strain at failure or toughness of the composite. Addition of ND to epoxy not only affects the area surrounding the crack, but, the entire epoxy matrix is strengthened. On the contrary, in case of pure epoxy, the area apart from the cracks is also found to be really very weak and is almost destroyed, as seen with very low modulus value in the maps.

Thus, nanoscale modulus-mapping is a great tool to understand the actual quality of reinforcement dispersion, matrix-reinforcement interaction and their behaviour during load sharing. More interestingly, the effect of loading on redistribution of ND and its significant effect on toughening can also be revealed by it.

4.2.3 Evaluation of Elastic Property using Numerical Analysis

Numerical analysis of mechanical properties of these composites structures has been carried out to investigate whether the physical distribution and modulus, found through modulus-mapping, corroborates the property at macroscale or not. The homogenized elastic property of polymer matrix composite, reinforced with hard particles with similar spatial distribution as ascertained through modulus maps, was obtained using finite element analysis. The outcomes, thus obtained, were compared with the experimental results on composite structure. Also the fibrous structure evolved due to redistribution of ND, when subjected to load (as found in modulus-mapping in figure 4.12) was compared with that obtained through finite element analysis. The hard particles i.e. nanodiamonds, were of the order of ~10 nm. However, due to high surface energy they start to form dense colonies of size 500-600 nm inside polymer matrix, as assessed from modulus mapping (figure 4.11). These colonies were not completely circular, but for the ease of analysis they are assumed to be circular in shape with diameter of 600 nm. Nanodiamond possesses elastic modulus of 1 TPa and Poisson's ratio of 0.2 [228]. Epoxy has elastic modulus of 4.6 GPa, as obtained from instrumented indentation and Poisson's ratio of 0.35 (from material datasheet as provided by vendor). Approximate density of domains/particles present in 1 wt% ND-epoxy composite was calculated from modulus maps (figure 4.11). The density of particles present in the rest compositions were than approximated from the ratio of the value obtained for 1 wt%. In order to obtain the homogenized response of heterogeneous material, it is required to define the RVE. Physical and geometrical properties of a composite were evaluated using a suitable RVE. Therefore, the proper choice of RVE determines the accuracy of modeling of a heterogeneous material. The 2D RVE with length and width of 10 μm x 10 μm, having randomly distributed non-overlapping circular particles of uniform size with diameter of 600 nm, was selected for simulation (figure 4.16(a)). This was adopted based

on the actual distribution obtained in modulus-mapping. Periodic boundary conditions were applied to evaluate the elastic properties. Four node bilinear elements (CPS4R) were used for RVE analysis figure 4.16(b). The interface between particles and matrix is modeled as perfect bond in ABAQUS software. Principle of strain energy equivalence was implemented in ABAQUS software using Python script to evaluate the effective elastic properties of the composite.

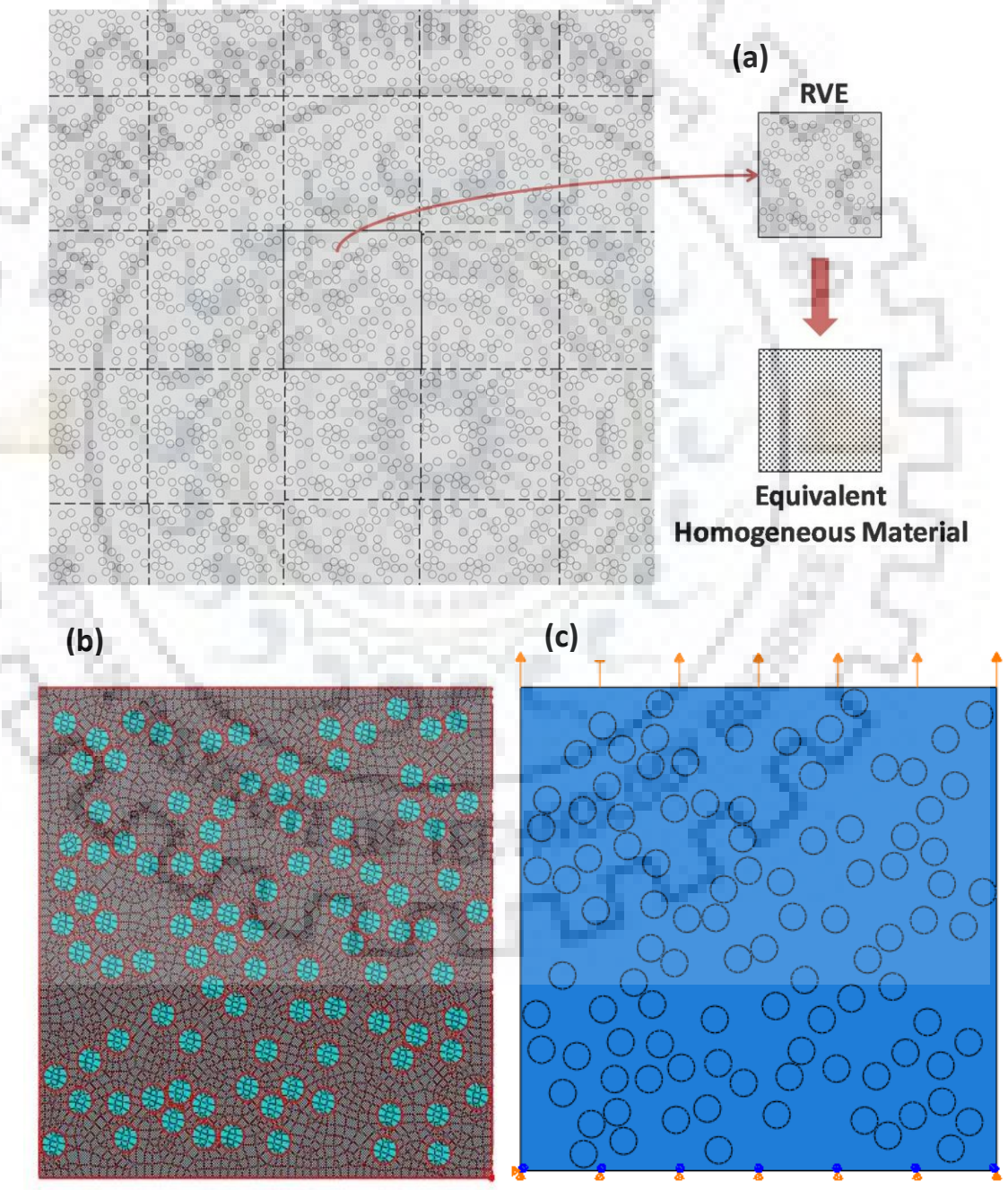

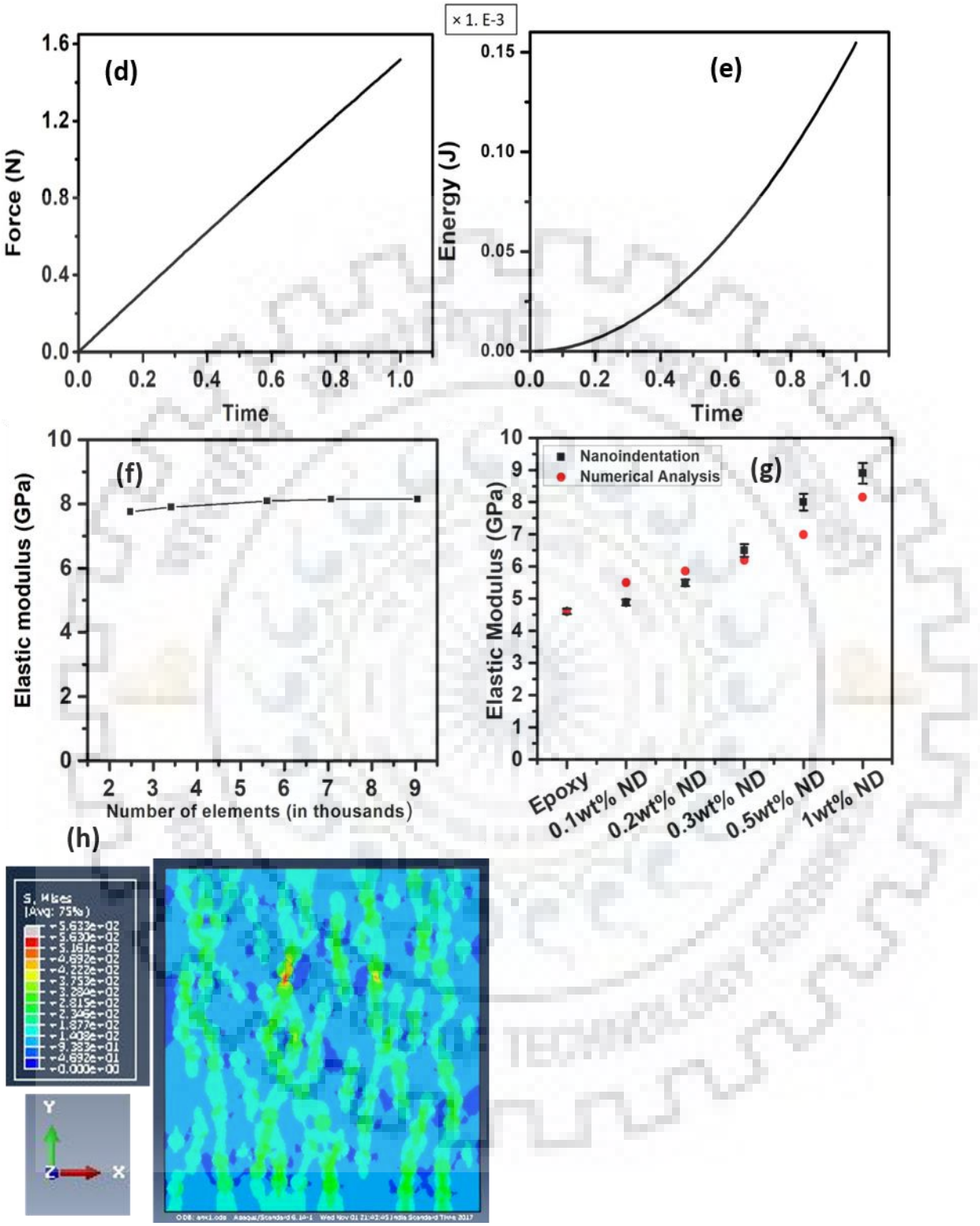

Figure 4.16 (a) Schematic representation of the homogenization approach for the periodic microstructure, **(b)** meshed RVE containing randomly distributed circular particles in the continuous matrix, **(c)** RVE subjected to the uniaxial tensile strain, **(d & e)** reaction force and strain energy

curve obtained under the specific loading and boundary conditions, **(f)** convergence study for modulus evaluation against number of elements, **(g)** comparative variation of the effective elastic modulus with weight fraction of the ND obtained from the numerical and experimental analysis and **(g)** the von Mises stress distribution for the RVE.

In this method, the strain energy of the heterogeneous composite is compared with the strain energy of the equivalent homogeneous material under similar loading and boundary conditions. The total strain energy of a body is given by

$$\bar{U} = \frac{1}{2}\int_V \sigma_{ij}\ \varepsilon_{ij} dV \tag{3}$$

To evaluate the elastic modulus (E), a uniaxial tensile strain was applied in the x-direction, as shown in figure 4.16(c), then the strain energy of homogenous medium is given as,

$$U_{xx} = \frac{1}{2}\int_V \sigma_{xx}\ \varepsilon_{xx} dV \tag{4}$$

As a response of this, reaction force and strain energy were obtained under specific loading and boundary conditions (figure 4.16(d & e)), which are given in table 3. By equating the strain energy of the equivalent homogenous medium with the strain energy of the heterogeneous composite, the elastic modulus is obtained using the following expression:

$$\bar{U} = \frac{1}{2}\int_V \sigma_{xx}\ \varepsilon_{xx} dV \tag{5}$$

Where σ_{xx} and ε_{xx} are the stress and strain components respectively. $\bar{U}$ is the numerically calculated strain energy of heterogeneous medium, due to the action of uniaxial tensile strain.

The effective modulus, obtained from numerical analysis, is compared to that experimentally measured using instrumented indentation. Before evaluating the material properties, a convergence study has been performed on the 2D RVE of 10 μm x 10 μm size with 1 wt% ND particles for

various mesh size (i.e. number of elements). Figure 4.16(f) shows the results of convergence study for effective material property evaluation against number of elements. The variation of equivalent elastic modulus of composite with weight fraction of nanodiamond is shown in figure 4.16(g). It can be clearly seen that the result obtained from numerical analysis are in good agreement with the experimental results. At low ND loading, the size of these domains might be smaller than 600 nm. This might be the reason why the elastic modulus value obtained from numerical analysis for low loading is overestimated. But the effect of size is not yet taken into consideration in this study.

Table 3. Load, strain energy and elastic modulus of the ND-epoxy composites obtained from numerical analysis

Nanodiamond (wt%)	**Particles**	**Load (N)**	**Strain Energy x 10^{-4} (J)**	**E (GPa)**
0.1	10	1.125	1.12	5.51
0.2	20	1.198	1.20	5.87
0.3	33	1.263	1.26	6.19
0.5	50	1.436	1.44	6.99
1	100	1.632	1.63	8.15

Further, the von Mises stress distribution map, obtained for 1 wt% ND-epoxy composite, is shown in figure 4.16(h), while for all other compositions it is shown in figure 4.17. It can be clearly seen from the von Mises stress distribution (figure 4.16(h)) that the stress field in the direction of applied stress tend to align the particles in the same direction. The particles, thus lying in almost an array, which tend to share the load like a long fibrous network. This observation is in agreement, both, experimentally through modulus mapping (figure 4.12(b)) and by numerical analysis (figure 4.16(h)). It can be also seen from figure 4.16(h) that ND domains lying in very close contact with

each other and creating a big agglomeration, leads to a sudden increase in the von Mises stress, generated at their interface. This eventually may lead to failure from the interface itself, once the stress increases above the elastic limit. These corroborations in observations are again a proof of the capability of 2D modulus-mapping in evaluating the physical and mechanical distribution of nano-phase reinforcements and their role in strengthening behaviour of the composite structure

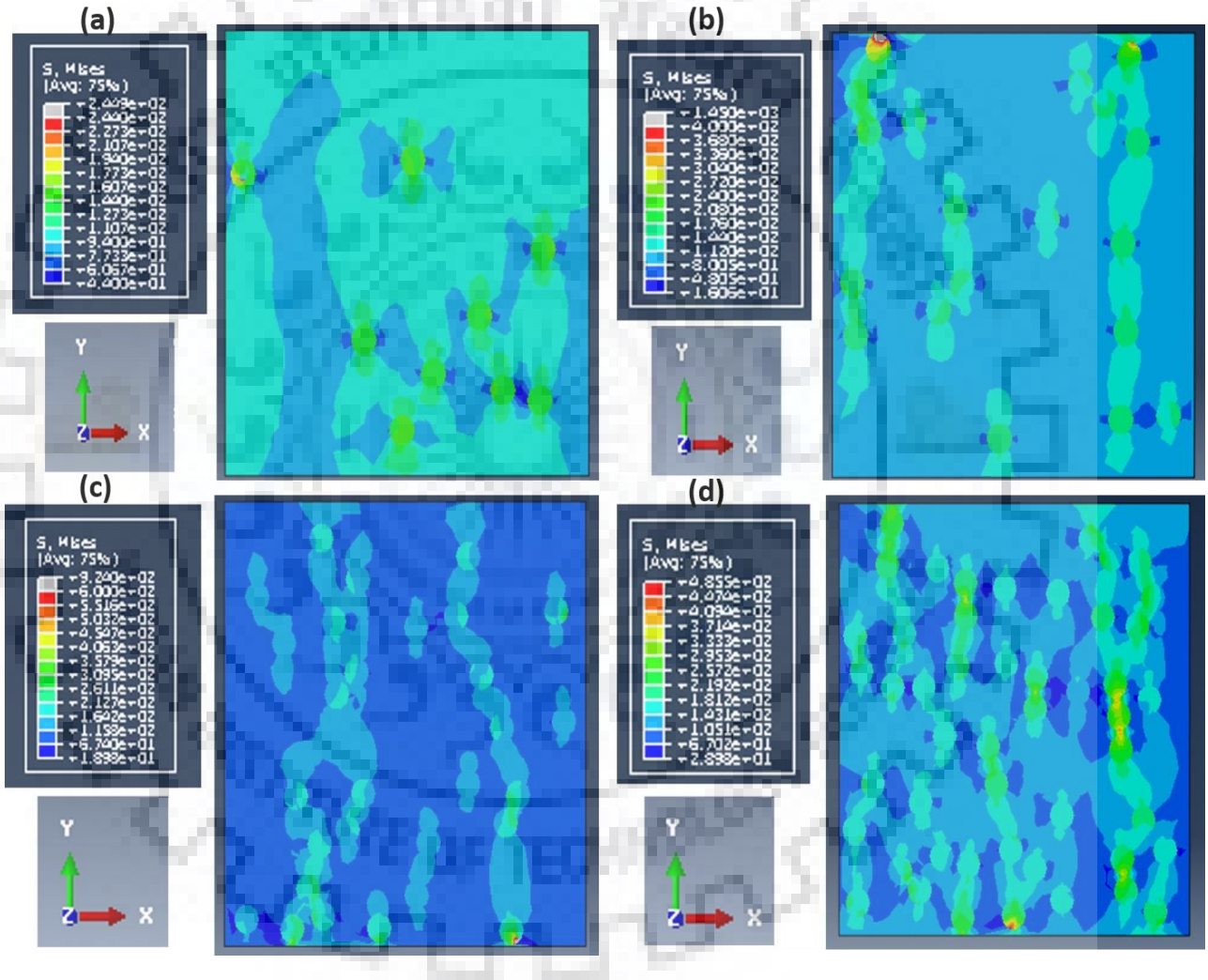

Figure 4.17 von Mises stress distribution for **(a)** 0.1 wt% ND-epoxy, **(b)** 0.2 wt% ND-epoxy, **(c)** 0.3 wt% ND-epoxy and **(d)** 0.5 wt% ND-epoxy composites

.

4.2.4 Summary

2D modulus-mapping is a great tool to understand the distribution of nanophase reinforcement in polymer matrix and their behaviour during loading. This study clearly shows the potential of using 2D modulus-mapping for detailed analysis of the role of nanophase reinforcement in mechanical behaviour of composites. The analysis of maps gives an idea of distribution of nanodiamond in matrix, in terms of spatial distribution of micron level higher modulus regions in the composite structure. It also gives insight into the matrix reinforcement interaction and its behaviour during loading. The NDs efficiently shares the load transferred from the matrix and provides high resistance to the matrix against deformation, thereby increasing the modulus by ~94%. TEM analysis revealed uniform dispersion and strong interaction of ND with epoxy matrix. Elastic modulus value obtained from numerical analysis, done based on the findings from modulus-mapping, was in good agreement with that obtained from nanoindentation. Apart from these findings, this study also develops 2D modulus mapping technique as a generalized tool for evaluating the quality of dispersion of the nanoscale reinforcement phases and their role in mechanical behaviour of the macro-scale composite structures.

4.3 Synergistic Effect of Nanodiamond in Binary Combinations with Carbon Nanotube and Graphene in Epoxy Composite

The previous studies verified the potential of ND as a reinforcement to epoxy matrix, both, individually as well as in comparison to CNT and Gr, the two most preferred reinforcement for polymer matrix, as seen from literature. The large surface area and the high aspect ratio allows the better stress transfer between CNT/Gr and polymer. However, the poor dispersion, due to entanglement of CNTs and stacking of Gr sheets, restricts their potential as a reinforcement in polymer matrix. The present study has taken the initiative to study the potential of ND in exfoliating Gr, using very simple, easily adoptable and scalable technique, using the power of ultrasonication. The extent of exfoliation of CNT/Gr, both with and without the help of ND, was investigated through TEM and FE-SEM. The capacity of ND assisted exfoliated CNT and Gr, as a potential reinforcement to epoxy matrix, is then explored in terms of mechanical properties. Tensile test and fracture toughness was performed for composites to evaluate their mechanical performance. The fractured surfaces of the tensile samples were investigated through FE-SEM to get insight of dispersion, interfacial interaction of fillers with matrix and active strengthening mechanism.

In case of binary combinations, two compositions are studied. The first composition is the highest of the individual best of each filler in binary combination. While, a sum of individual best was selected as second composition. As concluded from chapter 4.1, 0.3 wt% for CNT, 0.2 wt% for Gr and 0.5 wt% for ND offered best combination of properties. Hence, 0.3 wt% was selected as first composition (highest of the two), 0.6 wt% (CNT-ND hybrid) and 0.5 wt% (Gr-ND hybrid) as second composition (sum of two) for this study. Composites were compared for different combinations i.e. 0:100, 25:75, 50:50, 75:25 and 100:0 of CNT:ND and Gr:ND in epoxy matrix at these compositions.

4.3.1 Microstructural Characterization to Confirm Morphology of Binary Combinations of Nanofillers

FE-SEM and TEM images for CNT, CNT-ND hybrid, Gr and Gr-ND hybrid are shown in figure 4.18. Figure 4.18(i)(a & b) reveal tube like morphology of CNT with outer diameter of ~40 nm. Due to their high aspect ratio and fiber like morphology, CNTs are found entangled together, which reduces the overall exposed surface area. Thus, the total interface area with the polymer matrix is reduced in the composite structure. As the entanglement is weak, on the application of stress they tend to open-up, which reduces their reinforcement efficiency. This entanglement also leads to improper impregnation of epoxy in these regions.

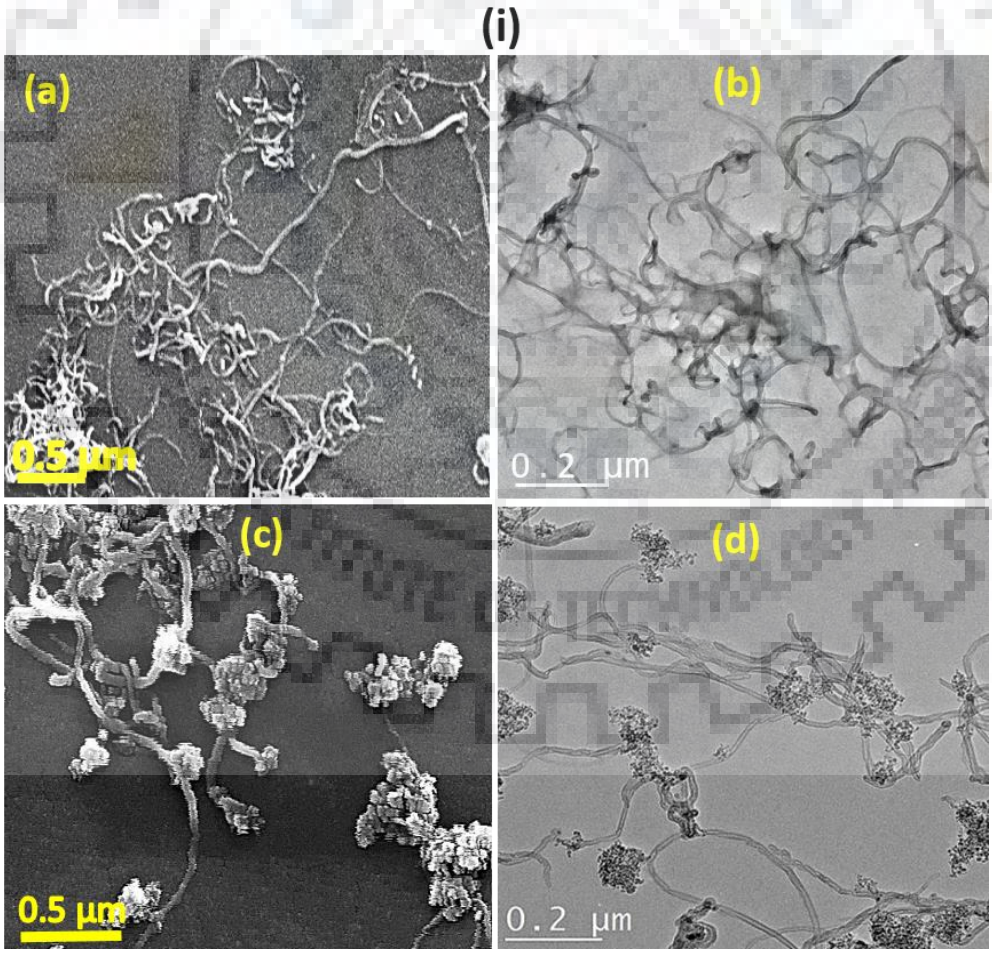

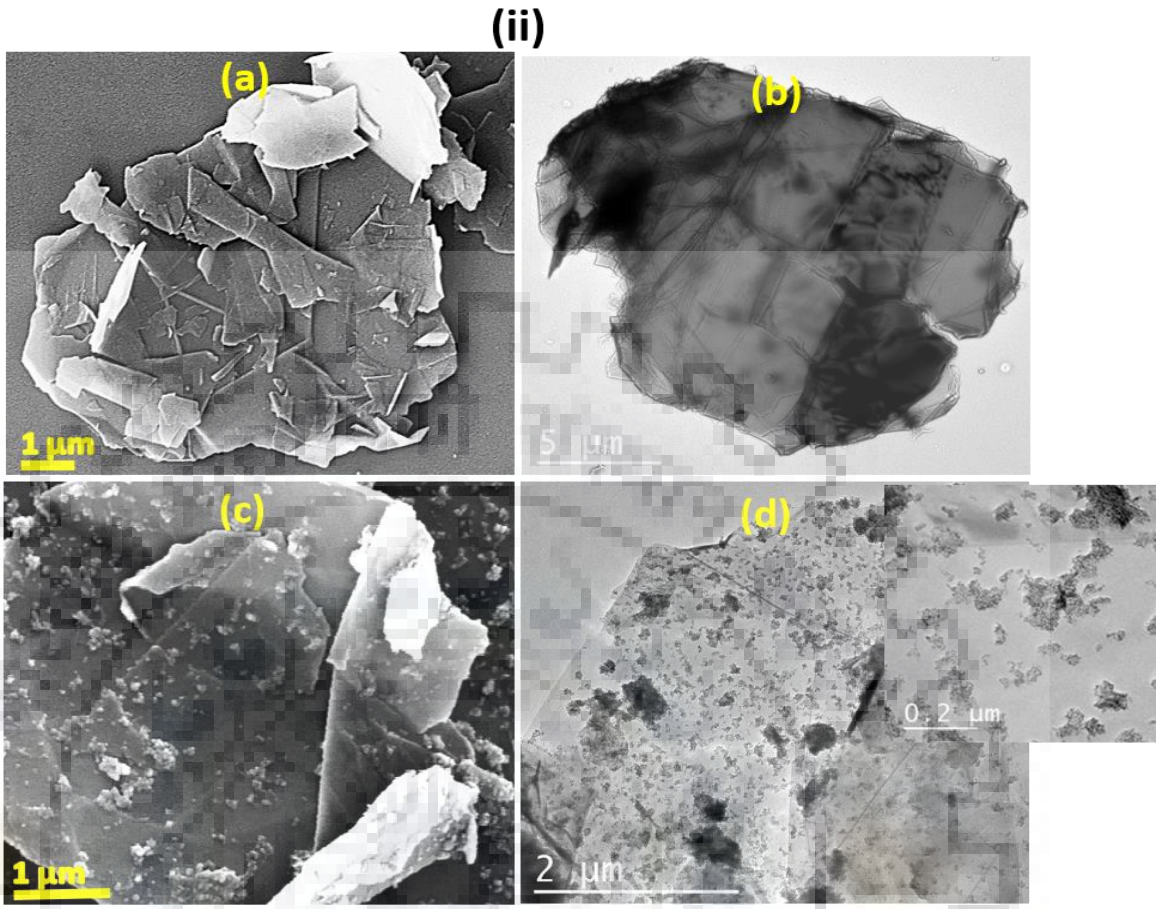

Figure 4.18 TEM and FE-SEM images for **(i) (a, b)** CNT, **(i) (c, d)** CNT-ND, **(ii) (a, b)** Gr and **(ii) (c, d)** Gr-ND

After sonicating CNT in the presence of ND, the NDs cluster attach themselves to the ends of CNTs, bridging them together into long chains (figure 4.18(i)(c & d)). This prevents the entanglement of CNTs to some extent, thus increasing the overall aspect ratio in the hybrid structure. The morphology of Gr is in the form of wrinkled nanoplatelet with nanosheet dimensions of ~15 µm along the length and ~10 µm along the width, as confirmed from figure 4.18(ii)(a & b). However, the thickness of the Gr or the number of nanosheets stacking is high, as evidenced from the opaque dark black colour, which reduces the overall aspect ratio. Thus, the total surface area of Gr, in contact with the polymer, is reduced. Further, the sheets are stacked with weak van der Waals force, which make them less effective as reinforcement for strengthening and toughening, due to slipping of sheets

during application of stress. All these declines the effectiveness of Gr in improving the property of the composite as a whole. Thus, exfoliation of Gr sheets is very important

Addition of ND to Gr, during sonication, is seen to improve exfoliation of Gr sheets. The Gr sheets, which appear opaque and black due to stacking of multiple sheets (figure 4.18(ii)(a & b)) before addition of ND, are found to be quite transparent after the addition of ND figure 4.18(ii)(c & d). The transparency indicates less number of graphene sheets stacked in the structure. The surface of Gr sheets is also seen decorated with ND (figure 4.18(ii)(d)), which restricted the π–π stabilization and hence inhibited stacking of Gr sheets, thus, improving its overall efficiency as reinforcement.

Further, the size of ND clusters in hybrid structures is found to be similar or smaller than the ultrasonically dispersed NDs, when used as an individual reinforcement (figure 4.18(d)). This reveals that the addition of ND promotes effective dispersion of Gr. Both, TEM and FE-SEM image analysis confirm the improved exfoliation of Gr, with the addition of ND.

4.3.2 Fracture Surface Analysis to Confirm Dispersion, Proper Integration and Strengthening Imparted by Binary Combinations of Nanofillers to Epoxy Matrix

FE-SEM, the most widely used characterization technique, was used to investigate the dispersion of nanofillers and the strengthening effect imparted by them. Figure 4.19(a-g) shows the FE-SEM images for fractured surface of CNT-epoxy, Gr-epoxy, ND-epoxy, Gr-ND epoxy and CNT-ND epoxy composite. As seen from figure 4.4, the tensile properties for CNT-epoxy and Gr-epoxy composite decreases beyond 0.3 wt% and 0.2 wt% reinforcement content, respectively, due to agglomeration of nanofillers. Therefore, the potential of ND in exfoliating CNT/Gr is investigated above 0.2 wt%, i.e. 0.3 wt% and 0.6 wt% for CNT- epoxy composite and 0.3wt% and 0.5wt% for Gr-ND epoxy composite. However, the fractured surface of epoxy, reinforced with hybrid fillers,

were analyzed only at higher filler content, for five different ratios, i.e., 100:0, 75:25, 50:50, 25:75 and 0:100 (figure 4.19(d-i)).

Dispersion of nanofillers is a very challenging task and it becomes even more challenging at higher filler content. On other hand, reinforcement efficiency of nanofiller reinforced composite is highly influenced by the dispersion of nanofillers in the matrix. Therefore, if the dispersion and interfacial interaction is found good with higher filler content of 0.6 wt% and 0.5 wt%, it is expected be good for lower filler content of 0.2 wt% and 0.3 wt%. Figure 4.19(a-c) shows the images for fractured surface of epoxy composite with CNT-epoxy, Gr-epoxy and ND-epoxy composite, with 0.5 wt% reinforcement content. Comparative analysis of these images shows the severity of agglomeration of nanofiller in each case with similar reinforcement content. The agglomeration of Gr is most significant and severe in comparison to CNT and ND. Partially pulled out Gr can be seen in the fracture surface (figure 4.19(b)), with only one end embedded in the matrix, while the rest dangling out of matrix. CNTs also segregate, instead of uniformly distributing throughout the matrix, with their ends protruding out. The CNTs are coated with epoxy, with no traces of porosity or voids due to weak bonding being visible (figure 4.19(a)). In case of ND at 0.5 wt%, the agglomerate size is quite small and completely coated with epoxy, making it less severe or prone to failure, than Gr (figure 4.19(c)).

Figure 4.19(d-f) show the fractured surface morphology for different combinations of 0.5 wt% ND decorated Gr reinforced epoxy composite. The presence of effectively embedded Gr on fracture surface can be evidenced by the sharp edges of the 2D Gr sheets. However, the presence of ND on the Gr surface obstructs the clear visualization of wrinkles, as seen in case of Gr epoxy composite at lower filler content (figure 4.2(g)). Due to the small size of ND, the presence of ND can’t be witnessed very clearly on the fractured surface of these composites, until the ratio of ND is

much higher than Gr, as seen in figure 4.19(f). No signs of agglomeration of Gr can be seen on the fractured surface, which clearly shows the potential of ND in improving the exfoliation of Gr

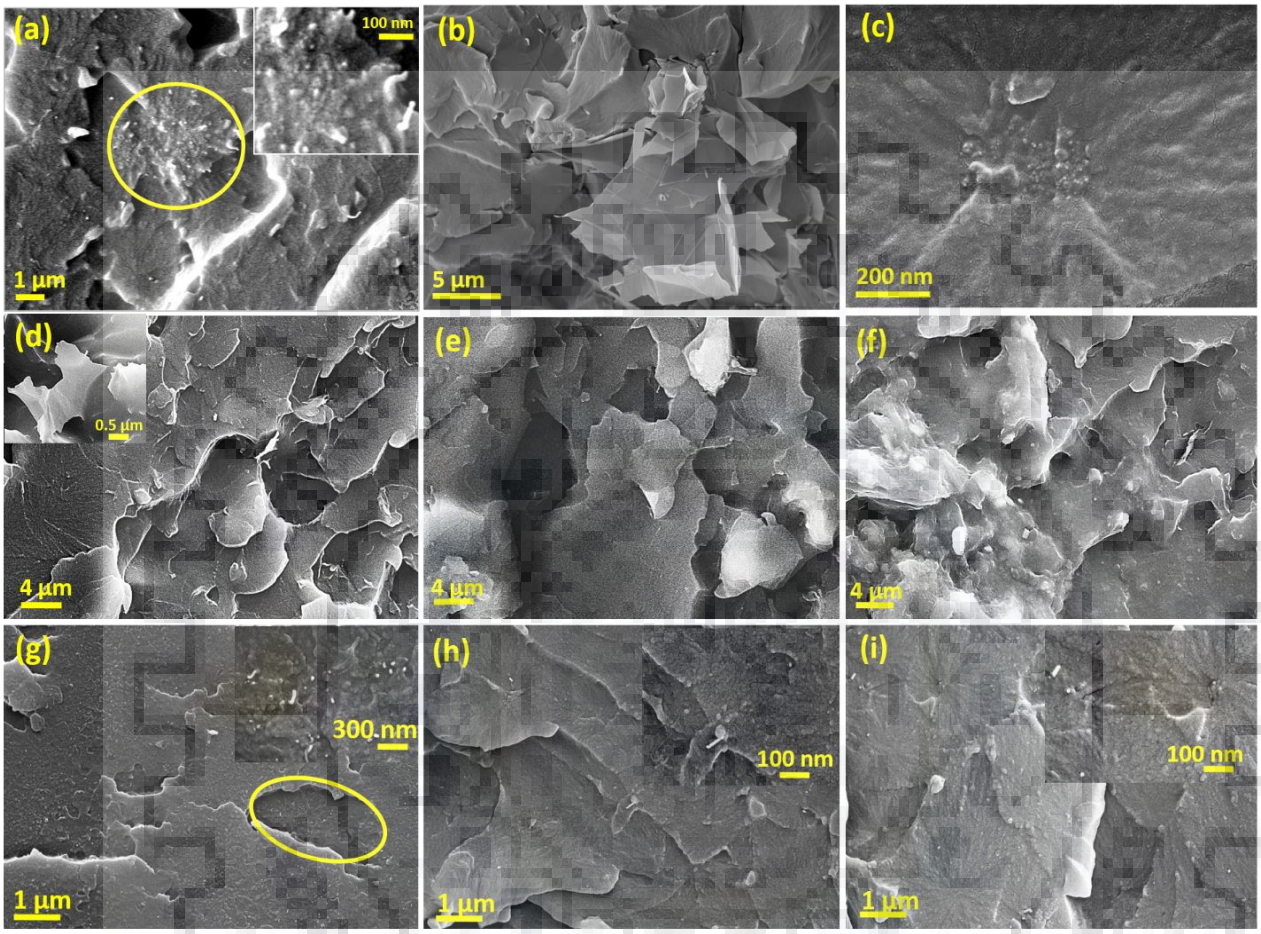

Figure 4.19 FE-SEM images for fractured surface of **(a)** 0.5 wt% CNT, **(b)** 0.5 wt% Gr, (c) 0.5 wt% ND, **(d)** 0.5 wt % (75Gr:25ND), **(f)** 0.5 wt% (50Gr:50ND), **(g)** 0.5 wt % (25Gr:75ND), **(h)** 0.6 wt% (75 CNT:25ND), **(i)** 0.6 wt% (50CNT:50ND) and **(j)** 0.6 wt% (25CNT:75ND) epoxy composite

Figure 4.19 (g-i) show the fractured surface morphology for different combinations of 0.6 wt% ND bridged CNT reinforced epoxy composite. The presence of effectively embedded CNTs on fracture surface can be evidenced by their one end protruding out, for the CNTs that are aligned along the applied load direction or exposed surface for CNTs aligned transverse to the load direction. On the other hand, presence of ND on fractured surface can be evidenced by the bow out or

hemispherical morphology, which is very typical of ND. This morphological feature becomes more prominent as we move from combinations having lower ND content (figure 4.19(g)) to higher ND content (figure 4.19(i)). No signs of agglomeration of CNT can be seen on the fractured surface, which clearly shows the potential of ND in reducing the agglomeration.

4.3.3 Mechanical Behaviour of Epoxy Matrix Reinforced with Binary Combinations of Nanofillers

To further investigate the effect of ND in assisting the exfoliation of CNT and Gr, mechanical properties of CNT-epoxy and Gr-epoxy composite were compared with and without ND. One of the aims of the study is to improve the effectiveness of CNT and Gr as a reinforcement by achieving better exfoliation and integrating them with the matrix. To improve the mechanical behavior of the composite, as a whole. The biggest challenge is to assimilate the improvement in exfoliation achieved for CNT/Gr with addition of ND into the composite fabricated, especially when the production is scaled up. Thus, tensile properties and fracture toughness were studied for the bulk composites.

4.3.3.1 Tensile Study to Assess the Strengthening Imparted by Binary Combinations of Nanofillers to Epoxy Matrix

Representative stress-strain plots for different combinations of CNT-Gr epoxy, with 0.3 wt% and 0.6 wt% filler content, and Gr-ND epoxy, with 0.3 wt% and 0.5 wt% filler content, are shown in figure 4.20(a-d). The quantitative values of UTS and % strain for different compositions and combinations, calculated from the stress strain curve, are presented in table 4. The composites, with

ND bridged CNT and ND exfoliated Gr as reinforcement, showed better tensile properties than CNT epoxy and Gr epoxy composite. The highest improvement, with 0.3 wt.% filler, is obtained with the filler ratio of 25CNT:75ND and 25Gr:75ND. The improvement noted in tensile strength and % strain is ~16% and 84%, as compared to 0.3 wt% CNT epoxy composite and ~37% and ~57%, as compared to pure epoxy, with 25CNT:75ND. While, the improvement in tensile strength and % strain with 25Gr:75ND are ~17% and ~54%, as compared to 0.3 wt% Gr-epoxy composite and ~34% and ~38%, as compared to epoxy. This improvement in properties clearly shows the effect of ND addition to CNT and Gr.

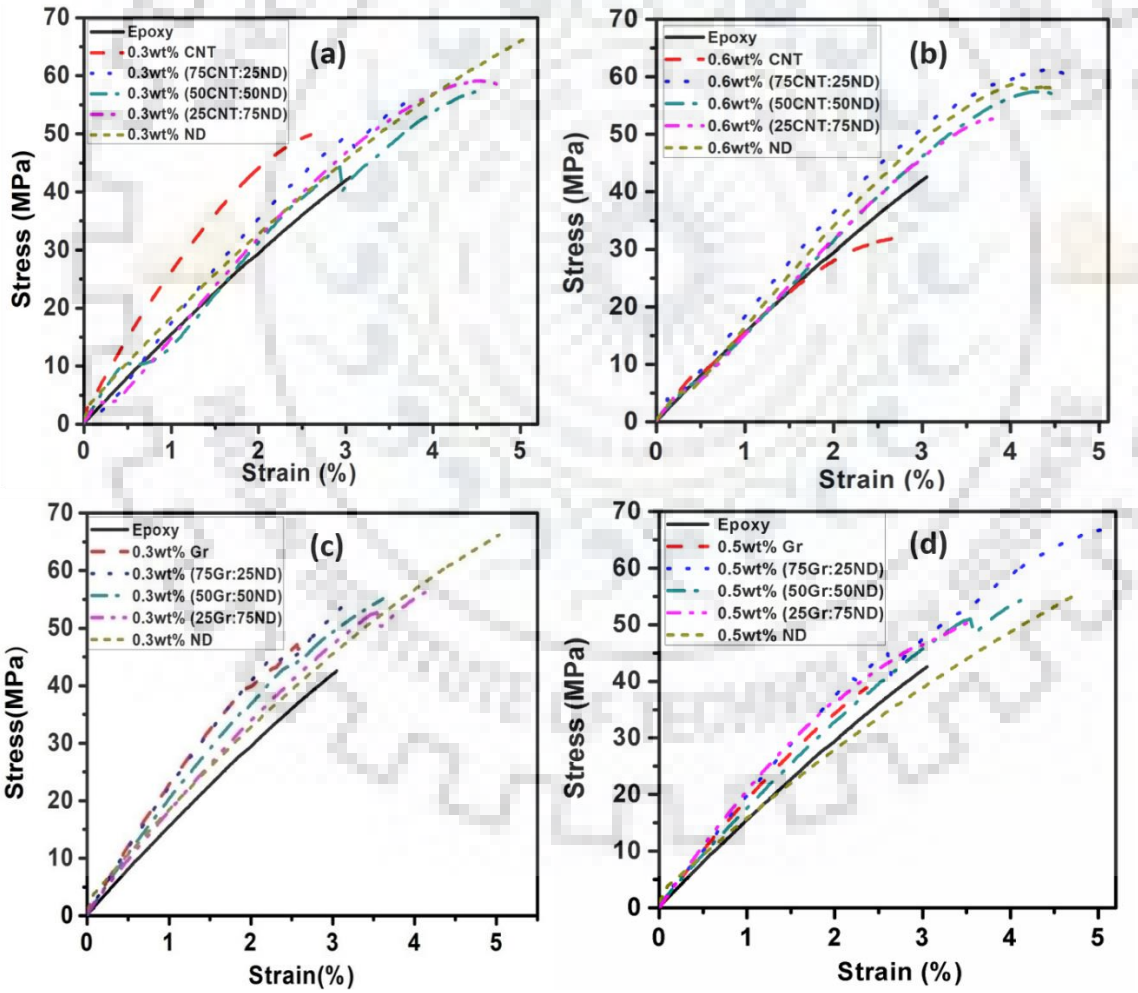

Figure 4.20 Representative stress-strain plots for various combinations of Gr-ND epoxy with **(a)** 0.3 wt% & **(b)** 0.5 wt% reinforcement

Table 4. Ultimate tensile strength, % strain, % improvement in fracture toughness for epoxy and various composition and combination of Gr-ND epoxy composite

Composition		UTS (MPa)	% strain	Improvement in K_{IC} (%)
Epoxy		42.5 ± 1.2	3.05 ± 0.2	-
0.3 wt%	100CNT:0ND	49.8 ± 1.4	2.61 ± 0.3	129
	75CNT:25ND	55.4 ± 1.5	3.68 ± 0.3	139
	50CNT:50ND	57.3 ± 1.5	4.53 ± 0.3	123
	25CNT:75ND	58.1 ± 1.5	4.79 ± 0.3	100
	0CNT:100ND	66.2 ± 1.6	5.03 ± 0.4	91
0.6 wt%	100CNT:0ND	31.9 ± 1.7	2.74 ± 0.4	97
	75CNT:25ND	60.1 ± 1.4	4.65 ± 0.2	163
	50CNT:50ND	56.3 ± 1.3	4.55 ± 0.2	140
	25CNT:75ND	52.5 ± 1.3	3.86 ± 0.2	117
	0CNT:100ND	57.6 ± 1.4	4.49 ± 0.3	54
0.3 wt%	100Gr:0ND	48.6 ± 1.5	2.72 ± 0.1	101
	75Gr:25ND	54.7 ± 1.3	3.19 ± 0.1	114
	50Gr:50ND	55.1 ± 1.2	3.61 ± 0.2	103
	25Gr:75ND	56.9 ± 1.2	4.21 ± 0.2	95
	0Gr:100ND	66.2 ± 0.8	5.03 ± 0.2	90
0.5 wt%	100Gr:0ND	38.9 ± 2.0	2.36 ± 0.1	74
	75Gr:25ND	66.7 ± 1.8	5.03 ± 0.2	131
	50Gr:50ND	55.1 ± 1.6	4.21 ± 0.1	126
	25Gr:75ND	50.4 ± 1.2	3.52 ± 0.1	107
	0Gr:100ND	55.4 ± 1.0	4.76 ± 0.2	60

As seen in chapter 4.1, for reinforcement content higher than 0.3 wt% for CNT and 0.2 wt% for Gr, the tensile properties reduced. This detrimental effect is due commencement of agglomeration of fillers due to high surface energy at higher filler content. However, addition of ND inhibits this agglomeration, as observed earlier through high energy electron micrographs. Thus, to

investigate the effectiveness of ND in exfoliating CNT/Gr, tensile properties were studied at higher total reinforcement content i.e. 0.6 wt% for CNT-ND and 0.5 wt% for Gr-ND. The ultimate tensile strength and % strain improvement was highest with 0.6 wt% (75Gr:25ND), which were ~88% and ~70%, respectively, as compared to 0.6 wt% CNT and ~41% and 52%, respectively, as compared to pure epoxy. With 0.5 wt% filler (75Gr:25ND) reinforced epoxy composite, the improvement in ultimate tensile strength and % strain is found to be higher by ~57%, and ~65%, respectively, as compared to epoxy and ~72% and ~112%, as compared to 0.5 wt% Gr. In fact, the improvement in ultimate tensile strength and % strain was ~17% and ~20% higher than the highest improvement achieved with 0.3 wt% (25Gr:75ND). Thus, this clearly proves the effectiveness of ND in exfoliating CNT/Gr, even at higher filler content.

It can be evidenced from figure 4.19 that the fractured surfaces of composite with 0.5 wt% CNT and 0.5 wt% Gr show agglomeration. The micrographs clearly show that the agglomerated reinforcement phases themselves act as sites for stress concentration and crack generation, instead of acting as an anchor to crack propagation. At 0.5 wt%, CNTs can be seen segregated in a small region leading to agglomeration, instead of uniformly distributing throughout the matrix. The Gr, sheets, on the other hand, appear to be on the surface with only one end embedded into the matrix and the rest is dangling out with no epoxy traces on the surface. This suggests a weak interface between the Gr and the epoxy matrix, which leads to catastrophic failure. However, with the addition of ND, even at higher concentrations, the fractured surface of composite, with ND bridged CNT and ND decorated Gr as reinforcement, showed no agglomeration (figure 4.19(d-i)).

With the improvement in strength, the simultaneous improvement in % strain of epoxy matrix is recorded. This improvement is due to the high resistance to crack propagation offered by the high aspect ratio CNTs, which causes the crack to travel long path before failure. Addition of

ND increased the overall aspect ratio of CNTs, by reducing entanglement and bridging them end to end, which increased the resistance to crack propagation further. On the other hand, with improved exfoliation of Gr, the population of impenetrable obstacles in the form of Gr increased and instead of acting as a site for crack generation they inhibited its growth. The spherical morphology of NDs is also believed to play the key role. Once a tensile stress is applied to a polymer composite, sliding of the polymer chains starts. The motion/rotation of NDs, attached to Gr surface, further facilitates this process, thus increasing failure strain or ductility [224].

4.3.3.2 Fracture toughness to assess the Toughening Imparted by Binary Combinations of Nanofillers to Epoxy Matrix

Fracture toughness is another very important mechanical property, especially for structural applications. The effect of exfoliation of CNT and Gr on the Mode I fracture toughness of epoxy is studied here. The fracture toughness for all compositions were higher than that of the epoxy, which is 1.75 MPa.$m^{1/2}$ as seen from figure 4.21. This is due to the fact that the presence of reinforcement changes the fracture mode by obstructing the path of crack. When the crack propagates through the matrix, the crack front encounters impenetrable obstacle in the form of CNT, Gr sheets or ND. As a result, the crack is deflected, which increases the requirement of energy for further propagation of crack. A crack may encounter a series of obstacles on the way, which cause the crack to suppress or bow out between particles, leading to crack pinning or the crack may finally find the path of least resistance and propagate, after repeated deflections, causing failure. At higher filler content, the fracture toughness for all composites, i.e. CNT-epoxy, Gr-epoxy and ND-epoxy, reduced. This is due to the agglomeration of filler at higher wt%, as seen from figure 4.19 (a-c). As agglomeration

not only reduces the probable sites for crack deflection, but also acts as a site for stress concentration, which may lead to premature fracture of the composite. Further, the weak interface between matrix and agglomerate allows the crack to easily propagate through the interface, reducing the overall fracture toughness of the composite

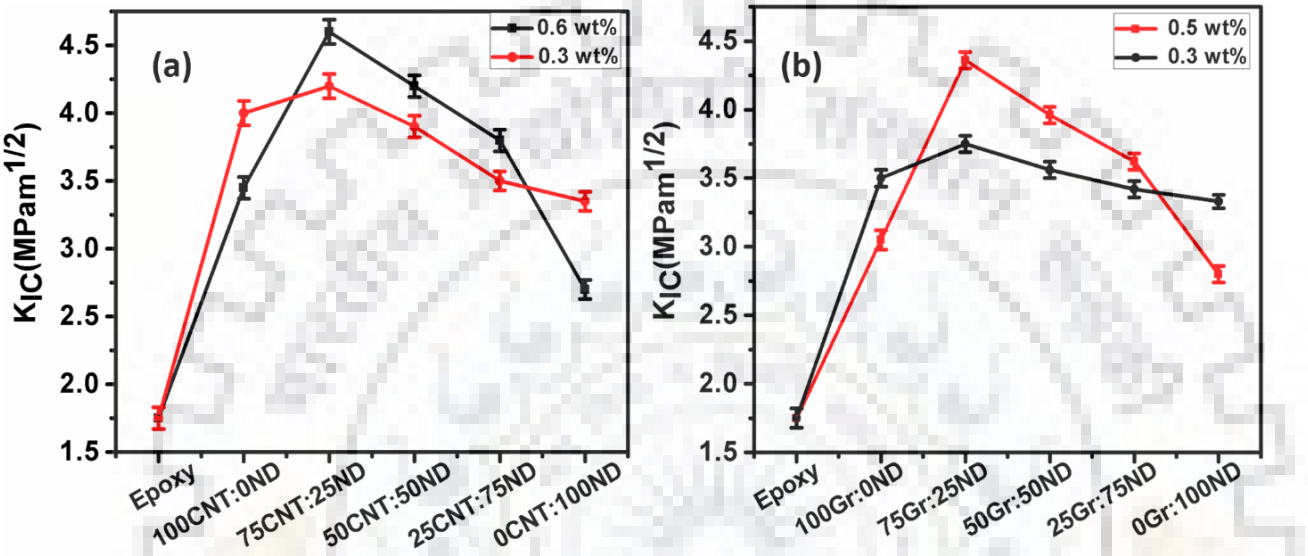

Figure 4.21 Fracture toughness plot for various combinations of **(a)** CNT-ND epoxy composite and **(b)** Gr- ND epoxy composite

With ND bridged CNT and ND decorated Gr as reinforcement to epoxy, the fracture toughness is seen to improve both at lower and higher filler content. Further, all combinations of ND bridged CNT epoxy composite and ND decorated Gr epoxy composites showed better fracture toughness than only CNT epoxy and only Gr epoxy composite with same filler loading. Sonicating CNT, in presence of ND, bridged the CNTs end to end. This increase in the aspect ratio for ND bridged CNT resulted in better crack bridging and improved the fracture toughness in 0.6 wt% (75CNT:25ND) composition, by ~163%, ~12% and ~33%, as compared to epoxy, 0.3 wt% (75CNT:25ND) and 0.6 wt% CNT, respectively.

Addition of ND to Gr during sonication improved dispersion of Gr, as the ND got attached to the surface of Gr sheet, preventing further stacking of sheets. Better dispersion signifies higher number of impenetrable obstacle encountering the crack front, which leads to greater fracture toughness. The highest improvement in fracture toughness was ~131 % with 0.5 wt% filler (75Gr:25ND), as compared to epoxy. The same was ~7% and ~36 %, as compared to 0.3 wt% (75Gr:25ND) and 0.5 wt% Gr, respectively. Hence, the improvement achieved in the mechanical properties with the addition of ND to Gr-epoxy composite, clearly proves the potential of ND in assisting exfoliation of Gr.

4.3.4 Thermal Analysis of Epoxy Reinforced with Binary Combinations of Nanofillers

4.3.4.1 Effect of Addition of Binary Combinations of Nanofillers on Thermal Degradation of Epoxy Matrix

As seen from figure 4.7. in chapter 4.1, the incorporation of CNT, Gr and ND as a unary filler to epoxy did not have any significant effect on its thermal stability. Only 5% mass loss occurs up to 300°C for nanofiller reinforced composites, which is due to the evaporation of moisture or volatile impurities. The degradation temperature was found to be ~340°C in each case, which is defined as the point of inflection on the TGA curve. The major mass loss of about 50% occurs between 350°C to 450°C. The thermal properties of nanofiller-epoxy composites are majorly governed by extent of dispersion/exfoliation of nanofillers. As, it controls the extent of interfacial interaction between the nanofiller and epoxy matrix. Thermal stability of nanodiamonds assisted exfoliated CNT and Gr as a reinforcement to epoxy composites were investigated by thermogravimetric analysis (TGA) in nitrogen atmosphere. Degradation in mass, as a function of

temperature, is presented in figure. 4.22(a, b &c). Initial mass loss, degradation temperature and response was similar to that mentioned above for unary fillers.

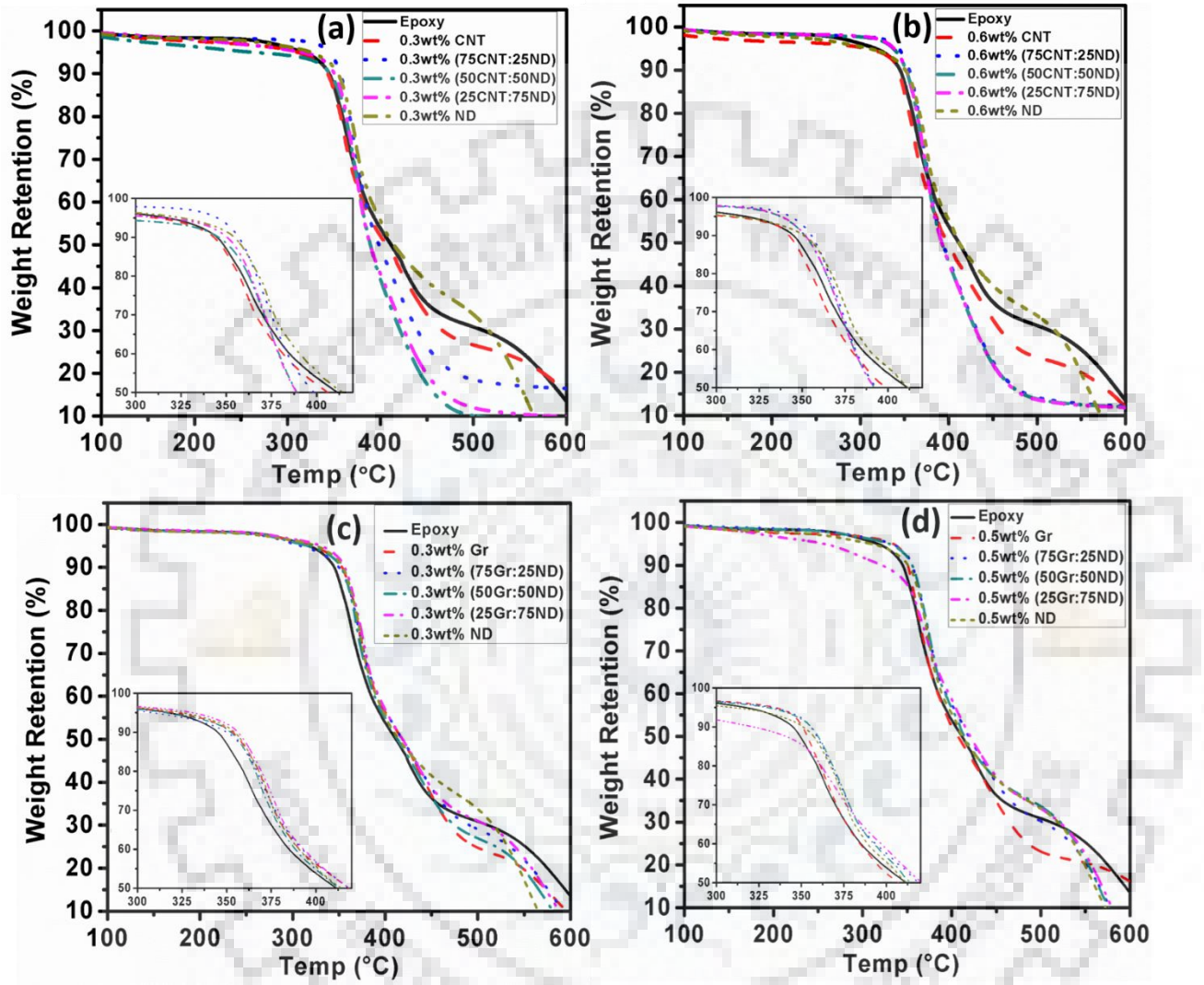

Figure 4.22 TGA thermogram for various combinations of **(a, b)** CNT-ND epoxy composite and **(c, d)** Gr- ND epoxy composite

A careful observation at the initial degradation temperature between 300 °C and 380 °C (inset in the figure 4.22) shows the improvement in thermal stability or degradation temperature of epoxy by ~10-15°C below ~340°C, with incorporation of ND exfoliated nanofiller. The improvement in

the thermal stability below the degradation temperature of epoxy is due to the presence of uniformly distributed and strongly integrated nanofillers, having higher thermal stability than epoxy. Once the temperature, rises above the degradation temperature, the epoxy starts becoming thermally unstable. Presence of ND bridged CNTs in epoxy, further degrade the thermal stability. The reduction in thermal stability is ~15-20°C over epoxy and around ~10°C over only CNT around 380°C, was seen, which further degraded at a much higher rate with increase in temperature. This reduced thermal stability is due to the bridging of CNTs by NDs which formed a long conducting network. Increasing the filler content from 0.3 wt% to 0.6 wt% reduced the thermal stability by 3-5°C. This is due to the more no. of thermally conducting networks formed at higher concentration.

Thermal stability of epoxy which reduced at higher temperature with incorporation of ≥ 0.3 wt% Gr, due to agglomeration, is seen to improve with ND exfoliated Gr by ~10-15°C for all compositions. The improved thermal stability of epoxy with incorporation of ND exfoliated Gr is evidenced for all compositions and combinations, both above and below the degradation temperature of epoxy. The improvement in thermal stability of the ND exfoliated Gr epoxy composite is postulated due to a sheet barrier effect or torturous path effect, which prevents the entry of oxygen and exit of volatile products evolved at high temperature or during thermal degradation. Addition of ND improved the exfoliation of Gr, which increased the total no. of sheets available to interact with epoxy matrix, thereby increasing the overall thermal stability of epoxy.

However, in either case, the thermal stability is found to be quite similar for hybrid filler irrespective of the difference in ratio.

4.3.4.2 Thermomechanical Analysis for Different Combinations of Binary Nanofiller Reinforced Epoxy Composite

As seen from the above studies, addition of ND to CNT and Gr during sonication led to improved exfoliation. DMA was done to gauge the effect of addition of fillers on the mobility of surrounding polymer through glass transition temperature. So, the effect of addition of, ND bridged CNT epoxy composite with 0.3 wt% and 0.6 wt% filler content and ND decorated Gr epoxy composite with 0.3 wt% and 0.5 wt% filler content, respectively on the mobility of epoxy matrix was studied through DMA. Temperature-dependent mechanical properties like storage modulus and damping factor, of a material when subjected to dynamic loading were evaluated using single cantilever mode at a ramp rate of 2^0C/min, constant frequency of 1 Hz and dynamic loading range of 0 to 10 N. DMA.

Figure 4.23 shows the typical storage modulus vs temperature plots for various combinations of CNT-ND epoxy and Gr-ND epoxy composite. It can be seen from the figure 4.23 that with the addition of 0.3 wt% CNT and 0.3 wt% Gr the storage modulus of epoxy increases by ~29% and ~26%, respectively. This improvement is due to improved load sharing by epoxy matrix with the addition of fillers. The storage modulus of Gr epoxy composite is less than CNT epoxy composite at 0.3 wt% reinforcement content, this is due to the sheet like morphology and extra π-π bonding of Gr they have the tendency to agglomerate at lower reinforcement content than CNT. Increasing the reinforcement, content from 0.3 wt% to 0.6 wt% and 0.5 wt% for CNT and Gr, respectively, improvement in storage modulus reduced to ~20% and ~8%, respectively. This reduction is due to the agglomeration of nanofillers at higher reinforcement content, which reduces the overall filler matrix interaction, which is more severe with Gr, as seen in figure 4.2.

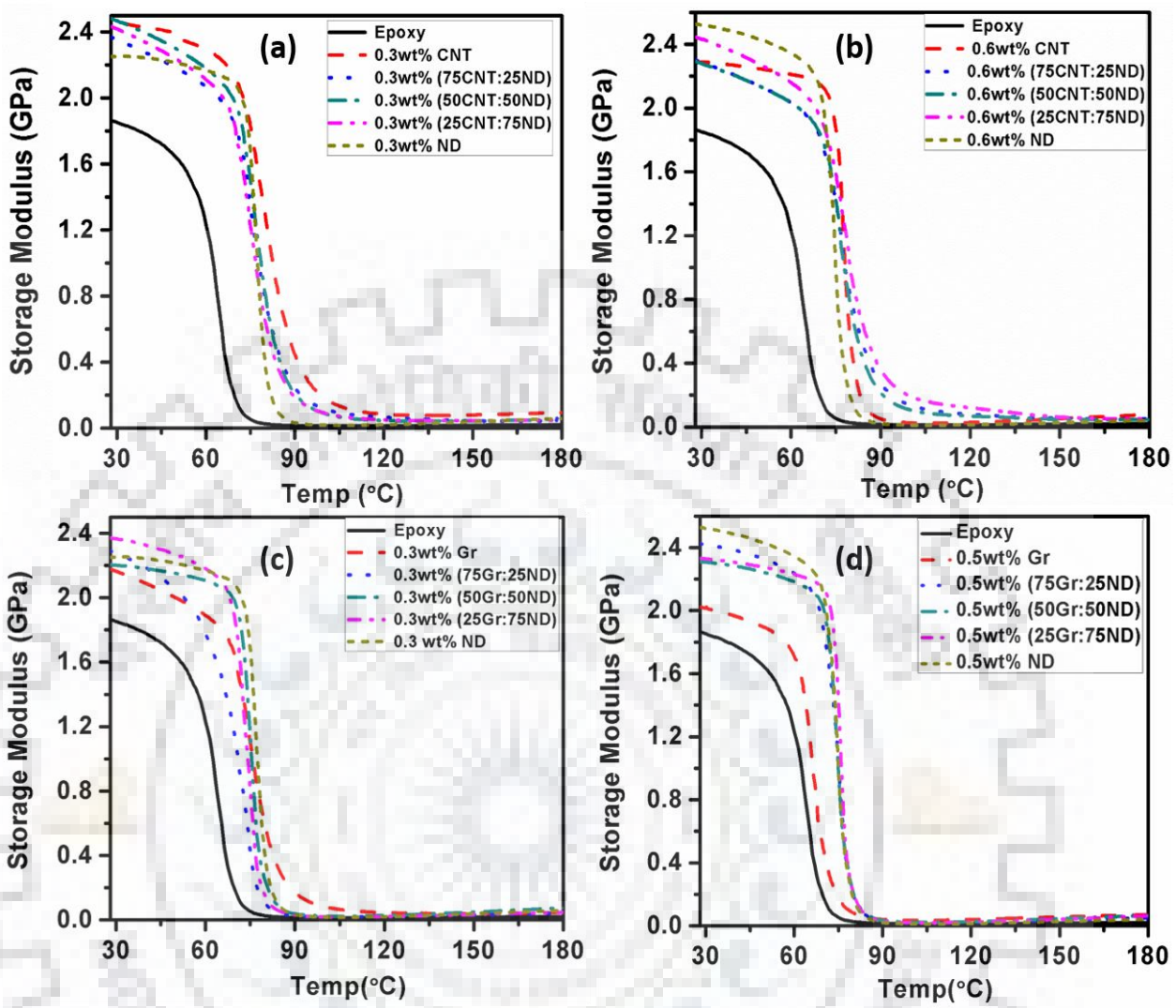

Figure 4.23 Storage modulus for various combinations of **(a)** 0.3 wt% CNT-ND epoxy, **(b)** 0.6 wt% CNT-ND epoxy, (c) 0.3 wt% Gr-ND epoxy and **(d)** 0.5 wt% Gr-ND epoxy composite as function of temperature

Addition of ND improved the storage modulus of CNT, with highest improvement with 0.5 wt% (25CNT:75ND), by ~11% and ~33%, over 0.6 wt% CNT and pure epoxy, respectively. Further, the highest improvement in storage modulus with ND decorated Gr was ~12 % and ~28%, over 0.5 wt% Gr and pure epoxy, respectively, with 0.5 wt% (75Gr:25ND). This improvement in storage modulus at room temperature is due to the improved filler matrix interaction, as ND reduces the entanglement of CNT by bridging/connecting them end to end. It also improves the exfoliation of

Gr, by adhering to its surface, which prevents the stacking of sheets due to strong π-π bonding. The retention of higher modulus by composites above room temperature, as compared to neat epoxy, is due to the restricted segmental mobility of the polymer chains in the structure.

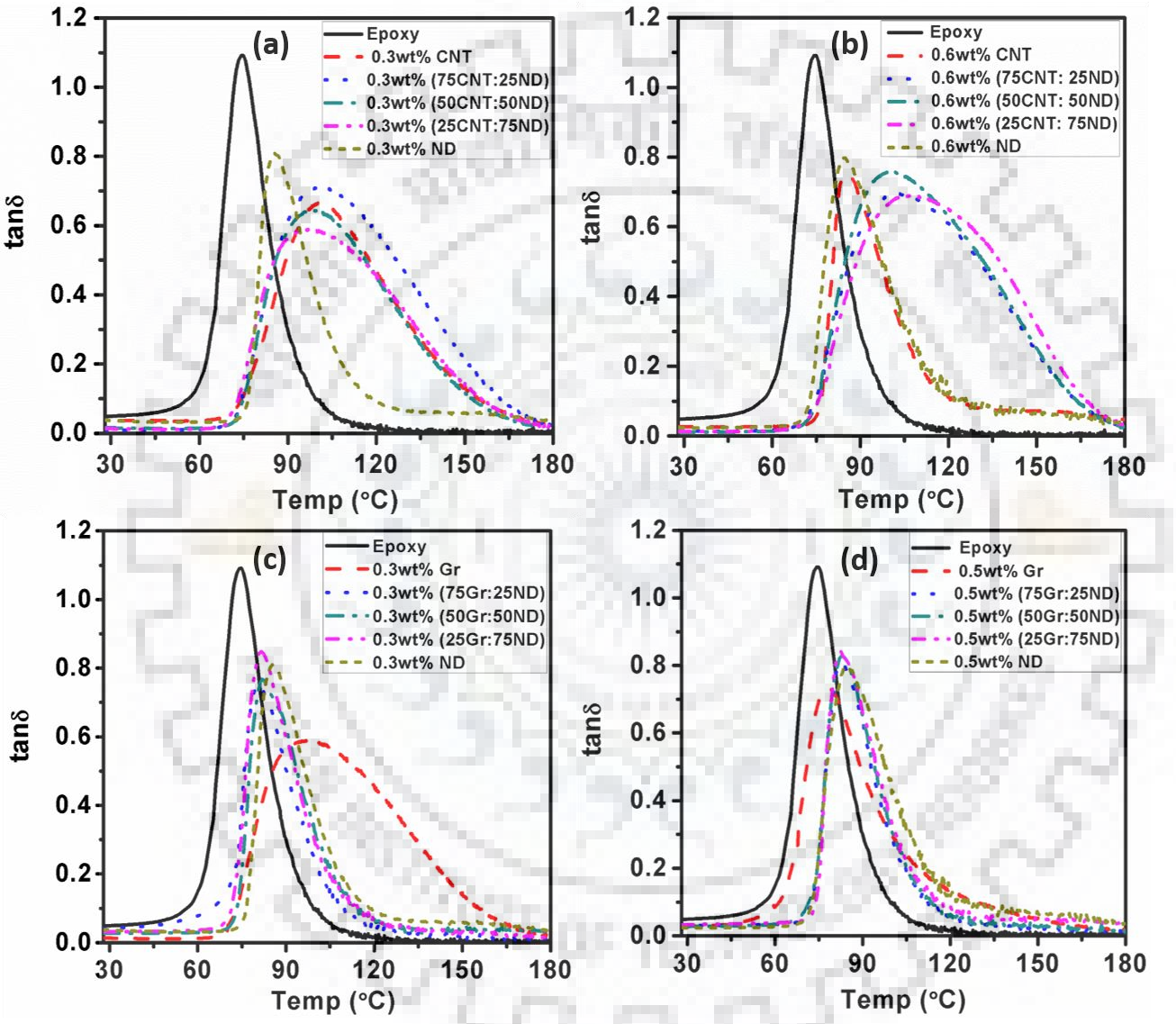

Figure 4.24 tanδ for various combinations of **(a)** 0.3 wt% CNT-ND epoxy, **(b)** 0.6 wt% CNT-ND epoxy, (c) 0.3 wt% Gr-ND epoxy and **(d)** 0.5 wt% Gr-ND epoxy composite as function of temperature

Representative tanδ (loss factor) vs. temperature plots for various combinations of CNT-ND epoxy with 0.3 wt% and 0.6 wt% reinforcement content and for Gr-ND epoxy with 0.3 wt% and 0.5 wt% reinforcement content is shown in figure 4.24. The peak value of these plots suggest the glass transition temperatures (T_g). The increase or decrease in T_g of a composite depends on the interaction between the filler and the matrix. If the interaction between the filler and the polymer is strong, the segmental mobility is less, which increases the T_g of the composite.

As explained by the dual monolayer theory, the first layer, formed next to the filler surface, is firmly bind to the stiff filler hinders the motion of polymer chain. The second layer is somewhat loosely bound, as it is formed little away from filler surface. As we move away from the filler surface the layers tend to becomes more and more mobile. Increase in filler content increases the number of first layers formed and reduces the distance between the fillers, thereby reducing the volume of immobile region. These events leads to higher T_g and lower tan δ. The glass transition temperature for epoxy was ~75 ^{0}C, addition of CNT improved T_g to ~100^{0}C, with further increase in CNT content to 0.6 wt% CNT, the T_g reduces to 85.3^{0}C, due to agglomeration of CNT. Addition of ND at higher reinforcement content, improves the T_g of CNT by 18-22°C, over 0.6 wt% CNT.

Addition of 0.3 wt% Gr, increased the glass transition of epoxy from ~75 ^{0}C to ~98^{0}C, further increase in Gr content to 0.5 wt%, the T_g reduces to ~78^{0}C, due to severe agglomeration. Addition of ND to Gr improved the T_g by 5-8°C, as compared to 0.5 wt% Gr. The improvement in glass transition temperature is due to the improved exfoliation of CNT and Gr with the addition of ND. Improved exfoliation led to stronger and increased filler matrix interaction, which restricted the segmental mobility of chains. Also, the ND which did not participate in exfoliation, helps reducing the free volume of the matrix. However, the improvement in T_g with ND is less than that with CNT, which is due to the spherical morphology of NDs. With, application of dynamic load at escalated

temperature, the ND attached to Gr surface, due to their spherical morphology promotes sliding of the polymer chains. Thus, the improvement achieved in the storage modulus and T_g due enhanced exfoliation of Gr with the addition of ND, is somewhat suppressed by the increased segmental mobility of polymer chain by ND. Higher the exfoliation, more the no of Gr decorated sheets having uniformly distributed ND over its surface. Therefore, more no. of ND interacting with polymer chains. So, a compromised improvement of around 10^0C-13^0C, as compared to epoxy and around 5^0C-8^0C, as compared to 0.5 wt% Gr, is achieved.

4.3.5 Summary

ND assisted exfoliation of CNT and Gr was successfully achieved using simple ultrasonication technique. Transmission electron microscopy and scanning electron microscopy confirmed the reduced entanglement of CNT by ND bridging their ends and improved exfoliation of Gr and proper integration of ND to the Gr surface. The composites, fabricated with ND bridged CNT and ND decorated Gr, revealed improved mechanical behaviour at both filler contents. The highest improvement in tensile strength and fracture toughness was seen with 0.6 wt% (75CNT:25ND) and 0.5 wt% (75Gr:25ND). These improvements are attributed to good exfoliation and strong interaction between filler and epoxy, as investigated through scanning electron microscopy of the fractured surface. Storage modulus and glass transition temperature also improved as a result of improved exfoliation by ND. The nanofillers did not affect the thermal stability significantly, especially below the degradation temperature of epoxy.

4.4 Nanodiamonds Assisted Exfoliation of Graphene and its Effect on Toughening Behaviour of Epoxy

Graphene (Gr) is one of the most preferred reinforcement for polymer matrix. The large surface area, offered by its 2D structure, allows better stress transfer between Gr and polymer. However, poor dispersion, due to stacking of Gr sheets, restricts their potential as a reinforcement in polymer matrix. Therefore, exfoliation of multi layered graphene (Gr) sheets through ultrasonication is done in the presence of nanodiamond (ND). TEM was done to confirm the role played by the ND in hindering restacking of graphene, by restricting the π–π stabilization. The extent of exfoliation achieved is further verified by measuring the thickness of Gr sheets for different combinations of Gr:ND through SPM. Numerical analysis is done to predict the effect of ND assisted exfoliation of Gr in terms of change in total interface area, on toughening behaviour of epoxy matrix. The predicted results are then compared to the experimental results, in order to evaluate the reinforcement efficiency of ND exfoliated Gr.

4.4.1 TEM Analysis to confirm the Nanodiamonds Assisted Exfoliation of Graphene

TEM images for Gr and Gr-ND hybrid, at different magnifications, are shown in figure 4.25(a-j). It can be seen from the figure 4.25(a & d) that the morphology of Gr is in the form of wrinkled nanoplatelet, with nanosheet dimensions of ~15 μm along the length and ~10 μm along the width. However, the thickness of the Gr or the number of nanosheets stacking is high, as evidenced from the opaque dark black colour, which reduces its overall aspect ratio. Thus, the total surface area of Gr in contact with the polymer is reduced.

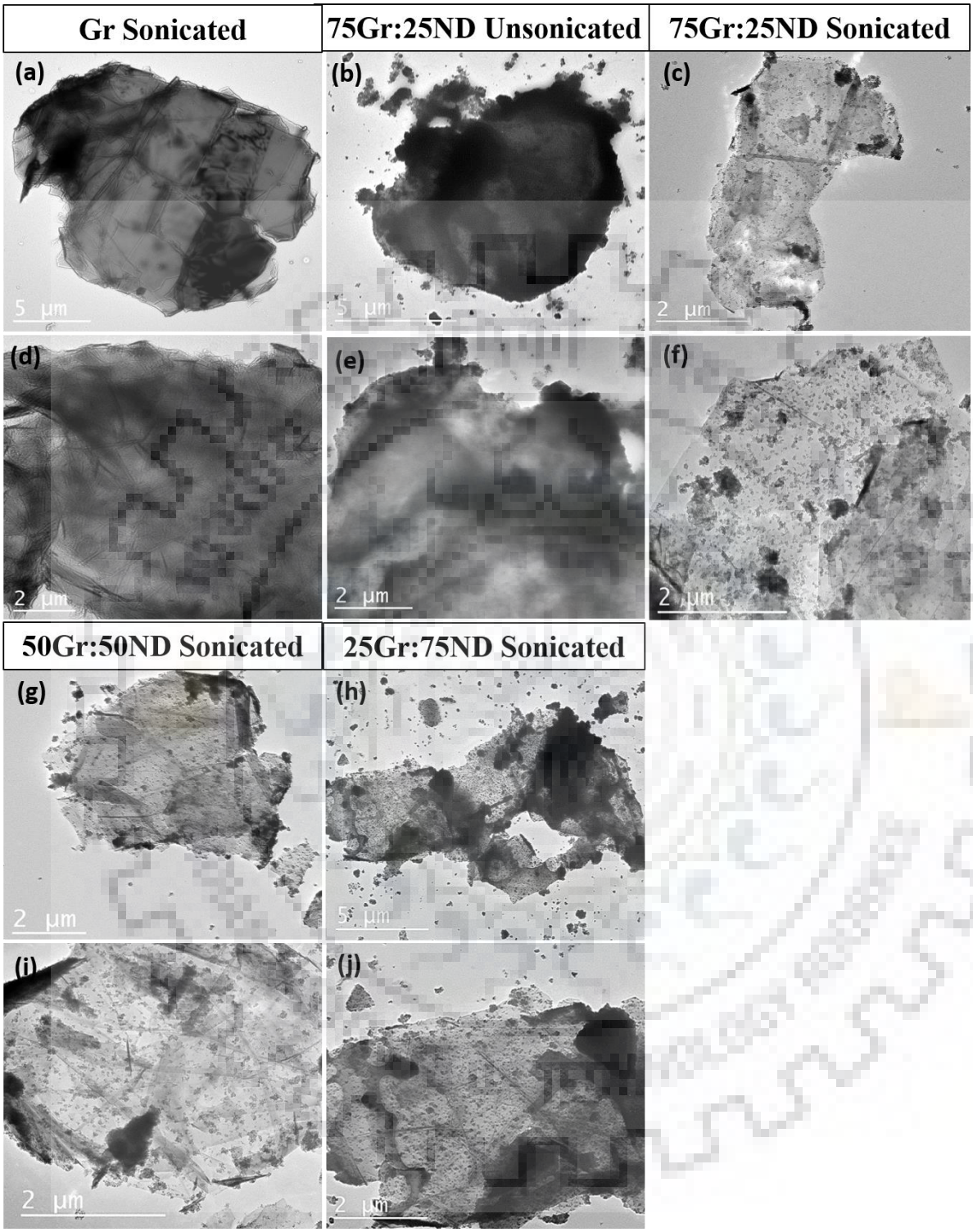

Figure 4.25 TEM images at different magnifications for **(a, f)** 0.5 wt% (100Gr:0ND), **(b, g)** 0.5 wt% (75Gr : 25ND) unsonicated, **(c, h)** 0.5 wt% (75Gr:25ND) sonicated **(d, i)** 0.5 wt% (50Gr:50ND) and **(e, j)** 0.5 wt% (25Gr:75ND)

Figure 4.25(b & e) shows the TEM image for 75Gr:25ND solution, which was not sonicated post mixing. As mentioned in materials and methods section, both Gr and ND were first sonicated separately for preparing Gr:ND hybrid. Once they were properly dispersed, they were mixed together and the mixture was further sonicated. Figure 4.25(c & f) shows the TEM images for 75Gr:25ND sonicated, post mixing. Comparative analysis of figures clearly shows that in order to achieve good exfoliation it is necessary to sonicate Gr in the presence of ND. Comparing figure 4.25 (b & e) with figure 4.25(c & f) clearly shows the increase in opaqueness of Gr sheets, with sonication. Sonicating Gr in the presence of ND, improved exfoliation of Gr, which can be clearly evidenced from the TEM images for different combinations of Gr:ND in figure (c, f, g-j). The Gr sheets, which were opaque and black due to stacking of multiple sheets (Figure 4.25(a)) before addition of ND, is found to be quite transparent after the addition of ND. Even, the size/area of the sheets are found to be maintained, post ultrasonication, with no sign of significant damage or fragmentation. The surfaces of Gr sheets are seen to be decorated with NDs, which restricted the π–π stabilization and hence inhibited stacking of Gr sheets.

The extent of exfoliation decreases, with the increase in the ND content in mixture beyond certain level, it starts agglomerating (figure 4.25(g - j)). This is due to the fact that with starting of agglomeration of ND its spatial availability for participating in exfoliation reduces. However, the exfoliation achieved is better for all combinations of Gr:ND, as compared to only Gr. Highest exfoliation is found at 75Gr:25ND combination. Thus, it can be concluded from TEM analysis that Gr should be sonicated in this presence of ND to achieve good exfoliation.

4.4.2 Assessing Exfoliation of Graphene with Addition of Nanodiamond by Surface Topography Imaging

The number of layers (thickness), size of the sheets, shape and presence and concentration of ND on the Gr surface highly affects its material property like elastic modulus, tensile strength, fracture toughness and others. Due to the nanoscopic nature of these features, the tool that can handle morphological characterization on this scale is required. Scanning probe microcopy is such a tool that allows evaluation of surface topography with nanometer scale resolution. 2D image, 3D profiling and line scan showing variation of thickness for ND, Gr, and Gr-ND, obtained through SPM technique, are shown in figure 4.26.

The potential of ND in exfoliating Gr is measured as difference in thickness of Gr with addition of ND, for different ratio. The thickness value for different combinations of Gr:ND nanofillers, are presented in table 5. The Gr:ND thickness values in table 5 are the average values, obtained from line scan in four different spots, in five different scanned images, chosen randomly. Out of all the line scans, the scan with highest thickness values are presented in figure 4.26, while the other three are presented in figure 4.27, along with a black and white 2D images showing contrast, confirming the exfoliation for all composition.

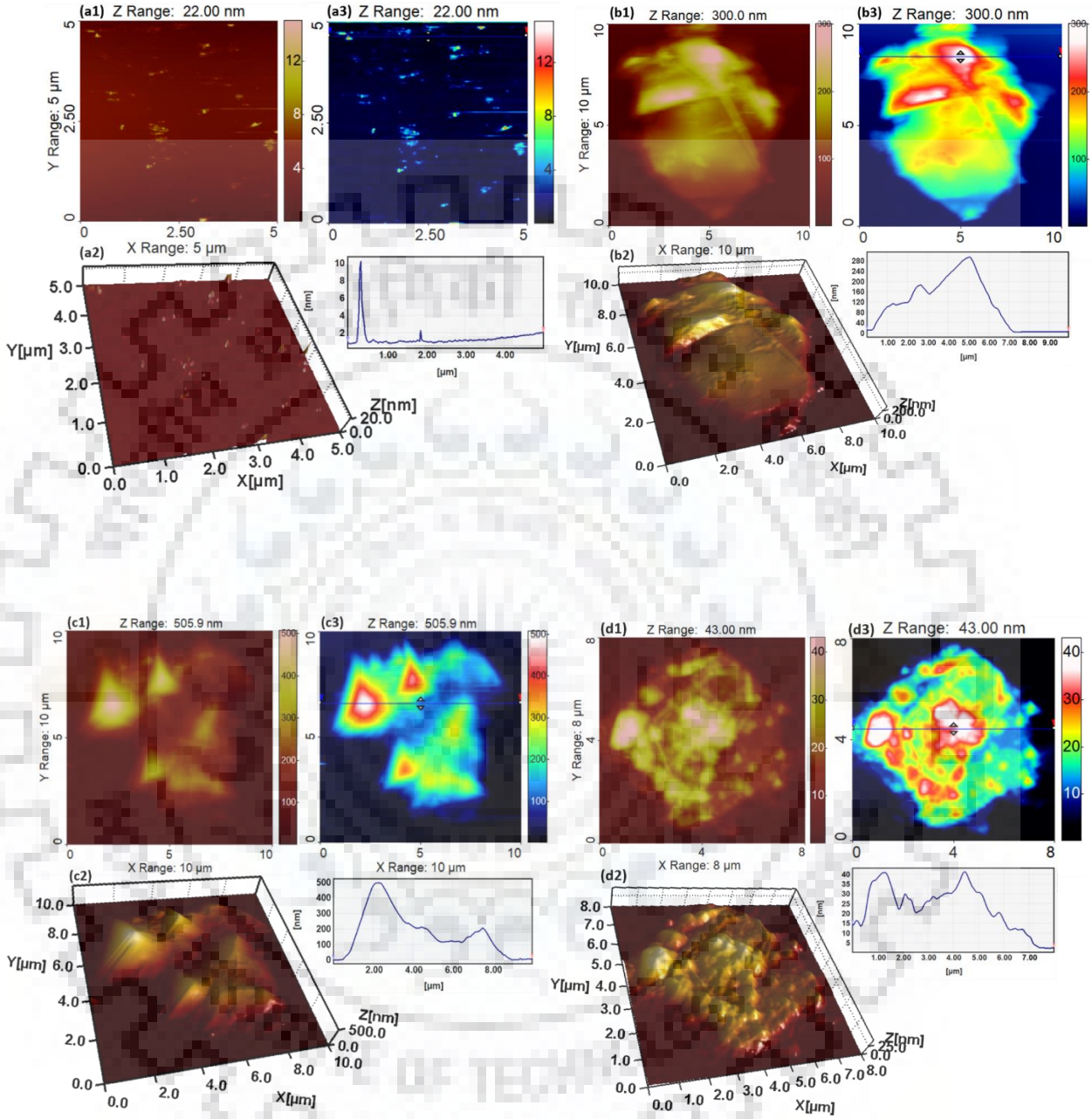
(a1) Z Range: 22.00 nm
(a3) Z Range: 22.00 nm
(b1) Z Range: 300.0 nm
(b3) Z Range: 300.0 nm
Y Range: 5 µm
Y Range: 10 µm
(a2) X Range: 5 µm
(b2) X Range: 10 µm
Y[µm]
X[µm]
Z[nm]
(c1) Z Range: 505.9 nm
(c3) Z Range: 505.9 nm
(d1) Z Range: 43.00 nm
(d3) Z Range: 43.00 nm
Y Range: 8 µm
(c2) X Range: 10 µm
(d2) X Range: 8 µm
[µm]
[nm]

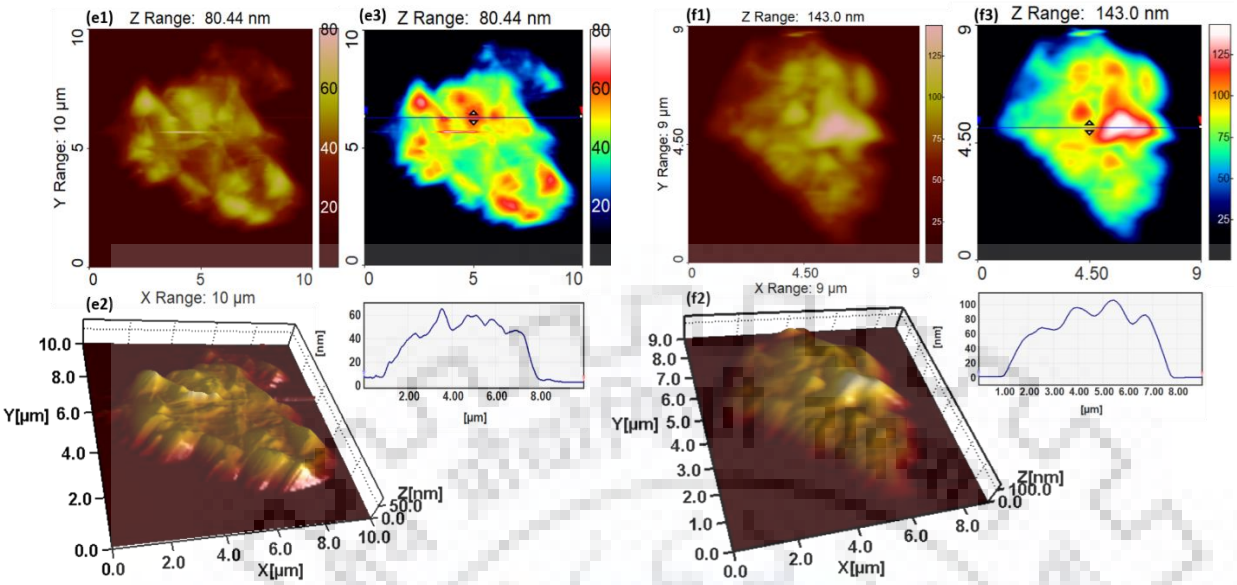

Figure 4.26 Surface morphology, 3D profiling and line scan with showing variation of thickness for **(a)** NDs, **(b)** Gr, **(c)** 75Gr:25ND unsonicated, **(d)** 75Gr:25ND sonicated, **(e)** 50Gr:50ND unsonicated and **(f)** 25Gr:75ND sonicated, processed through SPIP^{TM} software

Table 5. Shows the value for thickness and change in thickness for different combinations of Gr:ND

	Compositions	Thickness (nm)	Change in thickness
0.5 wt%	**0Gr:100ND**	8 ± 2	-
	100Gr:0ND	130 ± 15	-
	75Gr:25ND (unsonicated)	170 ± 20	↑ 1.3 fold
	75Gr:25ND	17 ± 2	↓ 7.6 fold
	50Gr:50ND	37 ± 3	↓ 3.5 fold
	25Gr:75ND	55 ± 5	↓ 2.4 fold

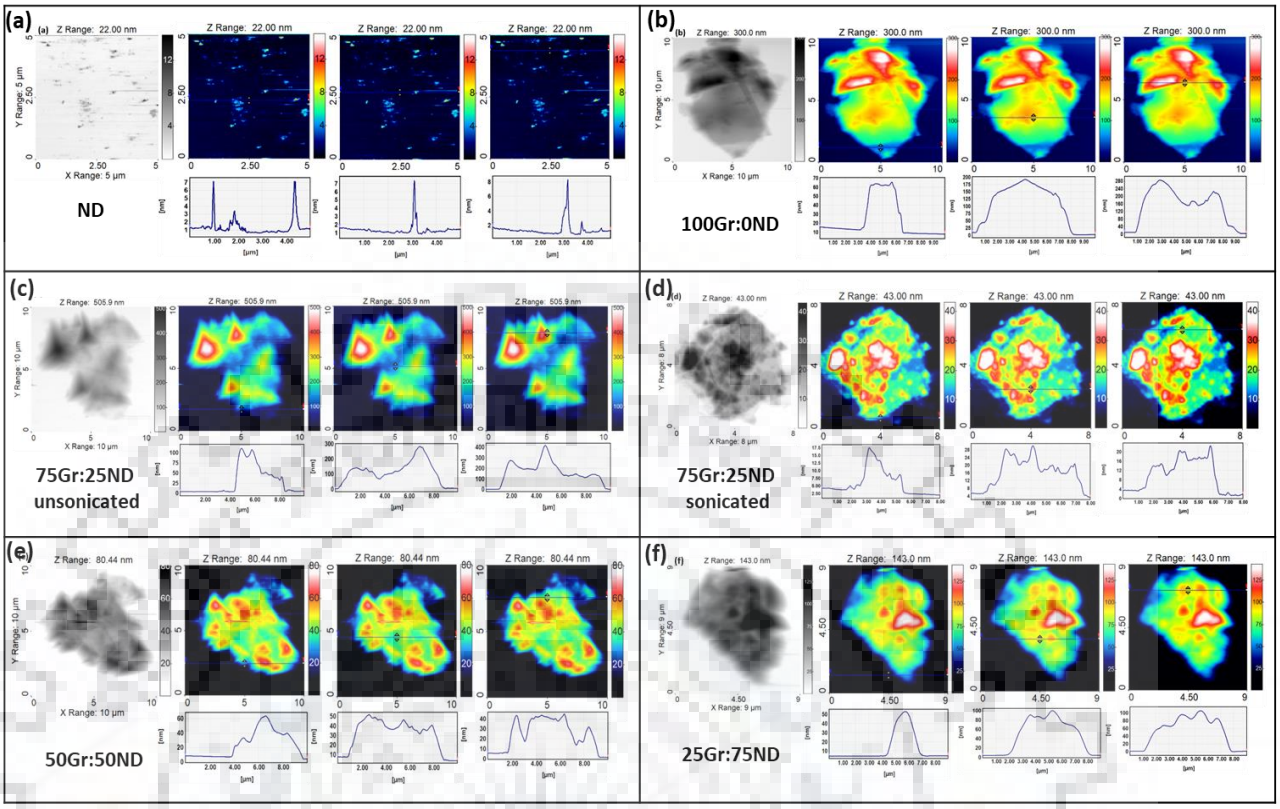

Figure 4.27 Surface morphology and line scan with surface thickness at three different locations **(a)** NDs, **(b)** Gr, **(c)** 75Gr:25ND unsonicated, **(d)** 75Gr:25ND sonicated, **(e)** 50Gr:50ND unsonicated and **(f)** 25Gr:75ND sonicated, processed through SPIP^{TM} software

The thickness values, (table 5) clearly shows that the addition of ND during exfoliation of Gr inhibited stacking of Gr sheets. The ND decorated Gr has offered thickness, as low as, 17 nm, as compared to 130 nm for Gr. However, it was not the case when dispersed ND was added to disperse Gr, but no sonication was done post mixing. The surface thickness was seen to increase to 170 nm for 75Gr:25ND, unsonicated. This clearly proves that just mixing the two together does not offer any exfoliation. Rather, Gr needs to be sonicated in the presence of ND to have efficient exfoliation.

The highest reduction in thickness is achieved with 75Gr:25ND, which is around 7.6 fold as compared to Gr. The NDs can be seen uniformly distributed throughout the Gr sheet (figure 4.26(d)), with the 3D profiling showing multiple spikes. With increase in ND content further, the thickness of

Gr is seen to increase, as compared to 75Gr:25ND. However, it is always less than only Gr. This increase in Gr thickness with increase in ND content is due to the increased affinity of ND to cluster at higher concentrations, as evinced from both TEM and SPM images.

4.4.3 Numerical Analysis to Predict the Effect of Exfoliation on Toughening Behaviour of Epoxy

It is confirmed from TEM and SPM analysis that sonicating Gr in the presence of ND improves exfoliation. The thickness data, obtained from SPM, shows that the thickness of Gr is reduced upto 7.6 times. Improved exfoliation means more number of impenetrable obstacles in crack path, which leads to improved fracture toughness. Thus, numerical analysis was done to predict this behaviour of epoxy reinforced with both Gr and ND exfoliated Gr,. However, there are several limitations in this study. To simulate crack initiation and its successive propagation damage models needs to be applied. Each damage models in abaqus need various material properties as input for e.g. Hashin damage model for composite requires longitudinal tensile strength, longitudinal compressive strength, transverse tensile strength, transverse compressive strength, longitudinal shear strength, transverse shear strength, longitudinal tensile fracture energy, longitudinal compressive fracture energy, transverse tensile fracture energy, transverse compressive fracture energy, which were not available in this study. Another limitation is the small thickness of Gr, which becomes even smaller with exfoliation. If the dimension of specimen for numerical analysis is chosen similar to that used in experimental analysis, than the number of Gr in each sample of size 44 mm x 10 mm x 5 mm would be in the order of 10^5. It is, therefore, not possible to perform simulation for such huge population of reinforcement, having such small size. A solution to this limitation is to use a sub size

2D model. However, the results, predicted by sub size specimen, cannot be absolutely compared tothose from full size experimental specimen.

Therefore, 2D analysis of SENB specimen (figure 4.28(a).) having geometry and dimension similar to experimental specimen are performed in this study, under plane stress condition, using finite element code in ABAQUS software. A typical FE mesh of 2D analysis is shown in figure 4.28(b). SENB specimen are modeled using four node bilinear plane stress quadrilateral (CPS4R) element, with reduced integration approach. The number of elements and node in FE meshes ranged from 5855 elements/6048 nodes to 7580 elements/7779 nodes. SENB specimen is subjected to a uniaxial tensile strain at the middle of top surface and lower ends are hinged and roller supported, as shown in figure 4.28(c). As a response, force and displacement were obtained under specific loading and boundary conditions. Element typs CPS$R were used to avoid problems associated with incompressiblity reduced integration element within ABAQUS. Elastic properties obtained using Hashin-Shtrikman approach (eq. 6 & 7) are used in the FE analysis.

$$E^{HS+} = \frac{9K^{HS+}\mu^{HS+}}{3K^{HS+}+\mu^{HS+}} \tag{6}$$

$$E^{HS-} = \frac{9K^{HS-}\mu^{HS-}}{3K^{HS-}+\mu^{HS-}} \tag{7}$$

$$K_{HS}^{\pm} = K_2 + \frac{\emptyset}{(K_1-K_2)^{-1}+(1-\emptyset)(K_2+\frac{4}{3}\mu_2)^{-1}} \tag{8}$$

$$\mu_{HS}^{\pm} = \mu_2 + \frac{\emptyset}{(\mu_1-\mu_2)^{-1}+\frac{2(1-\emptyset)(K_2+2\mu_2)}{5\mu_2\left(K_2+\frac{4}{3}\mu_2\right)}} \tag{9}$$

Where, $\emptyset$ is the volume fraction (V), E^{HS+} and E^{HS-} are the upper bounds and lower bound for elastic modulus for $\mu^{HS+}$and μ^{HS-} shear modulus and K^{HS+} and $K^{HS-}$are bulk modulus, obtained using Hashin–Shtrikman equations 8 & 9. The upper bound is computed when $K_2 > K_1$. The lower bound is computed by interchanging the indices in the equations. For upper bound $\emptyset$ is V_2 and for lower bound $\emptyset$ is V_1. As seen from literature, both Gr and ND possess almost similar elastic modulus of 1 TPa and Poisson's ratio of 0.2 [229]. Epoxy has elastic modulus of 4.6 GPa, as obtained from instrumented indentation and Poisson's ratio of 0.35 [228]. For calculating elastic property for composites through Hashin-Shtrikman model, the weight percent of reinforcement was first converted to volume percent. The contribution of Gr and ND in that voulme percent is then calculated based on their ratio for each composition using eq 10.

$$V_{EG} = V_G I_E + V_{ND} \quad (10)$$

V_{EG} is the volume fraction of exfoliated graphene, V_G is the volume fraction of graphene in Gr-ND hybrid mixture, I_E is the no. of times increment achieve in exfoliation and V_{ND} is the volume fraction of ND in Gr-ND hybrid mixture. Hence, the total voulme of reinforcement post exfoliation is the voulme fraction of Gr added in Gr-ND hybrid miture, multiplied by the number of times the exfoliation improved plus the volume fraction of ND in Gr-ND hybrid miture. The upper bound and the lower bound for elastic propeties, thus obtained from Hashin-Shtrikman, contains the effect of exfoliation. These elastic properties were then used for numerical analysis of 2D SENB specimen.

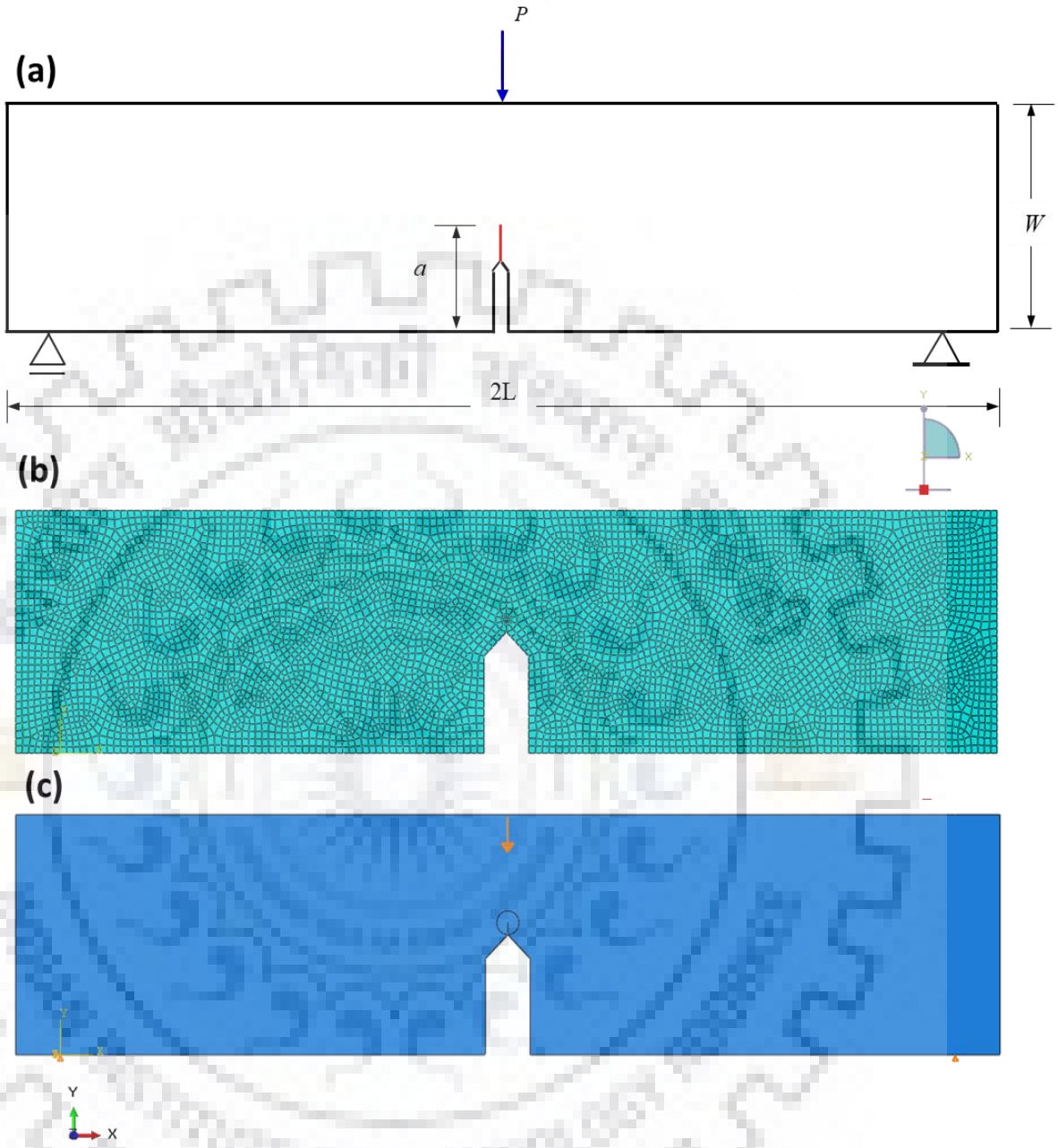

Figure 4.28 (a) Schematic representation of the SENB specimen, **(b)** meshed SENB specimen and **(c)** RVE subjected to the uniaxial tensile strain

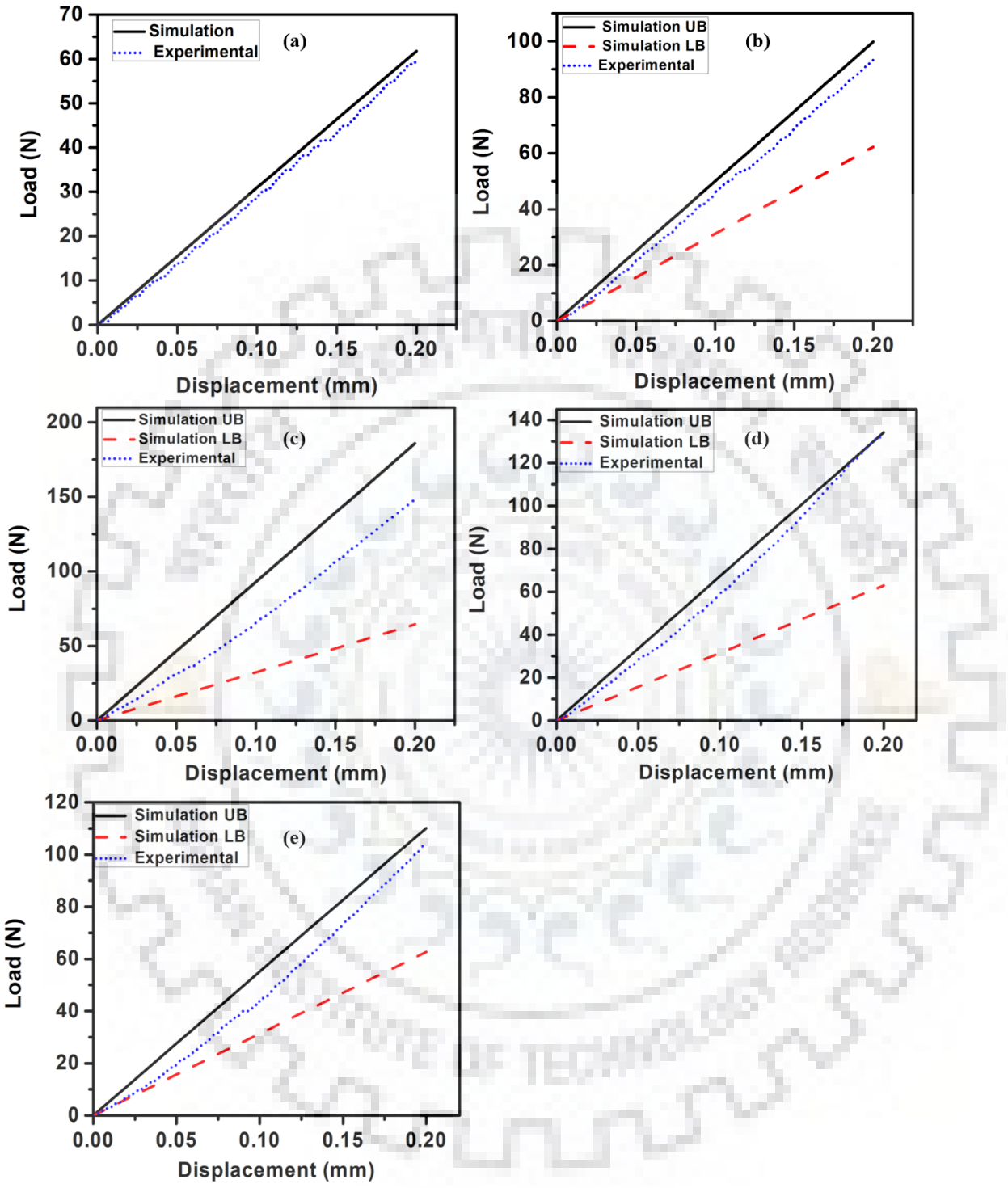

Figure 4.29 Comparison of load vs displacement plot obtained from numerical analysis of SENB analysis through Hashin-Shtrikman bounds and experimentally for **(a)** epoxy, **(b)** 0.5 wt% (100Gr:0ND) epoxy, **(c)** 0.5 wt% (75Gr:25ND) epoxy, **(d)** 0.5 wt% (50Gr:50ND) epoxy and **(e)** 0.5 wt% (25Gr:75ND) epoxy composite

The load (force) vs displacement plot for loaded 2D SENB specimens are obtained through numerical analysis . Two plots were obtained for each composition , corresponding tomlower and upper bound elastic properties, except for pure epoxy. These plots are compared to experimental load vs displacement plots for (figure 4.29). The plots obtained from numerical analysis for pure epoxy is a very close match with that obtained from experimental analysis, as seen from figure 4.29(a). For ND exfoliated Gr epoxy composite, the experimental plots lie between the predicted plots, for all composition. Further, the experimental plots are more towards the upper bound, which signifies the efficiency of ND in exfoliating Gr. The upper bound means the maximum load a crack tip can sustain for a particular strain, before its start to propagate. It basically signifies the maximum reinforcement efficiency. On the other hand, the lower bound defines the minimum load at which the crack propagates, which signifies almost negligible or zero reinforcement efficiency. As the experimental plots in this study are a better match with upper bound, it clearly indicates the efficiency of ND in exfoliating Gr, followed by the toughening of epoxy matrix..

The load, sustained by a notched specimen for same strain, is higher for Gr and Gr-ND epoxy composites, as compared to epoxy. The highest load is sustained by 75Gr:25ND, which is due to the better exfoliation leading to higher interfacial area to share the load. Hence, more load is required for opening the crack tip or for crack to propagate. All compositions of Gr-ND epoxy composite showed higher load carrying capacity than Gr-epoxy composite. However, for Gr-ND hybrid filler with ND ratio > 25, the load carrying capacity decreased due to reduced exfoliation. The results, thus predicted, are in good agreement with results obtained from experimental, SPM and TEM analysis.

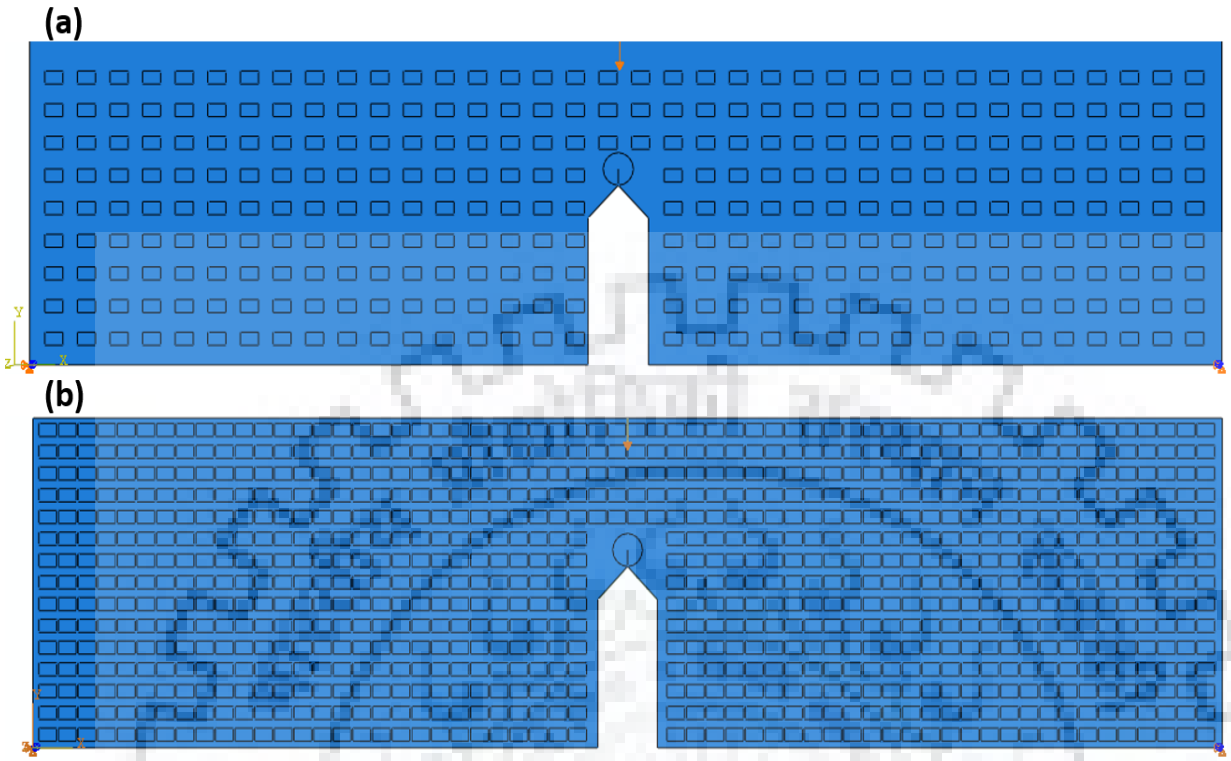

Figure 4.30 SENB specimen containing different volume fraction of Gr, distributed in the continuous epoxy matrix for **(a)** Gr and **(b)** 75Gr:25ND

The von Mises stress distribution, obtained for full sized specimen, does not help in understanding and visualising the effect of exfoliation of Gr in toughening the epoxy matrix. Hence, the sub size 2D specimen, having length of 1 mm and width of 0.22 mm, with different population of Gr for different composition distributed inside epoxy was analysed (figure 4.30). The boundary conditions and loading was similar to that of full sized specimen. Similar to full size specimen, the number of Gr was increased by the number of times the exfoliation improved for each combination. The von Mises stress distributions for all compositions are shown in figure 4.31. The load vs displacement plot, obtained for sub sized specimen, does not have any significance and hence, they are not presented.

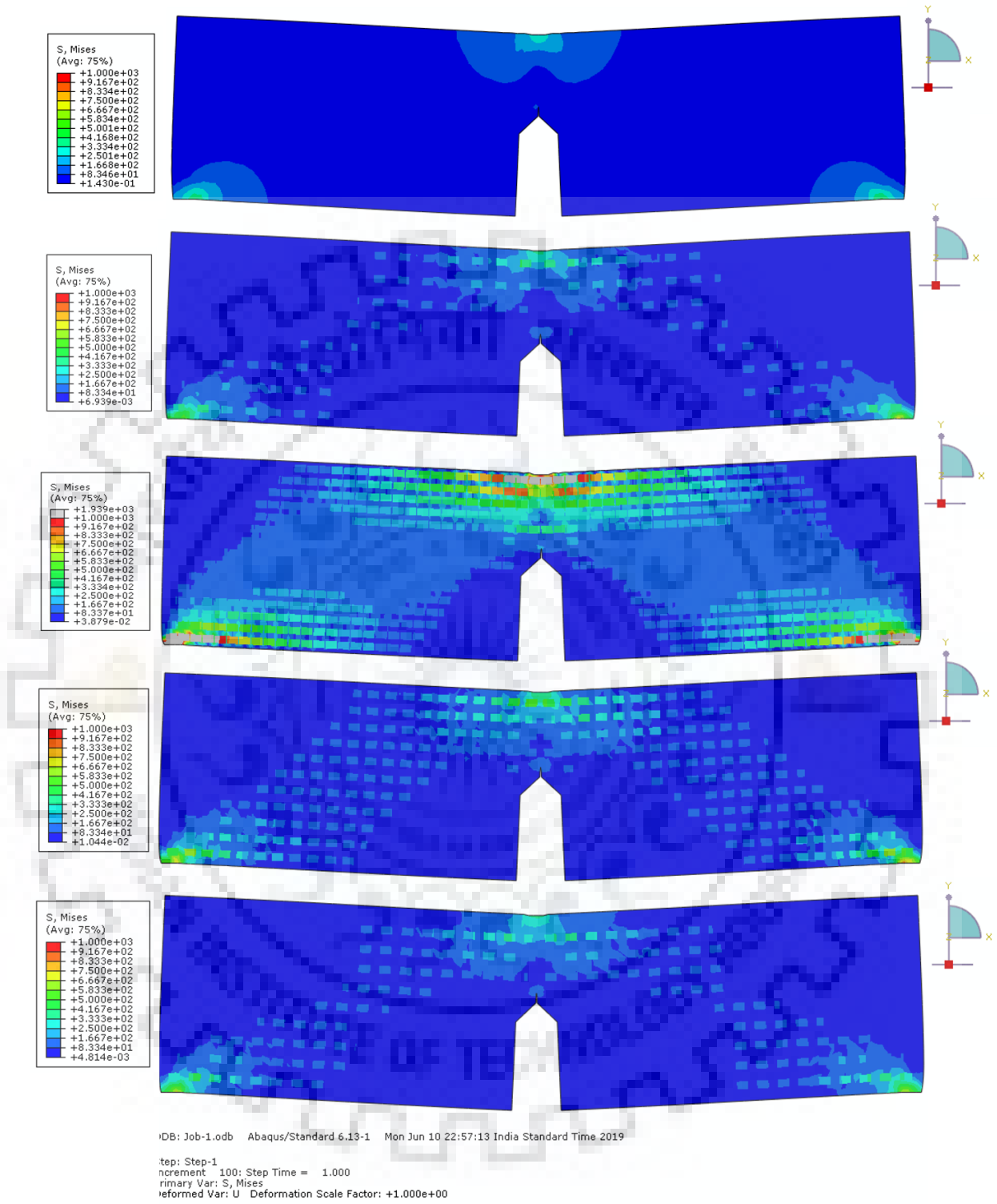

Figure 4.31 von-Mises stress distribution for **(a)** epoxy, **(b)** 0.5 wt% (100Gr:0ND) epoxy, **(c)** 0.5 wt% (75Gr:25ND) epoxy, **(d)** 0.5 wt% (50Gr:50ND) epoxy and **(e)** 0.5 wt% (25Gr:75ND) epoxy composite

It can be clearly seen from von Mises stress distribution that when a SENB specimen is loaded, crack propagation in epoxy require less load as compared to Gr epoxy and Gr-ND epoxy composite. In case of epoxy (figure 4.31 a), as there is no reinforcement to share load, the stress is localized at the points where specimen is loaded (above the crack tip) and where it is supported. The stress, is not shared by the entire sample and it is localized near the crack tip, therefore the crack propagates at low load figure 4.29(a). With the inclusion of Gr in epoxy matrix, the stress is equally shared and distributed among the Gr available in the vicinity of applied load as seen from figure 4.31(b). Hence, the load required for crack to propagate is higher than that for epoxy as seen from figure 4.29(b). With addition of ND, the exfoliation of Gr is improved, increasing the total no. of Gr available per unit area for sharing load. This reduces the space between two adjacent Gr, forming a well-connected network, as a result the stress is distributed uniformly throughout the matrix, as seen from figure 4.31(c). Thus, the load required for crack to propagate will be higher than Gr-epoxy as well as only epoxy as seen from figure 4.29(c). Hence, it can be concluded that if the exfoliation is better, the number of Gr available to interact with epoxy matrix is more and higher is the load shared by them. Therefore, the von Mises stress distribution clearly depicts the toughening imparted by ND exfoliated Gr to epoxy

4.4.4 Summary

ND assisted exfoliation of Gr was successfully achieved using simple ultrasonication technique in proper sequence, as confirmed from TEM and SPM analysis. NDs attach themselves to the surface of Gr, which restricts the π–π stabilization and hence inhibits the re-stacking of Gr sheets. The exfoliation achieved with 75Gr:25ND is 7.6 folds, which is the highest exfoliation among all

composition. Improved exfoliation of Gr resulted in better toughening, which is even confirmed through von Mises distribution. The load vs displacement plots, obtained from numerical analysis, are in good agreement with the experimental results. All of these also prove that the exfoliation of Gr plays a key role in improving the mechanical behaviour of the Gr-epoxy composite.

4.5 Investigating the Potential of Nanodiamonds in Boosting the Synergistic Effect of Gr-CNT Hybrid Filler in Epoxy

In this section, the potential of ND in improving synergistic effect of Gr-CNT hybrid and there after its potential as a reinforcement to epoxy matrix is explored. In depth TEM and FE-SEM analysis of fillers at different stages of exfoliation, with different combinations of nanofillers are investigated. Once the desired exfoliation is achieved, the composite is fabricated and tested for mechanical and thermal properties. The fractured surfaces of the tensile samples are then investigated through FE-SEM to get insight of dispersion, interfacial interaction of fillers with matrix and thus validating the differential mechanical properties across compositions.

The optimized composition in unary reinforcement with each filler, is used as an input for selecting the composition for binary reinforcement. Similarly, the composite with binary reinforcement is tested and analyzed, the optimized composition and combination of binary fillers is used as an input for ternary reinforcement. The composites with all the combinations of fillers are evaluated for tensile test and fracture toughness.

4.5.1 Microstructural Characterization to Verify the Synergistic Effect of Nanodiamond Addition on Graphene-Carbon Nanotube Hybrid filler

The TEM micrographs, revealing morphology of Gr, Gr-CNT and Gr-CNT-ND hybrids are shown in figure 4.32. The TEM image in figure 4.32(a) shows that the morphology of Gr is in the form of stacked wrinkled nanoplatelets, as evidenced from the opaque dark black color. To, improve exfoliation and prevent the restacking of Gr nanosheets during exfoliation the sonicated solution of CNTs were added to Gr solution during sonication. The improved exfoliation of Gr with the addition of CNT can be evidenced in figure 4.32(c). CNTs attach to the surface of Gr sheets preventing them

from restacking. However, as already mentioned and seen from figure 4.1(d) CNTs tend to entangle due to the tube like morphology, thus reducing the total number of CNTs interacting with the Gr sheets.

In order to overcome this drawback and to further improve the exfoliation, NDs were added to Gr-CNT hybrid. The TEM analysis (figure. 4.1(f)) of the ND revealed the spherical morphology and the size of individual ND, which is ~10 nm. However due to the small size and high surface energy, NDs tends to cluster in a group of 10-15 in number. All three nanofillers i.e. Gr, CNT and ND were exfoliated separately. Then, half of ND solution was added to Gr and the other half to CNT and sonicated. The TEM image of these binary combinations are presented in figure 4.32(c & d). Addition of ND improved exfoliation of Gr sheets. The Gr sheets, which appear opaque and black due to stacking of multiple sheets (figure 4.32(a)) before addition of ND, are found to be quite transparent after the addition of ND (figure 4.32(c)). The transparency indicates less number of graphene sheets stacked in the structure. The surface of Gr sheets is also seen decorated with ND, which restricted the π–π stabilization and hence inhibited stacking of Gr sheets. In case of CNT-ND mixture, the NDs cluster and attach themselves to the ends of CNTs bridging them together into long chains (figure 4.32(d)). This prevents the entanglement of CNTs to some extent, thus increasing the overall aspect ratio in the hybrid structure and hence its efficiency as reinforcement. Gr-ND and CNT-ND solutions are then added together and sonicated. The hybrid mixture with ternary combination of nanofillers thus obtained is shown in figure 4.32(e). The addition of ND to the pre-synthesized Gr-CNT mixture did not lead to good exfoliation as shown in figure 4.32(f). Infact, exfoliating all three separately and then mixing them together in one shot and sonicating also gave exfoliation similar to figure 4.32(f). The exfoliation achieved for ternary nanofillers in figure 4.32(e)

was better compared to what was achieved in figure 4.32(f). Comparing figure 4.32(b) with figure 4.32(e) confirms the improved exfoliation of Gr-CNT with the addition of ND.

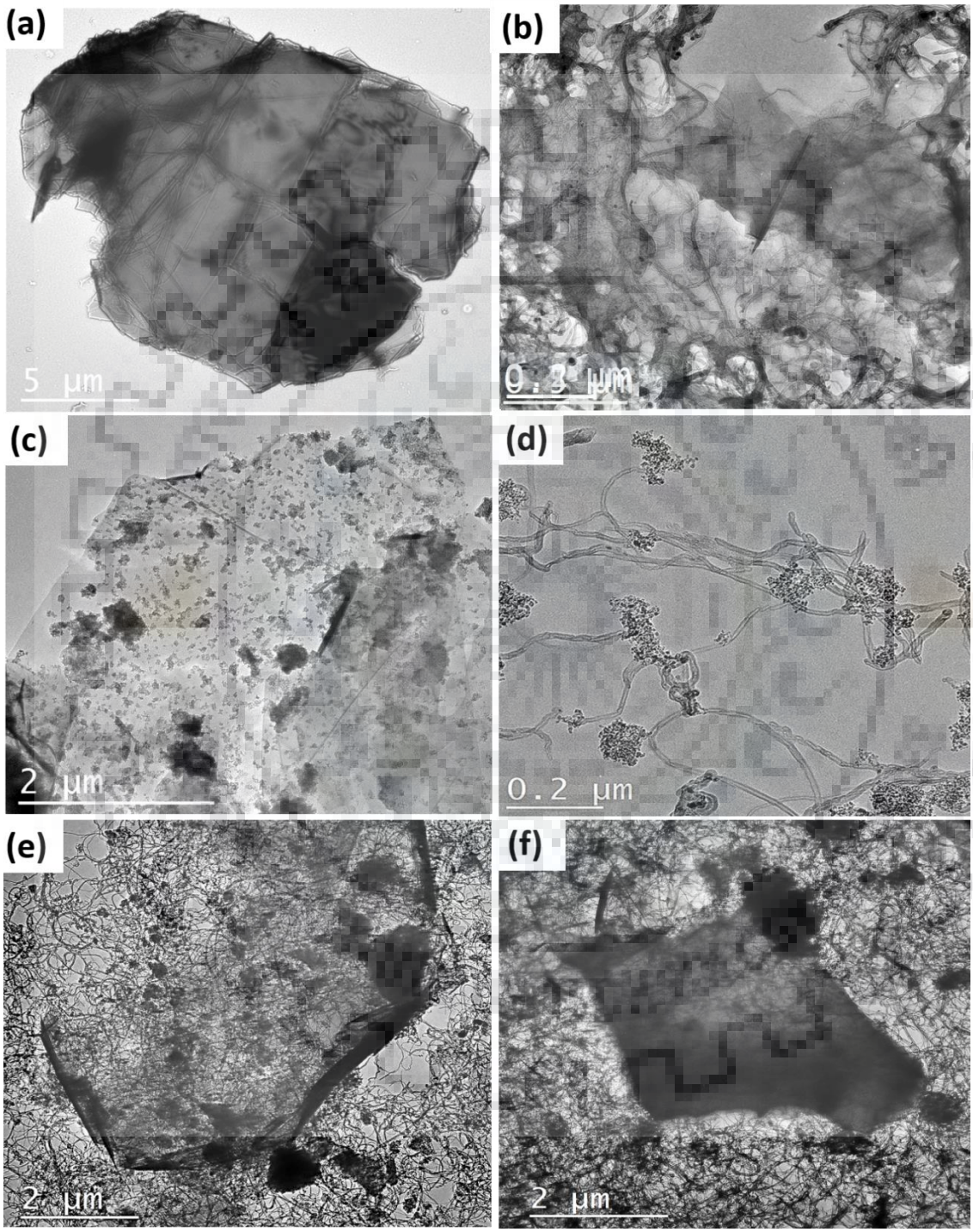

Figure 4.32 TEM images of **(a)** Gr, **(b)** Gr-CNT, **(c)** Gr-ND, **(d)** CNT-ND, **(e)** Gr-CNT-ND (exfoliated) and **(f)** Gr-CNT-ND agglomerated

The morphology, exfoliation and placement of nanofillers for Gr, Gr-CNT and Gr-CNT-ND combinations were further verified through FE-SEM images (figure 4.33(a-f)). For unary nanofillers, the FE-SEM images reaffirms the size and stacking of Gr sheets. FE-SEM images for binary combinations of nanofillers confirms the improved exfoliation of Gr sheets, with the addition of CNTs and NDs (figure 4.33(b & c)). A comparison of Gr, Gr-CNT and Gr-ND images (figure 4.33 (a, d & e)), clearly shows that the Gr sheets get exfoliated with addition of both CNT and ND. However, the exfoliation achieved with ND is better. Graphene sheets appear thick, torn, folded due to multiple sheets of different sizes stacked randomly one over other in figure 4.33(a). They transform to, thin, less crumpled sheets with CNTs uniformly distributed over the entire surface (figure 4.33(b)) and extremely thin ones with no traces of broken or folded sheets on the surface with ND covering the entire surface uniformly (figure 4.33(c)). The exfoliation achieved with ND is much better than that with CNTs, due to entanglement in the latter reducing their effective number to restricting the stacking of Gr. This is evidenced by the presence of only few CNTs on Gr surface and more clustered on the surrounding area (figure 4.33(b)). Figure 4.33(d) confirms the bridging of CNTs by ND clusters, preventing the entanglement of CNTs. The FE-SEM image for ternary combination of Gr-CNT-ND (by method adopted for this study) reveals improved exfoliation (figure 4.33(e)), as compared to all binary combinations, as well as, the ternary combination achieved by adding ND to the pre-mixed Gr-CNT combination (figure 4.33(f)). Therefore, both TEM and FE-SEM analysis confirms that the addition of ND improves the exfoliation of the binary combination of Gr-CNT, increasing its efficiency as a reinforcement.

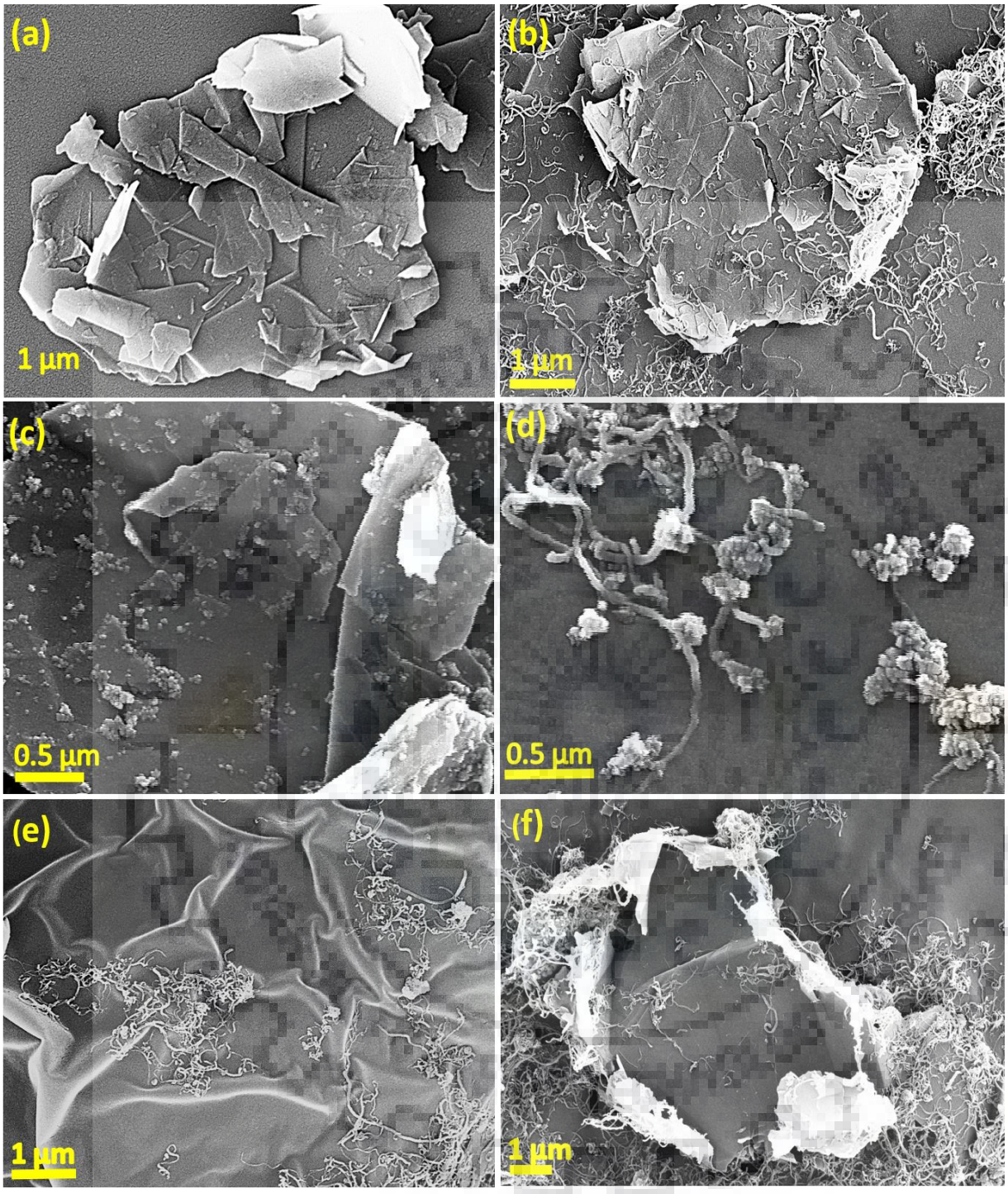

Figure 4.33 FE-SEM images of **(a)** Gr, **(b)** Gr-CNT, **(c)** Gr-ND, **(d)** CNT-ND, **(e)** Gr-CNT-ND (exfoliated) and **(f)** Gr-CNT-ND agglomerated

4.5.2 Fracture Surface Analysis of Epoxy Reinforced with Gr-CNT, and Gr-CNT-ND hybrid

The fractured surfaces of composites were investigated through FE-SEM to study the dispersion of nanofillers and the strengthening effect imparted as a result (figure 4.34). At 0.3 wt% Gr addition, the fractured surface of composite shows agglomeration at few places (figure 4.34(a)), while CNT and ND reveal good dispersion and compatibility with the epoxy matrix (figure 4.34(b & c)). The agglomeration of Gr, even though is not that severe, may still act as a site for failure, when subjected to stress due stress concentration and weak interface. With increase in reinforcement content further from 0.3 wt% to 0.5 wt%, the size and severity of agglomeration becomes detrimental in case of Gr, with only one end embedded in epoxy matrix and rest suspended out (figure 4.34(d)). Unlike Gr, the agglomerate size is quite small and completely coated with epoxy in case of CNT and ND, making it less prone to failure (figure 4.34(e & f)).

Figure 4.34(g-i) shows the fractured surface morphology for various combination of Gr-CNT hybrid composite. As compared to Gr/CNT-epoxy composite, the Gr-CNT hybrid epoxy composite showed better dispersion and interaction with the epoxy matrix at 0.5 wt% content. The addition of CNT to Gr led to improved dispersion, as, CNTs bridged the Gr sheets, thus preventing their restacking and thereby reducing entanglement of CNTs. The presence of uniformly dispersed Gr-CNT lead to strong interaction with the matrix, which can be witnessed by the sharp edges of the Gr sheets and the ends of CNTs protruding from all the three combinations. However, still the sharp edges of Gr sheets at some places can be seen devoid of epoxy, especially with the combinations having high Gr ratio.

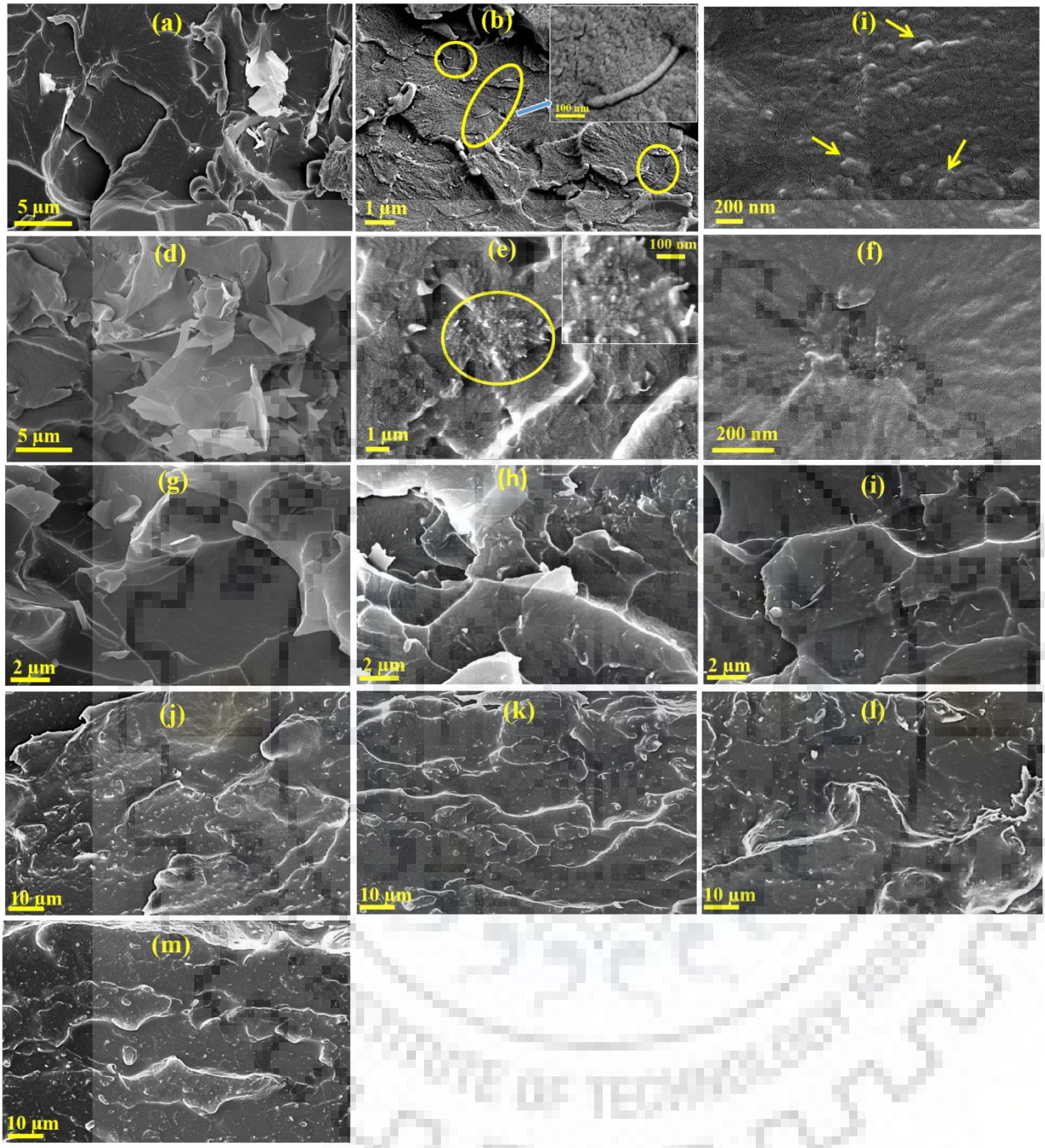

Figure 4.34. FE-SEM images for fractured surface of **(a)** 0.3 wt% Gr, **(b)** 0.3 wt% CNT, **(c)** 0.3 wt% ND, **(d)** 0.5 wt% Gr, **(e)** 0.5 wt% CNT, **(f)** 0.5 wt% ND, **(g)** 0.5 wt % (75Gr:25CNT), **(h)** 0.5 wt% (50Gr:50CNT), **(i)** 0.5 wt % (25Gr:75CNT), **(j)** 0.8 wt% (50Gr:25CNT:25ND), **(k)** 0.8 wt% (25Gr:50CNT:25ND), **(l)** 0.8 wt% (25Gr:25CNT:50ND) and **(m)** 0.8 wt% (33Gr:33CNT:33ND) epoxy composite

To further improve the dispersion, ND was added to Gr-CNT Hybrid. As already mentioned in the previous section, instead of adding complete ND to Gr-CNT hybrid. It was divided in two equal halves, each of which was separately added to Gr and CNT. Both the solutions were sonicated separately, then mixed together and further sonicated. Comparative analysis of FE-SEM images in figure 4.34(j-m) show that the dispersion and the interfacial interaction with the matrix for ternary reinforcement was much better even at high content of 0.8 wt%. In fact, the dispersion in this case was even much better than binary (figure 4.34(g-i)) and unary reinforcement (figure 4.34(a-f)) at even lower content. No traces of agglomeration can be seen on the fractured surface for all combinations with ternary reinforcement. The fracture surface morphology of composite with ternary reinforcement looks very similar. However, the addition of ND to Gr-CNT has changed the morphology of fractured surface significantly. Sharp edges and wrinkles on the 2D Gr sheets, which are predominant on the fracture surface of Gr-epoxy composite (figure 4.34(a & d)) diminishes in Gr-CNT epoxy composite (figure 4.34(g-i)), subsided considerably in presence of NDs. Attachment of NDs on the surface of Gr not only helps in inhibiting the stacking of Gr sheets by restricting π-π stabilization, but also knits the CNTs into a network, thereby reducing the entanglement. This increases the number of CNTs available for interaction, which further inhibits the stacking of Gr and improves the efficiency of CNTs as a reinforcement. The improved number and interaction of CNTs and ND on the Gr surface and edges prevent the Gr features to be reflected evidently on fractured surface of composite. This proves that the interaction between the Gr-CNT is improved both quantitatively and qualitatively with the addition of ND.

4.5.3 Mechanical Behaviour of Gr-CNT and Gr-CNT-ND Reinforced Epoxy Composites

4.5.3.1 Tensile Studies to Assess the Strengthening Imparted to Epoxy by Gr-CNT and Gr-CNT-ND fillers

Tensile properties were studied to understand the effect of improved exfoliation of nanofillers with binary and ternary combinations on epoxy matrix. The representative stress strain plots for Gr-CNT epoxy and Gr-CNT-ND epoxy composite for different compositions are shown in figure 4.35(a-d). The values of UTS and % strain for different compositions and combinations, calculated from the stress strain plots, are presented in table 6. The highest improvement in UTS was ~25% and ~18% with 0.2 wt% Gr and 0.3 wt% CNT, above which it reduces and becomes less than that for pure epoxy with ≥ 0.5 wt % Gr or CNT-epoxy composite (figure 4.4). The FE-SEM micrographs in figures 4.34 confirm the same. The micrographs clearly show that with 0.3 wt% Gr the agglomeration is not that evident (figure 4.34(a)). However, with 0.5 wt% Gr, the agglomeration becomes severe with multiple Gr sheets settled at one place with their edges dangling out, having no traces of epoxy on the surface (figure 4.34(a)). This clearly indicates weak interface between Gr and epoxy matrix at high content, thereby leading to failure of composite at considerably low load. On the other hand, CNTs can be seen properly dispersed throughout the matrix. The ones which were aligned along the direction of applied load protruding out of the fractured surface as marked by an arrow, while the one encircled is aligned in the transverse direction have their surface exposed, as seen in the inset in figure 4.34(b). Agglomeration starts with increase in CNTs content to 0.5 wt%. But it is not as severe as with 0.5 wt% Gr, as the CNT clusters can be seen coated with epoxy. The agglomerated CNTs act as a site for stress concentration and crack generation, which leads to premature failure and low UTS.

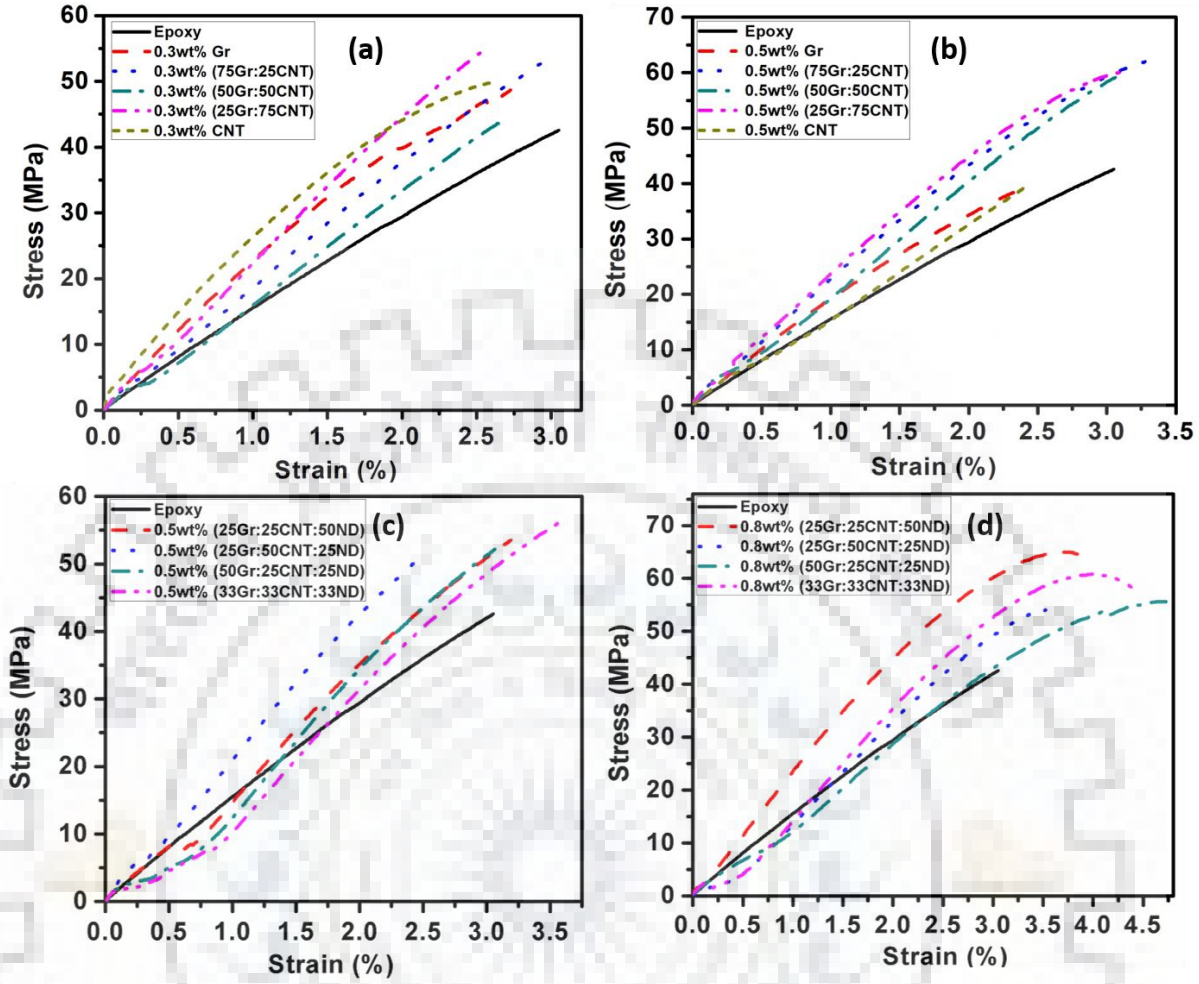

Figure 4.35 Representative stress-strain plots for various combinations of **(a)** 0.3 wt% Gr-CNT, **(b)** 0.5 wt% Gr-CNT, **(c)** 0.5 wt% Gr-CNT-ND and **(d)** 0.8 wt% Gr-CNT-ND epoxy composite

The highest UTS value was recorded with 0.2 wt% Gr and 0.3 wt% CNT. So, two compositions were selected for Gr-CNT hybrid composite as following: the highest value out of the individual best i.e. 0.3 wt% and; sum of individual best i.e. 0.5 wt%. These two compositions were tested for 5 different combinations of Gr:CNT i.e. 100:0, 75:25, 50:50, 25:75 and 0:100, the representative stress strain plots for which is shown in figure 4.35(a & b)). The UTS was higher for all combinations of Gr:CNT epoxy composite as compared to epoxy matrix and Gr/CNT-epoxy composite. The maximum improvement achieved in UTS was ~42% and ~60% in 0.5 wt% (75 Gr: 25CNT), as compared to pure epoxy and 0.5 wt% Gr, respectively. The fractured surface of Gr-CNT

hybrid does not show any traces of severe agglomeration with 0.3 wt % or 0.5 wt % reinforcement content (figure 4.34(g-i)). This reveals that the CNTs have the potential to improve the exfoliation of Gr. However, the combination with high Gr content (figure 4.34(g)) at few places shows small edges of pulled out Gr.

Table 6. Ultimate tensile strength, % strain, % improvement in fracture toughness for various composition and combination of Gr-CNT and Gr-CNT-ND epoxy composites

Composition		UTS (MPa)	% Strain	Improvement in K_{IC} (%)
Epoxy		42.5 ± 1.2	3.05 ± 0.2	-
0.3 wt%	**100Gr:0CNT**	48.7 ± 1.5	2.72 ± 0.3	101
	75Gr:25CNT	53.9 ± 1.4	3.02 ± 0.2	111
	50Gr:50CNT	43.8 ± 1.3	2.65 ± 0.2	117
	25Gr:75CNT	54.9 ± 1.3	2.56 ± 0.2	123
	0Gr:100CNT	49.9 ± 1.4	2.6 ± 0.3	128
0.5 wt%	**100Gr:0CNT**	38.9 ± 1.5	2.36 ± 0.4	74
	75Gr:25CNT	62.1 ± 1.3	3.28 ± 0.2	123
	50Gr:50CNT	59.2 ± 1.2	3.06 ± 0.2	128
	25Gr:75CNT	60.0 ± 1.2	3.10 ± 0.2	140
	0Gr:100CNT	39.5 ± 1.3	2.42 ± 0.4	154
0.5 wt%	**25Gr:25CNT:50ND**	53.5 ± 1.2	2.47 ± 0.3	80
	25Gr:50CNT:25ND	51.0 ± 1.3	3.18 ± 0.3	91
	50Gr:25CNT:25ND	52.2 ± 1.3	3.06 ± 0.3	78
	33Gr:33CNT:33ND	56.8 ± 1.2	3.62 ± 0.3	87
0.8 wt%	**25Gr:25CNT:50ND**	64.2 ± 1.2	3.95 ± 0.2	155
	25Gr:50CNT:25ND	54.2 ± 1.2	3.52 ± 0.2	165
	50Gr:25CNT:25ND	55.9 ± 1.2	4.72 ± 0.2	148
	33Gr:33CNT:33ND	59.8 ± 1.2	4.38 ± 0.2	158

For further improving the synergistic effect of Gr-CNT hybrid, ND was added. The tube like morphology of CNT, having high aspect, tend to cause entanglement. This leads to reduction in the overall aspect ratio, surface area and efficiency of CNT in exfoliating Gr, as well as, reinforcement. The Gr-CNT-ND hybrid were tested for two compositions, i.e., 0.5 wt% and 0.8 wt% for 4 different combinations of Gr:CNT:ND i.e. 25:25:50, 25:50:25, 50:25:25 and 33:33:33. The highest improvement in UTS was ~34% with 0.5 wt% (33Gr:33CNT:33ND) as compared to pure epoxy. However, the improvement is not as much as expected, it is less than that obtained with Gr-CNT hybrid. As seen from the table 6 that combinations of Gr-CNT-ND having higher ND ratio had higher UTS. This means that the amount of ND is not enough to achieve the desired exfoliation leading to the morphology similar to figure 4.33(f), where Gr is not properly exfoliated and ND bridged CNTs are seen sitting at very few places. To overcome this drawback, the reinforcement content was raised from 0.5 wt% to 0.8 wt% for the same ratios of nanofillers. This was decided as the total reinforcement content being the sum of individual best (optimized composition) of Gr, CNT and ND-epoxy composites, i.e., 0.2 wt%, 0.3 wt% and 0.3 wt%, respectively. The highest improvement in UTS was obtained with 0.8 wt% (25Gr:25CNT:50ND) to be ~51% and ~20%, respectively, as compared to pure epoxy and 0.5 wt% (25Gr:25CNT:50ND). The higher value of UTS for all combinations with increase in reinforcement content from 0.5 wt% to 0.8 wt% proves the potential of ND in improving exfoliation of Gr and reducing entanglement of CNTs. The fracture surface morphology in figure 4.34(j-m) shows very uniform dispersion, with no trace of agglomeration or free lying Gr, CNT or ND. These observations suggest strong interfacial interaction and no discontinuity or stress concentration.

The fractured surface morphology for ternary reinforcement has more resemblance to ND epoxy composite, rather than wave or ripple like morphology of Gr epoxy composite formed due to

the sharp edges of Gr. As, due to the good exfoliation of Gr sheets, its surface as well as the edges are completely covered with ND and ND bridged CNT which is then effectively wrapped in epoxy, making their presence less evident on fractured surface. Similarly, the ends of CNTs, which were earlier seen protruding out of the fractured surface throughout the matrix, are rarely seen due to the ends of CNTs bridged by NDs. This uniformly dispersed well connected network of Gr-CNT-ND, having strong interfacial interaction with epoxy, is the key to efficient load transfer from matrix to reinforcement. Any discontinuity, whether agglomeration (stress concentration or crack generation) or weak interface, will lead to inefficient load transfer or premature failure when loaded externally.

4.5.3.2 Fracture Toughness to Assess the Toughening Imparted to Epoxy by Gr-CNT and Gr-CNT-ND fillers

The composites were also evaluated for fracture toughness, as it is another very important mechanical property that needs to be evaluated for structural applications, especially with brittle epoxy matrix. The presence of reinforcement not only changes the fracture toughness of matrix, but its morphology affects the mode of fracture and the active toughening mechanism. Thus, fracture toughness is the property, which is affected the most by the extent of dispersion as well as the morphology of reinforcement. The fracture toughness values, calculated from 3-point bend test, are shown in figure 4.36(a & b) for binary and ternary compositions. The fracture toughness values for all compositions and combinations are higher than that for pure epoxy and the % improvement in fracture toughness w.r.t epoxy is presented in table 6. The increase in fracture toughness is due to the presence of nanofillers, which changes the mode of fracture by impeding the path of crack. In case of epoxy, the crack once initiated propagates through the sample up till fracture, without getting deflected, bridged or pinned down by any impenetrable obstacle. However, with the addition of

nanofillers, the crack front encounters a series of impenetrable obstacle in the form of Gr, CNT or ND.

In case of nanofiller reinforced epoxy composite, the toughening is caused by matrix deformation, interfacial debonding, nanofiller rupture, crack deflection, crack bridging or crack pinning. The crack is deflected, bridged or pinned due to interaction with nanofillers, which creates the requirement of more energy for further propagation of the crack. A crack may even get fully suppressed after encountering multiple of such occasions or it may finally find the path of least resistance and propagate causing failure. The increase the fracture toughness of epoxy matrix is noted as ~101%, 154%, 140% and 165% with 0.3 wt% Gr, 0.5 wt% CNT, 0.5 wt% (25Gr:75CNT) and 0.8 wt% (25Gr:50CNT:25ND), respectively.

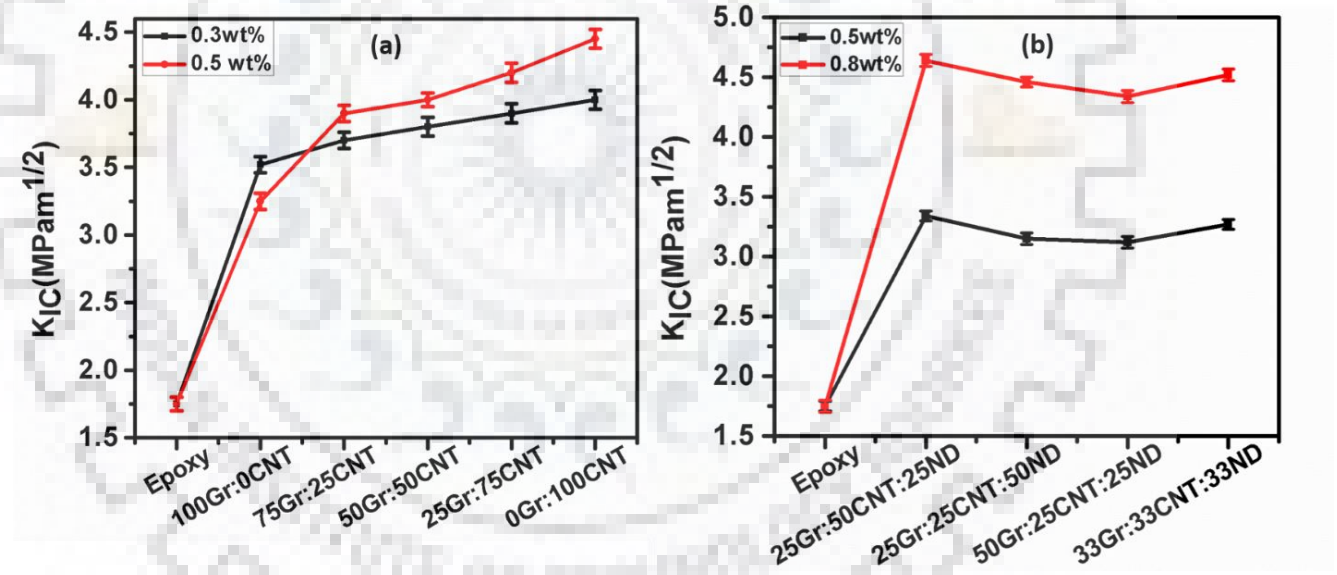

Figure 4.36 Fracture toughness plots for various compositions and combinations of **(a)** Gr-CNT and **(b)** Gr-CNT-ND epoxy composite

Higher filler content for Gr-epoxy (0.5 wt%) and Gr-CNT (1 wt%) composites lead to reduction in fracture toughness, due to agglomeration of reinforcement phases, as seen from figure 4.34(d & e). Agglomerated nanofillers act as sites for crack generation, due to stress concentration. Further, agglomeration reduces the effective spatial distribution of reinforcement phases, leading to

reduction in number of probable sites for crack deflection. In addition, weak interface between matrix and agglomerate allows the crack to easily propagate through the interface. All of these result into deterioration of overall fracture toughness of the composite structure.

Addition of CNTs improved the fracture toughness of Gr epoxy composite. The improvement was ~31% and ~9%, as compared to 0.5 wt% Gr and 0.3 wt% (25Gr:75CNT), respectively, with 0.5 wt% (25Gr:75CNT). The CNTs gets attached to the surface of Gr, preventing the restacking of Gr during exfoliation. To improve the dispersion further, specifically at higher filler concentration, ND was added to Gr-CNT epoxy composite. With 0.5 wt% filler content, the Gr-CNT-ND epoxy composite showed higher fracture toughness than epoxy but lower than Gr-CNT epoxy composite. The quantity of ND was not sufficient to achieve the desired exfoliation, as confirmed from tensile test. Hence, the total reinforcement content was increased from 0.5 wt% to 0.8 wt%. The improvement in fracture toughness was found quite significant with increase in content to 0.8 wt% (25Gr:50CNT:25ND). The resulting improvement was ~40% and ~44%, as compared to 0.5 wt% (25Gr:75CNT) and 0.5 wt% Gr. The improvement achieved was the highest, out of all the compositions so far. This proves the potential of ND in achieving better synergy of Gr-CNT hybrid at higher reinforcement content and the key is better exfoliation and dispersion.

4.5.4 Thermal Analysis of Gr-CNT Epoxy and Gr-CNT-ND Epoxy Composites

4.5.4.1 Effect of Addition of Gr-CNT and Gr-CNT-ND fillers on the Thermal Stability of Epoxy

As seen from figure 4.22. in chapter 4.3, addition of Gr-ND and CNT-ND hybrid filler to epoxy, affected its thermal stability to a much higher extent as compared to the incorporation of CNT, Gr and ND as a unary filler to epoxy (figure 4.7. in chapter 4.1). This effect was due to the

improved exfoliation of Gr and reduced entanglement of CNT when sonicated in the presence of ND. Thus, the effect of addition of ND to improve the synergy between Gr-CNT hybrid filler on the thermal stability of epoxy was studied through TGA.

TGA for Gr-CNT and Gr-CNT-ND reinforced epoxy composite was done in nitrogen atmosphere. Degradation in mass as a function of temperature is presented in figure 4.37. The initial response, of the composite was similar, to that observed in the previous studies. 5% mass loss occurs up to 300°C for both set of composites, which is due to the evaporation of moisture or volatile impurities. The degradation temperature was found to be ~340°C in each case, which is defined as the point of inflection on the TGA curve. The major mass loss of about 50% occurs between 350°C to 450°C.

Comparative analysis of TGA curve for Gr-CNT and Gr-CNT-ND reinforced epoxy composite at the initial degradation temperature between 300 °C and 380 °C (inset in the figure 4.37) shows better thermal stability with Gr-CNT than Gr-CNT-ND. Improvement in thermal stability of epoxy with Gr-CNT and degradation in thermal stability of epoxy with Gr-CNT-ND is only ~5°C which is not very significant. Above 380°C the thermal stability of Gr-CNT epoxy composite reduced significantly. The reduction in thermal stability is ~15-20°C over epoxy which kept increasing with temperature. This reduced thermal stability is due to CNTs bridging Gr sheets and preventing them from stacking, which also reduced entanglement of CNTs. The increase in the no. of thermal conductive channels as a result of reduced entanglement of CNT, is more dominant than the sheet barrier effect due to improved exfoliation of Gr. As seen the exfoliation achieved for Gr with addition of CNT is not high as with ND (figure 4.32(c)).

Gr-CNT-ND reinforced epoxy composite on the other hand is seen to have thermal stability very similar to epoxy, with only ~5°C improvement post 380°C. This is due to the well exfoliated

close knitted 3D network of reinforcement achieved post addition of ND to Gr-CNT hybrid. The degradation of thermal stability because of the presence of well-connected conductive thermal channels of CNTs is overcome by the dominant sheet barrier effect due to the improved exfoliation of Gr which prevents the thermal stability. The filler content as well as composition did not affect the thermal stability significantly, the thermal stability is found to be quite similar.

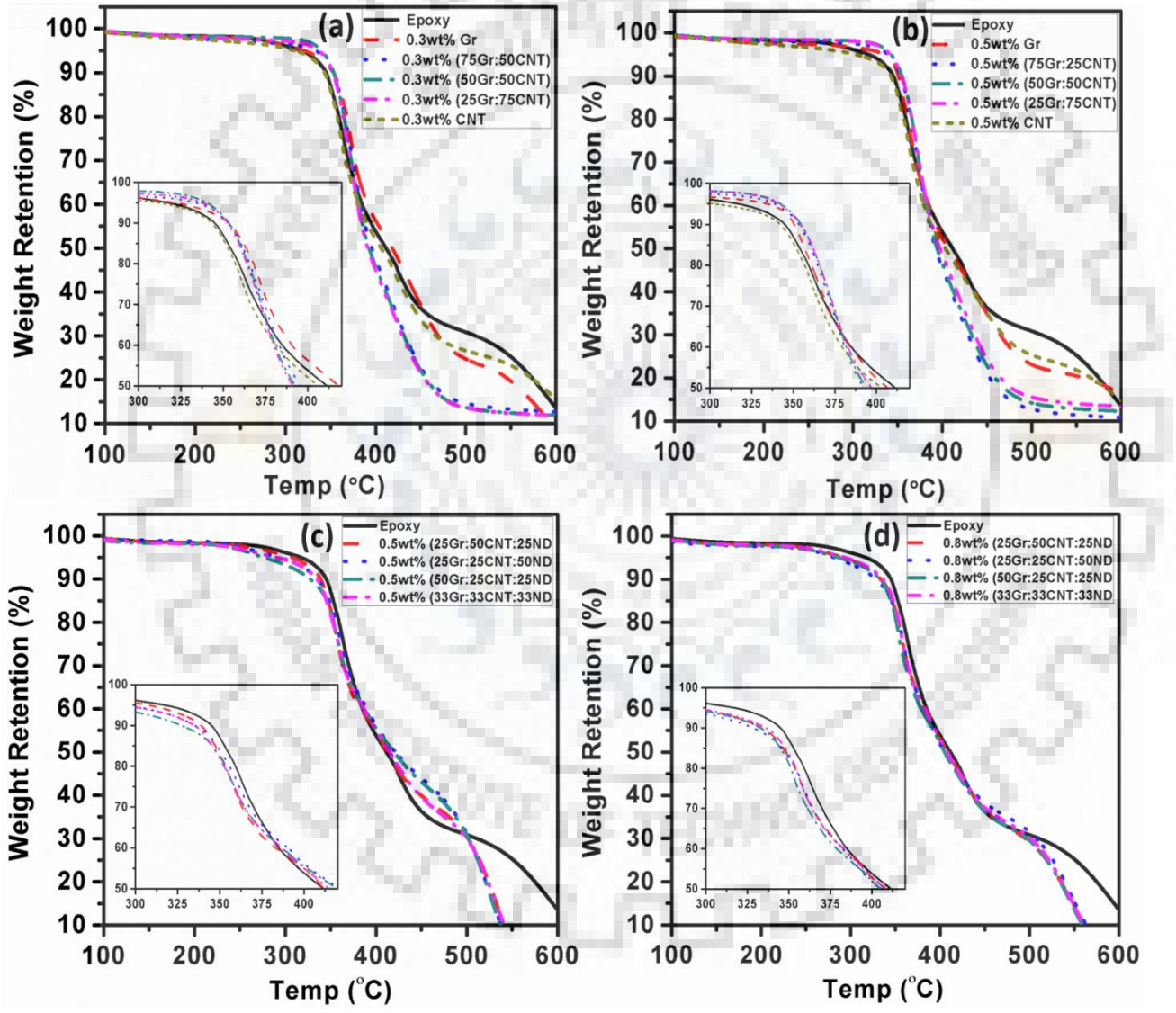

Figure 4.37 TGA thermogram for various combinations of **(a, b)** Gr-CNT epoxy composite and **(c, d)** Gr- CNT-ND epoxy composite

Above, 500°C the thermal stability reduces rapidly and becomes quite significant. However, at this temperature the weight degradation is already 70%. As for a material used for structural applications the working temperature is generally chosen as the temperature at which material retains 90-95% of its weight during its service life, which is < 300°C in this study. Therefore, we can conclude that the effect of incorporation of Gr-CNT and Gr-CNT-ND on thermal stability is insignificant or the thermal stability of epoxy is retained even after being reinforced by nanofillers.

4.5.4.1 Thermomechanical Analysis of Gr-CNT and Gr-CNT-ND Epoxy Composites

Comparative analysis of synergy offered by Gr-CNT as a hybrid filler with Gr-CNT-ND hybrid filler in modulating the mechanical property of epoxy subjected to dynamic loading as a function of temperature is done through DMA. Representative storage modulus vs temperature and tan δ (loss factor) vs temperature plots for various combinations of 0.3 wt% and 0.5 wt% Gr-CNT epoxy composite and 0.5 wt% and 0.8 wt% Gr-CNT-ND epoxy composite is shown in figure 4.38. Plots in figure 4.38 clearly shows that the improvement in storage modulus is between 10-20% for all compositions and combinations. However, with Gr-CNT hybrid the storage modulus retention at higher temperature is better than Gr-CNT-ND composites. This is due to the ND forming long conducting networks by connecting CNTs end to end which reduces the thermal stability of polymer chain. As, a result their might be diffusion or evaporation of volatile impurities or small molecules present in the matrix or filler surface, which generates defect at the interface while escaping the sample. This suppresses the effect of increased surface area available for efficient load transfer from matrix to reinforcement as a result of improved exfoliation at higher temperature

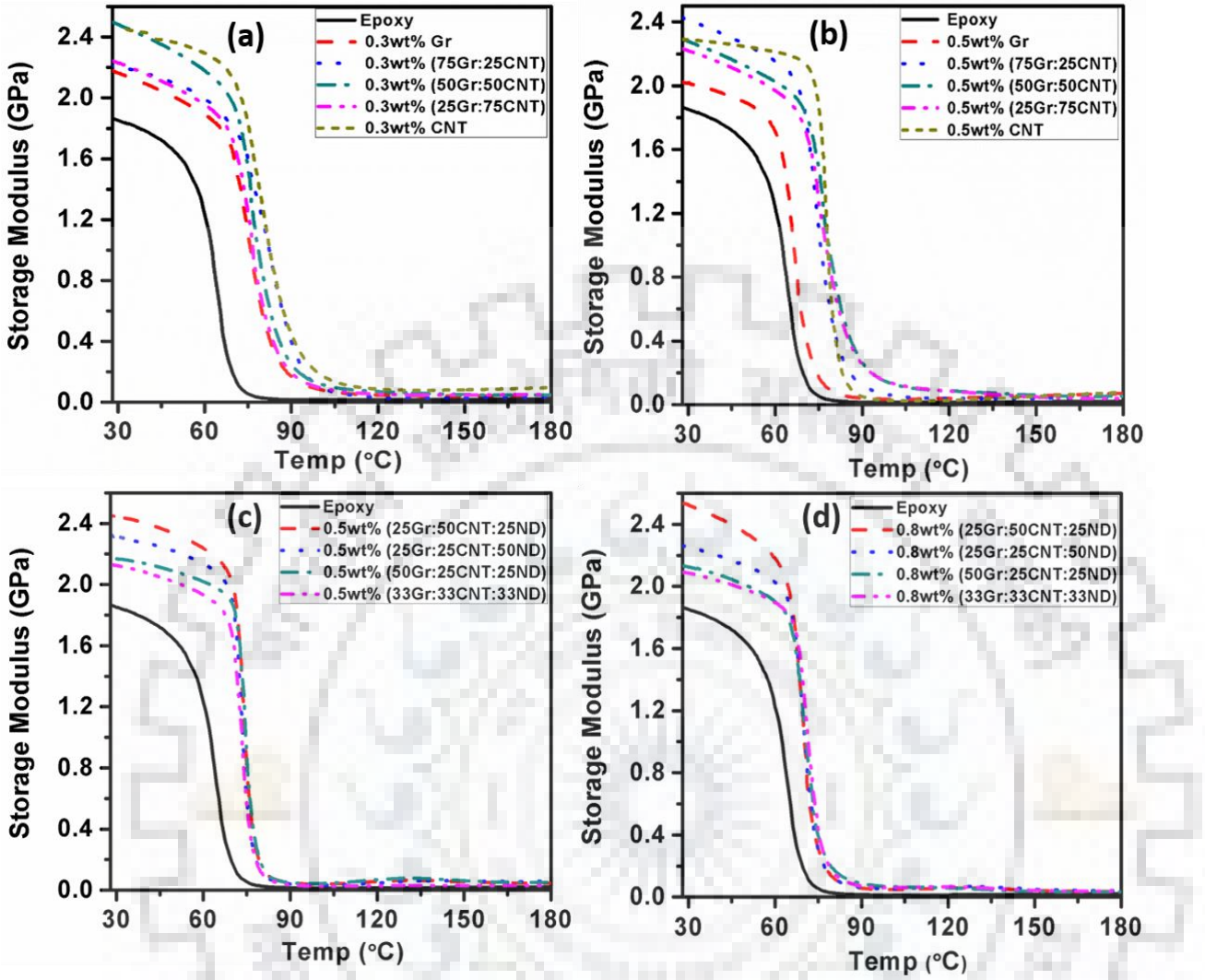

Figure 4.38 Storage modulus for various combinations of **(a)** 0.3 wt% Gr-CNT epoxy, **(b)** 0.5 wt% Gr-CNT epoxy, **(c)** 0.5 wt% Gr-CNT-ND epoxy and **(d)** 0.8 wt% Gr-CNT-ND epoxy composite as function of temperature

Similar behaviour was observed with glass transition temperature (figure 4.39). Incorporating, Gr-CNT hybrid filler to epoxy improved its T_g by ~20-25ºC, which is ~5 ºC higher than the improvement achieved with Gr-CNT-ND hybrid filler. The increase in filler content did not have any significant effect on T_g. The addition of Gr-CNT-ND hybrid also improved the glass transition temperature of epoxy. The improvement in T_g ~10 ºC with 0.5 wt% filler content which improved to ~20 ºC with 0.8 wt% filler content. As, higher filler content suggests more number of

stiffer particle interacting with polymer chain. The increase in glass transition temperature with the addition of fillers is the result of resistance to the motion of polymer chain by stiff fillers uniformly distributed throughout the matrix.

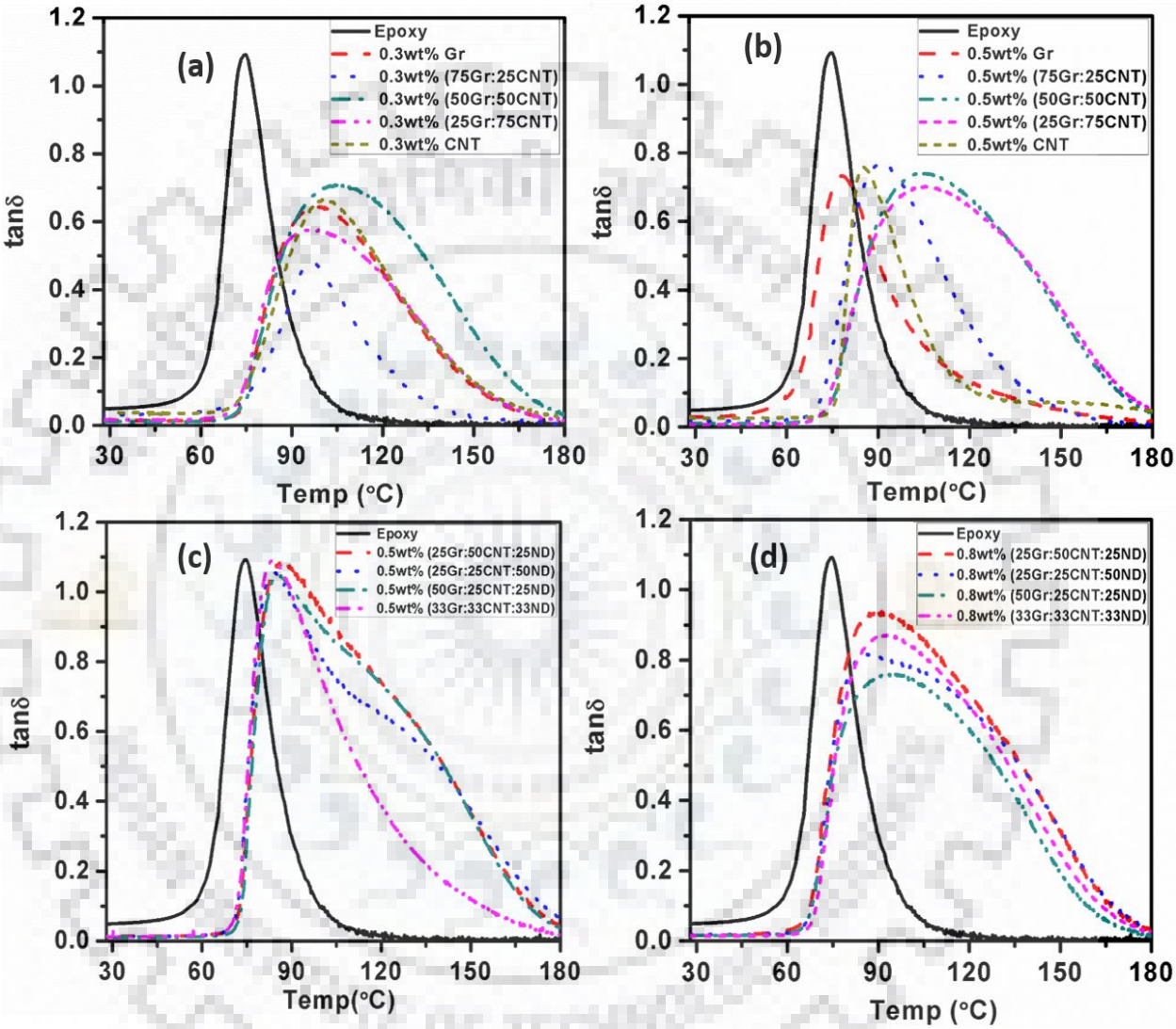

Figure 4.39 tanδ for various combinations of **(a)** 0.3 wt% Gr-CNT epoxy, **(b)** 0.5 wt% Gr-CNT epoxy, **(c)** 0.5 wt% Gr-CNT-ND epoxy and **(d)** 0.8 wt% Gr-CNT-ND epoxy composite as function of temperature

It is seen from figure 4.39(c) that with 0.5 wt% Gr-CNT-ND reinforcement the improvement in glass transition was lowest among all. Apart from the significant peak around 90 ºC, there is a

deflection or shift in the curve post 105ºC with 25Gr:50CNT:25ND, 25Gr:25CNT:50ND and 50Gr:25CNT:25ND. This shift or deflection in the curve is due to unexfoliated or agglomerated nanofillers with uncured epoxy trapped inside them. With increase in the temperature, the uncured epoxy trapped inside these agglomerate tends to cure. This phenomenon tries to shift T_g to high temperature, but as the temperature is already above T_g of fully cured epoxy, i.e. ~75 ºC, the impact is weak [230]. The improvement in T_g is ~10ºC, over pure epoxy for all compositions of nanofiller reinforced epoxy composite. This clearly proves that there is agglomeration but it is no quite severe and does not exist throughout the matrix.

The lower T_g achieved with 0.8 wt% Gr-CNT-ND hybrid filler as compared to 0.5 wt% Gr-CNT filler, is because of the conducting channels or networks formed due to the presence of ND. The interfacial interaction between filler and matrix becomes weak, due to the reduced thermal stability of polymer chains. The weak interfacial interaction allows the mobility of polymer chains at much lower temperature.

4.5.5 Summary

Addition of ND to Gr-CNT hybrid helped in achieving a well exfoliated close knitted 3D network of reinforcement, which improved both tensile strength and fracture toughness quite significantly. ND improved exfoliation of Gr by acting as a barrier and prevented the entanglement of CNTs by acting as a bridge which connects CNTs end to end. Transmission electron microscopy and scanning electron microscopy analysis of nanofillers performed at different stages gave an insight into the role of ND on dispersion of Gr and CNT. The fractured surfaces of composites, fabricated with Gr-CNT-ND as reinforcement, revealed good dispersion and strong interfacial interaction. The same was translated to improved tensile strength and fracture toughness of the

structures. Addition of ND to Gr-CNT epoxy composite improved the tensile strength from ~42% with 0.5 wt% (75Gr:25CNT) and ~51% with 0.8 wt% (25Gr:25CNT:50ND), as compared to neat epoxy. Fracture toughness got improved by ~140% with 0.5 wt% (25Gr:75CNT) and 165% with 0.8 wt% (25Gr:50CNT:25ND). The composition that offered the best combination of mechanical properties (tensile strength and fracture toughness) was 0.8 wt% (33Gr:33CNT:33ND). The improvement in tensile strength and fracture toughness was ~41% and ~158%, as compared to epoxy. This combination was hard to achieve in Gr-CNT epoxy composite, as composite with higher Gr ratio offered better tensile strength, while the ones with higher CNT ratio showed better fracture toughness

4.6 Role of 3D Network of Carbon Nanofillers in Improving the Properties of Carbon Fiber Epoxy Laminated Composite

This study aims to investigate the effect of addition of the well exfoliated close knitted 3D network of Gr-CNT-ND into the epoxy matrix of a conventional carbon fiber-reinforced composites. Carbon fiber reinforced epoxy composites are used in numerous structural applications. However, the out of plane and transverse properties of these composites is always less than expected. Therefore, potential of carbon nanofillers in improving these properties with, three different morphologies, i.e. CNT (1D), Gr (2D) and nanodiamond (3D), in a well-connected 3D network is evaluated. Thorough evaluation of mechanical properties, which include tensile test, interlaminar shear strength, interlaminar and intralaminar Mode I fracture toughness, were conducted to investigate the effect of addition of 3D network of Gr-CNT-ND on interfacial properties of CF-epoxy composite. In depth fracture surface analysis, through FE-SEM, was carried out to get an insight into the active strengthening and toughening mechanism in the interface as well as matrix regions of the laminated composites structure.

The composite laminate was fabricated for pure epoxy, 0.8 wt% (25Gr:25CNT:50ND), 0.8 wt% (25Gr:50CNT:25ND) and 0.8 wt% (33Gr:33CNT:33ND) and will be referred hereafter as, CF-epoxy, 225 GCN CF-epoxy, 252 GCN CF-epoxy and 333 GCN CF-epoxy composite. The compositions selected here are optimized from the systematic studies conducted for each nanofillers at different compositions and combinations over the course of study.

4.6.1 Investigating the Wettability and Infiltration of Carbon Fiber by Epoxy and Nanofiller Modified Epoxy

In order to achieve effective load transfer and improved mechanical properties, strong interfacial adhesion between the reinforcement and matrix is required. In order to achieve strong interface, it is important for the epoxy to properly infiltrate the carbon fiber. Addition of nanofillers may increase the viscosity of the epoxy. Therefore, wettability and infiltration of epoxy with and without addition of nanofillers (Gr-CNT-ND) was evaluated through sessile drop technique, as a function of time, as shown in figure 4.40.

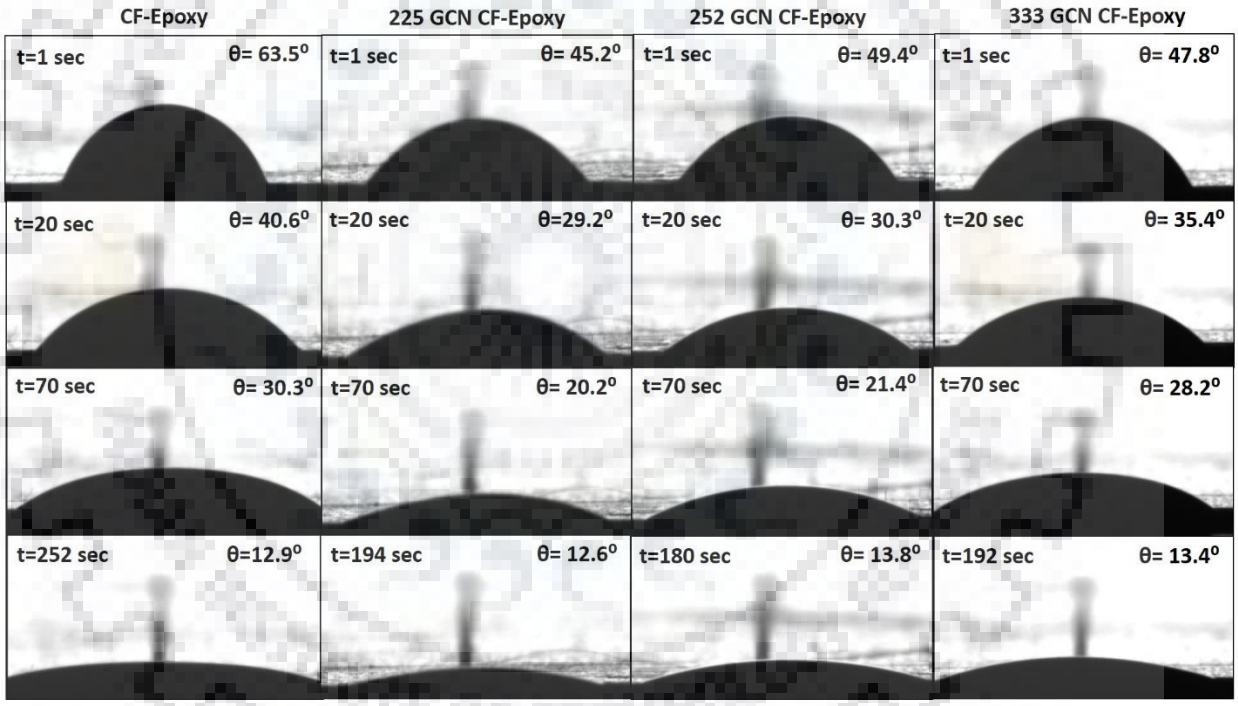

Figure 4.40 Images showing wetability and infiltration of epoxy on CF without and with addition of nanofillers as a function of time

Due to low viscosity of epoxy, there was a continuous flow of epoxy and it took time for the drop to detach from that flow and be released on carbon surface, which resulted in an immediate contact angle of 63.5 º. Similarly, observation was made in case of nanofiller modified epoxy and immediate contact angle was found reduced by approximately 14º-18º. This was followed by gradual

decrease in contact angle for all compositions. Nanofillers modified epoxy reached a contact angle of ~13º in almost a minute ahead of pure epoxy. However, once the contact angle reached the range of 12º-13º, the further reduction in contact angle or the infiltration slowed down. It took almost another 2-3 mins for the contact angles to become zero. This proves that the addition of 0.8 wt% of Gr:CNT:ND it improved the wettability and infiltration of epoxy.

4.6.2 Fracture Surface Analysis to Confirm Role Played by 3D Network of Nanofiller in Strengthening and Improving the Interfacial Bonding between CF and Epoxy matrix

The morphology of the fractured surface of CF epoxy with and without Gr-CNT-ND modification, post tensile test were observed under FE-SEM. Figure 4.41(a-d) shows the fractured surface morphology of bidirectional woven fibers aligned along (interfiber debonding) and transverse to the applied load direction (interlayer debonding). The micrographs clearly show the difference between the fracture morphology of CF-epoxy composite with and without Gr-CNT-ND. Fractography for the fibers aligned along the transverse direction to applied load/ interlayer debonding (figure 4.41(a1, b1, c1 & d1)) shows, debonded matrix (figure 4.41(a3, b3, c3 & d3)) and debonded fiber (figure 4.41(a4, b4, c4 & d4)).

Comparative analysis of matrix region for epoxy and Gr-CNT-ND modified epoxy clearly shows the resistance offered by the 3D network of Gr-CNT-ND to crack propagation. The cracks, once generated in CF-epoxy, propagate though the matrix without being deflected, bridged, pinned or bifurcated by nanofillers (figure 4.41(a1)). However, the addition of Gr-CNT-ND makes the crack propagation difficult as a result of the resistance, offered by the multiple encounters with the well exfoliated 3D network of nanofillers, making crack path tortuous and sometimes they even subside midway losing all its energy (figure 4.41(b1, c1 & d1)). The crack, once reached the fiber matrix

interface, propagates further through interface due to weak bonding between fiber and epoxy. This is evidenced by clear fiber surface with no traces of epoxy on the fractured surface as seen in figure 4.41(a4). Also, the presence of an alternate fiber on fractured surface proves that the crack propagated through interface due to weak bonding between fiber and epoxy matrix. While, in case of Gr-CNT-ND modified epoxy composite, crack gets deflected in the matrix due to strong interfacial bonding, as evidenced by traces of epoxy on fiber surface (figure 4.41(b4, c4 & d4)). The improved interaction between fiber and matrix can further be verified by the presence of consecutive fibers (figure 4.41(b1)) or the rippled morphology (figure 4.41(c1 & d1)) on ditches created due to debonded fiber on fractured surface. The fractured surface of Gr-CNT-ND modified CF-epoxy composite do not show any traces of agglomeration of either CNT, Gr or ND. The nanofillers can be seen properly dispersed and strongly integrated with the fiber and matrix (figure 4.41b(3&5), c(3&5) and d(3&5)).

Similarly, for fibers aligned along the applied load direction, the comparative analysis of figure 4.41(a2) with figure 4.41(b2, c2 & d2) verifies the effect of addition of Gr-CNT-ND on interfiber bonding. As seen from figure 4.41(a2) (encircled region) that a bunch of fiber is pulled out when subjected to loading due to weak interfacial bonding between carbon fiber and epoxy. However, with the addition of nanofillers the interfacial bonding improved with only one or two fibers pulled out at different sites as seen from figure 4.41(b2, c2 & d2). Therefore, the failure or crack propagation did not happen due to debonding of fibers in presence of nanofillers, on contrary to that in case of CF-epoxy. Rather, the failure in the former occurred due to breakage of fibers.

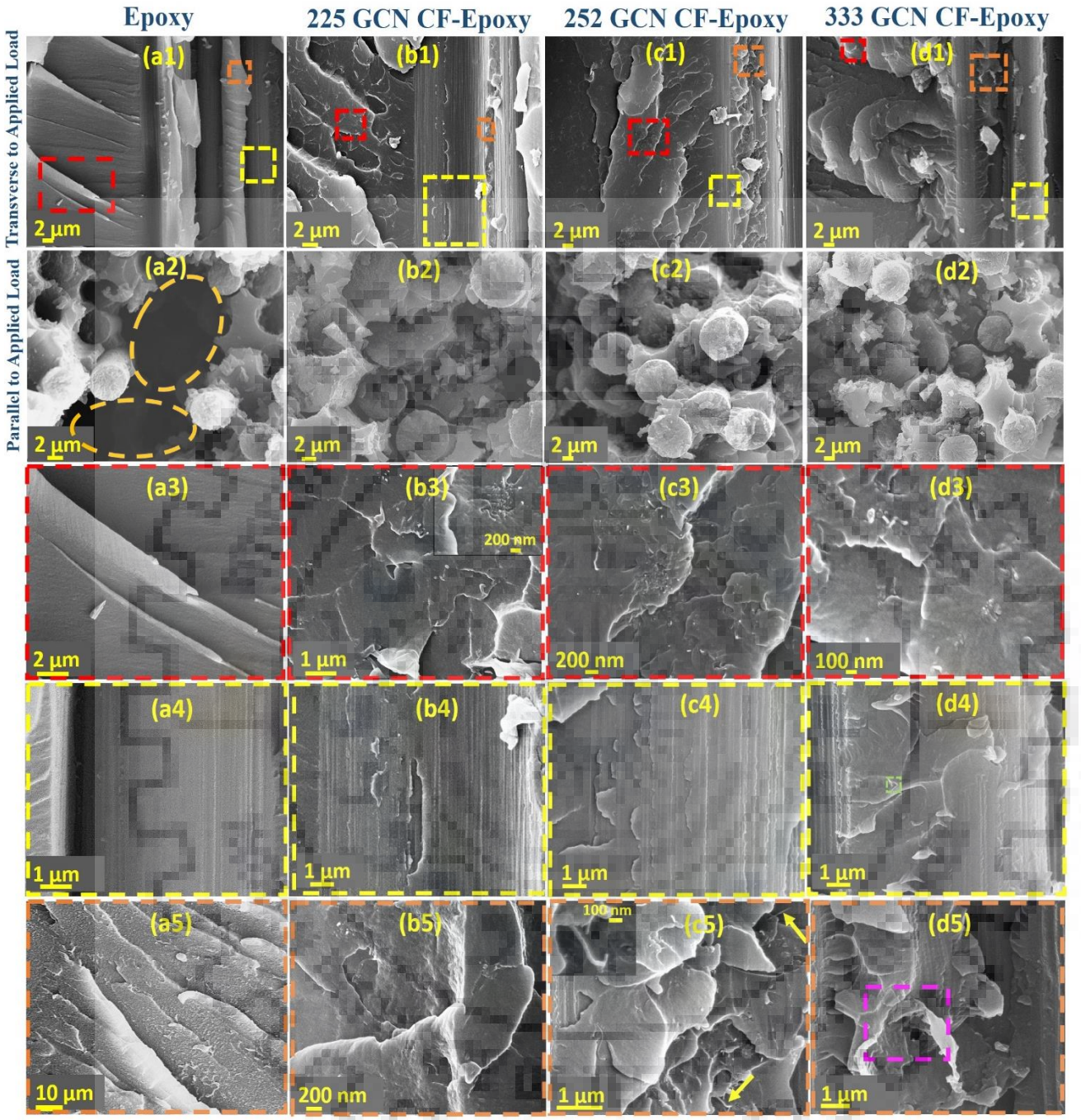

Figure 4.41 FE-SEM images of the fractured surface cross-sections both along and transverse to the direction of applied load for **(a(1-5))** CF-Epoxy, **(b(1-5))** 225 GCN CF-Epoxy, **(c(1-5))** 252 GCN CF-Epoxy and **(d(1-5))** 333 GCN CF-Epoxy composites at different magnifications

The delaminated surface of all the composites were also evaluated using FE-SEM to examine the effect of Gr-CNT-ND on inter laminar fracture mechanics on CF-epoxy composite. A comparative analysis of figure 4.42(b) with figure 4.42(e, h & k) clearly shows that with the addition of nanofillers a lot of resistance was offered to crack propagation. The crack path in matrix was diverted multiple times as it encountered the nanofillers, which required additional energy to advance the crack. The main mode of failure, as observed from figure 4.42(b & c), is debonding of fiber and matrix, which can be verified by the smooth fracture surface of epoxy in the debonded fiber region and no trace of epoxy on the fiber surface. Therefore, debonding of fiber matrix interface is the main mode of failure in CF-epoxy composite. On, the contrary, the inclusion of Gr-CNT-ND made the fractured surface of epoxy quite rippled with evidences of pulled out Gr and CNT, having strong adhesion to the fiber surface, along with chunks of matrix bonded to the fiber surface, as seen from the figure 4.42(e, h & k) and their magnified images. This is due to the presence of nanofillers, having high surface area, offering strong adhesion between matrix and fiber and thus, diverting the crack path several times, finally deflecting it away from the fiber matrix interface. Therefore, the improved fiber matrix interface suggested improved ILFT.

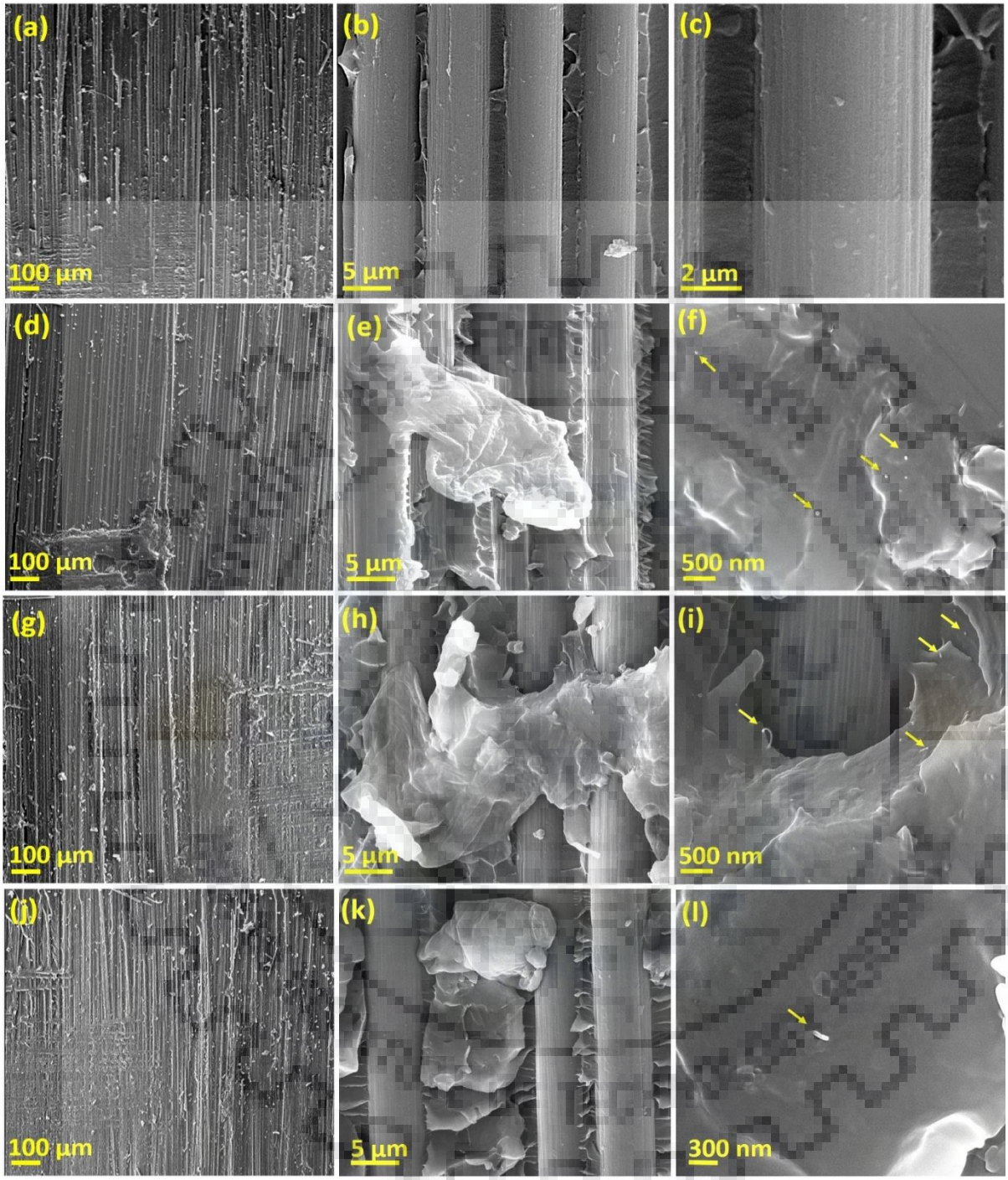

Figure 4.42 FE-SEM images at different magnifications for delaminated **(a-c)** CF-epoxy, **(d-f)** 25Gr:25CNT:75ND CF-epoxy, **(g-i)** 25Gr:50CNT:25ND CF-epoxy and **(j-l)** 33Gr:33CNT:33ND CF-epoxy composites.

4.6.3 Investigating Mechanical Properties of Multiscale Composites

4.6.3.1 Tensile Test for CF epoxy and Nanofiller Reinforced Carbon Fiber Epoxy Composite

The results of tensile test for different compositions of Gr-CNT-ND CF-epoxy composites are shown in figure 4.43. The tensile properties of the composites were compared to evaluate the effect of addition of nanofillers on mechanical behaviour of CF-epoxy composite. The properties calculated from stress– strain curve include young's modulus (E), ultimate tensile strength (UTS), and % strain (at failure). The quantitative values for the same are present in table 7. Young's modulus was determined from the slope of stress-strain plots. The maximum stress value in the stress-strain plots was the estimated tensile strength, while the strain value at the last data point was the strain (at failure) for the composites.

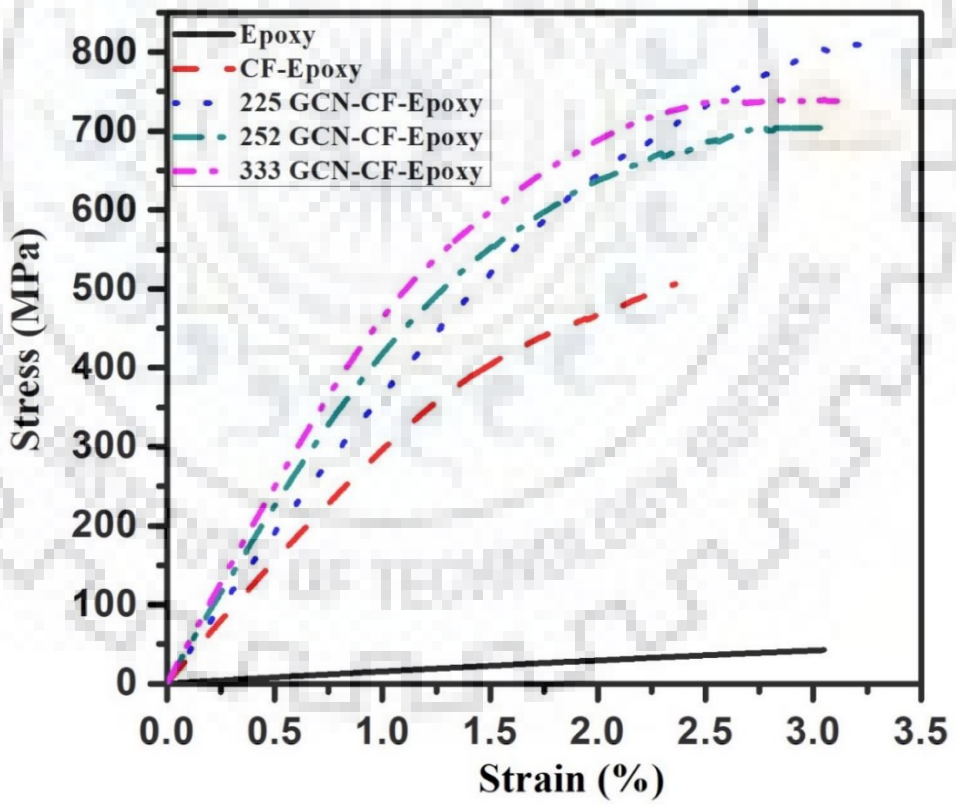

Figure 4.43 Stress-Strain plots for various combination of Gr:CNT:ND CF-epoxy composite

The improvement in tensile strength of CF-epoxy is ~1090 %, as compared to epoxy. Further, nanofillers modified epoxy CF composite offers the highest improvement of ~1805% over epoxy and ~60% over CF-epoxy with 225 GCN CF-epoxy. The tensile strength of the composites is generally governed by the tensile strength of the fibers oriented along the applied load direction. While, the fibers are oriented perpendicular to the applied load direction, the failure is through matrix or fiber-matrix debonding at much lower load. As the load is applied to the composite, the cracks present in the epoxy matrix starts to propagate. In case of CF-epoxy, with increase in load, the cracks propagate further and reaches straight into the vicinity of fiber without any resistance being offered. As, the crack approaches near to the fiber, the stress intensity increases, which leads to fiber matrix debonding. The crack propagates further, either causing fiber breakage (strong interface) or through the interface eventually leading to fiber pullout. The major failure mechanisms for CF epoxy composite are brittle failure of matrix and fiber pullout as seen in figure 4.41(a). The same for nanofillers modified epoxy CF composite are ductile failure of matrix and fiber breakage, as evidenced from figure 4.41(b, c & d).

The reasons behind higher tensile strength of nanofillers modified epoxy CF composite, as compared to CF epoxy composite, are uniformly dispersed well-connected 3D network of nanofillers and relatively improved fiber matrix interaction, which effectively improved load transfer efficiency. CF being the major reinforcements in the composite, E of composite mostly depends on the stiffness of CF. Therefore, addition of nanofillers does not change the Young's modulus of epoxy as significantly as by CF, though the improvement is still quite significant. The improvement in modulus of CF-epoxy composite is ~567%, as compared to epoxy. Addition of nanofillers further improved the modulus by ~57% over CF-epoxy, in case of 333 GCN CF-epoxy composite. An

improvement of ~57% is quite significant considering the modulus of CF-epoxy composite is already high i.e. 30.67 ± 1.3 GPa.

Reinforcing epoxy with CF improves the strength along with reduction in % strain by ~29%. Interestingly, with the addition of nanofillers, there is simultaneous improvement in % strain and strength of composite. In fact, in case of 225 GCN CF-epoxy, the strain regains its value and becomes ~7% more than pure epoxy with a total regain of ~38% over CF-epoxy composite, NDs is believed to play the key role in improvement in % strain with strength. When, a tensile stress is applied to a ND epoxy composite, sliding of the polymer chains starts. The motion/rotation of NDs, further, facilitates this process, thus increasing failure strain or ductility. Along with the high resistance to crack propagation which causes the crack to travel long path before failure, offered by the CNTs, having high aspect ratio as a result of less entanglement and end to end bridging by NDs.

Table 7. Elastic modulus, ultimate tensile strength and % strain, for various composition and combination of Gr:CNT:ND CF-epoxy composites

Composition		E (GPa)	UTS (MPa)	% strain
Epoxy		4.6 ± .08	42.5 ± 1.2	3.05 ± 0.2
0.8 wt%	**CF-Epoxy**	30.67 ± 1.3	506 ± 7	2.36 ± 0.1
	25Gr:25CNT:50ND CF-Epoxy	37.84 ± 1.5	810 ± 10	3.26 ± 0.2
	25Gr:50CNT:25ND CF-Epoxy	44.21 ± 1.8	705 ± 8	3.09 ± 0.2
	33Gr:33CNT:33ND CF-Epoxy	48.12 ± 1.9	740 ± 10	3.17 ± 0.2

4.6.3.2 Intralaminar Fracture Toughness for CF Epoxy and Nanofiller Reinforced Carbon Fiber Epoxy Composite

The composites were evaluated for fracture toughness using 3-point bend test, the values obtained are presented in figure 4.44. As far as structural applications are concerned, fracture toughness is a very important mechanical property that needs to be evaluated especially with brittle matrix like epoxy. Fracture toughness values, obtained for all combinations of Gr-CNT-ND reinforced CF-epoxy composites, are higher than that with CF-epoxy composite.

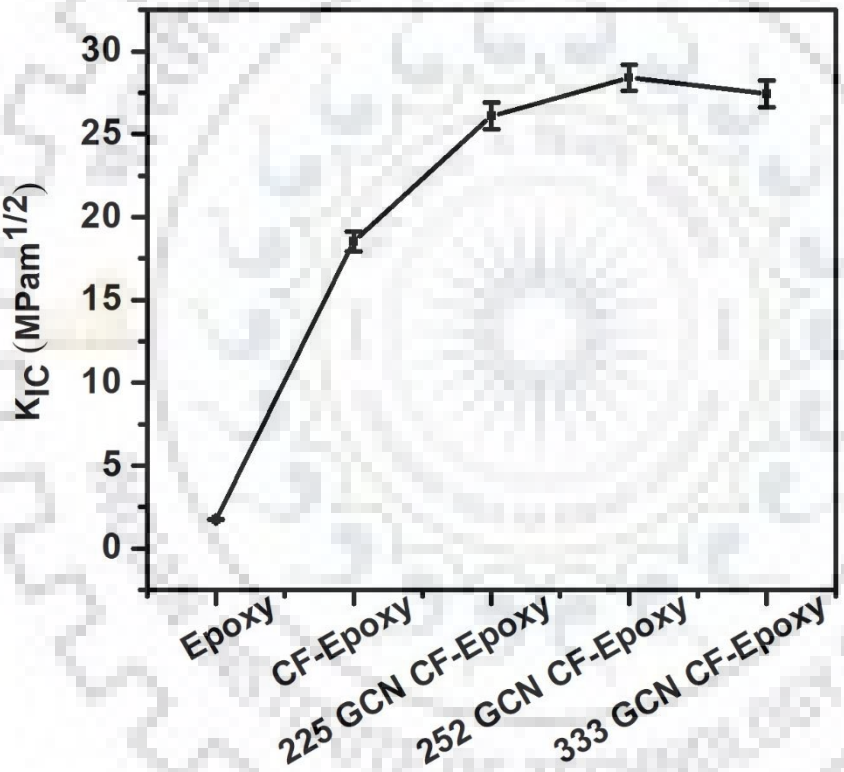

Figure 4.44 Fracture toughness plots for various combination of Gr:CNT:ND CF-epoxy composite

Addition of CF as reinforcement itself improved the fracture toughness of epoxy by ~959%. Matrix fiber debonding, crack deflection by twisting and tilting around the fiber, fiber pullout, fiber breaking etc. are the major toughening mechanism. Addition of nanofillers further improved the fracture toughness of the composite by ~53% with 252 GCN CF-epoxy composite, as compared to

CF-epoxy, noting a total improvement of ~1523% over pure epoxy. Resistance to the crack propagation or matrix cracking by uniformly distributed well-connected 3D network of nanofillers is the reason behind improved toughness. The major toughening mechanism include crack deflection, bridging, pinning and even ceasing of crack propagation. The improved interfacial interaction between fiber and matrix also plays a major role by increased resistance to matrix fiber debonding, twisting and tilting of crack around the fiber and fiber pullout.

4.6.4 Assessing the Role of 3D Network of Carbon Nanofillers in Improving the Interfacial Properties of Multiscale Composite

4.6.4.1 Mode - I Interlaminar Fracture Toughness

Failure to delamination is one of the major drawback of laminated composite structures. Therefore, it is very important to be aware of the resistance offered by laminated composite to interlaminar fracture. The interlaminar fracture toughness values for CF-epoxy and CF-nanofillers modified epoxy composites, calculated from the load displacement curves figure 4.45(a) of DCB test are shown in figure 4.45(b). The values represent the fracture toughness corresponding to crack propagation in different composites. The initial response for all composites was linear, indicating elastic loading followed by a sudden drop in load. This drop is due to the crack propagation, which is again followed by increase in load. Throughout the test for all the composites, increase in load was observed after a large sudden drop in load.

All compositions of CF- nanofillers modified epoxy composites showed higher ILFT than the CF-epoxy composite at all crack displacements. The delamination generally occurs due to cracking of matrix between two layers of fibers. The adhesion of matrix to fiber increases with the addition of well exfoliated nanofillers, well, which improves the resistance to delamination. The FE-

SEM images in figure 4.42(e, h & k) reveal the Gr adhered to the fiber surface with CNTs protruding out as seen from magnified images in figure 4.42(f, i & l). The additional energy, consumed by the crack tip to propagate, is due to bridging and improved interfacial adhesion by CNTs and Gr. High aspect ratio and surface area of these nanofillers attribute towards better adhesion. The improved toughness of nanofiller reinforced matrix also contributed to the overall improvement in the ILFT.

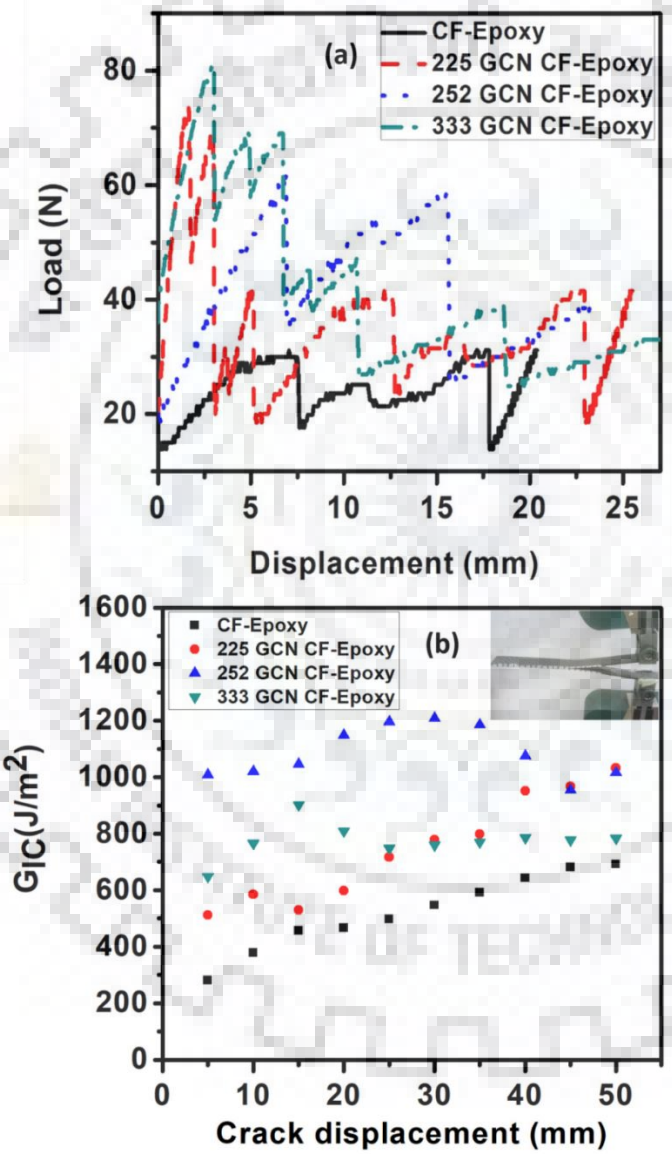

Figure 4.45 (a) Representative load vs displacement curves obtained from modified beam theory (MBT) method **(b)** variation of ILFT as a function of crack length for different combination of Gr:CNT:ND CF-epoxy composite

The fracture toughness value increases almost linearly with increase in crack length for CF-epoxy. Similar trend is followed by 225 GCN CF-epoxy composite with drop in fracture toughness values at 15 mm, which may be due to some discontinuity or minor agglomeration, as the ILFT is higher than pure epoxy. For the other two compositions, (252 GCN and 333 GCN) having relatively higher CNT content, a sudden jump is observed in fracture toughness values, which subdues with increase in crack displacement. This jump may be due to the more population of CNTs available to bridge the crack in that particular region of crack displacement. The results show that the highest improvement in interlaminar fracture toughness is ~260 % with 252 GCN CF-epoxy composite, as compared to CF-epoxy composite. The improvement was ~36% and ~97% higher than the 333 GCN CF-epoxy and 252 GCN CF-epoxy composite. This is due to the higher amount of CNTs, which provide higher resistance to crack propagation by crack bridging. Crack bridging is one of the most efficient toughening mechanism, it is more effective with CNTs, having fiber like morphology with very high aspect ratio.

4.6.4.2 Interlaminar Shear Strength

ILSS values, derived from load vs displacement plot figure 4.46(a) of short beam shear test using equation 2, are shown in figure 4.46(b). All, load vs displacement curves show almost a linear behaviour. The first major drop in each plot is due to the compression failure as result of first discontinuity generated under the applied load. The curve rises again and suffers drop due to shear failure or delamination. In case of CF-epoxy, the composite suffered multiple shear failure in the central area all connected together which led to final drop in the curve as seen from figure 4.46(b).

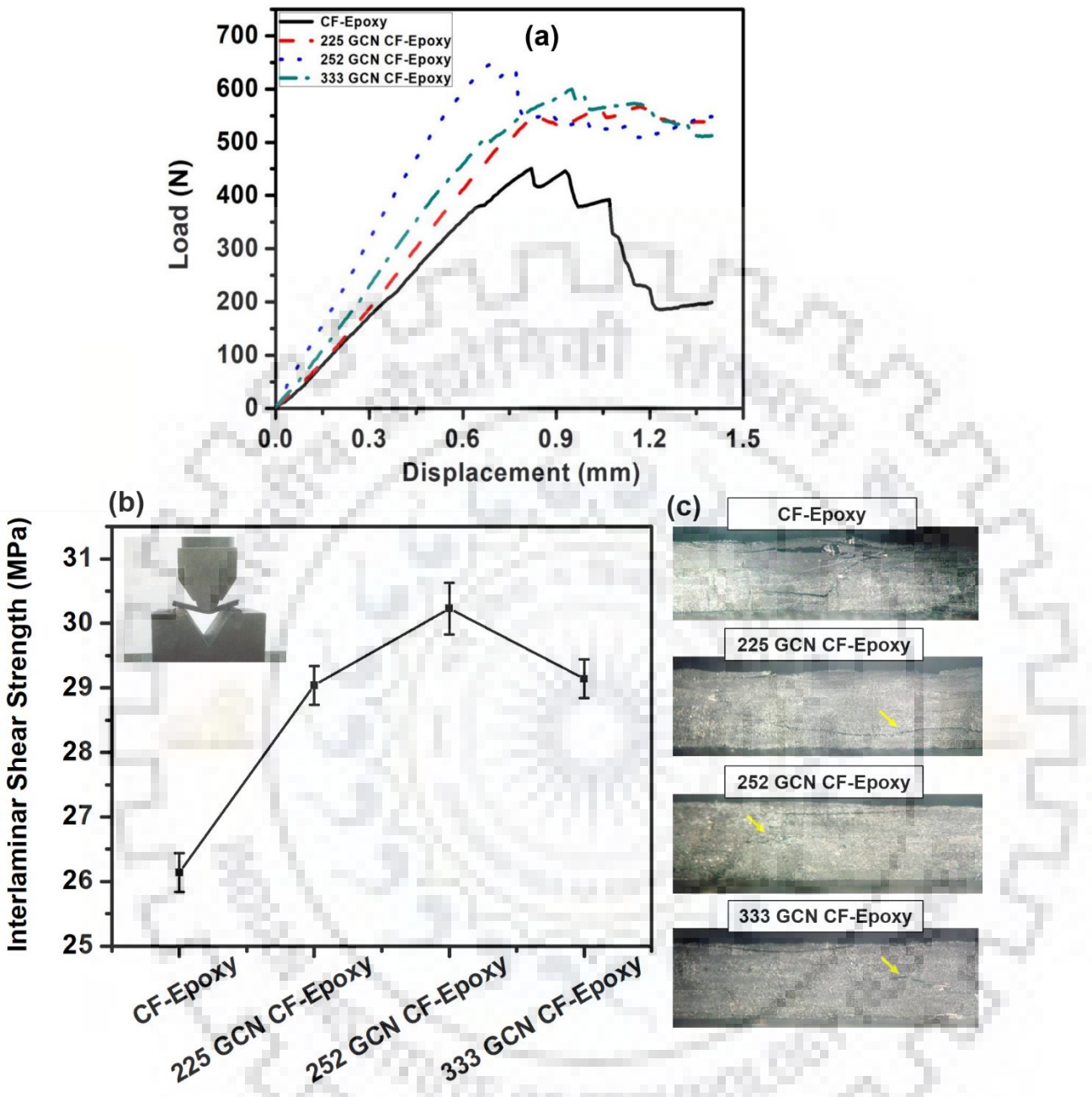

Figure 4.46 (a) Representative load vs displacement curves obtained from short beam shear test **(b)** ILSS plots for CF-epoxy and various combination of Gr:CNT:ND CF-epoxy composite and **(c)** digital images of failed samples

For all compositions of CF nanofillers modified epoxy composite, apart from compression failure only single shear failure mode was observed marked by an arrow as shown in figure 4.46(c).

The ILSS value for CF-epoxy composite is 26.14 ± 0.3 MPa. Not much difference was found for the measured ILSS values for different composite. The maximum improvement in ILSS was 15.6% with 252 GCN CF-epoxy composite as compared to CF-epoxy composite. This improvement is attributed to the increase in the contact area or better interfacial interaction between CF and matrix, along with the stiffening and strengthening of the matrix, due to the incorporation of nanofillers in epoxy matrix. The higher surface area offered by the 2D structure of Gr majorly contributed to improved bonding between the CF and epoxy. While, the bridging of cracks by the CNTs, due to their fiber like morphology, led to improved stiffening and strengthening of epoxy matrix. This has been possible due to the addition of ND. As, ND improved exfoliation of Gr by acting as a barrier and prevented the entanglement of CNTs by acting as a bridge which connects CNTs end to end. Thus, increasing the total interface area with the polymer matrix in the composite structure. In addition, improved wettability of CF by epoxy resin, with incorporation of nanofillers, also contributed to improve ILSS. These, mechanism together led to improved mechanical interlocking between fiber-matrix, and, in the matrix (between polymer chains). As a result, the ILSS of CF epoxy improved. This is even confirmed from the digital images for various composition of CF-epoxy composite in figure 4.46(c). The CF-epoxy composite due to weak interfacial bonding between CF and epoxy led to interlayer as well as interfiber debonding, as a result the composite failed due to multiple shear failure all connected together. While, CF-nanofiller modified epoxy composite due to improved interfacial interaction between CF and modified epoxy failed by single shear failure.

4.6.5 Thermal Analysis of Carbon Fiber and Nanofiller Reinforced Carbon Fiber Epoxy Composite

4.6.5.1 Effect of Addition of Nanofillers on Thermal Stability of CF Epoxy Composite

The effect of addition of well knitted 3D network of nanofiller on the thermal stability of CF epoxy composite was studied through TGA. The TGA curve for epoxy, CF epoxy composite and CF nanofiller modified epoxy composite is shown in figure 4.47. The initial decomposition of ~5% weight loss occurs up to 300°C for epoxy, CF epoxy composite and CF nanofiller modified epoxy composite, which is due to the evaporation of moisture or volatile impurities. The degradation temperature was found to be ~340°C in each case, which is defined as the point of inflection on the TGA curve. Below this temperature, the thermal stability was seen to be almost similar for all compositions. The major mass loss of about 50% was seen between 350°C to 750°C for CF epoxy composites with and without nanofiller. While, in case of epoxy it was between 350°C to 450°C.

Reinforcing epoxy matrix with CF is seen to improve the thermal stability of epoxy quite significantly. As, CF has higher thermal stability, the strong interaction of epoxy matrix with CF, improved its stability. Comparative analysis of TGA curve for CF epoxy and Gr-CNT-ND CF epoxy composite reveals, that the decomposition temperature of the CF epoxy composite is decreased with the addition of nanofillers. Infact, nanofiller reinforced CF epoxy composite showed lower thermal stability at higher temperature. The reduction in thermal stability was ~25°C at the beginning of decomposition, which increased upto 100-125°C between 650°C to 750°C with 25Gr:50CNT:25ND and 33Gr:33CNT:33ND CF epoxy composite. This clearly indicates nanofiller modified CF epoxy composite shows lower thermal stability than CF epoxy composite specially with the composition having higher CNT content and at higher temperatures.

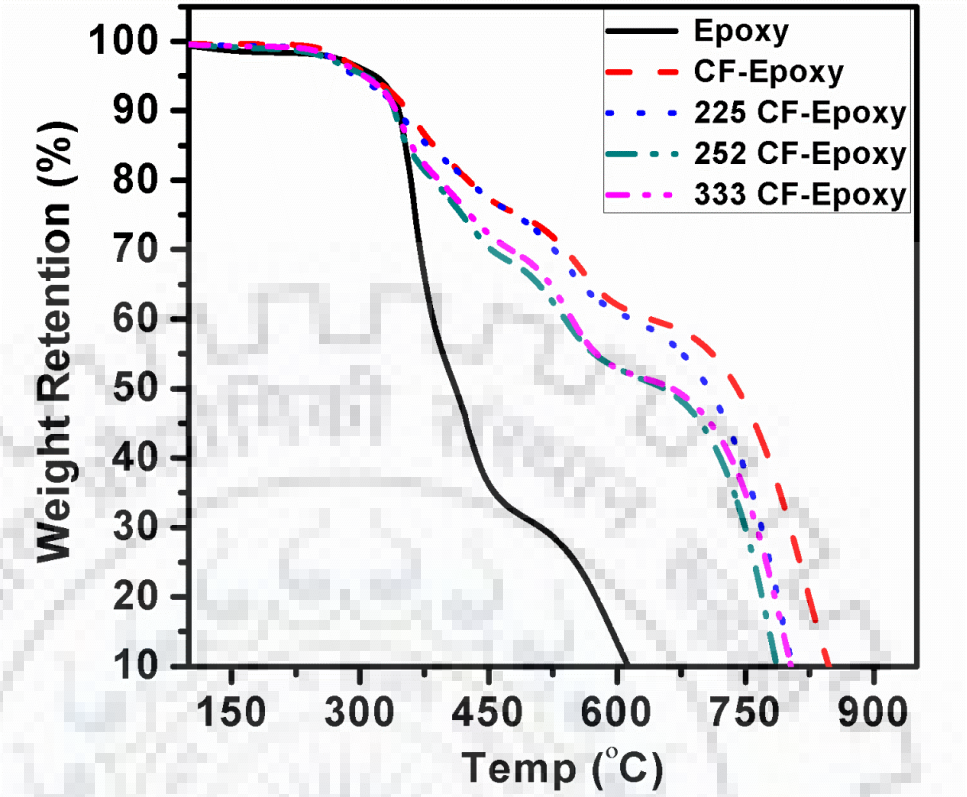

Figure 4.47 TGA thermogram for epoxy, CF epoxy composite and CF nanofiller modified epoxy composite

The thermal stability of CF nanofiller epoxy composite is expected to increase with improved exfoliation due to the sheet barrier effect or torturous path effect. The highly exfoliated well connected network of nanofillers have higher and strong interaction with the epoxy matrix, thus preventing the entry of oxygen and exit of volatile products evolved at high temperature or during thermal degradation. However, as seen, the presence of ND improves the exfoliation and synergy between nanofillers. This results into well connected thermally conducting network of nanofillers throughout the matrix degrading it, at a much faster rate. The compositions with lower CNT ratios are seen to have relatively higher thermal stability as due to less no. of CNTs available for the formation of conductive network.

However, for structural applications, the preferable working temperature for a composite system is the temperature at which the mass loss is no more than 10%, during its service life, which is below 350°C in this study. Upto, 350°C the thermal stability is similar for CF epoxy composites both with and without carbon nanofiller.

4.6.5.2 Thermomechanical Analysis of CF Epoxy Composite with and without Nanofillers

DMA was done to verify the improvement in interfacial interaction between the CF and epoxy with the addition of 3D network of nanofiller, through storage modulus and glass transition temperature. As, it is a very sensitive technique, so even a small disturbance in the interface in the form of agglomeration or weak interfacial bonding, can be easily translated to reduced storage modulus and glass transition temperature. It also helps to gauge the change in interfacial interaction over the course/range of temperature. Storage modulus and damping factor of epoxy, CF epoxy and Gr-CNT-ND CF epoxy composite, under dynamic loading of 0 to 10 N were evaluated using single cantilever mode at a ramp rate of 2^0C/min, constant frequency of 1 Hz.

Figure 4.48 shows the typical storage modulus vs temperature plots for CF epoxy and other three optimized combinations of Gr-CNT-ND CF epoxy composite. It can be seen from the figure that addition of CF to epoxy matrix increases its storage modulus by 670%. As, CF is much stiffer, stronger and resistant to temperature, as compared to epoxy, so it prevents the deformation of matrix and help share higher load over the range of temperature. Adding Gr-CNT-ND, further improved the storage modulus for all compositions, even at higher temperatures. The highest improvement in modulus was ~60% with 33Gr:33CNT:33ND CF epoxy composite.

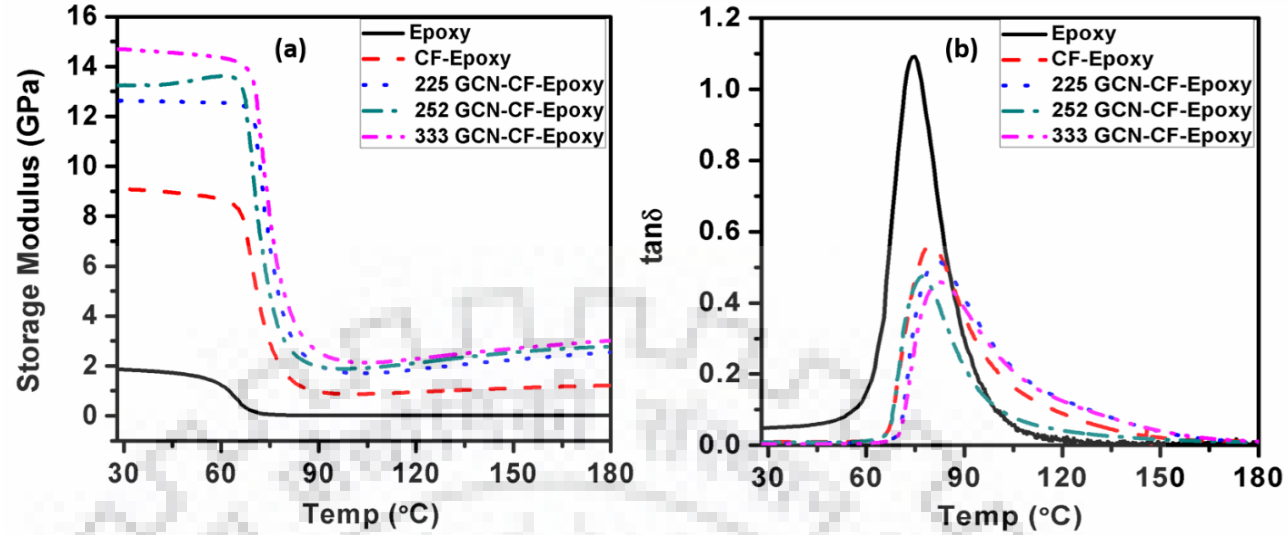

Figure 4.48 Typical DMA results **(a)** Storage modulus and **(b)** tanδ curve for various composition of Gr:CNT:ND CF epoxy composite as a function of temperature

Reinforcing epoxy with CF improved the T_g by ~5^{0}C. Incorporation 3D network of nanofillers further to CF epoxy, did not have any significant effect on T_g. As, already seen over the course of this study, that when ND is added as reinforcement, whether it's a unary or binary filler system the improvement in T_g is not as high. The spherical morphology of NDs is believed to promote sliding of the polymer chains at higher temperature.

Therefore, with increase in temperature, the resistance offered to segmental mobility of polymer chain due to improved interfacial interaction between reinforcement and matrix, is suppressed by the increased segmental mobility of polymer chain by ND. Also, the long conducting networks formed by ND by connecting CNTs end to end reduces the overall thermal stability of polymer chain at high temperature. As, a result the epoxy polymer chains starts becoming unstable, which leads to diffusion or evaporation of volatile impurities or small molecules present in the matrix or filler surface, generating defect at the interface. This, effect is translated more evidently in multiscale composite, as nanofillers itself acts as an interface between CF and epoxy. Thus, at higher

temperatures, the effect of reduced segmental mobility of polymer chain due to increased matrix reinforcement interaction as a result of improved exfoliation is suppressed.

4.6.6 Summary

The potential of carbon nanofillers, with three different morphologies, i.e., CNT (tube), Gr (sheet), and nanodiamond (particle), integrated in a 3D network for improving the fracture toughness of a laminated CF epoxy composite is investigated. Mode I interlaminar and intralaminar fracture toughness values obtained clearly suggest the potential of uniformly dispersed hybrid well connected 3D network of Gr-CNT-ND in improving the fracture toughness of the carbon fiber epoxy composite. In addition, the tensile strength and interlaminar shear strength showed significant improvement with the addition of nanofillers. Improved adhesion between matrix and fiber, due to high surface area and aspect ratio offered by nanofillers, led to better load sharing, improved resistance to crack propagation by deflection, bridging and pinning, which eventually improved the overall mechanical properties of CF epoxy composite. The FE-SEM images corroborates the same. Out of the different composition of nanofillers, the composition having highest CNT content offered maximum improvement in the fracture toughness and interlaminar shear strength, due to crack bridging. Thermal stability was not affected by incorporation of 3D network of nanofiller upto 350°C, post which the thermal stability reduced as nanofillers formed thermally conducting networks. Storage modulus showed improvement, while T_g was not affected by the addition of nanofillers. Thus, the present study clearly shows the potential of well-connected 3D network of Gr-CNT-ND in improving the interfacial and mechanical properties of CF-epoxy composite without degrading its thermal stability, significantly.

CHAPTER 5

CONCLUSIONS

The work done in this thesis has explored the possibility of developing carbon nanofiller modified carbon fiber epoxy composite for structural application. In this regard, the epoxy was modified with carbon nanofiller, having different morphologies, e.g., carbon nanotubes (CNT) with 1D structure, graphene (Gr) with 2D shape and nanodiamonds (ND) with 3D morphology. The potential of each nanofiller and the synergy that exist between them both in binary and ternary combination and its effect on mechanical and thermal properties of epoxy was investigated. The epoxy, modified with optimized combination and composition of nanofillers, was then used to fabricate the multiscale composite. Comparative analysis of multiscale composite, with conventional CF epoxy composite, was done in terms of mechanical, interfacial and thermal properties.

The following are the specific conclusions drawn out of the present work:

- Addition of carbon based nanofillers (CNT, Gr and ND), having three different morphologies, are found to improve the mechanical and thermal properties of the epoxy matrix. ND showed better reinforcement efficiency in terms of Young's modulus, hardness, storage modulus and strength, along with strain as compared to the other two reinforcements. CNT showed better improvement in properties than Gr, both in fracture toughness and elastic modulus. Infact, CNT showed highest improvement in fracture toughness.
- The modulus mapping studies, carried out on composites with and without application of uniaxial tensile stresses, reveals the active role played by nanodiamond in modulating the mechanical behaviour of the epoxy matrix. This study develops 2D modulus mapping technique as a generalized tool for evaluating the quality of dispersion of the nanoscale

reinforcement phases and their role in controlling the mechanical behaviour of the macro-scale composite structures.

- Great synergy was offered by CNT-ND and Gr-ND hybrid fillers. Addition of ND, to CNT and Gr during sonication, led to enhanced exfoliation, improving the tensile strength and fracture toughness with 0.6 wt% (75CNT:25ND) and 0.5 wt% (75Gr:25ND)
- ND assisted exfoliation of Gr was successfully achieved using simple ultrasonication technique, confirmed through TEM and SPM. The exfoliation improved by 7.6 folds with 75Gr:25ND, which resulted in better toughening, verified through both experimental and numerical analysis.
- Addition of ND to Gr-CNT hybrid helped in achieving a well exfoliated close knitted 3D network of reinforcement. When reinforced in epoxy it improved both tensile strength and fracture toughness quite significantly. Addition of ND to Gr-CNT epoxy composite improved both tensile strength and fracture toughness.
- The improvement in ILFT, ILSS and tensile strength of CF epoxy composite was observed with the addition of uniformly dispersed hybrid well connected 3D network of Gr-CNT-ND. It clearly reveals the potential of carbon nanofillers and the technique used in modulating the interface efficiently. Improved interfacial adhesion between matrix and fiber, due to high surface area and aspect ratio offered by nanofillers, led to better load sharing, improved resistance to crack propagation by deflection, bridging and pinning, which eventually improved the overall properties of CF epoxy composite.

CHAPTER 6

RECOMMENDATIONS FOR FUTURE WORK

The findings of this study establish the carbon nanofiller modified CF epoxy composite to be a potential alternate to conventional CF epoxy composite for structural applications. However, some of the topics need further investigations to progress further forweard. Following is a tentative list of recommendations for the same.

- In situ mechanical testing of the composite can be a good study to observe delamination propagation under tensile loading and interlaminar cracking under Mode I fracture test, in real time. Microstructural strain evolution by digital image correlation (DIC) analysis needs to be done to gain insight into the active mechanisms during deformation.
- In situ indentation studies, on the surface as well as along the cross-section, needs to be carried out in order to understand the role of filler in reducing the anisotropy in mechanical properties along the matrix dominated direction.
- Effect of functionalization of carbon nanofillers, on the synergistic effect of the well-connected 3D network of nanofillers in epoxy matrix, needs to be thoroughly investigated.
- Comparative study is recommended to validate the optimized composition used in this approach. Instead of fabricating multiscale composite, using only the optimized ternary compositions of nanofiller, multiscale composite should be fabricated and tested for all the compositions of unary, binary and ternary fillers. The optimized composition and properties achieved, using both the approaches, should be compared. Any discrepancy or very significant difference in properties or composition should be further validated.

LIST OF PUBLICATIONS

Published Papers

1. **Ankita Bisht,** Manoj Kumar R., Kinshuk Dasgupta, Debrupa Lahiri, "Evaluation of Physical Distribution of Nanodiamond and its Effect on Mechanical Behaviour of Epoxy Based Composite using 2D Modulus Mapping" **Mechanics of Materials, 2019,** Vol. 135, pp. 114-128. **(Journal Impact Factor: 2.958)**
2. **Ankita Bisht**, Kinshuk Dasgupta, Debrupa Lahiri, "Effect of Graphene and CNT Reinforcement on Mechanical and Thermomechanical Behaviour of Epoxy - A Comparative Study" **Journal of Applied Polymer Science,** 2018, 135 (14), 46101 **(Journal Impact Factor: 2.188)**
3. **Ankita Bisht**, Vijayesh Kumar, Lu Hua Li, Ying Chen, Arvind Agarwal, Debrupa Lahiri, "Effect of warm rolling and annealing on the mechanical properties of aluminum composite reinforced with boron nitride nanotubes" **Materials Science & Engineering A;** Vol. 710, 2018, pp. 366-373. **(Journal Impact Factor: 4.081)**
4. **Ankita Bisht**, Mukul Srivastava, R. Manoj Kumar, Indranil Lahiri, Debrupa Lahiri, "Strengthening mechanism in graphene nanoplatelets reinforced aluminium composite fabricated through spark plasma sintering" **Materials Science and Engineering A,** Vol 695, 2017, pp. 20-28. **(Journal Impact Factor: 4.0081)**
5. Andy Nieto, **Ankita Bisht**, Debrupa Lahiri, Cheng Zhang, Arvind Agarwal, "Graphene reinforced metal and ceramic matrix composites: a review" **International Materials Reviews**; Vol. 62; 2016, pp. 241-302. **(Journal Impact Factor: 21.086)**

Manuscripts under Review

1. **Ankita Bisht,** Vijayesh Kumar, Palash Chandra Maity, Indranil Lahiri, Debrupa Lahiri, "Strong and transparent PMMA sheet reinforced with amine functionalized BN nanoflakes for UV-shielding application" **Composites Part B: Engineering**

2. **Ankita Bisht**, Kinshuk Dasgupta, Debrupa Lahiri, "Investigating the role of 3D network of carbon nanofillers in improving the mechanical properties of carbon fiber epoxy laminated composite" **Composites Part A: Applied Science and Manufacturing**
3. **Ankita Bisht**, Sanjay Singh Samant, Satish jaiswal, Kinshuk Dasgupta, Debrupa Lahiri, "Nanodiamonds assisted exfoliation of graphene and its effect on toughening of composite structure" **Carbon**
4. **Ankita Bisht**, Kinshuk Dasgupta, Debrupa Lahiri, "Evaluating the effect of addition of nanodiamond on the synergistic effect of graphene-carbon nanotube hybrid on the mechanical properties of epoxy based composites" **Materials and Manufacturing Processes**

Conferences

1. **Ankita Bisht**, Pallavi Gupta, Debrupa Lahiri, "**Influence of Carbon Nanotube and Graphene on Mechanical and Damping Characteristics of Epoxy Matrix Composite- A Comparative Analysis**", TMS Annual Meeting 2017, San Diego, USA, 26th February -2nd March, 2017
2. **Ankita Bisht,** Pallavi Gupta, Debrupa Lahiri, **"Nanodiamond: A Potential Reinforcement for Epoxy Composites",** TMS Annual Meeting 2017, San Diego, USA, 26th February -2nd March, 2017
3. **Ankita Bisht**, R. Manoj. Kumar, Kinshuk Dasgupta, Debrupa Lahiri, **"Effect of introduction of nanodiamond on the mechanical behaviour of epoxy matrix under tensile stress"**, Nanoyantrika, Thiruvananthapuram, India, 17th-20th September 2017.
4. **Ankita Bisht**, Manoj. Kumar, Debrupa Lahiri, **"Investigating the nanomechanical behaviour of nanodiamond reinforced epoxy matrix through nanoindentation",** 55th National Metallurgists' Day NMD ATM 2017, Goa, India, 11th-14th November, 2017
5. **Ankita Bisht**, Vijayesh Kumar, Debrupa Lahiri, **"The Reinforcing Effect of BNNT on Mechanical Properties and Microstructural Evaluation of Warm Rolled and Annealed Aluminum"**, 55th National Metallurgists' Day, NMD ATM 2017, Goa, India, 11th-14th November, 2017

6. Jijo Christudasjustus, **Ankita Bisht**, Debrupa Lahiri, **"Mechanical behaviour of Al-Gr composite as a result of thermo-mechanical treatment"**, 55th National Metallurgists' Day NMD ATM 2017, Goa, India, 11th-14th November, 2017
7. **Ankita Bisht,** Vijayesh Kumar, Palash Chandra Maity, Indranil Lahiri, Debrupa Lahiri **"Mechanical and UV-Shielding Properties of Boron Nitride Nanoflakes Reinforced Poly(methyl methacrylate) Composite"** AMPCO, IIT Roorkee, India, 30th November - 2nd December, 2017
8. Jijo Christudasjustus, **Ankita Bisht**, Debrupa Lahiri, **"Effect on Mechanical behaviour of Al-Gr composite due to work hardening"** AMPCO, IIT Roorkee, India, 30th November - 2nd December, 2017
9. **Ankita Bisht**, Mukul Srivastava, Manoj Kumar R, Indranil Lahiri, Debrupa Lahiri **"Effect of Graphene Nanoplatelet (GNP) addition on Aluminium based Composite"** 54th Annual Technical Meeting of Indian Institute of Metals, IIT Kanpur, Indian, 13th-16th November, 2016.
10. **Ankita Bisht**, Debrupa Lahiri, **"Thermal and Mechanical Properties of Nanodiamond Reinforced Epoxy Composites"**, 54th National Metallurgists' Day IIT Kanpur, India, 11th-14th November, 2016
11. **Ankita Bisht**, Debrupa Lahiri, **"Carbon Nanofiller Reinforced Epoxy Composites for Structural Application"**, 53rd National Metallurgists' Day, NMD ATM 2015, Coimbatore, India, 13th-16th November, 2015.

REFERENCES

[1] D. De Cicco, Z. Asaee, F. Taheri, Use of Nanoparticles for Enhancing the Interlaminar Properties of Fiber-Reinforced Composites and Adhesively Bonded Joints—A Review, Nanomaterials. 7 (2017) 360.

[2] C. Soutis, Fibre reinforced composites in aircraft construction, Prog. Aerosp. Sci. 41 (2005) 143-151.

[3] P.K. Mallick, Fiber reinforced composites: materials, manufaturing and design, CRC Press, 3rd Edition, 2008.

[4] Y. Liu, S. Kumar, Recent progress in fabrication, structure, and properties of carbon fibers, Polym. Rev. 52 (2012) 234–258.

[5] S.R. Dhakate, O.P. Bahl, Effect of carbon fiber surface functional groups on the mechanical properties of carbon-carbon composites with HTT, Carbon N. Y. 41 (2003) 1193-1203.

[6] H. Dvir, J. Jopp, M. Gottlieb, Estimation of polymer-surface interfacial interaction strength by a contact AFM technique, J. Colloid Interface Sci. 304 (2006) 58-66.

[7] E. Fitzer, K.H. Geigl, W. Hüttner, R. Weiss, Chemical interactions between the carbon fibre surface and epoxy resins, Carbon N. Y. 18 (1980) 389-393

[8] W. Qin, F. Vautard, L.T. Drzal, J. Yu, Mechanical and electrical properties of carbon fiber composites with incorporation of graphene nanoplatelets at the fiber-matrix interphase, Compos. Part B Eng. 69 (2015) 335-341.

[9] K.V. Kundan, P. Katti, S. Kumar, S. Bose, Assessing the interfacial properties in carbon fiber/epoxy nanocomposites: From ‘interlayers’ to ‘interconnects,’ Nano-Structures and Nano-Objects. 12 (2017) 194-209.

[10] M. Sharma, S. Gao, E. Mäder, H. Sharma, L.Y. Wei, J. Bijwe, Carbon fiber surfaces and composite interphases, Compos. Sci. Technol. 102 (2014) 35-50.

[11] M.M.J. Treacy, T.W. Ebbesen, J.M. Gibson, Exceptionally high Young’s modulus observed

for individual carbon nanotubes, Nature. 381 (1996) 678–680.

[12] J.P. Salvetat, J.M. Bonard, N.B. Thomson, A.J. Kulik, L. Forró, W. Benoit, L. Zuppiroli, Mechanical properties of carbon nanotubes, Appl. Phys. A Mater. Sci. Process. 69 (1999) 255-260.

[13] W. Choi, I. Lahiri, R. Seelaboyina, Y.S. Kan, Synthesis of Graphene and Its Applications: A Review, Crit. Rev. Solid State Mater. Sci. 35 (2010) 52–71.

[14] V.K. Srivastava, T. Gries, D. Veit, T. Quadflieg, B. Mohr, M. Kolloch, Effect of nanomaterial on mode I and mode II interlaminar fracture toughness of woven carbon fabric reinforced polymer composites, Eng. Fract. Mech. 180 (2017) 73–86.

[15] M. Siegfried, C. Tola, M. Claes, S. V Lomov, I. Verpoest, L. Gorbatikh, Impact and residual after impact properties of carbon fiber/epoxy composites modified with carbon nanotubes, Compos. Struct. 111 (2014) 488–496.

[16] Y. Wang, S.K. Raman Pillai, J. Che, M.B. Chan-Park, High Interlaminar Shear Strength Enhancement of Carbon Fiber/Epoxy Composite through Fiber- and Matrix-Anchored Carbon Nanotube Networks, ACS Appl. Mater. Interfaces. 9 (2017) 8960−8966.

[17] J.L. Abot, Y. Song, M.J. Schulz, V.N. Shanov, Novel carbon nanotube array-reinforced laminated composite materials with higher interlaminar elastic properties, Compos. Sci. Technol. 68 (2008) 2755-2760.

[18] W. Zhang, X. Deng, G. Sui, X. Yang, Improving interfacial and mechanical properties of carbon nanotube-sized carbon fiber/epoxy composites, Carbon N. Y. 145 (2019) 629–639.

[19] J.K. Park, I.H. Do, P. Askeland, L.T. Drzal, Electrodeposition of exfoliated graphite nanoplatelets onto carbon fibers and properties of their epoxy composites, Compos. Sci. Technol. 68 (2008) 1734-1741.

[20] M. Tehrani, A.Y. Boroujeni, T.B. Hartman, T.P. Haugh, S.W. Case, M.S. Al-Haik, Mechanical characterization and impact damage assessment of a woven carbon fiber reinforced carbon nanotube-epoxy composite, Compos. Sci. Technol. 75 (2013) 42-48.

[21] E. Kandare, A.A. Khatibi, S. Yoo, R. Wang, J. Ma, P. Olivier, N. Gleizes, C.H. Wang,

Improving the through-thickness thermal and electrical conductivity of carbon fibre/epoxy laminates by exploiting synergy between graphene and silver nano-inclusions, Compos. Part A Appl. Sci. Manuf. 69 (2015) 72-82.

[22] A.Y. Boroujeni, M. Al-Haik, Carbon nanotube – Carbon fiber reinforced polymer composites with extended fatigue life, Compos. Part B Eng. 164 (2019) 537–545.

[23] G. Szebényi, D. Faragó, C. Lámfalusi, R. Göbl, Interfacial adhesion improvement in carbon fiber/carbon nanotube reinforced hybrid composites by the application of a reactive hybrid resin initiated by gamma irradiation, Radiat. Phys. Chem. 164 (2018) 537-545.

[24] E. Mannov, H. Schmutzler, S. Chandrasekaran, C. Viets, S. Buschhorn, F. Tölle, R. Mülhaupt, K. Schulte, Improvement of compressive strength after impact in fibre reinforced polymer composites by matrix modification with thermally reduced graphene oxide, Compos. Sci. Technol. 87 (2013) 36-41.

[25] S.P. Sharma, S.C. Lakkad, Effect of CNTs growth on carbon fibers on the tensile strength of CNTs grown carbon fiber-reinforced polymer matrix composites, Compos. Part A Appl. Sci. Manuf. 42 (2011) 8-15.

[26] E. Bekyarova, E.T. Thostenson, A. Yu, H. Kim, J. Gao, J. Tang, H.T. Hahn, T.W. Chou, M.E. Itkis, R.C. Haddon, Multiscale carbon nanotube-carbon fiber reinforcement for advanced epoxy composites, Langmuir. 23 (2007) 3970-3974.

[27] S.Y. Huang, G.P. Wu, C.M. Chen, Y. Yang, S.C. Zhang, C.X. Lu, Electrophoretic deposition and thermal annealing of a graphene oxide thin film on carbon fiber surfaces, Carbon N. Y. 52 (2013) 613-616.

[28] X. He, F. Zhang, R. Wang, W. Liu, Preparation of a carbon nanotube/carbon fiber multi-scale reinforcement by grafting multi-walled carbon nanotubes onto the fibers, Carbon N. Y. 45 (2007) 2559-2563.

[29] F.H. Zhang, R.G. Wang, X.D. He, C. Wang, L.N. Ren, Interfacial shearing strength and reinforcing mechanisms of an epoxy composite reinforced using a carbon nanotube/carbon fiber hybrid, J. Mater. Sci. 44 (2009) 3574–3577.

[30] F. Zhao, Y. Huang, L. Liu, Y. Bai, L. Xu, Formation of a carbon fiber/polyhedral oligomeric silsesquioxane/carbon nanotube hybrid reinforcement and its effect on the interfacial properties of carbon fiber/epoxy composites, Carbon N. Y. 49 (2011) 2624-2632.

[31] Y. Huang, Preparation of carbon fiber hierarchical reinforcement and its effect on the interfacial property of carbon fiber/epoxy composites, Mater. China. 32 (2013) 211-216.

[32] X. Chen, H. Xu, D. Liu, C. Yan, Y. Zhu, A novel and facile fabrication of polyphosphazene nanotube/carbon fiber multi-scale hybrid reinforcement and its enhancing effect on the interfacial properties of epoxy composites, Compos. Sci. Technol. 169 (2019) 34-44.

[33] M. Tehrani, M. Safdari, A.Y. Boroujeni, Z. Razavi, S.W. Case, K. Dahmen, H. Garmestani, M.S. Al-Haik, Hybrid carbon fiber/carbon nanotube composites for structural damping applications, Nanotechnology. 24 (2013) 155704.

[34] S.Y. Yang, W.N. Lin, Y.L. Huang, H.W. Tien, J.Y. Wang, C.C.M. Ma, S.M. Li, Y.S. Wang, Synergetic effects of graphene platelets and carbon nanotubes on the mechanical and thermal properties of epoxy composites, Carbon N. Y. 49 (2011) 793–803.

[35] S. Chatterjee, F. Nafezarefi, N.H. Tai, L. Schlagenhauf, F.A. Nuesch, B.T.T. Chu, Size and synergy effects of nanofiller hybrids including graphene nanoplatelets and carbon nanotubes in mechanical properties of epoxy composites, Carbon N. Y. 50 (2012) 5380–5386.

[36] P.N. Wang, T.H. Hsieh, C.L. Chiang, M.Y. Shen, Synergetic effects of mechanical properties on graphene nanoplatelet and multiwalled carbon nanotube hybrids reinforced epoxy/carbon fiber composites, J. Nanomater. 2015 (2015) 838032.

[37] W. Li, A. Dichiara, J. Bai, Carbon nanotube-graphene nanoplatelet hybrids as high-performance multifunctional reinforcements in epoxy composites, Compos. Sci. Technol. 74 (2013) 221–227.

[38] F. Aghadavoudi, H. Golestanian, K.A. Zarasvand, Elastic behaviour of hybrid cross-linked epoxy-based nanocomposite reinforced with GNP and CNT: experimental and multiscale modelling, Polym. Bull. 76 (2018) 4275–4294.

[39] N.R. Bandyopadhyay, S. Ghosh, A. Basumallick, New generation metal matrix composites,

Mater. Manuf. Process. 22 (2007) 679–682.

[40] J. Pusch, B. Wohlmann, Chapter 2 - Carbon Fibers, in: B. Mahltig, Y. Kyosev (Eds.), Inorg. Compos. Fibers, Woodhead Publishing, 2018: pp. 31–51.

[41] M.C. Paiva, C.A. Bernardo, M. Nardin, Mechanical, surface and interfacial characterization of pitch and PAN-based carbon fibres, Carbon N. Y. 38 (2000) 1323-1337.

[42] S.J. Park, B.J. Kim, Roles of acidic functional groups of carbon fiber surfaces in enhancing interfacial adhesion behavior, Mater. Sci. Eng. A. 408 (2005) 269-273.

[43] J. Bustillos, C. Zhang, B. Boesl, A. Agarwal, Three-Dimensional Graphene Foam-Polymer Composite with Superior Deicing Efficiency and Strength, ACS Appl. Mater. Interfaces. 10 (2018) 5022-5029.

[44] A.K. Yadav, S. Banerjee, R. Kumar, K.K. Kar, J. Ramkumar, K. Dasgupta, Mechanical Analysis of Nickel Particle-Coated Carbon Fiber-Reinforced Epoxy Composites for Advanced Structural Applications, ACS Appl. Nano Mater. 1 (2018) 4332-4339.

[45] M. Das, D. Ray, S. Bandyopadhyay, S. Banerjee, N.R. Bandyopadhyay, A. Basumallik, Thermogravimetric and resistivity study of Ex situ and in situ poly(methyl methacrylate)/carboxylic acid group functionalized multiwall carbon nanotubes composites, J. Appl. Polym. Sci. 120 (2011) 2954–2961.

[46] R. Kumar, P. Bhargava, Fabrication of low specific resistance ceramic carbon composites by slip casting, J. Asian Ceram. Soc. 3 (2015) 262-265.

[47] P. Nautiyal, C. Rudolf, A. Loganathan, C. Zhang, B. Boesl, A. Agarwal, Directionally Aligned Ultra-Long Boron Nitride Nanotube Induced Strengthening of Aluminum-Based Sandwich Composite , Adv. Eng. Mater. 18 (2016) 1747–1754.

[48] O. Gohardani, M.C. Elola, C. Elizetxea, Potential and prospective implementation of carbon nanotubes on next generation aircraft and space vehicles: A review of current and expected applications in aerospace sciences, Prog. Aerosp. Sci. 70 (2014) 42–68.

[49] M.F.L. De Volder, S.H. Tawfick, R.H. Baughman, a J. Hart, Carbon nanotubes: present and future commercial applications., Science. 339 (2013) 535–9.

[50] A. Pandey, A. Patel, A. S., V. Kumar, R. Sharma, S. Kanhed, V. Nigam, A. Keshri, A. Agarwal, K. Balani, Enhanced Tribological and Bacterial Resistance of Carbon Nanotube with Ceria- and Silver-Incorporated Hydroxyapatite Biocoating, Nanomaterials. 8 (2018) 363.

[51] P. Jojibabu, M. Jagannatham, P. Haridoss, G.D. Janaki Ram, A.P. Deshpande, S.R. Bakshi, Effect of different carbon nano-fillers on rheological properties and lap shear strength of epoxy adhesive joints, Compos. Part A Appl. Sci. Manuf. 82 (2016) 53-64.

[52] S. V. Sawant, S. Banerjee, A.W. Patwardhan, J.B. Joshi, K. Dasgupta, Effect of in-situ boron doping on hydrogen adsorption properties of carbon nanotubes, Int. J. Hydrogen Energy. 44 (2019) 18193–18204.

[53] L. Vertuccio, L. Guadagno, G. Spinelli, P. Lamberti, M. Zarrelli, S. Russo, G. Iannuzzo, Smart coatings of epoxy based CNTs designed to meet practical expectations in aeronautics, Compos. Part B Eng. 147 (2018) 42-46.

[54] M.R. Gude, S.G. Prolongo, A. Ureña, Toughening effect of carbon nanotubes and carbon nanofibres in epoxy adhesives for joining carbon fibre laminates, Int. J. Adhes. Adhes. 62 (2015) 139-145.

[55] S. Kanagaraj, F.R. Varanda, T. V. Zhil'tsova, M.S.A. Oliveira, J.A.O. Simões, Mechanical properties of high density polyethylene/carbon nanotube composites, Compos. Sci. Technol. 67 (2007) 3071-3077.

[56] S. Arun, S. Kanagaraj, Performance enhancement of epoxy based sandwich composites using multiwalled carbon nanotubes for the application of sockets in trans-femoral amputees, J. Mech. Behav. Biomed. Mater. 59 (2016) 1-10.

[57] S. Arun, S. Kanagaraj, Effect of Reinforcement and Processing Methods in PP/MWCNTs Nanocomposites, Adv. Mater. Res. 747 (2013) 575-578.

[58] S.R. Bakshi, D. Lahiri, A. Agarwal, Carbon nanotube reinforced metal matrix composites - a review, Int. Mater. Rev. 55 (2010) 41–64.

[59] B. Boesl, D. Lahiri, S. Behdad, A. Agarwal, Direct observation of carbon nanotube induced strengthening in aluminum composite via in situ tensile tests, Carbon N. Y. 69 (2014) 79-85.

[60] A. Jiménez-Suárez, M. Campo, S.G. Prolongo, M. Sánchez, A. Ureña, Effect of filtration in functionalized and non-functionalized CNTs and surface modification of fibers as an effective alternative approach, Compos. Part B Eng. 94 (2016) 286-291.

[61] M.H.G. Wichmann, J. Sumfleth, F.H. Gojny, M. Quaresimin, B. Fiedler, K. Schulte, Glass-fibre-reinforced composites with enhanced mechanical and electrical properties - Benefits and limitations of a nanoparticle modified matrix, Eng. Fract. Mech. 73 (2006) 2346-2359.

[62] B. Rogers, J. Adams, S. Pennathur. Nanotechnology: understanding small systems, 3rd edition, CRC Press, (2013).

[63] M. Arena, M. Viscardi, G. Barra, L. Vertuccio, L. Guadagno, Multifunctional Performance of a Nano-Modified Fiber Reinforced Composite Aeronautical Panel, Materials (Basel). 12 (2019) 869.

[64] S. Wang, R. Downes, C. Young, D. Haldane, A. Hao, R. Liang, B. Wang, C. Zhang, R. Maskell, Carbon Fiber/Carbon Nanotube Buckypaper Interply Hybrid Composites: Manufacturing Process and Tensile Properties, Adv. Eng. Mater. 17 (2015) 1442-1453.

[65] S. Aldajah, Y. Haik, Transverse strength enhancement of carbon fiber reinforced polymer composites by means of magnetically aligned carbon nanotubes, Mater. Des. 34 (2012) 379-383.

[66] R. Sadeghian, S. Gangireddy, B. Minaie, K.T. Hsiao, Manufacturing carbon nanofibers toughened polyester/glass fiber composites using vacuum assisted resin transfer molding for enhancing the mode-I delamination resistance, Compos. Part A Appl. Sci. Manuf. 37 (2006) 1787-1795.

[67] Z. Fan, M.H. Santare, S.G. Advani, Interlaminar shear strength of glass fiber reinforced epoxy composites enhanced with multi-walled carbon nanotubes, Compos. Part A Appl. Sci. Manuf. 39 (2008) 540-554.

[68] M. Eizenberg, J.M. Blakely, Carbon monolayer phase condensation on Ni(111), Surf. Sci. 82 (1979) 228-236.

[69] K.S. Novoselov, A.K. Geim, S. V. Morozov, D. Jiang, Y. Zhang, S. V. Dubonos, I. V.

Grigorieva, A.A. Firsov, Electric field in atomically thin carbon films, Science. 306 (2004) 666-669.

[70] C. Lee, X. Wei, J.W. Kysar, J. Hone, Measurement of the Elastic Properties and Intrinsic Strength of Monolayer Graphene, Science. 321 (2008) 385–388.

[71] A.A. Balandin, S. Ghosh, W. Bao, I. Calizo, D. Teweldebrhan, F. Miao, C.N. Lau, Superior thermal conductivity of single-layer graphene, Nano Lett. 8 (2008) 902–907.

[72] J.S. Bunch, S.S. Verbridge, J.S. Alden, A.M. Van Der Zande, J.M. Parpia, H.G. Craighead, P.L. McEuen, Impermeable atomic membranes from graphene sheets, Nano Lett. 8 (2008) 2458-2462.

[73] C. Rudolf, B. Boesl, A. Agarwal, In situ indentation behavior of bulk multi-layer graphene flakes with respect to orientation, Carbon N. Y. 94 (2015) 872-878.

[74] S.S. Nemala, P. Kartikay, S. Prathapani, H.L.M. Bohm, P. Bhargava, S. Bohm, S. Mallick, Liquid phase high shear exfoliated graphene nanoplatelets as counter electrode material for dye-sensitized solar cells, J. Colloid Interface Sci. 499 (2017) 9-16.

[75] M. Koller, H. Seiner, M. Landa, A. Nieto, A. Agarwal, Anisotropic elastic and acoustic properties of bulk graphene nanoplatelets consolidated by spark plasma sintering, Acta Phys. Pol. A, 2015 (2015) 670-673.

[76] J.H. Ouyang, S. Sasaki, T. Murakami, K. Umeda, Tribological properties of spark-plasma-sintered ZrO2(Y 2O3)-CaF2-Ag composites at elevated temperatures, Wear. 258 (2005) 1444-1454.

[77] M. Raimondo, L. Guadagno, V. Speranza, L. Bonnaud, P. Dubois, K. Lafdi, Multifunctional graphene/POSS epoxy resin tailored for aircraft lightning strike protection, Compos. Part B Eng. 140 (2018) 44-56.

[78] P. Jojibabu, G.D.J. Ram, A.P. Deshpande, S.R. Bakshi, Effect of carbon nano-filler addition on the degradation of epoxy adhesive joints subjected to hygrothermal aging, Polym. Degrad. Stab. 140 (2017) 84-94.

[79] R. Moriche, A. Jiménez-Suárez, M. Sánchez, S.G. Prolongo, A. Ureña, High sensitive damage

sensors based on the use of functionalized graphene nanoplatelets coated fabrics as reinforcement in multiscale composite materials, Compos. Part B Eng. 149 (2018) 31-37.

[80] S.G. Prolongo, A. Jimenez-Suarez, R. Moriche, A. Ureña, In situ processing of epoxy composites reinforced with graphene nanoplatelets, Compos. Sci. Technol. 86 (2013) 185–191.

[81] J.A. King, D.R. Klimek, I. Miskioglu, G.M. Odegard, Mechanical properties of graphene nanoplatelet/epoxy composites, J. Appl. Polym. Sci. 128 (2013) 4217–4223.

[82] S.G. Prolongo, A. Jiménez-Suárez, R. Moriche, A. Ureña, Graphene nanoplatelets thickness and lateral size influence on the morphology and behavior of epoxy composites, Eur. Polym. J. 53 (2014) 292–301.

[83] R. Atif, J. Wei, I. Shyha, F. Inam, Use of morphological features of carbonaceous materials for improved mechanical properties of epoxy nanocomposites, RSC Adv. 6 (2016) 1351–1359.

[84] M.G. Prolongo, C. Salom, C. Arribas, M. Sánchez-Cabezudo, R.M. Masegosa, S.G. Prolongo, Influence of graphene nanoplatelets on curing and mechanical properties of graphene/epoxy nanocomposites, J. Therm. Anal. Calorim. 125 (2016) 629–636.

[85] Y. Wang, J. Yu, W. Dai, Y. Song, D. Wang, L. Zeng, N. Jiang, Enhanced Thermal and Electrical Properties of Epoxy Composites Reinforced With Graphene Nanoplatelets, Polym. Compos. 36 (2014) 556-565.

[86] Y. Zhou, F. Pervin, L. Lewis, S. Jeelani, Experimental study on the thermal and mechanical properties of multi-walled carbon nanotube-reinforced epoxy, Mater. Sci. Eng. a-Structural Mater. Prop. Microstruct. Process. 452 (2007) 657–664.

[87] L.C.O. Silva, G.G. Silva, P.M. Ajayan, B.G. Soares, Long-term behavior of epoxy/graphene-based composites determined by dynamic mechanical analysis, J. Mater. Sci. 50 (2015) 6407–6419.

[88] Y. Zhang, Y. Wang, J. Yu, L. Chen, J. Zhu, Z. Hu, Tuning the interface of graphene platelets/epoxy composites by the covalent grafting of polybenzimidazole, Polym. (United

Kingdom). 55 (2014) 4990–5000.

[89] M.A. Rafiee, J. Rafiee, Z. Wang, H. Song, Z.Z. Yu, N. Koratkar, Enhanced mechanical properties of nanocomposites at low graphene content, ACS Nano. 3 (2009) 3884–3890.

[90] Q. Meng, J. Jin, R. Wang, H.-C. Kuan, J. Ma, N. Kawashima, A. Michelmore, S. Zhu, C.H. Wang, Processable 3-nm thick graphene platelets of high electrical conductivity and their epoxy composites., Nanotechnology. 25 (2014) 125707.

[91] R. Sengupta, S. Chakraborty, S. Bandyopadhyay, S. Dasgupta, R. Mukhopadhyay, K. Auddy, a S. Deuri, A Short Review on Rubber / Clay Nanocomposites With Emphasis on Mechanical Properties, Engineering. 47 (2007) 21–25.

[92] A.S. Wajid, H.S.T. Ahmed, S. Das, F. Irin, A.F. Jankowski, M.J. Green, High-Performance Pristine Graphene/Epoxy Composites With Enhanced Mechanical and Electrical Properties, Macromol. Mater. Eng. 298 (2013) 339–347.

[93] H. Feng, X. Wang, D. Wu, Fabrication of Spirocyclic Phosphazene Epoxy-Based Nanocomposites with Graphene via Exfoliation of Graphite Platelets and Thermal Curing for Enhancement of Mechanical and Conductive Properties, Ind. Eng. Chem. Res. 52 (2013) 10160–10171.

[94] Y. Yang, W. Rigdon, X. Huang, X. Li, Enhancing graphene reinforcing potential in composites by hydrogen passivation induced dispersion., Sci. Rep. 3 (2013) 2086.

[95] A.M. Izzuddin Zaman , Hsu-Chiang Kuan , Qingshi Meng, and J.M. Nobuyuki Kawashima , Terry Pitt , Liqun Zhang , Sherif Gouda , Lee Luong, A Facile Approach to Chemically Modified Graphene and its Polymer Nanocomposites, Adv. Funct. Mater. (2012) 2735–2743.

[96] W. Liu, K.L. Koh, J. Lu, L. Yang, S. Phua, J. Kong, Z. Chen, X. Lu, Simultaneous catalyzing and reinforcing effects of imidazole-functionalized graphene in anhydride-cured epoxies, J. Mater. Chem. 22 (2012) 18395.

[97] X. Huang, C. Zhi, P. Jiang, Toward effective synergetic effects from graphene nanoplatelets and carbon nanotubes on thermal conductivity of ultrahigh volume fraction nanocarbon epoxy composites, J. Phys. Chem. C. 116 (2012) 23812–23820.

[98] J.Q. Pham, C. a Mitchell, J.L. Bahr, J.M. Tour, R. Krishanamoorti, P.F. Green, Glass transition of polymer/single-walled carbon nanotube composite films, J. Polym. Sci. Part B-Polymer Phys. 41 (2003) 3339–3345.

[99] Y.-J. Wan, L.-C. Tang, D. Yan, L. Zhao, Y.-B. Li, L.-B. Wu, J.-X. Jiang, G.-Q. Lai, Improved dispersion and interface in the graphene/epoxy composites via a facile surfactant-assisted process, Compos. Sci. Technol. 82 (2013) 60–68.

[100] A. Hameed, M. Islam, I. ahmad, N. Mahmood, S. Saeed, H. Javed, Thermal and mechanical properties of carbon nanotube/epoxy nanocomposites reinforced with pristine and functionalized multiwalled carbon nanotubes, Polym. Compos. 36 (2015) 1891–1898.

[101] S.U. Khan, J.R. Pothnis, J.-K. Kim, Effects of carbon nanotube alignment on electrical and mechanical properties of epoxy nanocomposites, Compos. Part A Appl. Sci. Manuf. 49 (2013) 26–34.

[102] C.E. Corcione, F. Freuli, A. Maffezzoli, The aspect ratio of epoxy matrix nanocomposites reinforced with graphene stacks, Polym. Eng. Sci. 53 (2013) 531–539.

[103] V.N. Mochalin, O. Shenderova, D. Ho, Y. Gogotsi, The properties and applications of nanodiamonds, Nat. Nanotechnol. 7 (2012) 11–23.

[104] A. Shakun, J. Vuorinen, M. Hoikkanen, M. Poikelispää, A. Das, Hard nanodiamonds in soft rubbers: Past, present and future - A review, Compos. Part A Appl. Sci. Manuf. 64 (2014) 49–69.

[105] I. Neitzel, V. Mochalin, J.A. Bares, R.W. Carpick, A. Erdemir, Y. Gogotsi, Tribological properties of nanodiamond-epoxy composites, Tribol. Lett. 47 (2012) 195–202.

[106] M.R. Ayatollahi, E. Alishahi, S. Doagou-R, S. Shadlou, Tribological and mechanical properties of low content nanodiamond/epoxy nanocomposites, Compos. Part B Eng. 43 (2012) 3425–3430.

[107] A. Stravato, R. Knight, V. Mochalin, S.C. Picardi, HVOF-sprayed nylon-11 + nanodiamond composite coatings: Production & characterization, J. Therm. Spray Technol. 17 (2008) 812–817.

[108] K.D. Behler, A. Stravato, V. Mochalin, G. Korneva, G. Yushin, Y. Gogotsi, Nanodiamond-polymer composite fibers and coatings, ACS Nano. 3 (2009) 363–369.

[109] V.N. Mochalin, Y. Gogotsi, Diamond & Related Materials Nanodiamond – polymer composites, Diam. Relat. Mater. 58 (2015) 161–171.

[110] A. Nieto, J. Kim, O. V. Penkov, D.E. Kim, J.M. Schoenung, Elevated temperature wear behavior of thermally sprayed WC-Co/nanodiamond composite coatings, Surf. Coatings Technol. 315 (2017) 283-293.

[111] A. Nieto, L. Jiang, J. Kim, D.E. Kim, J.M. Schoenung, Synthesis and Multi Scale Tribological Behavior of WC-Co/Nanodiamond Nanocomposites, Sci. Rep. 7 (2017) 7060.

[112] Q. Zhang, V.N. Mochalin, I. Neitzel, I.Y. Knoke, J. Han, C.A. Klug, J.G. Zhou, P.I. Lelkes, Y. Gogotsi, Fluorescent PLLA-nanodiamond composites for bone tissue engineering, Biomaterials. 32 (2011) 87–94.

[113] V.N. Khabashesku, J.L. Margrave, E. V. Barrera, Functionalized carbon nanotubes and nanodiamonds for engineering and biomedical applications, Diam. Relat. Mater. 14 (2005) 859–866.

[114] R. Lam, M. Chen, E. Pierstorff, H. Huang, E. Osawa, D. Ho, Nanodiamond-embedded microfilm devices for localized chemotherapeutic elution, ACS Nano. 2 (2008) 2095–2102. doi:10.1021/nn800465x.

[115] D. Ho, Nanodiamonds: Applications in biology and nanoscale medicine, Springer, 2010.

[116] C. Portet, G. Yushin, Y. Gogotsi, Electrochemical performance of carbon onions, nanodiamonds, carbon black and multiwalled nanotubes in electrical double layer capacitors, Carbon N. Y. 45 (2007) 2511–2518.

[117] O.A. Shenderova, D.M. Gruen, Ultrananocrystalline Diamond: Synthesis, Properties and Applications, William Andrew, 2012.

[118] T. Subhani, M. Latif, I. Ahmad, S.A. Rakha, N. Ali, A.A. Khurram, Mechanical performance of epoxy matrix hybrid nanocomposites containing carbon nanotubes and nanodiamonds, Mater. Des. 87 (2015) 436–444.

[119] I. Neitzel, V. Mochalin, I. Knoke, G.R. Palmese, Y. Gogotsi, Mechanical properties of epoxy composites with high contents of nanodiamond, Compos. Sci. Technol. 71 (2011) 710–716.

[120] U. Maitra, K.E. Prasad, U. Ramamurty, C.N.R. Rao, Mechanical properties of nanodiamond-reinforced polymer-matrix composites, Solid State Commun. 149 (2009) 1693–1697.

[121] M.R. Ayatollahi, E. Alishahi, S. Shadlou, Mechanical behavior of nanodiamond/epoxy nanocomposites, Int. J. Fract. 170 (2011) 95–100.

[122] V.N. Mochalin, I. Neitzel, B.J.M. Etzold, A. Peterson, G. Palmese, Y. Gogotsi, Covalent incorporation of aminated nanodiamond into an epoxy polymer network, ACS Nano. 5 (2011) 7494–7502.

[123] Y.J. Zhai, Z.C. Wang, W. Huang, J.J. Huang, Y.Y. Wang, Y.Q. Zhao, Improved mechanical properties of epoxy reinforced by low content nanodiamond powder, Mater. Sci. Eng. A. 528 (2011) 7295–7300.

[124] I. Neitzel, V.N. Mochalin, J. Niu, J. Cuadra, A. Kontsos, G.R. Palmese, Y. Gogotsi, Maximizing Young's modulus of aminated nanodiamond-epoxy composites measured in compression, Polym. (United Kingdom). 53 (2012) 5965–5971.

[125] A. Aris, A. Shojaei, R. Bagheri, Cure Kinetics of Nanodiamond-Filled Epoxy Resin : In fl uence of Nanodiamond Surface Functionality, 54, (2015) 8954-8962.

[126] E.P. Koumoulos, P. Jagadale, A. Lorenzi, A. Tagliaferro, C.A. Charitidis, Evaluation of surface properties of epoxy-nanodiamonds composites, Compos. Part B Eng. 80 (2015) 27–36.

[127] Y.A. Haleem, D. Liu, W. Chen, C. Wang, C. Hong, Z. He, J. Liu, P. Song, S. Yu, L. Song, Surface functionalization and structure characterizations of nanodiamond and its epoxy based nanocomposites, Compos. Part B. 78 (2015) 480–487.

[128] T.S. Kurkin, E.P. Tikunova, A. V. Solopchenko, M.Y. Yablokova, A.N. Ozerin, Polymer composite materials based on thermoset epoxy binders modified with diamond-containing nanofillers, Polym. Sci. Ser. C. 58 (2016) 50–61.

[129] S.A. Rakha, R. Raza, A. Munir, Reinforcement effect of nanodiamond on properties of epoxy

matrix, Polym. Compos. 34 (2013) 811–818.

[130] S.A. Rakha, N. Ali, Y.A. Haleem, F. Alam, A.A. Khurram, A. Munir, Comparison of Mechanical Properties of Acid and UV Ozone Treated Nanodiamond Epoxy Nanocomposites, J. Mater. Sci. Technol. 30 (2014) 753–758.

[131] R.S. Ruoff, D.C. Lorents, Mechanical and thermal properties of carbon nanotubes, Carbon N. Y. 33 (2013) 925-930.

[132] J.N. Coleman, U. Khan, W.J. Blau, Y.K. Gun'ko, Small but strong: A review of the mechanical properties of carbon nanotube-polymer composites, Carbon N. Y. 44 (2006) 1624–1652.

[133] J. Hone, M.C. Llaguno, M.J. Biercuk, A.T. Johnson, B. Batlogg, Z. Benes, J.E. Fischer, Thermal properties of carbon nanotubes and nanotube-based materials, Appl. Phys. A Mater. Sci. Process. 74 (2002) 339–343.

[134] R. Krupke, F. Hennrich, H. V. Löhneysen, M.M. Kappes, Separation of metallic from semiconducting single-walled carbon nanotubes, Science. 301 (2003) 344-347.

[135] X. Xu, R. Ray, Y. Gu, H.J. Ploehn, L. Gearheart, K. Raker, W.A. Scrivens, Electrophoretic analysis and purification of fluorescent single-walled carbon nanotube fragments, J. Am. Chem. Soc. 126 (2004) 12736-7.

[136] H.H. Gommans, J.W. Alldredge, H. Tashiro, J. Park, J. Magnuson, A.G. Rinzler, Fibers of aligned single-walled carbon nanotubes: Polarized Raman spectroscopy, J. Appl. Phys. 88 (2000) 2509.

[137] J. Guo, C. Lu, F. An, S. He, Preparation and characterization of carbon nanotubes/carbon fiber hybrid material by ultrasonically assisted electrophoretic deposition, Mater. Lett. 66 (2012) 382-384.

[138] J. Guo, C. Lu, Continuous preparation of multiscale reinforcement by electrophoretic deposition of carbon nanotubes onto carbon fiber tows, Carbon N. Y. 50 (2012) 3101-3103.

[139] A.J. Rodriguez, M.E. Guzman, C.S. Lim, B. Minaie, Mechanical properties of carbon nanofiber/fiber-reinforced hierarchical polymer composites manufactured with multiscale-

reinforcement fabrics, Carbon N. Y. 49 (2011) 937-948.

[140] Q. Zhang, J. Liu, R. Sager, L. Dai, J. Baur, Hierarchical composites of carbon nanotubes on carbon fiber: Influence of growth condition on fiber tensile properties, Compos. Sci. Technol. 69 (2009) 594-601.

[141] F. Ghaemi, R. Yunus, A. Ahmadian, F. Ismail, M.A.M. Salleh, S.A. Rashid, Few- and multi-layer graphene on carbon fibers: Synthesis and application, RSC Adv. 5 (2015) 81266.

[142] S. Zhu, C.H. Su, S.L. Lehoczky, I. Muntele, D. Ila, Carbon nanotube growth on carbon fibers, Diam. Relat. Mater. 12 (2003) 1825-1828.

[143] K. Otsuka, Y. Abe, N. Kanai, Y. Kobayashi, S. Takenaka, E. Tanabe, Synthesis of carbon nanotubes on Ni/carbon-fiber catalysts under mild conditions, Carbon N. Y. 42 (2004) 727-736.

[144] Z.G. Zhao, L.J. Ci, H.M. Cheng, J.B. Bai, The growth of multi-walled carbon nanotubes with different morphologies on carbon fibers, Carbon N. Y. 43 (2005) 455-678.

[145] N. Sonoyama, M. Ohshita, A. Nijubu, H. Nishikawa, H. Yanase, J. Ichiro Hayashi, T. Chiba, Synthesis of carbon nanotubes on carbon fibers by means of two-step thermochemical vapor deposition, Carbon N. Y. 44 (2006) 1754-1761.

[146] K.J. Kim, W.R. Yu, J.H. Youk, J. Lee, Degradation and healing mechanisms of carbon fibers during the catalytic growth of carbon nanotubes on their surfaces, ACS Appl. Mater. Interfaces. 4 (2012) 2250-2258.

[147] H. Qian, A. Bismarck, E.S. Greenhalgh, G. Kalinka, M.S.P. Shaffer, Hierarchical composites reinforced with carbon nanotube grafted fibers: The potential assessed at the single fiber level, Chem. Mater. 20 (2008) 1862-1869.

[148] P. Lv, Y.Y. Feng, P. Zhang, H.M. Chen, N. Zhao, W. Feng, Increasing the interfacial strength in carbon fiber/epoxy composites by controlling the orientation and length of carbon nanotubes grown on the fibers, Carbon N. Y. 49 (2011) 4665-4673.

[149] E.T. Thostenson, W.Z. Li, D.Z. Wang, Z.F. Ren, T.W. Chou, Carbon nanotube/carbon fiber hybrid multiscale composites, J. Appl. Phys. 91 (2002) 6034.

[150] M.F. De Riccardis, D. Carbone, T.D. Makris, R. Giorgi, N. Lisi, E. Salernitano, Anchorage of carbon nanotubes grown on carbon fibres, Carbon N. Y. 44 (2006) 671-674.

[151] R.B. Mathur, S. Chatterjee, B.P. Singh, Growth of carbon nanotubes on carbon fibre substrates to produce hybrid/phenolic composites with improved mechanical properties, Compos. Sci. Technol. 68 (2008) 1608-1615.

[152] F. An, C. Lu, Y. Li, J. Guo, X. Lu, H. Lu, S. He, Y. Yang, Preparation and characterization of carbon nanotube-hybridized carbon fiber to reinforce epoxy composite, Mater. Des. 33 (2012) 197-202.

[153] R.J. Sager, P.J. Klein, D.C. Lagoudas, Q. Zhang, J. Liu, L. Dai, J.W. Baur, Effect of carbon nanotubes on the interfacial shear strength of T650 carbon fiber in an epoxy matrix, Compos. Sci. Technol. 69 (2009) 898-904.

[154] J.D.H. Hughes, The carbon fibre/epoxy interface-A review, Compos. Sci. Technol. 41 (1991) 13-45.

[155] H. Qian, A. Bismarck, E.S. Greenhalgh, M.S.P. Shaffer, Carbon nanotube grafted carbon fibres: A study of wetting and fibre fragmentation, in: Compos. Part A Appl. Sci. Manuf., 41 (2010) 1107-1114.

[156] S.A. Steiner, R. Li, B.L. Wardle, Circumventing the mechanochemical origins of strength loss in the synthesis of hierarchical carbon fibers, ACS Appl. Mater. Interfaces. 5 (2013) 4892-4903.

[157] R. Li, N. Lachman, P. Florin, H.D. Wagner, B.L. Wardle, Hierarchical carbon nanotube carbon fiber unidirectional composites with preserved tensile and interfacial properties, Compos. Sci. Technol. 117 (2015) 139-145.

[158] Y. Yun, V. Shanov, Y. Tu, S. Subramaniam, M.J. Schulz, Growth mechanism of long aligned multiwall carbon nanotube arrays by water-assisted chemical vapor deposition, J. Phys. Chem. B. 110 (2006) 23920-23925.

[159] N. De Greef, A. Magrez, E. Couteau, J.P. Locquet, L. Forró, J.W. Seo, Growth of carbon nanotubes on carbon fibers without strength degradation, Phys. Status Solidi Basic Res. 249

(2012) 2420–2423.

[160] Y. Dzenis, Materials science: Structural nanocomposites, Science (80-.). 319 (2008) 419-420.

[161] H. Zhou, X. Du, H.Y. Liu, H. Zhou, Y. Zhang, Y.W. Mai, Delamination toughening of carbon fiber/epoxy laminates by hierarchical carbon nanotube-short carbon fiber interleaves, Compos. Sci. Technol. 140 (2017) 46-53.

[162] E.J. Garcia, B.L. Wardle, A. John Hart, Joining prepreg composite interfaces with aligned carbon nanotubes, Compos. Part A Appl. Sci. Manuf. 39 (2008) 1065-1070.

[163] H. Ning, J. Li, N. Hu, C. Yan, Y. Liu, L. Wu, F. Liu, J. Zhang, Interlaminar mechanical properties of carbon fiber reinforced plastic laminates modified with graphene oxide interleaf, Carbon N. Y. 91 (2015) 224-233.

[164] L. Chen, H. Jin, Z. Xu, J. Li, Q. Guo, M. Shan, C. Yang, Z. Wang, W. Mai, B. Cheng, Role of a gradient interface layer in interfacial enhancement of carbon fiber/epoxy hierarchical composites, J. Mater. Sci. 50 (2015) 112-121.

[165] O. Boura, E.K. Diamanti, S.A. Grammatikos, D. Gournis, A.S. Paipetis, Carbon nanotube growth on high modulus carbon fibres: Morphological and interfacial characterization, Surf. Interface Anal. 45 (2013) 1372-1381.

[166] A. Godara, D. Raabe, Influence of fiber orientation on global mechanical behavior and mesoscale strain localization in a short glass-fiber-reinforced epoxy polymer composite during tensile deformation investigated using digital image correlation, Compos. Sci. Technol. 67 (2007) 2417-2427.

[167] A. Ashori, H. Rahmani, R. Bahrami, Preparation and characterization of functionalized graphene oxide/carbon fiber/epoxy nanocomposites, Polym. Test. 48 (2015) 82-88.

[168] X. Zhang, X. Fan, C. Yan, H. Li, Y. Zhu, X. Li, L. Yu, Interfacial microstructure and properties of carbon fiber composites modified with graphene oxide, ACS Appl. Mater. Interfaces. 4 (2012) 1543-1552.

[169] P. Drescher, M. Thomas, J. Borris, U. Riedel, C. Arlt, Strengthening fibre/matrix interphase

by fibre surface modification and nanoparticle incorporation into the matrix, Compos. Sci. Technol. 74 (2013) 60-66.

[170] L. Zhang, N. De Greef, G. Kalinka, B. Van Bilzen, J.-P. Locquet, I. Verpoest, J.W. Seo, Carbon nanotube-grafted carbon fiber polymer composites: Damage characterization on the micro-scale, Compos. Part B Eng. 126 (2017) 202–210.

[171] J.L. Thomason, L.J. Adzima, Sizing up the interphase: An insider's guide to the science of sizing, Compos. Part A Appl. Sci. Manuf. 32 (2001) 313-321.

[172] N. Dilsiz, J.P. Wightman, Surface analysis of unsized and sized carbon fibers, Carbon N. Y. 37 (1999) 1105-1114.

[173] J.W. Shim, S.J. Park, S.K. Ryu, Effect of modification with HNO3 and NaOH on metal adsorption by pitch-based activated carbon fibers, Carbon N. Y. 39 (2001) 1635-1642.

[174] B. Xu, X. Wang, Y. Lu, Surface modification of polyacrylonitrile-based carbon fiber and its interaction with imide, Appl. Surf. Sci. 253 (2006) 2695-2701.

[175] C. Jones, Effects of electrochemical and plasma treatments on carbon fibre surfaces, Surf. Interface Anal. 20 (1993) 357-367.

[176] J. Liu, Y. Tian, Y. Chen, J. Liang, Interfacial and mechanical properties of carbon fibers modified by electrochemical oxidation in (NH4HCO3)/(NH4)2C2O4·H2O aqueous compound solution, Appl. Surf. Sci. 256 (2010) 6199-6204.

[177] K.B. Hung, J. Li, Q. Fan, Z.H. Chen, The enhancement of carbon fiber modified with electropolymer coating to the mechanical properties of epoxy resin composites, Compos. Part A Appl. Sci. Manuf. 39 (2008) 1133-1140.

[178] Y.Q. Dai, D.M. Zhou, K.K. Shiu, Permeability and permselectivity of polyphenylenediamine films synthesized at a palladium disk electrode, Electrochim. Acta. 52 (2006) 297-303.

[179] N. Dilsiz, N.K. Erinç, E. Bayramli, G. akovali, Surface energy and mechanical properties of plasma-modified carbon fibers, Carbon N. Y. 33 (1995) 853-858.

[180] Z. Xu, Y. Huang, C. Zhang, L. Liu, Y. Zhang, L. Wang, Effect of γ-ray irradiation grafting on the carbon fibers and interfacial adhesion of epoxy composites, Compos. Sci. Technol. 67

(2007) 3261-3270.

[181] J.Q. Li, Y.D. Huang, S.Y. Fu, L.H. Yang, H. tao Qu, G. shun Wu, Study on the surface performance of carbon fibres irradiated by γ-ray under different irradiation dose, Appl. Surf. Sci. 256 (2010) 2000-2004.

[182] S.J. Park, Y.S. Jang, Interfacial characteristics and fracture toughness of electrolytically Ni-plated carbon fiber-reinforced phenolic resin matrix composites, J. Colloid Interface Sci. 237 (2001) 91-97.

[183] T. Ramanathan, A. Bismarck, E. Schulz, K. Subramanian, Investigation of the influence of acidic and basic surface groups on carbon fibres on the interfacial shear strength in an epoxy matrix by means by single-fibre pull-out test, Compos. Sci. Technol. 61 (2001) 595-605.

[184] S. Osbeck, R.H. Bradley, C. Liu, H. Idriss, S. Ward, Effect of an ultraviolet/ozone treatment on the surface texture and functional groups on polyacrylonitrile carbon fibres, Carbon N. Y. 49 (2011) 4322-4330.

[185] N. Dilsiz, J.P. Wightman, Effect of acid-base properties of unsized and sized carbon fibers on fiber/epoxy matrix adhesion, Colloids Surfaces A Physicochem. Eng. Asp. 164 (2000) 325-336.

[186] X. Zhang, Latent Curing Agent Modified Epoxy Sizing Agent for High Modulus Carbon Fiber, Open Mater. Sci. J. 5 (2011) 104-108.

[187] B. Fernández, A. Arbelaiz, A. Valea, F. Mujika, I. Mondragon, A comparative study on the influence of epoxy sizings on the mechanical performance of woven carbon fiber-epoxy composites, Polym. Compos. 25 (2004) 319-330.

[188] C.L. Weitzsacker, M. Bellamy, P.M.A. Sherwood, Studies of the effect of size on carbon fiber surfaces, J. Vac. Sci. Technol. A Vacuum, Surfaces, Film. 12 (2002) 2392-2397.

[189] Z. Dai, B. Zhang, F. Shi, M. Li, Z. Zhang, Y. Gu, Chemical interaction between carbon fibers and surface sizing, J. Appl. Polym. Sci. 124 (2012) 2127-2132.

[190] R.L. Zhang, Y.D. Huang, D. Su, L. Liu, Y.R. Tang, Influence of sizing molecular weight on the properties of carbon fibers and its composites, Mater. Des. 34 (2012) 649-654.

[191] L.T. Drzal, V.K. Raghavendran, Adhesion of thermoplastic matrices to carbon fibers: Effect of polymer molecular weight and fiber surface chemistry, J. Thermoplast. Compos. Mater. 16 (2003) 21-30.

[192] L.T. Drzal, Fiber-Matrix Interphase Structure and Its Effect on Adhesion and Composite Mechanical Properties, in: Control. Interphases Compos. Mater., (1990) 309-320.

[193] T.H. Cheng, J. Zhang, S. Yumitori, F.R. Jones, C.W. Anderson, Sizing resin structure and interphase formation in carbon fibre composites, Composites. 25 (1994) 661-670.

[194] Y. Yang, C.X. Lu, X.L. Su, G.P. Wu, X.K. Wang, Effect of nano-SiO2 modified emulsion sizing on the interfacial adhesion of carbon fibers reinforced composites, Mater. Lett. 61 (2007) 3601-3604.

[195] E. Mäder, S. lin Gao, R. Plonka, Static and dynamic properties of single and multi-fiber/epoxy composites modified by sizings, Compos. Sci. Technol. 67 (2007) 1105-1115.

[196] X. Zhang, Y. Huang, T. Wang, L. Liu, Influence of fibre surface oxidation-reduction followed by silsesquioxane coating treatment on interfacial mechanical properties of carbon fibre/polyarylacetylene composites, Compos. Part A Appl. Sci. Manuf. 38 (2007) 936-944.

[197] Z. Xu, L. Chen, Y. Huang, J. Li, X. Wu, X. Li, Y. Jiao, Wettability of carbon fibers modified by acrylic acid and interface properties of carbon fiber/epoxy, Eur. Polym. J. 44 (2008) 494-503.

[198] L.G. Tang, J.L. Karoos, A review of methods for improving the interfacial adhesion between carbon fiber and polymer matrix, Polym. Compos. 18 (1997) 100-113.

[199] J. Bijwe, M. Sharma, Carbon Fabric-Reinforced Polymer Composites and Parameters Controlling Tribological Performance, J.P. Davim, editor Wear Adv. Mater., ISTE Wiley, (2011) 1-59.

[200] S. Tiwari, J. Bijwe, S. Panier, Tribological studies on polyetherimide composites based on carbon fabric with optimized oxidation treatment, Wear. 271 (2011) 2252-2260.

[201] E. Pamula, P.G. Rouxhet, Bulk and surface chemical functionalities of type III PAN-based carbon fibres, Carbon N. Y. 41 (2003) 1905-1915.

[202] L.M Manocha, Role of fiber surface-matrix combination incarbon fiber reinforced epoxy composites, J. Mater. Sci. 17 (1982) 3039-3044

[203] K.F. Köster, P. Schwartz, Influence of acetylene plasma treatment on the torsional fatigue of carbon-fiber-reinforced composite strands, Compos. Sci. Technol. 60 (2000) 2005-2010.

[204] K. Tsutsumi, K. Ban, K. Shibata, S. Okazaki, M. Kogoma, Wettability and adhesion characteristics of plasma-treated carbon fibers, J. Adhes. 57 (1996) 45-53.

[205] S. Mujin, H. Baorong, W. Yisheng, T. Ying, H. Weiqiu, D. Youxian, The surface of carbon fibres continuously treated by cold plasma, Compos. Sci. Technol. 34 (1989) 353-364.

[206] Y.J. Ma, J.L. Wang, X.P. Cai, The effect of electrolyte on surface composite and microstructure of carbon fiber by electrochemical treatment, Int. J. Electrochem. Sci. 8 (2013) 2806-2815.

[207] S.J. Park, M.K. Seo, K.Y. Rhee, Effect of Ar+ ion beam irradiation on the physicochemical characteristics of carbon fibers [5], Carbon N. Y. 41 (2003) 592-594.

[208] A.P. Kettle, A.J. Beck, L. O'Toole, F.R. Jones, R.D. Short, Plasma polymerisation for molecular engineering of carbon-fibre surfaces for optimised composites, Compos. Sci. Technol. 57 (1997) 1023-1032.

[209] P.C. Varelidis, R.L. McCullough, C.D. Papaspyrides, The effect on the mechanical properties of carbon/epoxy composites of polyamide coatings on the fibers, Compos. Sci. Technol. 59 (1999) 1813-1823.

[210] F. An, C. Lu, J. Guo, S. He, H. Lu, Y. Yang, Preparation of vertically aligned carbon nanotube arrays grown onto carbon fiber fabric and evaluating its wettability on effect of composite, Appl. Surf. Sci. 258 (2011) 1069-1076. doi:10.1016/j.apsusc.2011.09.003.

[211] H. Qian, A. Bismarck, E.S. Greenhalgh, M.S.P. Shaffer, Synthesis and characterisation of carbon nanotubes grown on silica fibres by injection CVD, Carbon N. Y. 48 (2010) 277-286.

[212] K.A. Dransfield, L.K. Jain, Y.-W. Mai, On the effects of stitching in CFRPs—I. mode I delamination toughness, Compos. Sci. Technol. 58 (2002) 815-827.

[213] K. Dransfield, C. Baillie, Y.W. Mai, Improving the delamination resistance of CFRP by

stitching-a review, Compos. Sci. Technol. 50 (1994) 305-317.

[214] V.A. Guénon, T.W. Chou, J.W. Gillespie, Toughness properties of a three-dimensional carbon-epoxy composite, J. Mater. Sci. 24 (1989) 4168-4175.

[215] L.K. Jain, K.A. Dransfield, Y.W. Mai, On the effects of stitching in CFRPs - II. Mode II delamination toughness, Compos. Sci. Technol. 58 (1998) 829-837.

[216] V.K. Srivastava, T. Gries, D. Veit, T. Quadflieg, B. Mohr, M. Kolloch, Effect of nanomaterial on mode I and mode II interlaminar fracture toughness of woven carbon fabric reinforced polymer composites, Eng. Fract. Mech. 180 (2017) 73-86.

[217] K.L. Lu, R.M. Lago, Y.K. Chen, M.L.H. Green, P.J.F. Harris, S.C. Tsang, Mechanical damage of carbon nanotubes by ultrasound, Carbon N. Y. 34 (1996) 814–816.

[218] Z.A. Ghaleb, M. Mariatti, Z.M. Ariff, Properties of graphene nanopowder and multi-walled carbon nanotube-filled epoxy thin-film nanocomposites for electronic applications: The effect of sonication time and filler loading, Compos. Part A Appl. Sci. Manuf. 58 (2014) 77–83.

[219] I. Zaman, H.C. Kuan, Q. Meng, A. Michelmore, N. Kawashima, T. Pitt, L. Zhang, S. Gouda, L. Luong, J. Ma, A facile approach to chemically modified graphene and its polymer nanocomposites, Adv. Funct. Mater. 22 (2012) 2735-2743.

[220] M. Ullah, A. Kausar, M. Siddiq, M. Subhan, M. Abid Zia, Reinforcing Effects of Modified Nanodiamonds on the Physical Properties of Polymer-Based Nanocomposites: A Review, Polym. - Plast. Technol. Eng. 54 (2015) 861-879.

[221] S. Roy, K. Mitra, C. Desai, R. Petrova, S. Mitra, Detonation Nanodiamonds and Carbon Nanotubes as Reinforcements in Epoxy Composites—A Comparative Study, J. Nanotechnol. Eng. Med. 4 (2013) 011008.

[222] Y.J. Wan, L.C. Tang, D. Yan, L. Zhao, Y.B. Li, L. Bin Wu, J.X. Jiang, G.Q. Lai, Improved dispersion and interface in the graphene/epoxy composites via a facile surfactant-assisted process, Compos. Sci. Technol. 82 (2013) 60–68.

[223] R. Manoj Kumar, S.K. Sharma, B.V. Manoj Kumar, D. Lahiri, Effects of carbon nanotube aspect ratio on strengthening and tribological behavior of ultra high molecular weight

polyethylene composite, Compos. Part A Appl. Sci. Manuf. 76 (2015) 62–72.

[224] Y. Fu, Y. Huang, W. Meng, Z. Wang, Y. Bando, D. Golberg, C. Tang, C. Zhi, Highly ductile UV-shielding polymer composites with boron nitride nanospheres as fillers, Nanotechnology. 26 (2015) 115702.

[225] X. Wang, J. Jin, M. Song, An investigation of the mechanism of graphene toughening epoxy, Carbon N. Y. 65 (2013) 324–333.

[226] Y.E. Liu, C.E. He, R.G. Peng, W. Tang, Y.K. Yang, Ionic Liquid Assisted Dispersion of Reduced Graphene Oxide in Epoxy Composites with Improved Mechanical Properties, Adv. Mater. Res. 738 (2013) 56–60.

[227] G. Tsagaropoulos, A. Eisenberg, Dynamic Mechanical Study of the Factors Affecting the Two Glass Transition Behavior of Filled Polymers. Similarities and Differences with Random Ionomers, Macromolecules. 28 (1995) 6067-6077.

[228] M. Mohr, A. Caron, P. Herbeck-Engel, R. Bennewitz, P. Gluche, K. Brühne, H.J. Fecht, Young's modulus, fracture strength, and Poisson's ratio of nanocrystalline diamond films, J. Appl. Phys. 116 (2014) 124308 1-9.

[229] A. Politano, G. Chiarello, Probing the Young's modulus and Poisson's ratio in graphene/metal interfaces and graphite: a comparative study, Nano Res. 8 (2015) 1847-1856.

[230] W. Stark, Investigation of the curing behaviour of carbon fibre epoxy prepreg by Dynamic Mechanical Analysis DMA, Polym. Test. 32 (2013) 231-239.